

第43回 フラーレン・ナノチューブ・グラフェン 総合シンポジウム

The 43rd Fullerenes-Nanotubes-Graphene General Symposium

講演要旨集 Abstracts

会場：東北大学川内キャンパス 東北大学百周年記念会館 川内萩ホール
Tohoku University Centennial Hall (Kawauchi Hagi Hall), Kawauchi Campus

2012. 9. 5 wed.-7fri.

主催：フラーレン・ナノチューブ・グラフェン学会 The Fullerenes, Nanotubes and Graphene Research Society

共催：日本化学会 The Chemical Society of Japan

東北大学 大学院工学研究科 Graduate School of Engineering, Tohoku University

東北大学 大学院環境科学研究科 Graduate School of Environmental Studies, Tohoku University

協賛：日本物理学会 The Physical Society of Japan

応用物理学会 The Japan Society of Applied Physics

高分子学会 The Society of Polymer Science, Japan

電気化学会 The Electrochemical Society of Japan

カーボンナノチューブ

新製品のご紹介

単層カーボンナノチューブ※1 **NEW!**

- | | | |
|--|---------------------|----------------|
| ○ single-walled (98% semiconducting SWNTs) | 750522-1MG | ¥65,700 |
| ○ single-walled (98% metallic SWNTs) | 750530-1MG | ¥99,500 |
| ○ single-walled (<1% catalyst content) | 750514-25MG | ¥43,100 |
| ○ single-walled (<3.5% catalyst content) | 750492-100MG | ¥46,500 |

二層カーボンナノチューブ※2 **NEW!**

- | | | |
|--|------------------|----------------|
| ○ double-walled, short, <10% Metal Oxide | 755141-1G | ¥31,200 |
| ○ double-walled, <10% Metal Oxide | 755168-1G | ¥31,200 |

※1 NanoIntegris 社製 ※2 Nanocyl 社製

www.aldrich.com/nano-jp

SIGMA-ALDRICH®

シグマ アルドリッチ ジャパン

〒140-0002 東京都品川区東品川2-2-24
天王洲セントラルタワー4階

■製品に関するお問い合わせは、弊社テクニカルサポートへ
TEL : 03-5796-7330 FAX : 03-5796-7335
E-mail : sialjpts@sial.com

■在庫照会・ご注文方法に関するお問い合わせは、弊社カスタマーサービスへ
TEL : 03-5796-7320 FAX : 03-5796-7325
E-mail : sialjpcs@sial.com

<http://www.sigma-aldrich.com/japan>

Abstracts

The 43rd Fullerenes-Nanotubes-Graphene General Symposium

第43回フラーレン・ナノチューブ・グラフェン総合シンポジウム 講演要旨集

The Fullerenes, Nanotubes and Graphene Research Society

The Chemical Society of Japan

Graduate School of Engineering, Tohoku University

Graduate School of Environmental Studies, Tohoku University

The Physical Society of Japan

The Japan Society of Applied Physics

The Society of Polymer Science, Japan

The Electrochemical Society of Japan

主催： フラーレン・ナノチューブ・グラフェン学会

共催： 日本化学会・東北大学 大学院工学研究科・
東北大学 大学院環境科学研究科

協賛： 日本物理学会・応用物理学会・高分子学会・電気化学学会

Date: September 5th (Wed.) – 7th (Fri.), 2012

Place: Tohoku University Centennial Hall (Kawauchi Hagi Hall)
40 Kawauchi, Aoba-ku, Sendai 980-8576, Japan
TEL: 022-795-3391 / FAX: 022-795-3390

Presentation: Plenary Lecture (40 min presentation, 5 min discussion)
Special Lecture (25 min presentation, 5 min discussion)
General Lecture (10 min presentation, 5 min discussion)
Poster Preview (1 min presentation, no discussion)

日時： 平成24年9月5日(水)～7日(金)

場所： 東北大学 東北大学百周年記念会館 川内萩ホール
〒980-8576 宮城県仙台市青葉区川内40
TEL: 022-795-3391 / FAX: 022-795-3390

発表時間： 基調講演 (発表 40分・質疑応答 5分)
特別講演 (発表 25分・質疑応答 5分)
一般講演 (発表 10分・質疑応答 5分)
ポスタープレビュー (発表 1分・質疑応答 なし)

展示団体御芳名（五十音順、敬称略）

(株)ATR
アイクストロン(株)
アルバック販売(株)
コスモ・バイオ(株)
サーモフィッシャーサイエンティフィック(株)
(株)島津製作所
(株)セントラル科学貿易
ナカライテスク(株)
(株)ニューメタルス エンド ケミカルス コーポレーション
(株)堀場製作所
(株)名城ナノカーボン
和光純薬工業(株)

広告掲載団体御芳名（五十音順、敬称略）

アイクストロン(株)
アルバック販売(株)
イデア・インターナショナル(株)
エクセルソフト(株)
(株)エリオニクス
コスモ・バイオ(株)
サーモフィッシャーサイエンティフィック(株)
ジェー・エー・ウーラム・ジャパン (株)
シグマ アルドリッチ ジャパン (株)
(株)島津製作所
(株)セントラル科学貿易
(株)東京インスツルメンツ
(株)東北サイエンス
東洋炭素(株)
ナカライテスク(株)
日本電気(株)
ブルカー・ダルトニクス(株)
フロンティアカーボン(株)
(株)フロンティア出版
(株)日立ハイテクノロジーズ
日立工機(株)
和光純薬工業(株)

Contents

Time Table	i
Chairperson	iii
Program Japanese	iv
English	xix
Abstracts Plenary Lecture, Special Lecture	1
General Lecture	7
Poster Preview	47
Author Index	181

目次

プログラム早見表	i
座長一覧	iii
プログラム 和文	iv
英文	xix
講演予稿 基調講演・特別講演	1
一般公演	7
ポスター発表	47
発表索引	181

プログラム早見表

9月5日(水)	
8:20	受付開始 8:20～ 講演開始 9:30～
9:20	オープニング
9:30	一般講演 5件 (ナノチューブの生成と精製・ ナノチューブの物性) 9:30-10:45
10:45	休憩 10:45-11:00
11:00	特別講演 (岡崎俊也) 11:00-11:30
11:30	一般講演 4件 (フラーレンの化学・ 金属内包フラーレン) 11:30-12:30
12:30	昼食 (幹事会) 12:30-13:45
13:45	一般講演 3件 (フラーレンの応用) 13:45-14:30
14:30	特別講演 (Kosmas Prassides) 14:30-15:00
15:00	休憩 15:00-15:15
15:15	一般講演 4件 (グラフェンの応用) 15:15-16:15
16:15	特別講演 (尾辻泰一) 16:15-16:45
16:45	休憩 16:45-17:00
17:00	ポスタープレビュー (1P-1 ~ 1P-50) 17:00-17:50
17:50	ポスターセッション 17:50-19:35

19:35

9月6日(木)	
8:30	受付開始 8:30～ 講演開始 9:00～
9:00	大澤賞受賞対象者講演 4件 飯島賞受賞対象者講演 2件 9:00-11:00
11:00	休憩 11:00-11:15
11:15	基調講演 (水谷孝) 11:15-12:00
12:00	昼食 12:00-13:00
13:00	若手奨励賞表彰式
13:15	総会 13:15-13:45
13:45	ポスタープレビュー (2P-1 ~ 2P-41) 13:45-14:25
14:25	ポスターセッション 14:25-16:10
16:10	フォーラム 安全安心社会とナノ科学技術 (含:東日本大震災現地調査) 16:10-18:30
18:30	懇親会 (ウエスティンホテル) 18:30-20:30

20:30

9月7日(金)	
8:30	受付開始 8:30～ 講演開始 9:00～
9:00	一般講演 5件 (ナノチューブの生成と精製・ ナノチューブの応用・ 内包ナノチューブ) 9:00-10:15
10:15	休憩 10:15-10:30
10:30	一般講演 4件 (ナノチューブの物性) 10:30-11:30
11:30	特別講演 (R. Mohan Sankaran) 11:30-12:00
12:00	昼食 12:00-13:15
13:15	一般講演 6件 (グラフェンの物性) 13:15-14:45
14:45	特別講演 (吾郷浩樹) 14:45-15:15
15:15	休憩 15:15-15:30
15:30	一般講演 3件 (ナノホーン・ナノ炭素粒子) 15:30-16:15
16:15	ポスタープレビュー (3P-1 ~ 3P-42) 16:15-17:00
17:00	ポスターセッション 17:00-18:45

18:45

基調講演 発表40分・質疑5分
特別講演 発表25分・質疑5分
大澤賞飯島賞対象者講演
発表10分・質疑10分
一般講演 発表10分・質疑5分
ポスタープレビュー 発表1分・質疑なし

Time Table

September 5 [Wed.]		September 6 [Thu.]		September 7 [Fri.]	
8:20	Registration begins at 8:20 Lecture begin at 9:30	8:30	Registration begins at 8:30 Lecture begin at 9:00	8:30	Registration begins at 8:30 Lecture begin at 9:00
9:20	Opening	9:00	General Lectures [6] Lectures by Candidates for the Osawa Award and the Iijima Award 9:00-11:00	9:00	General Lectures [5] [Formation and Purification of Nanotubes · Applications of Nanotubes · Endohedral Nanotubes]
9:30	General Lectures [5] [Formation and Purification of Nanotubes · Properties of Nanotubes] 9:30-10:45	11:00		Coffee Break 11:00-11:15	
10:45	Coffee Break 10:45-11:00	11:15	Prenary Lecture [T. Mizutani] 11:15-12:00	10:30	General Lectures [4] [Properties of Nanotubes] 10:30-11:30
11:00	Special Lecture [T. Okazaki] 11:00-11:30	12:00	Lunch 12:00-13:00	11:30	Special Lecture [R. Sankaran] 11:30-12:00
11:30	General Lectures [4] [Chemistry of Fullerenes · Endohedral Metallofullerenes] 11:30-12:30	13:00	Poster Awards Ceremony	12:00	Lunch 12:00-13:15
12:30	Lunch [Administrative Meeting] 12:30-13:45	13:15	General Meeting 13:15-13:45	13:15	General Lectures [6] [Properties of Graphene] 13:15-14:45
13:45	General Lectures [3] [Applications of Fullerenes] 13:45-14:30	13:45	Poster Preview [2P-1 through 2P-41] 13:45-14:25	14:45	
14:30	Special Lecture [K. Prassides] 14:30-15:00	14:25	Poster Session 14:25-16:10	15:15	Coffee Break 15:15-15:30
15:00	Coffee Break 15:00-15:15	16:10		Forum	15:30
15:15	General Lectures [4] [Applications of Graphene] 15:15-16:15	16:10	Safety · Security Society and Nano Science · Technology [Field investigation of the Great East Japan Earthquake included] 16:10-18:30	16:15	Poster Preview [3P-1 through 3P-42] 16:15-17:00
16:15	Special Lecture [T. Otsuji] 16:15-16:45	18:30		Banquet [Westin Hotel] 18:30-20:30	17:00
16:45	Coffee Break 16:45-17:00	18:30	Banquet [Westin Hotel] 18:30-20:30	17:00	Poster Session 17:00-18:45
17:00	Poster Preview [1P-1 through 1P-50] 17:00-17:50	18:30		Banquet [Westin Hotel] 18:30-20:30	
17:50	Poster Session 17:50-19:35	18:30	Banquet [Westin Hotel] 18:30-20:30	18:45	Prenary Lecture : 40min.[Presentation]+5min.[Discus.] Special Lecture : 25min.[Presentation]+5min.[Discus.] General Lecture by Candidate for Osawa Award and Iijima Award : 10min.[Presentation]+10min.[Discus.] General Lecture : 10min.[Presentation]+5min.[Discus.]
19:35		20:30			

座長一覽

9月5日(水)

(敬称略)

	時 間	座 長
一般講演	9:30 ~ 10:45	小松 直樹
特別講演(岡崎)	11:00 ~ 11:30	松田 一成
一般講演	11:30 ~ 12:30	阿知波 洋次
一般講演	13:45 ~ 14:30	村田 靖次郎
特別講演(Prassides)	14:30 ~ 15:00	赤阪 健
一般講演	15:15 ~ 16:15	宮本 良之
特別講演(尾辻)	16:15 ~ 16:45	畠山 力三
ポスタープレビュー	17:00 ~ 17:50	小久保 研
ポスターセッション	17:50 ~ 19:35	高野 勇太

9月6日(木)

	時 間	座 長
大澤賞対象者講演 飯島賞対象者講演	9:00 ~ 11:00	北浦 良
基調講演(水谷)	11:15 ~ 12:00	丸山 茂夫
ポスタープレビュー	13:45 ~ 14:25	千足 昇平
ポスターセッション	14:25 ~ 16:10	小林 慶太
フォーラム	16:10 ~ 18:30	田路 和幸

9月7日(金)

	時 間	座 長
一般講演	9:00 ~ 10:15	片浦 弘道
一般講演	10:30 ~ 11:30	前田 優
特別講演(Sankaran)	11:30 ~ 12:00	金子 俊郎
一般講演	13:15 ~ 14:45	岡田 晋
特別講演(吾郷)	14:45 ~ 15:15	野田 優
一般講演	15:30 ~ 16:15	若林 知成
ポスタープレビュー	16:15 ~ 17:00	梅山 有和
ポスターセッション	17:00 ~ 18:45	阿多 誠介

9月5日(水)

特別講演 発表25分 ・ 質疑応答5分
一般講演 発表10分 ・ 質疑応答5分
ポスタープレビュー 発表1分 ・ 質疑応答なし

一般講演 (9:30-10:45)

ナノチューブの生成と精製・ナノチューブの物性

- | | | |
|-----|--|----|
| 1-1 | カイラリティ制御における2元金属触媒の効果
○阿知波 洋次, 兒玉 健, 橋本 健朗, 城丸 春夫, 岡崎 俊也 | 7 |
| 1-2 | X線照射した二層カーボンナノチューブのラマン散乱研究
○村上 俊也, 山本 勇樹, 木曾田 賢治, 伊東 千尋 | 8 |
| 1-3 | 単層カーボンナノチューブへの電気化学的手法によるヨウ素ドーピング
○川崎 晋司, ソン ハヨン, アルズバイディ アヤル, 石井 陽祐, 酒井 武信 | 9 |
| 1-4 | 単層カーボンナノチューブの選択的化学反応
○前田 優, 天谷 優里, 肥後 淳基, 松井 淳, 山田 道夫, 長谷川 正, Lu Jing, 永瀬 茂, 赤阪 健 | 10 |
| 1-5 | 拡散プラズマ反応による窒素置換単層カーボンナノチューブの合成と電気伝導特性
○加藤 俊顕, 村越 幸史, 安久津 誠, 畠山 力三, 金子 俊郎 | 11 |

>>>>> 休憩 (10:45-11:00) <<<<<<

特別講演 (11:00-11:30)

- | | | |
|------|-------------------------------|---|
| 1S-1 | カーボンナノチューブ複合物質の創製と評価
岡崎 俊也 | 1 |
|------|-------------------------------|---|

一般講演 (11:30-12:30)

フラーレンの化学・金属内包フラーレン

- | | | |
|-----|--|----|
| 1-6 | C ₇₀ への求核的環式付加反応: 反応性の振電相互作用密度解析
○春田 直毅, 佐藤 徹, 田中 一義 | 12 |
| 1-7 | Thermodynamic Stability and Exohedral Derivatization of Hepta-Fullerene
○Wang Wei-Wei, Dang Jing-Shuang, Xiang Zhao | 13 |
| 1-8 | リチウムイオン内包フラーレンの電子移動還元反応
○大久保 敬, 川島 雄樹, 福住 俊一 | 14 |
| 1-9 | 塩化チタンによる金属フラーレンの迅速分離
○秋山 和彦, 竹内 絵里奈, 王志永, 千葉 和喜, 中西 勇介, 野田 祥子, 篠原 久典 | 15 |

>>>>> 昼食 (12:30-13:45) <<<<<<

一般講演 (13:45-14:30)

フラーレンの応用

- | | | |
|------|---------------------------------------|----|
| 1-10 | フラーレン添加GaAs薄膜の結晶学的特性
○西永 慈郎, 堀越 佳治 | 16 |
|------|---------------------------------------|----|

9月5日(水)

- 1-11 有機薄膜太陽電池変換効率に対するホスホン酸エステルを有するフラーレン誘導体の側鎖による影響 17
○三浦 匠悟, Jaebuem Oh, Misun Ryu, Haeseong Lee, Jin Jang, 朴 鐘震, 森山 広思
- 1-12 水溶性水酸化フラーレンを用いたCu-CMP研磨スラリーの新世代 18
○小久保 研, 林 照剛, 田名田 祐樹, 田近 英之, 岸田 裕貴, 鹿野 和昌, 村井 亮太
道畑 正岐, 大島 巧, 高谷 裕浩

特別講演 (14:30-15:00)

- 1S-2 Superconductivity proximate to antiferromagnetism in fullerene superconductors 2
Kosmas Prassides

>>>>> 休憩 (15:00-15:15) <<<<<

一般講演 (15:15-16:15)

グラフェンの応用

- 1-13 ポルフィリンが共有結合で修飾された化学変換グラフェンの合成と光物性 19
○梅山 有和, 三原 潤也, 今堀 博
- 1-14 ポリグリセロール修飾による水溶性グラフェンの合成 20
○保田 徳, 趙 利, 劉 剛, 青沼 秀児, 木村 隆英, 小松 直樹
- 1-15 グラフェン FET デバイスを用いたTHz波検出とGHz 帯伝送 21
○マハジューブ アカラム, 阿部 拓斗, 磯 優平, 大内 隆寛, 鈴木 信一, 福田 秀人, 青木 伸之, 宮本 克彦, 尾松 孝茂, バード ジョナサン, フェリー デイビッド, 石橋 幸治, 落合 勇一
- 1-16 Synthesis of carbon nanosheet films from a solid carbon source and their applications to solar cell 22
○Zhipeng Wang, Mao Shoji, Toshiyuki Ito, Hironori Ogata

特別講演 (16:15-16:45)

- 1S-3 グラフェンテラヘルツ波レーザーの創出に向けて 3
尾辻 泰一, 佐藤 昭, リズィー ヴィクトール

>>>>> 休憩 (16:45-17:00) <<<<<

ポスタープレビュー (17:00-17:50)

ポスターセッション (17:50-19:35) (☆)若手奨励賞候補 フラーレン

- 1P-1 C₆₀-C₇₀ 2成分フラーレンナノウイスキーの成長研究 47
○平田 千佳, 下村 周一, 若原 孝次, 宮澤 薫一
- 1P-2 C₆₀フラーレンにおける近赤外フェムト秒パルス誘起振動ダイナミクス:時間依存断熱状態 48
☆ 法によるシミュレーション
○山崎 馨, 中村 堯祉, 新津 直幸, 菅野 学, 河野 裕彦

9月5日(水)

1P-3	光励起によるC ₆₀ フラレーン解離の動力学の理論的研究 ○中村 堯祉, 新津 直幸, 菅野 学, 河野 裕彦, 上田 潔	49
1P-4	C ₂₆ からなる二次元炭素結晶相の構造と電子状態 ☆ ○丸山 実那, 岡田 晋	50
1P-5	C ₆₀ に内包された水分子の電子密度分布 ○青柳 忍, 佐道 祐貴, 北浦 良, 篠原 久典, 西田 智子, 村田 靖次郎	51
1P-6	フラレーン成長機構再考 斎藤 晋	52

フラレーンの化学

1P-7	Fullerene Growth Mechanism and Regioselectivity of Dimeric Carbon Addition ○Dang Jing-Shuang, Wang Wei-Wei, Xiang Zhao	53
1P-8	塩化第二鉄を利用するフラレーン誘導体のレトロ反応 ○橋口 昌彦, 上野 隆生, 松尾 豊	54
1P-9	アザフレロイドのambidentな塩基性に起因する酸触媒芳香族化反応 ○伊熊 直彦, 土井 佑太, 三木江 翼, 中川 晃二, 小久保 研, 大島 巧	55
1P-10	ポリヒドロキシフラレーンの近赤外レーザー誘起振動ダイナミクスと高温状態の反応に関する理論的研究 ○池田 旭伸, Naoyuki Niitsu, Manabu Kanno, Stephan Irle, Hirohiko Kono	56
1P-11	高親水性かつ非界面活性な両親媒性コンカルフラレーンによる固体分散 ☆ ○新田 寛久, 原野 幸治, 中村 栄一	57
1P-12	アルコール-水混合溶媒中における水酸化フラレーンの凝集挙動に対するマジックナンバー効果 ○中村 友治, 上野 裕, 伊熊 直彦, 小久保 研, 大島 巧	58
1P-13	Synthesis and Photophysical Properties of [60]Fullerene-Cobalt Dyads and Triads ☆ ○丸山 優史, Drik M. Guldi, 中村 栄一, 松尾 豊	59
1P-14	アルコキシフラレーンの選択的合成と分子構造: アルコールによるオクタブロモフラレーンの置換反応 ○内山 幸也, 森山 広思, 与座 健治	60

金属内包フラレーン

1P-15	金属内包フラレーン生成における選択性の発現機構 ○阿知波 洋次, 兒玉 健, 橋本 健朗, 城丸 春夫	61
1P-16	医療応用を目指したカルボキシ金属フラレーンの合成に関する研究 ○竹内 絵里奈, 秋山 和彦, 川端 庸平, 久富木 志郎	62
1P-17	カチオン内包アニオンナノ粒子: リチウム内包水酸化フラレーンの合成 ☆ ○上野 裕, 中村 友治, 伊熊 直彦, 小久保 研, 大島 巧	63

9月5日(水)

- 1P-18 The Origin and Mechanism of Non-HPLC Rapid Purification of Metallofullerenes with TiCl_4 64
○王 志永, 中西 勇介, 野田 祥子, 秋山 和彦, 篠原 久典
- 1P-19 Single-crystal X-ray structural analyses of a series of divalent Yb@C_{82} isomers: 65
☆ $\text{Yb@C}_s(6)\text{-C}_{82}$, $\text{Yb@C}_2(5)\text{-C}_{82}$, $\text{Yb@C}_{2v}(9)\text{-C}_{82}$
○鈴木 光明, Xing Lu, Zdenek Slanina, 溝呂木 直美, 永瀬 茂, Marilyn M. Olmstead, Alan L. Balch, 赤阪 健
- 1P-20 プラズマ電位制御によるフラーレンへの窒素内包向上 66
○趙 順天, 畠山 力三, 金子 俊郎
- 1P-21 Application of MCD Spectroscopy and TD-DFT to Endohedral Metallofullerenes. New Insights into Characterization of Their Electron Transitions 67
○山田 道夫, Zdenek Slanina, 溝呂木 直美, 村中 厚哉, 前田 優, 永瀬 茂, 赤阪 健, 小林 長夫
- 1P-22 $[\text{Li@C}_{60}](\text{PF}_6)$ 塩からの Li@C_{60} 単分子層の作製 68
○山田 洋一, 田中 健, 佐々木 正洋, 笠間 泰彦, 河地 和彦, 境 誠司
- 1P-23 リチウム内包フラーレンクラスターのキャラクタリゼーション 69
○權 根相, 小松 健一郎, 奥田 慎一, 河地 和彦, 笠間 泰彦, 遠藤 智明

フラーレンの応用

- 1P-24 水酸化フラーレンの形態制御と固体物性 70
○馬場 啓輔, 伊藤 寿之, 緒方 啓典
- 1P-25 水溶性フラーレンベシクルの疎水性表面上におけるポリマーナノカプセルのテンプレート 71
☆ 合成
○ゴルゴル リカルド ミヅグチ, 原野 幸治, 中村 栄一
- 1P-26 光渦の集光照射によるフラーレン薄膜の光重合 72
☆ ○鳥海 直人, 土井 達也, 粕山 大輝, 穂山 航, 宮本 克彦, 尾松 孝茂, ジョナサン バード, 青木 伸之, 落合 勇一
- 1P-27 水溶性アミノフラーレン誘導体を用いたsiRNAデリバリー 73
○南 皓輔, 岡本 好司, 野入 英世, 原野 幸治, 中村 栄一

ナノチューブの生成と精製

- 1P-28 分子ノギスによる単層カーボンナノチューブの直径分離 74
○小松 直樹, 劉 剛, 木村 隆英
- 1P-29 単層CNTのCVD合成過程の分子動力学: オクトパスとVLSモード 75
○丸山 茂夫, 久間 馨, 野口 拓哉, 川鈴木 智哉, 高木 勇輝, 塩見 淳一郎, 千足 昇平
- 1P-30 触媒微粒子アレイの調整方法による単層CNTフォレストの構造制御 76
○桜井 俊介, 稲熊 正康, フタバドン, 湯村 元雄, 畠 賢治
- 1P-31 らせん型最短ナノチューブのボトムアップ化学合成 77
☆ ○一杉 俊平, 中西 和嘉, 山崎 孝史, 磯部 寛之

9月5日(水)

1P-32	アルコール濃度制御による単層カーボンナノチューブの凝集体の形成と高純度化 ○河合 英輝, 長谷川 凱, 藤原 正澄, 竹内 繁樹, 片浦 弘道, 中津 亨, 柳 和宏	78
1P-33	多孔質ガラスを用いたACCVD法により作製した単層カーボンナノチューブの分散 伊藤 洋介, ○鈴木 信三, 長澤 浩, 小野 晶, 阿知波 洋次	79
1P-34	表面分解法によるカーボンナノチューブ生成のその場NEXAFS測定 ○丸山 隆浩, 石黒 祐樹, 榊原 悟史, 成塚 重弥, 雨宮 健太	80
1P-35	高真空ガスソース法によるZnO(0001)Zn面へのカーボンナノチューブ成長の試み ○河合 起, 成塚 重弥, 丸山 隆浩	81
1P-36	高真空アルコールガスソース法によるPt触媒からの単層カーボンナノチューブの低温成長 ○近藤 弘基, 福岡 直也, Yoshihiro Mizutani, ラナジツト ゴーン, 成塚 重弥, 丸山 隆浩, 飯島 澄男	82
1P-37	SiC表面分解カーボンナノチューブ生成において成長温度が成長速度に与える影響 ○矢嶋 孝敏, 榊原 悟史, 成塚 重弥, 丸山 隆浩	83
1P-38 ★	SDS溶液中におけるカーボンナノチューブとゲルの相互作用の熱力学: 金属型/半導体型分離の理解に向けて ○平野 篤, Takeshi Tanaka, Hiromichi Kataura	84
1P-39 ★	安定的電界誘起層形成法による半導体型単層カーボンナノチューブ高純度分離 ○佐々木 扶紗子, 井原 和紀, 斎藤 毅, 二瓶 史行	85
1P-40	ロゼッタ型冷却容器を用いたプローブ型超音波照射による単層カーボンナノチューブの可溶化 ○倉渕 祐太, Tatsuki Yasumitsu, Gang Liu, Jean-Marc LeVêque, Shinji Aonuma, Laurent Duclaux, Takahide Kimura, Naoki Komatsu	86
1P-41	The simplest separation of single-chirality carbon nanotubes by temperature-controlled gel chromatography ○劉 華平, 卜部 泰子, 田中 丈士, 片浦 弘道	87
1P-42	湿式微粒化装置を用いてカゼイン水溶液に分散したSW-CNTに対するダメージの評価 ○高島 正, 井上 大輔, 前田 寧, 小野 慎	88
1P-43	CVD法における単層カーボンナノチューブ合成の触媒としてのナノダイヤモンドの安定性 ○海野 貴徳, 中村 謙太, 井上 泰輝, 平松 典大, 千足 昇平, 本間 芳和, 丸山 茂夫	89
1P-44	¹³ C炭素源を利用したeDIPS法CNT成長機構に関する解析検討 ○平井 孝佳, 星 和明, 桑原 有紀, 柴田 怜那, 清宮 維春, 仲野 瞬, 斎藤 毅	90
1P-45	水平配向単層カーボンナノチューブの合成: 触媒担持法および水晶表面の影響 ○井ノ上 泰輝, Grace Meikle, Saifullah Badar, 長谷川 大祐, 千足 昇平, 丸山 茂夫	91
1P-46 ★	カイラリティ分布の狭い単層カーボンナノチューブの大量合成に向けたパルスプラズマCVD ○村越 幸史, 加藤 俊顕, 畠山 力三, 金子 俊郎	92

9月5日(水)

1P-47 ガラスビーズろ過法による超長尺SWCNTの分離 93
○片浦 弘道, 都築 真由美, 藤井 俊治郎, 田中 丈士

1P-48 金属ナノ粒子を触媒としたカーボンナノ材料の合成 94
○バラチャンドラン ジャヤデワン, 長田 至弘, 佐藤 義倫, 砂山 裕貴

ナノホーン

1P-49 シンバスタチン担持カーボンナノホーンが骨形成に与える影響 95
○山内 貴紀子, 松村 幸子, 飯塚 正, 芝 清隆, 湯田坂 雅子, 飯島 澄男, 横山 敦郎

ナノ環境と安全評価

1P-50 Biodistribution and biocompatibility of water-soluble carbon nanotubes 96
○Shigeaki Abe, Sachiko Itoh, Toshihisa Kobayashi, Takayuki Kiba, Tsukasa Akasaka,
Yasutaka Yawaka, Shin-Ichiro Sato, Motohito Uo, Fumio Watari, Daisuke Hayashi,
Tomoya Takada

9月6日(木)

基調講演 発表40分 ・ 質疑応答5分
大澤賞飯島賞対象者講演 発表10分 ・ 質疑応答10分
ポスタープレビュー 発表1分 ・ 質疑応答なし

大澤賞対象者講演 (9:00-10:20)

- 2-1 Synthesis of Endohedral Fullerene C₆₀ Encapsulating a Single Molecule of Water 23
○黒飛 敬, 村田 靖次郎
- 2-2 陽イオン内包フラーレン, [Li⁺@C₆₀], の化学 24
○岡田 洋史, 丸山 優史, 小室 貴士, 渡邊 孝仁, 笠間 泰彦, 飛田 博実, 松尾 豊
- 2-3 金属内包フラーレンを鍵分子とした分子内電子授受システムの構築 25
○高野 勇太, Naomi Mizorogi, M. Angeles Herranz, Nazario Martin, Dirk M. Guldi, Shigeru Nagase, Takeshi Akasaka
- 2-4 Room Temperature Observation of Single-Electron Tunneling via Fullerene Quantum Dots in a Si-based Device Structure 26
○早川 竜馬, Chikyow Toyohiro, Yutaka Wakayama

飯島賞対象者講演 (10:20-11:00)

- 2-5 A patternable CNT-Cu composite possessing hundred-times higher electrical current-carrying-capacity than metals 27
○Chandramouli Subramaniam, Takeo Yamada, Don N. Futaba, Motoo Yumura, Kenji Hata
- 2-6 Effect of Mechanical Strain on Polycrystalline Graphene 28
○Mark Bissett, Wataru Izumida, Riichiro Saito, Hiroki Ago

>>>>> 休憩 (11:00-11:15) <<<<<<

基調講演 (11:15-12:00)

- 2S-4 グラフェン電極を有するカーボンナノチューブ電界効果トランジスタ 4
水谷 孝

>>>>> 昼食 (12:00-13:00) <<<<<<

若手奨励賞表彰式 (13:00-13:15)

総会 (13:15-13:45)

ポスタープレビュー (13:45-14:25)

ポスターセッション (14:25-16:10) (☆)若手奨励賞候補

ナノチューブの物性

- 2P-1 ホールドープ単層カーボンナノチューブにおける発光スペクトルの温度依存性 97
○毛利 真一郎, 岩村 宗千代, 秋月 直人, 宮内 雄平, 松田 一成

9月6日(木)

2P-2	CNT分散溶液の凝集状態評価 ○永徳 丈, 丹下 将克, 加藤 晴久, 岡崎 俊也	98
2P-3	単層カーボンナノチューブのRBMへの水蒸気の影響に関する分子動力学計算 ○本間 直樹, 佐藤 慎太郎, 千足 昇平, 本間 芳和, 山本 貴博	99
2P-4	X線光電子分光法を用いたCNT表面官能基の評価 ○二井 裕之, 野口 俊輔, 本行 乾一, 中川 浜三	100
2P-5	有限長の金属単層ナノチューブにおけるディラックコーン傾斜とノギススペクトル ○泉田 渉, 辰巳 由樹, 齋藤 理一郎	101
2P-6 ☆	Theory of electronic Raman scattering in metallic single wall carbon nanotubes ○Eddwi H. Hasdeo, Ahmad R.T. Nugraha, 佐藤 健太郎, 齋藤 理一郎	102
2P-7 ☆	Excitonic effects on coherent phonons in single wall carbon nanotubes ○ヌグラハ アフマドリドワントレスナ, サンダース ゲイリー, クリストファー スタントン, 齋藤 理一郎	103
2P-8	Thermoelectric Power of Metallic and Semiconducting Single-Wall Carbon Nanotube Buckypaper ○本田 和也, Yusuke Nakai, Kazuhiro Yanagi, Yutaka Maniwa	104
2P-9 ☆	電界下における水素終端カーボンナノチューブの静電ポテンシャル ○山中 綾香, 岡田 晋	105
2P-10 ☆	Analysis of Operation Mechanisms of SWNT Network Field-Effect Transistors Studied via Scanning Gate Microscopy ○Masahiro Matsunaga, Xiaojun Wei, Kenji Maeda, Taturou Yahagi, Kazuaki Tanaka, Jonathan P. Bird, Koji Ishibashi, Yuichi Ochiai, Nobuyuki Aoki	106
2P-11 ☆	キャリアドープした単層カーボンナノチューブの発光励起分光 ○秋月 直人, 岩村 宗千代, 毛利 真一郎, 宮内 雄平, 松田 一成	107
2P-12 ☆	Coherent AC Transport in Metallic Carbon Nanotubes with Disorder ○平井 大介, 山本 貴博, 渡邊 聡	108
2P-13	Electronic States in Flattened Carbon Nanotubes with Effective-Mass Approximation ○中西 毅, 安藤 恒也	109
2P-14	超微小径単層カーボンナノチューブの光学特性 ○中村 俊也, 宮田 耕充, 犬飼 恵理, 北浦 良, 片浦 弘道, 篠原 久典	110
2P-15	Non-linear and Non-planar Free Thermal Vibration of Single-walled Carbon Nanotubes in Molecular Dynamic Simulation ○Heeyuen Koh, James Cannon, Shohei Chiashi, Junichiro Shiomi, Shigeo Maruyama	111
2P-16	CNT-SiC界面における電流挙動 ○稲葉 優文, 渋谷 恵, 大原 一慶, 落合 拓海, 増田 佳穂, 平岩 篤, 楠 美智子, 川原 田 洋	112

9月6日(木)

- 2P-17 Raman Imaging Spectroscopy of Horizontally Aligned Single-Walled Carbon Nanotubes on Crystal Quartz 113
○Saifullah Badar, Daisuke Hasegawa, Taiki Inoue, Shohei Chiashi, Shigeo Maruyama
- 2P-18 孤立架橋した二層カーボンナノチューブの作製と評価 114
○北河 友也, 北浦 良, 宮内 雄平, 宮田 耕充, 松田 一成, 篠原 久典
- 2P-19 多層カーボンナノチューブフォレストの結晶構造解析 115
○古田 寛, 八田 章光

ナノチューブの応用

- 2P-20 単層カーボンナノチューブ—シリコンヘテロ接合太陽電池の光電変換特性 116
○小澤 大知, 平岡 和志, 宮内 雄平, 毛利 真一郎, 松田 一成
- 2P-21 Micro-fabrication of stretchable and robust interconnects of conductive CNT rubber on a stretchable substrate 117
○Atsuko Sekiguchi, Tekao Yamada, Kazufumi Kobashi, Motoo Yumura, Kenji Hata
- 2P-22 複合材の導電性を向上させる単層カーボンナノチューブの分散構造 118
○尹 好苑, 山下 基, 阿多 誠介, 湯村 守雄, 畠 賢治
- 2P-23 スーパーグロス単層CNT導電性ゴムの大量生産を目指した押し出し成形の開発 119
○阿多 誠介, 水野 貴瑛, 尹 好苑, 湯村 守雄, 畠 賢治
- 2P-24 単一(6,5)カイラリティ単層カーボンナノチューブ厚膜におけるイオンゲルトランジスタ 120
○工藤 光, 野房 勇希, 片浦 弘道, 竹延 大志, 柳 和宏
- 2P-25 反応射出成型法を用いたポリマー／カーボンナノチューブ樹脂複合体の合成と電気特性評価 121
○ホアン テ バン, 重田 真宏, 上島 貢
- 2P-26 ビオチン修飾二層カーボンカーボンナノチューブを用いた特異的バイオセンサーの作製 122
○長屋 祐香, 久野 晃弘, 土屋 好司, 矢島 博文
- 2P-27 酸化二層カーボンナノチューブへのマンノースの修飾とバイオセンサーへの応用 123
○武居 修平, 久野 晃弘, 土屋 好司, 矢島 博文
- 2P-28 Dip法による高密度で均一なカーボンナノチューブ薄膜形成 124
☆ ○清水 麻希, 藤井 俊治郎, 田中 丈士, 片浦 弘道
- 2P-29 Conduction-Type Control of Carbon Nanotube Field-Effect Transistors by Pd and Ti Overlayer Doping 125
○Satoshi Ishii, Masato Tamaoki, Shigeru Kishimoto, Takashi Mizutani
- 2P-30 Switchable thermal conductivity enhancement of phase change composites with single walled carbon nanotube inclusions 126
☆ ○Sivasankaran Harish, Kei Ishikawa, Taiki Inoue, Shohei Chiashi, Junichiro Shiomi, Shigeo Maruyama

9月6日(木)

2P-31 ☆	その場電子顕微鏡法によるカーボンナノチューブ/金ナノ粒子接合の作製と電気伝導測定 ○荻田 基志, 安坂 幸師, 中原 仁, 齋藤 弥八	127
2P-32	気液界面プラズマを用いた間隔制御ナノ粒子複合カーボンナノチューブの合成 ○金子 俊郎, 陳 強, 畠山 力三	128
2P-33	Electrochemical durability of single-wall carbon nanotube electrode against anodic oxidation in water ○大森 滋和, 齋藤 毅	129
2P-34	ポリスチレン粒子を用いたパターンニングしたカーボンナノチューブ薄膜 ○葉原 有紀, 平井 孝佳, 齋藤 毅	130
2P-35 ☆	セシウム内包単層カーボンナノチューブによる安定なpn接合形成 ○安彦 嘉浩, 加藤 俊顕, 畠山 力三, 金子 俊郎	131
2P-36	スーパーキャパシタに向けたナノチューブベース・カーボン自立膜の開発 ○キンテーロ レストレポリカルド, 金 東榮, 長谷川 馨, 山田 裕貴, 山田 淳夫, 野田 優	132
2P-37	カーボンナノチューブと抗体の反応制御 ○飯泉 陽子, 岡崎 俊也, 池原 譲, 小倉 睦郎, 湯田坂 雅子	133
2P-38	フラーレン dendrimer による半導体単層カーボンナノチューブの選択的抽出 ○鈴木 浩紀, 岡崎 俊也, 飯泉 陽子, 丹下 将克, 和田 卓聡, 田島 智之, 高口 豊, 飯島 澄男	134
2P-39	化学ドーピング半導体単層カーボンナノチューブ/Siヘテロ接合ダイオードの作製と特性 ○庄司 真雄, 中野 陸, 緒方 啓典	135
2P-40	長期間による胸部軟組織のマクロフェージ内での化学修飾多層カーボンナノチューブの構造変形 ○佐藤 義倫, 横山 敦郎, 中澤 英子, Minfang Zhang, 湯田坂 雅子, 本宮 憲一, 田路 和幸	136
2P-41	交流電場と流動場の組み合わせによる配向CNTナノ薄膜の構築 ○松井 淳, 改田 茂, 宮下 徳治	137

フォーラム (16:10-18:30)
安全安心社会とナノ科学技術
(含: 東日本大震災現地調査)

9月7日(金)

特別講演 発表25分 ・ 質疑応答5分
一般講演 発表10分 ・ 質疑応答5分
ポスタープレビュー 発表1分 ・ 質疑応答なし

一般講演 (9:00-10:15)

ナノチューブの生成と精製・ナノチューブの応用・内包ナノチューブ

- | | | |
|-----|---|----|
| 3-1 | 蒸気拡散法によって作製した単層カーボンナノチューブ凝集体の性質
○柳 和宏, Hideki Kawai, Hikaru Kudo, Kai Hasegawa, Hiromichi Kataura, Ryo Nakatzu | 29 |
| 3-2 | カーボンナノチューブの欠陥性がゴム複合材料の劣化抑制及び電気伝導性に与える影響
○長岡 朋弥, 土屋 好司, 高橋 芳行, 矢島 博文 | 30 |
| 3-3 | カーボンナノチューブ-アルミナ複合材料の製造と応用
○大森 守, 山本 剛, 白須 圭一, 橋田 俊之 | 31 |
| 3-4 | 単層カーボンナノチューブを陽極として用いたフレキシブル有機薄膜太陽電池の作製
○藤井 俊治郎, 田中 丈士, 西山 聡子, 片浦 弘道 | 32 |
| 3-5 | 単層カーボンナノチューブを用いた細い単層窒化ホウ素ナノチューブの合成
○中西 亮, 北浦 良, 山本 悠太, 荒井 重勇, Jamie H Warner, 宮田 耕充, 篠原 久典 | 33 |

>>>>> 休憩 (10:15-10:30) <<<<<

一般講演 (10:30-11:30)

ナノチューブの物性

- | | | |
|-----|--|----|
| 3-6 | 細いカーボンナノチューブの光学応答
○是常 隆, 斎藤 晋 | 34 |
| 3-7 | 酸素ドーピングカーボンナノチューブの発光測定
○岩村 宗千代, 宮内 雄平, 毛利 真一郎, 川添 忠, 大津 元一, 松田 一成 | 35 |
| 3-8 | 単層カーボンナノチューブの多重励起子生成による光電流
○小鍋 哲, 岡田 晋 | 36 |
| 3-9 | Diameter reduction of SWNTs by nitrogen incorporation and encapsulation of a one-dimensional nitrogen gas
○Theerapol Thurakitserree, Christian Kramberger, Heeyuen Koh, Yudai Izumi, Toyohiko Kinoshita, Takayuki Muro, Shohei Chiashi, Erik Einarsson, Shigeo Maruyama | 37 |

特別講演 (11:30-12:00)

- | | | |
|------|--|---|
| 3S-5 | Plasma processing of carbon-based nanomaterials
R. Mohan Sankaran | 5 |
|------|--|---|

>>>>> 昼食 (12:00-13:15) <<<<<

9月7日(金)

一般講演 (13:15-14:45)

グラフェンの物性

- 3-10 ジグザグBC₂Nナノリボンにおけるエッジ状態に関する数値的研究 38
○針谷 喜久雄, 金子 智昭
- 3-11 積層構造がねじれた2層グラフェンにおけるGバンド強度と結合状態密度 39
○佐藤 健太郎, 齋藤 理一郎, Chunxiao Cong, Ting Yu, Mildred S. Dresselhaus
- 3-12 酸化グラフェンナノシートの光照射によるナノ空孔の形成とイオン伝導性の発現 40
○鯉沼 陸央, 緒方 盟子, 亀井 雄樹, 畠山 一翔, 立石 光, 枳原 健吾, 谷口 貴章, 松本 泰道
- 3-13 単層エピタキシャルグラフェンの近赤外光領域における発光ダイナミクス 41
○小山 剛史, 伊藤 由人, 吉田 和真, 吾郷 浩樹, 岸田 英夫, 中村 新男
- 3-14 Bilayer graphene sandwiched by ionic molecules: Band-gap and carrier type engineering 42
○Thanh Cuong Nguyen, Minoru Otani, Susumu Okada
- 3-15 水分子によるグラフェンの光化学的表面修飾 43
○野内 亮, 三苫 伸彦, 谷垣 勝己

特別講演 (14:45-15:15)

- 3S-6 グラフェンのエピタキシャルCVD成長 6
吾郷 浩樹

>>>>> 休憩 (15:15-15:30) <<<<<<

一般講演 (15:30-16:15)

ナノホーン・ナノ炭素粒子

- 3-16 窒素雰囲気下で生成したカーボンナノホーン集合体の構造と電子物性 44
○弓削 亮太, 眞子 隆志, 湯田坂 雅子, 當山 清彦, 山口 貴司, 飯島 澄男, 中野 嘉一郎
- 3-17 経口投与したカーボンナノホーンの消化管内における挙動 45
○中村 真紀, 田原 善夫, 村上 達也, 飯島 澄男, 湯田坂 雅子
- 3-18 AcBとCNBの混合による電気二重層キャパシタのエネルギー密度向上 46
○岡部 雄太, H.Izumi, 須田 善行, 滝川 浩史, 田上 英人, 植 仁志, 清水 一樹

ポスタープレビュー (16:15-17:00)

ポスターセッション (17:00-18:45) (☆)若手奨励賞候補

内包ナノチューブ

- 3P-1 単一カイラリティ(11,10)単層カーボンナノチューブへのC₆₀分子の内包 138
○河合 将利, 五十嵐 透, 客野 遥, 岡崎 俊也, 真庭 豊, 柳 和宏
- 3P-2 ペリレン/カーボンナノチューブ複合系の光学特性 139
○恒川 拓也, 小山 剛史, 安坂 幸師, 齋藤 弥八, 岸田 英夫, 中村 新男

9月7日(金)

- 3P-3 電子線照射下に於ける¹²CNTおよび¹³CNTに内包された臭化銀の寿命の差異 140
○小林 慶太, 斎藤 毅, 清宮 維春, 保田 英洋
- 3P-4 カーボンナノチューブ内における構造均一的な導電性ポリマーの創製と物性 141
☆ ○宮浦 健志, 宮田 耕充, 北浦 良, 篠原 久典
- 3P-5 TTFおよびF₄TCNQ内包による単層カーボンナノチューブへのキャリアドーピング 142
○伊藤 靖浩, 藤井 俊治郎, 清水 麻希, 田中 丈士, 片浦 弘道

グラフェン生成

- 3P-6 Microwave-assisted exfoliation of graphite in organic solvents without using strong oxidants 143
○沖本 治哉, Ryota Tada, Masahito Sano
- 3P-7 アルコールCVD法により直接合成したパターン化グラフェンのラマン評価 144
○鬼頭 佑典, Hiroya Yamauchi, Tomoya Kamizyukoku, Manabu Suzuki, 丸山 隆浩, 成塚 重弥
- 3P-8 Cu上の六角形グラフェンのドメイン境界の評価 145
○小川 友以, 河原 憲治, 宮下 雅大, 辻 正治, 吾郷 浩樹
- 3P-9 CVD Growth of Mono- and Bi-Layer Graphene from Ethanol 146
☆ ○Xiao Chen, Pei Zhao, Bo Hou, Shohei Chiashi, Shigeo Maruyama
- 3P-10 ヘキサゴナルドメイングラフェンのシリコン基板上への直接合成 147
○加藤 俊頭, 島山 力三, 金子 俊郎

グラフェンの物性

- 3P-11 BN単層シート中の炭素不純物に関する第一原理電子状態計算 148
○藤本 義隆, 是常 隆, 斎藤 晋
- 3P-12 電界下における二層グラフェンの電子状態 149
○小鍋 哲, 岡田 晋
- 3P-13 X線照射グラフェンのラマン散乱研究 150
○村上 俊也, 山崎 一樹, 鴨井 督, 蓮池 紀幸, 播磨 弘, 木曾田 賢治, 伊東 千尋
- 3P-14 グラフェンナリボンの熱起電力へのエッジ効果: 第一原理計算 151
○加藤 哲平, 白井 信志, 山本 貴博
- 3P-15 グラフェンナリボンの電気伝導特性に関する波束ダイナミクスシミュレーション 152
高田 幸宏, ○高島 健悟, 山本 貴博
- 3P-16 準周期的超格子にあるグラフェンにおける複数のディラックコーン 153
☆ ○田島 昌征, 羽田野 直道
- 3P-17 超音波ミストCVDにより銅箔上に作製した窒素ドーピンググラフェンの表面抵抗率 154
○水野 貴裕, 滝沢 守雄, 坂東 俊治

9月7日(金)

- 3P-18 自立グラフェンのヘリウムイオン顕微鏡によるイメージのシミュレーション 155
宮本 良之
- 3P-19 グラフェン/六方晶窒化ホウ素薄膜における格子整合とバンドギャップ 156
☆ ○酒井 佑規, 斎藤 晋
- 3P-20 グラフェン量子ドットの合成とその光学物性 157
☆ ○冬野 直人, 小澤 大知, 宮内 雄平, 毛利 真一郎, 松田 一成
- 3P-21 ハロゲン終端されたアームチェア型グラフェンナノリボンの構造及び電子状態に関する 158
☆ 第一原理計算
○實宝 秀幸, 大淵 真理
- 3P-22 Novel spintronic phenomena arising from pore-edge polarized spins of ferromagnetic 159
graphene nanomeshes
○Naoki Kosugi, Yasuki Hashimoto, Kenshi Sakuramoto, Keigo Takeuchi, Shota Kamikawa, Yuko Yagi, Junji Haruyama, Yoshiaki Hashimoto, Kazuhiro Fujita, Yuto Kato, Shingo Katsumoto, Yasuhiro Iye, Pei Zhao, Shigeo Maruyama, Apparao Rao
- 3P-23 Magnetic behaviors sensitive to foreign-atom termination of pore-edge in graphene 160
nanomeshes
○Keigo Takeuchi, Kenshi Sakuramoto, Naoki Kosugi, Yasuki Hashimoto, Yuko Yagi, Junji Haruyama, Pei Zhao, Shigeo Maruyama, Apparao Rao

グラフェンの応用

- 3P-24 トポロジカル欠陥のある六方晶系窒化ホウ素の電子構造 161
○富田 陽子, 岡田 晋
- 3P-25 電子線レジストによるCVDグラフェンへのホールドーピング 162
○小川 友以, 辻 正治, 吾郷 浩樹
- 3P-26 その場TEM観察に向けた架橋グラフェンナノリボンデバイスの作製 163
☆ ○鈴木 祥司, 北浦 良, 佐々木 祐生, 加門 慶一, 宮田 耕充, 篠原 久典
- 3P-27 グラフェン電極CNT-FETにおけるグラフェン層厚さのI-V特性への影響 164
○玉置 聖人, 岸本 茂, 水谷 孝
- 3P-28 酸化グラフェン還元物へのナノカーボン複合化 165
○Ellya Indahyanti, 横井 裕之, 畠山 一翔, 松本 泰道
- 3P-29 ゲート電界導入によるグラフェンDual-Doubleゲートトランジスタの第一原理シミュレー 166
ション
大淵 真理

ナノホーン

- 3P-30 Apoptotic Mechanism of RAW264.7 Induced by Carbon Nanohorns 167
○Mei Yang, Minfang Zhang, Yoshio Tahara, Sumio Iijima, Masako Yudasaka

9月7日(金)

- 3P-31 ガス導入水中アーク法による金属ナノ粒子分散カーボンナノホーンの合成 168
○佐野 紀彰, タットポーン ストーンロハナクン, チャンタマニー プーンジャランシン,
平間 大介, 谷口 幸助, 乗本 達彦, 石井 大河, 田門 肇, タワチャイ チャリンパニットク
ン

ナノワイヤー

- 3P-32 ポリイン及びシアノポリインの禁制遷移における振電相互作用 169
○若林 知成, 和田 資子, 富岡 万貴子

ナノ炭素粒子

- 3P-33 PtRu担持カーボンナノ材料のメタノール酸化反応特性 170
○尾崎 公洋, 須田 善行, 滝川 浩史, 田上 英人, 植 仁志, 清水 一樹
- 3P-34 無極性溶媒中におけるポリイン-ヨウ素錯体の赤外吸収スペクトル 171
○和田 資子, 森澤 勇介, 若林 知成
- 3P-35 カarbonナノチューブ上シリコンナノ粒子のジュール加熱によるカーボンナノカプセル 172
☆ の形成
○寺田 朋広, 安坂 幸師, 中原 仁, 齋藤 弥八
- 3P-36 直流アーク放電陰極堆積物中におけるランタン内包カーボンナノカプセルの分布 173
○山本 和典, 社本 真一, 赤阪 健

その他

- 3P-37 分散時間に対するカーボンナノコイルの長さ依存性 174
☆ ○丸山 皓司, 須田 善行, 田上 英人, 滝川 浩史, Hitoshi Ue, Kazuki Shimizu, Yoshito
Umeda
- 3P-38 酸化鉄ナノチューブへのフラーレンドーピング 175
○白木 勇喜, 三品 雄基, 坂東 俊治
- 3P-39 ゼオライト鑄型炭素に内包された水の過冷却およびガラス状態 176
○客野 遥, 松田 和之, 中井 祐介, 福岡 智子, 真庭 豊, 西原 洋知, 京谷 隆
- 3P-40 核磁気共鳴法によるゼオライト鑄型炭素(ZTC)の研究 177
○山田 健介, Yusuke Nakai, Kazuyuki Matsuda, Yutaka Maniwa, Hiroto Nishihara,
Takashi Kyotani
- 3P-41 SEM内におけるカーボンナノコイルの電気的特性の測定 178
○國本 隆司, 米村 泰一郎, 須田 善行, 田上 英人, 滝川 浩史, 植 仁志, 清水 一樹,
梅田 良人
- 3P-42 CNTを触媒担体とする燃料電池の開発 179
○藤ヶ谷剛彦, モハメド・レダ・バーバー, 中嶋直敏

September 5, Wed.

Special Lecture: 25min (Presentation) + 5min (Discussion)
General Lecture: 10min (Presentation) + 5min (Discussion)
Poster Preview: 1min (Presentation)

General Lecture (9:30-10:45)

Formation and Purification of Nanotubes · Properties of Nanotubes

- | | | |
|-----|--|----|
| 1-1 | Binary alloy effect on the chirality selection of carbon nanotubes
○Yohji Achiba, Takeshi Kodama, Kenro Hashimoto, Haruo Shiromaru, Toshiya Okazaki | 7 |
| 1-2 | Raman study on defects induced double walled carbon nanotube by X-ray irradiation
○Toshiya Murakami, Yuki Yamamoto, Kenji Kisoda, Chihiro Itoh | 8 |
| 1-3 | Electrochemical Iodine Doping of SWCNTs
○Shinji Kawasaki, Song Ha Yong, Ayar Al-zubaidi, Yosuke Ishii, Takenobu Sakai | 9 |
| 1-4 | Selective Functionalization of Single-Walled Carbon Nanotubes
○Yutaka Maeda, Yuri Amagai, Junki Higo, Jun Matsui, Michio Yamada, Tadashi Hasegawa, Jing Lu, Shigeru Nagase, Takeshi Akasaka | 10 |
| 1-5 | Fabrication of nitrogen substituted single-walled carbon nanotubes by diffusion plasma reaction and their electrical transport properties
○Toshiaki Kato, Koshi Murakoshi, Makoto Akutsu, Rikizo Hatakeyama, Toshiro Kaneko | 11 |

>>>>> **Coffee Break (10:45-11:00)** <<<<<

Special Lecture (11:00-11:30)

- | | | |
|------|---|---|
| 1S-1 | Synthesis and characterization of carbon-nanotube-based hybrid materials
Toshiya Okazaki | 1 |
|------|---|---|

General Lecture (11:30-12:30)

Chemistry of Fullerenes · Endohedral Metallofullerenes

- | | | |
|-----|---|----|
| 1-6 | Nucleophilic cycloadditions to C ₇₀ : Vibronic coupling density analysis for its reactivity
○Naoki Haruta, Tohru Sato, Kazuyoshi Tanaka | 12 |
| 1-7 | Thermodynamic Stability and Exohedral Derivatization of Hepta-Fullerene
○Wei-Wei Wang, Jing-Shuang Dang, Xiang Zhao | 13 |
| 1-8 | Electron-Transfer Reduction of Li Ion Encapsulated Fullerene
○Kei Ohkubo, Yuki kawashima, Shunichi Fukuzumi | 14 |
| 1-9 | Rapid Separation of Metallofullerenes by Titanium Chloride
○Kazuhiko Akiyama, Erina Takeuchi, Zhiyong Wang, Kazuki Chiba, Yusuke Nakanishi, Shoko Noda, Hisanori Shinohara | 15 |

>>>>> **Lunch Time (12:30-13:45)** <<<<<

September 5, Wed.

General Lecture (13:45-14:30)

Applications of Fullerenes

- | | | |
|------|--|----|
| 1-10 | Crystalline characteristics of fullerene doped GaAs layers grown by MBE
○ <i>Jiro Nishinaga, Yoshiji Horikoshi</i> | 16 |
| 1-11 | Structural effect of fullerene derivatives with phosphonic ester in organic photovoltaic devices
○ <i>Shogo Miura, Jaebuem Oh, Misun Ryu, Haeseong Lee, Jin Jang, Chyongjin Pac, Hiroshi Moriyama</i> | 17 |
| 1-12 | A New Generation of Cu-CMP Slurry using Water-Soluble Fullerenol
○ <i>Ken Kokubo, Terutake Hayashi, Hiroki Tanada, Hideyuki Tachika, Hirotaka Kishida, Kazumasa Kano, Ryota Murai, Masaki Michihata, Takumi Oshima, Yasuhiro Takaya</i> | 18 |

Special Lecture (14:30-15:00)

- | | | |
|------|---|---|
| 1S-2 | Superconductivity proximate to antiferromagnetism in fullerene superconductors
<i>Kosmas Prassides</i> | 2 |
|------|---|---|

>>>>> Coffee Break (15:00-15:15) <<<<<<

General Lecture (15:15-16:15)

Applications of Graphene

- | | | |
|------|--|----|
| 1-13 | Preparation and photophysical properties of chemically converted graphene covalently functionalized with porphyrins
○ <i>Tomokazu Umeyama, Junya Mihara, Hiroshi Imahori</i> | 19 |
| 1-14 | Water-soluble graphene through polyglycerol grafting
○ <i>Toku Yasuda, Li Zhao, Liu Gang, Shuji Aonuma, Takahide Kimura, Naoki Komatsu</i> | 20 |
| 1-15 | Utilizing graphene FET device for GHz transport and THz detection
○ <i>Akram Mahjoub, T. Abe, Y. Iso, T. Ouchi, S. Suzuki, H. Fukuda, N. Aoki, K. Miyamoto, T. Omatsu, J. P. Bird, D. K. Ferry, K. Ishibashi, Y. Ochiai</i> | 21 |
| 1-16 | Synthesis of carbon nanosheet films from a solid carbon source and their applications to solar cell
○ <i>Zhipeng Wang, Mao Shoji, Toshiyuki Ito, Hironori Ogata</i> | 22 |

Special Lecture (16:15-16:45)

- | | | |
|------|---|---|
| 1S-3 | Toward the Creation of Graphene Terahertz Lasers
<i>Taiichi Otsuji, Akira Satou, Victor Ryzhii</i> | 3 |
|------|---|---|

>>>>> Coffee Break (16:45-17:00) <<<<<<

Poster Preview (17:00-17:50)

Poster Session (17:50-19:35) (★)Candidates for the Young Scientist Poster Award

Fullerenes

- 1P-1 Growth investigation of C₆₀-C₇₀ two-component fullerene nanowhiskers 47
 ○Chika Hirata, Shuichi Shimomura, Takatsugu Wakahara, Kun'ichi Miyazawa
- 1P-2 Simulation of Near-Infrared Excitation of Raman Active Modes in Fullerene C₆₀ by a 48
 ☆ Time-Dependent Adiabatic State Approach
 ○Kaoru Yamazaki, Takashi Nakamura, Naoyuki Niitsu, Manabu Kanno, Hirohiko Kono
- 1P-3 Theroretical investigation of the fragmentation dynamics of photoexcited C₆₀ fullerene 49
 ○Takashi Nakamura, Naoyuki Niitsu, Manabu Kanno, Hirohiko Kono, Kiyoshi Ueda
- 1P-4 Geometric and electronic structures of two-dimensional networks of fused C₂₆ fullerenes 50
 ☆ ○Mina Maruyama, Susumu Okada
- 1P-5 Charge density distribution of water molecule encapsulated in fullerene C₆₀ 51
 ○Shinobu Aoyagi, Yuki Sado, Ryo Kitaura, Hisanori Shinohara, Tomoko Nishida, Yasujiro Murata
- 1P-6 Growth Mechanism of Fullerenes Revisited 52
 ○Susumu Saito

Chemistry of Fullerenes

- 1P-7 Fullerene Growth Mechanism and Regioselectivity of Dimeric Carbon Addition 53
 ○Jing-Shuang Dang, Wei-Wei Wang, Xiang Zhao
- 1P-8 FeCl₃-mediated retro-reaction of fullerene derivatives 54
 ○Masahiko Hashiguchi, Takao Ueno, Yutaka Matsuo
- 1P-9 Dual reactivity of azafulleroid due to its ambident n / π -basicity 55
 ○Naohiko Ikuma, Yuta Doi, Tsubasa Mikie, Koji Nakagawa, Ken Kokubo, Takumi Oshima
- 1P-10 Theoretical investigation on vibrational excitation and reaction dynamics of polyhydroxy 56
 fullerene induced by a near-infrared laser
 ○Akinobu Ikeda, Naoyuki Niitsu, Manabu Kanno, Stephan Irle, Hirohiko Kono
- 1P-11 Highly Hydrophilic Non-Surface-Active Conical Fullerene Amphiphiles for Dispersion 57
 ☆ of Solid Materials
 ○Hirohisa Nitta, Koji Harano, Eiichi Nakamura
- 1P-12 Magic number effects on aggregation of polyhydroxylated fullerenes in alcohol-water 58
 binary solvent
 ○Yuji Nakamura, Hiroshi Ueno, Naohiko Ikuma, Ken Kokubo, Takumi Oshima
- 1P-13 Synthesis and Photophysical Properties of [60]Fullerene-Cobalt Dyads and Triads 59
 ☆ ○Masashi Maruyama, Dirk M. Guldi, Eiichi Nakamura, Yutaka Matsuo
- 1P-14 Selective synthesis and molecular structure of alkoxyfullerenes: substitution reaction of 60
 octabromofullerene with alcohol
 ○Kouya Uchiyama, Hiroshi Moriyama, Kenji Yoza

September 5, Wed.

Endohedral Metallofullerenes

- 1P-15 What causes the selectivity of the metallofullerene formation? 61
○Yohji Achiba, Takeshi Kodama, Kenro Hashimoto, Haruo Shiromaru
- 1P-16 Synthesis of Carboxy Metallofullerenes for Medical Application 62
○Erina Takeuchi, Kazuhiko Akiyama, Youhei Kawabata, Shiro Kubuki
- 1P-17 Synthesis of Lithium-Encapsulated Fullerenol as “Cation-Encapsulated Anion Nanoparticle” 63
★ ○Hiroshi Ueno, Yuji Nakamura, Naohiko Ikuma, Ken Kokubo, Takumi Oshima
- 1P-18 The Origin and Mechanism of Non-HPLC Rapid Purification of Metallofullerenes with TiCl_4 64
○Zhiyong Wang, Yusuke Nakanishi, Shoko Noda, Kazuhiko Akiyama, Hisanori Shinohara
- 1P-19 Single-crystal X-ray structural analyses of a series of divalent Yb@C_{82} isomers: 65
★ $\text{Yb@C}_s(6)\text{-C}_{82}$, $\text{Yb@C}_{2(5)}\text{-C}_{82}$, $\text{Yb@C}_{2v(9)}\text{-C}_{82}$
○Mitsuaki Suzuki, Xing Lu, Zdenek Slanina, Naomi Mizorogi, Shigeru Nagase, Marilyn M. Olmstead, Alan L. Balch, Takeshi Akasaka
- 1P-20 Enhancement of nitrogen encapsulation into fullerene under control of plasma potential 66
○Soon. C. Cho, Rikizo Hatakeyama, Toshiro Kaneko
- 1P-21 Application of MCD Spectroscopy and TD-DFT to Endohedral Metallofullerenes. New Insights into Characterization of Their Electron Transitions 67
○Michio Yamada, Zdenek Slanina, Naomi Mizorogi, Atsuya Muranaka, Yutaka Maeda, Shigeru Nagase, Takeshi Akasaka, Nagao Kobayashi
- 1P-22 Fabrication of Li@C_{60} Monolayer from $[\text{Li@C}_{60}](\text{PF}_6)$ Salt 68
○Yoichi Yamada, Ken Tanaka, Masahiro Sasaki, Yasuhiko Kasama, Kazuhiko Kawachi, Seiji Sakai
- 1P-23 Characterization of Endohedral Lithium Metallofullerene Clusters 69
○Eunsang Kwon, Ken-ichirou Komatsu, Shin-ichi Okuda, Kazuhiko Kawachi, Yasuhiko Kasama, Tomoaki Endo

Applications of Fullerenes

- 1P-24 Fabrication and Solid State Properties of Fullerenol Nanostructures 70
○Keisuke Baba, Toshiyuki Ito, Hironori Ogata
- 1P-25 Templated Synthesis of Polymer Nanocapsules on Water-Soluble Fullerene Vesicles 71
★ ○Ricardo Mizoguchi Gorgoll, Koji Harano, Eiichi Nakamura
- 1P-26 Photo Polymerization of C_{60} Thin Film Using Focused Optical Vortex 72
★ ○Naoto Toriumi, Tatsuya Doi, Daiki Momiyama, Wataru Akiyama, Katsuhiko Miyamoto, Takashige Omatsu, Jonathan P. Bird, Nobuyuki Aoki, Yuichi Ochiai
- 1P-27 siRNA Delivery System Using Water-Soluble Amino-Fullerene Derivative 73
○Kosuke Minami, Koji Okamoto, Eisei Noiri, Koji Harano, Eiichi Nakamura

Formation and Purification of Nanotubes

1P-28	From nanotweezers to nanocalipers : Selective extraction of SWNTs with larger diameters ○Naoki Komatsu, Gang Liu, Takahide Kimura	74
1P-29	A molecular dynamics simulation of SWNT growth by CVD method : Octopus and VLS modes ○Shigeo Maruyama, Kaoru Hisama, Takuya Noguchi, Tomoya Kawasuzuki, Yuki Takaki, Junichiro Shiomi, Shohei Chiashi	75
1P-30	Catalyst Particle Array Formation Process Adjusted for Growth of Single-Walled Carbon Nanotube Forest with Different Structures ○Shunsuke Sakurai, Masayasu Inaguma, Don N. Futaba, Motoo Yumura, Kenji Hata	76
1P-31	Bottom-up synthesis of finite models of helical (n,m)-single-wall carbon nanotubes ☆ ○Shunpei Hitosugi, Waka Nakanishi, Takashi Yamasaki, Hiroyuki Isobe	77
1P-32	Purification of Single Wall Carbon Nanotubes by Formation of Aggregates Caused by Control of Alcohol Concentration ○Hideki Kawai, Kai Hasegawa, Masazumi Huziwaru, Shigeki Takeuchi, Hiromichi Kataura, Ryo Nakatsu, Kazuhiro Yanagi	78
1P-33	Dispersion of single-walled carbon nanotubes made by using ACCVD technique with porous glass Yosuke Ito, ○Shinzo Suzuki, Hiroshi Nagasawa, Akira Ono, Yohji Achiba	79
1P-34	In situ NEXAFS Study on Carbon Nanotube Growth Process by Surface Decomposition of SiC ○Takahiro Maruyama, Yuki Ishiguro, Satoshi Sakakibara, Shigeya Naritsuka, Kenta Amemiya	80
1P-35	Carbon Nanotube Growth on ZnO(0001) Zn-face using Gas Source Method in High Vacuum ○Takeshi Kawai, Shigeya Naritsuka, Takahito Maruyama	81
1P-36	Low Temperature Growth of SWNTs on Pt catalyst by Alcohol Gas Source Method in High Vacuum ○Hiroki Kondo, Naoya Fukuoka, Yoshihiro Mizutani, Ghosh Ranajit, Shigeya Naritsuka, Takahiro Maruyama, Sumio Iijima	82
1P-37	Effect of Growth Temperature on Growth Rate in Carbon Nanotube Formation by Surface Decomposition of SiC ○Takatoshi Yajima, Satoshi Sakakibara, Shigeya Naritsuka, Takahiro Maruyama	83
1P-38	Thermodynamics of the interaction of carbon nanotubes with hydrogels in SDS solutions: ☆ Toward understanding metal-semiconductor separation ○Hirano Atsushi, Takeshi Tanaka, Hiromichi Kataura	84
1P-39	Highly pure semiconducting single-wall carbon nanotubes obtained by stable electric-field-induced layer formation ☆ ○Fusako Sasaki, Kazuki Ihara, Takeshi Saito, Fumiyuki Nihey	85

September 5, Wed.

- 1P-40 A rosette cooling cell : more effective container for solubilization of single-walled carbon nanotubes under probe-type ultrasonic irradiation 86
○Yuta Kurabuchi, Tatsuki Yasumitsu, Gang Liu, Jean-Marc LeVêque, Shinji Aomuma, Laurent Duclaux, Takahide Kimura, Naoki Komatsu
- 1P-41 The simplest separation of single-chirality carbon nanotubes by temperature-controlled gel chromatography 87
○Huaping Liu, Yasuko Urabe, Takeshi Tanaka, Hiromichi Kataura
- 1P-42 Evaluation of damage to SWCNTs during dispersion process in casein aqueous solution by using a wet-type super atomizer 88
○Tadashi Takashima, Daisuke Inoue, Yasushi Maeda, Shin Ono
- 1P-43 Stability of Nano-Diamonds as the Catalyst for CVD Growth of Single-Walled Carbon Nanotubes 89
○Takanori Umino, Kenta Nakamura, Taiki Inoue, Norihiro Hiramatsu, Shohei Chiashi, Yoshikazu Homma, Shigeo Maruyama
- 1P-44 Reaction analysis on CNT growth mechanism by eDIPS method using ^{13}C carbon source 90
○Takayoshi Hirai, Kazuaki Hoshi, Yuki Kuwahara, Rena Shibata, Masaharu Kiyomiya, Shun Nakano, Takeshi Saito
- 1P-45 Growth of Horizontally Aligned Single Walled Carbon Nanotubes : Effect of Catalyst Preparation and Crystal Quartz Surface 91
○Taiki Inoue, Grace Meikle, Saifullah Badar, Daisuke Hasegawa, Shohei Chiashi, Shigeo Maruyama
- 1P-46 Pulse plasma CVD for mass production of narrow-chirality distributed single-walled carbon nanotubes 92
★
○Koshi Murakoshi, Toshiaki Kato, Rikizo Hatakeyama, Toshiro Kaneko
- 1P-47 Separation of ultra-long single-wall carbon nanotubes using glass beads filtration 93
○Hiromichi Kataura, Mayumi Tsuzuki, Shunjiro Fujii, Takeshi Tanaka
- 1P-48 Synthesis of Carbon Nanomaterials Using Metallic Nanoparticles as Catalysts 94
○Balachandran Jeyadevan, Yukihiro Osada, Yoshinori Sato, Yuuki Sunayama

Nanohorns

- 1P-49 The effect of CNHs absorbed simvastatin on bone regeneration 95
○Akiko Yamauchi, Sachiko Matsumura, Tadashi Iizuka, Kiyotaka Shiba, Masako Yudasaka, Sumio Iijima, Atsuro Yokoyama

Environmental / Safety Characterization of Nanomaterials

- 1P-50 Biodistribution and biocompatibility of water-soluble carbon nanotubes 96
○Shigeaki Abe, Sachiko Itoh, Toshihisa Kobayashi, Takayuki Kiba, Tsukasa Akasaka, Yasutaka Yawaka, Shin-Ichiro Sato, Motohito Uo, Fumio Watari, Daisuke Hayashi, Tomoya Takada

September 6, Thu.

Plenary Lecture: 40min (Presentation) + 5min (Discussion)

**General Lecture by Candidates for Osawa Award and Iijima Award
: 10min (Presentation) + 10min (Discussion)**

Poster Preview: 1min (Presentation)

General Lecture by Candidates for the Osawa Award (9:00-10:20)

- 2-1 Synthesis of Endohedral Fullerene C₆₀ Encapsulating a Single Molecule of Water 23
○*Kei Kurotobi, Yasujiro Murata*
- 2-2 Chemistry of Cation-Endohedral Fullerene: [Li⁺@C₆₀] 24
○*Hiroshi Okada, Masashi Maruyama, Takashi Komuro, Takahito Watanabe, Yasuhiko Kasama, Hiromi Tobita, Yutaka Matsuo*
- 2-3 Establishment of intra-molecular electron accepting and donating systems based on endohedral metallofullerenes 25
○*Yuta Takano, Naomi Mizorogi, M. Angeles Herranz, Nazario Martin, Dirk M. Guldi, Shigeru Nagase, Takeshi Akasaka*
- 2-4 Room Temperature Observation of Single-Electron Tunneling via Fullerene Quantum Dots in a Si-based Device Structure 26
○*Ryoma Hayakawa, Chikyow Toyohiro, Yutaka Wakayama*

General Lecture by Candidates for the Iijima Award (10:20-11:00)

- 2-5 A patternable CNT-Cu composite possessing hundred-times higher electrical current-carrying-capacity than metals 27
○*Chandramouli Subramaniam, Takeo Yamada, Don N. Futaba, Motoo Yumura, Kenji Hata*
- 2-6 Effect of Mechanical Strain on Polycrystalline Graphene 28
○*Mark A. Bissett, Wataru Izumida, Riichiro Saito, Hiroki Ago*

>>>>> Coffee Break (11:00-11:15) <<<<<<

Plenary Lecture (11:15-12:00)

- 2S-4 Carbon nanotube field effect transistors with graphene contacts 4
Takashi Mizutani

>>>>> Lunch Time (12:00-13:00) <<<<<<

Young Scientist Poster Award Ceremony (13:00-13:15)

General Meeting (13:15-13:45)

September 6, Thu.

Poster Preview (13:45-14:25)

Poster Session (14:25-16:10) (☆) Candidates for the Young Scientist Poster Award

Properties of Nanotubes

2P-1	Temperature Dependence of Photoluminescence Spectra in Hole-Doped Single-Walled Carbon Nanotubes ○Shinichiro Mouri, Munechiyo Iwamura, Naoto, Akizuki, Yuhei Miyauchi, Kazunari Matsuda	97
2P-2	Aggregation and agglomeration evaluation of dispersed carbon nanotubes ○Takeshi Eitoku, Masayoshi Tange, Haruhisa Kato, Toshiya Okazaki	98
2P-3	Effects of Water Vapor on RBM of Single-Walled Carbon Nanotubes : Molecular Dynamics Simulation ○Naoki Homma, Shintaro Sato, Shouhei Chiashi, Yoshikazu Homma, Takahiro Yamamoto	99
2P-4	Evaluation of Functionalized Single-Walled Carbon Nanotubes by X-ray Photoelectron Spectroscopy ○Hiroyuki Nii, Syunsuke Noguchi, Ken-ichi Hongyou, Hamazo Nakagawa	100
2P-5	Tilting of Dirac cones and vernier spectrum in finite-length metallic single-wall carbon nanotubes ○Wataru Izumida, Yuki Tatsumi, Riichiro Saito	101
2P-6 ☆	Theory of electronic Raman scattering in metallic single wall carbon nanotubes ○Eddwi H. Hasdeo, Ahmad R. T. Nugraha, Kentaro Sato, Riichiro Saito	102
2P-7 ☆	Excitonic effects on coherent phonons in single wall carbon nanotubes ○Ahmad Ridwan Tresna Nugraha, Gary D. Sanders, Christopher J. Stanton, Riichiro Saito	103
2P-8	Thermoelectric Power of Metallic and Semiconducting Single-Wall Carbon Nanotube Buckypaper ○Honda Kazuya, Yusuke Nakai, Kazuhiro Yanagi, Yutaka Maniwa	104
2P-9 ☆	Electrostatic Potential of Hydrogenated Finite-length Carbon Nanotubes under an Electric Field ○Ayaka Yamanaka, Susumu Okada	105
2P-10 ☆	Analysis of Operation Mechanisms of SWNT Network Field-Effect Transistors Studied via Scanning Gate Microscopy ○Masahiro Matsunaga, Xiaojun Wei, Kenji Maeda, Tatsuroou Yahagi, Kazuaki Tanaka, Jonathan P. Bird, Koji Ishibashi, Yuichi Ochiai, Nobuyuki Aoki	106
2P-11 ☆	Photoluminescence Excitation Spectroscopy of Carrier-Doped Single-Walled Carbon Nanotubes ○Naoto Akizuki, Munechiyo Iwamura, Shinichiro Mouri, Yuhei Miyauchi, Kazunari Matsuda	107
2P-12 ☆	Coherent AC Transport in Metallic Carbon Nanotubes with Disorder ○Daisuke Hirai, Takahiro Yamamoto, Satoshi Watanabe	108

September 6, Thu.

2P-13	Electronic States in Flattened Carbon Nanotubes with Effective-Mass Approximation ○ <i>Takeshi Nakanishi, Tsuneya Ando</i>	109
2P-14	Optical properties of ultrathin single-wall carbon nanotubes ○ <i>Toshiya Nakamura, Yasumitsu Miyata, Eri Inukai, Ryo Kitaura, Hiromichi Kataura, Hisanori Shinohara</i>	110
2P-15	Non-linear and Non-planar Free Thermal Vibration of Single-walled Carbon Nanotubes in Molecular Dynamic Simulation ○ <i>Heeyuen Koh, James Cannon, Shohei Chiashi, Junichiro Shiomi, Shigeo Maruyama</i>	111
2P-16	Electrical current behavior at CNT-SiC interface ○ <i>Masafumi Inaba, Megumi Shibuya, Kazuyoshi Oohara, Takumi Ochiai, Yoshiho Masuda, Atsushi Hiraiwa, Michiko Kusunoki, Hiroshi Kawarada</i>	112
2P-17	Raman Imaging Spectroscopy of Horizontally Aligned Single-Walled Carbon Nanotubes on Crystal Quartz ○ <i>Saifullah Badar, Daisuke Hasegawa, Taiki Inoue, Shohei Chiashi, Shigeo Maruyama</i>	113
2P-18	Fabrication and characterization of individually suspended DWCNTs ○ <i>Tomoya Kitagawa, Ryo Kitaura, Yuhei Miyauchi, Yasumitsu Miyata, Kazunari Matsuda, Hisanori Shinohara</i>	114
2P-19	Crystal structure analysis of MWNT forests ○ <i>Hiroshi Furuta, Akimitsu Hatta</i>	115

Applications of Nanotubes

2P-20	Photovoltaic Properties of Single-Walled Carbon Nanotube/Silicon Heterojunction Solar Cells ○ <i>Daichi Kozawa, Kazushi Hiraoka, Yuhei Miyauchi, Shinichiro Mouri, Kazunari Matsuda</i>	116
2P-21	Micro-fabrication of stretchable and robust interconnects of conductive CNT rubber on a stretchable substrate ○ <i>Atsuko Sekiguchi, Tekao Yamada, Kazufumi Kobashi, Motoo Yumura, Kenji Hata</i>	117
2P-22	Optimizing dispersion structure of SWNT for high electrically-conductive rubber composites ○ <i>Howon Yoon, Motoi Yamashita, Seisuke Ata, Motoo Yumura, Kenji Hata</i>	118
2P-23	Super-Growth SWNT/rubber composite with extruder for commercial applications ○ <i>Seisuke Ata, Takaaki Mizuno, Howon Yoon, Motoo Yumura, Kenji Hata</i>	119
2P-24	Ion-Gel Transistors on Thick Films in a Single Chiral State of (6,5) Single-Wall Carbon Nanotubes ○ <i>Hikaru Kudo, Yuki Nobusa, Hiromichi Kataura, Taishi Takenobu, Kazuhiro Yanagi</i>	120
2P-25	Synthesis and Electrical Conductivity of Polymer/CNT Composite Using the Reaction Injection Molding (RIM) Method ○ <i>Hoang The Ban, Masahiro Shigeta, Mitsugu Uejima</i>	121

September 6, Thu.

2P-26	Fabrication of biotin-labeled double-walled carbon nanotubes for a specific biosensor ○Yuka Nagaya, Akihiro Kuno, Koji Tsuchiya, Hirofumi Yajima	122
2P-27	Labeling of mannose to acid-treated double-walled carbon nanotubes for a sensitive and specific biosensor ○Shuhei Takesue, Akihiro Kuno, Koji Tsuchiya, Hirofumi Yajima	123
2P-28 ★	Formation of homogeneous and high density thin-film of single-wall carbon nanotube by dip coating ○Maki Shimizu, Shunjiro Fujii, Takeshi Tanaka, Hiromichi Kataura	124
2P-29	Conduction-Type Control of Carbon Nanotube Field-Effect Transistors by Pd and Ti Overlayer Doping ○Satoshi Ishii, Masato Tamaoki, Shigeru Kishimoto, Takashi Mizutani	125
2P-30 ★	Switchable thermal conductivity enhancement of phase change composites with single walled carbon nanotube inclusions ○Sivasankaran Harish, Kei Ishikawa, Taiki Inoue, Shohei Chiashi, Junichiro Shiomi, Shigeo Maruyama	126
2P-31 ★	In-situ transmission electron microscopy study on electric properties of a junction between a gold nanoparticle and carbon nanotubes ○Motoyuki Karita, Koji Asaka, Hitoshi Nakahara, Yahachi Saito	127
2P-32	Synthesis of carbon nanotubes conjugated with distance-controlled nanoparticles using gas-liquid interfacial plasmas ○Toshiro Kaneko, Qiang Chen, Rikizo Hatakeyama	128
2P-33	Electrochemical durability of single-wall carbon nanotube electrode against anodic oxidation in water ○Shigekazu Ohmori, Takeshi Saito	129
2P-34	Patterned Carbon Nanotubes Thin Films Fabricated by Polystyrene-Nanosphere Templating ○Yuki Kuwahara, Takayoshi Hirai, Takeshi Saito	130
2P-35 ★	Fabrication of stable p-n junction diode with Cs encapsulated single-walled carbon nanotubes ○Yoshihiro Abiko, Toshiaki Kato, Rikizo Hatakeyama, Toshiro Kaneko	131
2P-36	Nanotube-Based Self-Standing Carbon Films for Supercapacitors ○Ricardo Quintero, Dong Young Kim, Kei Hasegawa, Yuki Yamada, Atsuo Yamada, Suguru Noda	132
2P-37	Controlled Functionalization of Carbon Nanotubes with Antibody ○Yoko Iizumi, Toshiya Okazaki, Yuzuru Ikehara, Mutsuo Ogura, Masako Yudasaka	133
2P-38	Selective Extraction of Semiconducting Single-Walled Carbon Nanotubes by Fullerodendrons ○Hironori Suzuki, Toshiya Okazaki, Yoko Iizumi, Masayoshi Tange, Takaaki Wada, Tomoyuki Tajima, Yutaka Takaguchi, Sumio Iijima	134

September 6, Thu.

- 2P-39 Fabrication and properties of chemically doped semiconducting single-walled carbon nanotubes/Si heterojunction diodes 135
○*Mao Shoji, Atsushi Nakano, Hironori Ogata*
- 2P-40 Structural deformation of functionalized multi-walled carbon nanotubes in the macrophage of rat subcutaneous soft tissue over long time 136
○*Yoshinori Sato, Atsuro Yokoyama, Eiko Nakazawa, Minfang Zhang, Masako Yudasaka, Kenichi Motomiya, Kazuyuki Tohji*
- 2P-41 Ultrathin aligned CNTs film by combining AC electric field with liquid flow 137
○*Jun Matsui, Shigeru Kaida, Tokuji Miyashita*

Forum (16:10-18:30)

Safety · Security Society and Nano Science · Technology

(Field investigation of the Great East Japan Earthquake included)

September 7, Fri.

Special Lecture: 25min (Presentation) + 5min (Discussion)

General Lecture: 10min (Presentation) + 5min (Discussion)

Poster Preview: 1min (Presentation)

General Lecture (9:00-10:15)

Formation and Purification of Nanotubes · Applications of Nanotubes · Endohedral Nanotubes

- | | | |
|-----|---|----|
| 3-1 | Properties of Single Wall Carbon Nanotube Aggregates Formed by Vapor Diffusion Methods
○ <i>Kazuhiro Yanagi, Hideki Kawai, Hikaru Kudo, Kai Hasegawa, Hiromichi Kataura, Ryo Nakatzu</i> | 29 |
| 3-2 | Effects of the Defective Structures for Carbon Nanotube on the Antidegradation and Electrical Conductivity of Rubber Composites
○ <i>Tomoya Nagaoka, Koji Tsuchiya, Yoshiyuki Takahashi, Hirofumi Yajima</i> | 30 |
| 3-3 | Fabrication and applications of carbon nanotube-alumina composite
○ <i>Mamoru Omori, Go Yamamoto, Keiichi Shirasu, Toshiyuki Hashida</i> | 31 |
| 3-4 | Fabrication of flexible bulk-heterojunction organic solar cells using single-wall carbon nanotube thin films as transparent conducting anodes
○ <i>Shunjiro Fujii, Takeshi Tanaka, Satoko Nishiyama, Hiromichi Kataura</i> | 32 |
| 3-5 | Thin single-walled boron nitride nanotubes synthesized in single-wall carbon nanotubes
○ <i>Ryo Nakanishi, Ryo Kitaura, Yuta Yamamoto, Shigeo Arai, Jamie H. Warner, Yasumitsu Miyata, Hisanori Shinohara</i> | 33 |

>>>>> Coffee Break (10:15-10:30) <<<<<

General Lecture (10:30-11:30)

Properties of Nanotubes

- | | | |
|-----|--|----|
| 3-6 | Optical properties of small-diameter carbon nanotubes
○ <i>Takashi Koretsune, Susumu Saito</i> | 34 |
| 3-7 | Photoluminescence Spectroscopy of Oxygen-doped Carbon Nanotubes
○ <i>Munehiyo Iwamura, Yuhei Miyauchi, Shinichiro Mouri, Tadashi Kawazoe, Motoichi Ohtsu, Kazunari Matsuda</i> | 35 |
| 3-8 | Photocurrents with multiple exciton generation in single-walled carbon nanotubes
○ <i>Satoru Konabe, Susumu Okada</i> | 36 |
| 3-9 | Diameter reduction of SWNTs by nitrogen incorporation and encapsulation of a one-dimensional nitrogen gas
○ <i>Theerapol Thurakitserree, Christian Kramberger, Heeyuen Koh, Yudai Izumi, Toyohiko Kinoshita, Takayuki Muro, Shohei Chiashi, Erik Einarsson, Shigeo Maruyama</i> | 37 |

September 7, Fri.

Special Lecture (11:30-12:00)

- 3S-5 Plasma processing of carbon-based nanomaterials 5
R. Mohan Sankaran

>>>>> Lunch Time (12:00-13:15) <<<<<<

General Lecture (13:15-14:45)

Properties of Graphene

- 3-10 Numerical Study of Edge States in Zigzag BC₂N Nanoribbons 38
○*Kikuo Harigaya, Tomoaki Kaneko*
- 3-11 G band intensity and joint density of states of twisted bilayer graphene 39
○*Kentaro Sato, Riichiro Saito, Chunxiao Cong, Ting Yu, Mildred S. Dresselhaus*
- 3-12 Production of Nanopores and Proton Conduction in Graphene Oxide Nanosheets 40
Prepared by Photoreaction
○*Michio Koinuma, Chikako Ogata, Yuki Kamei, Kazuto Hatakeyama, Hikaru Tateishi, Kengo Gezuhara, Takaaki Taniguchi, Yasumichi Matsumoto*
- 3-13 Photoluminescence Kinetics of Monolayer Epitaxial Graphene in the Near-Infrared 41
Region
○*Takeshi Koyama, Yoshito Ito, Kazuma Yoshida, Hiroki Ago, Hideo Kishida, Arao Nakamura*
- 3-14 Bilayer graphene sandwiched by ionic molecules: Band-gap and carrier type engineering 42
○*Nguyen Thanh Cuong, Minoru Otani, Susumu Okada*
- 3-15 Photochemical modification of graphene surfaces with water molecules 43
○*Ryo Nouchi, Nobuhiko Mitoma, Katsumi Tanigaki*

Special Lecture (14:45-15:15)

- 3S-6 Epitaxial CVD Growth of Graphene 6
Hiroki Ago

>>>>> Coffee Break (15:15-15:30) <<<<<<

General Lecture (15:30-16:15)

Nanohorns • Carbon Nanoparticles

- 3-16 Structure and electronic properties of carbon nanohorn aggregates prepared under 44
nitrogen atmosphere
○*Ryota Yuge, Takashi Manako, Masako Yudasaka, Kiyohiko Toyama, Takashi Yamaguchi, Sumio Iijima, Kaichiro Nakano*
- 3-17 Gastrointestinal behavior of orally-administered single-walled carbon nanohorns 45
○*Maki Nakamura, Yoshio Tahara, Tatsuya Murakami, Sumio Iijima, Masako Yudasaka*

September 7, Fri.

- 3-18 Improvement in energy density of electric double-layer capacitors by mixture of AcB and CNB 46
○Yuta Okabe, H. Izumi, Yoshiyuki Suda, Hirohumi Takikawa, Hideto Tanoue, Hitoshi Ue, Kazuki Shimizu

Poster Preview (16:15-17:00)

Poster Session (17:00-18:45) (☆) Candidates for the Young Scientist Poster Award Endohedral Nanotubes

- 3P-1 Encapsulation of C₆₀ into the Single Chirality State of (11,10) Single Wall Carbon Nanotubes 138
○Masatoshi Kawai, Toru Igarashi, Haruka Kyakuno, Toshiya Okazaki, Yutaka Maniwa, Kazuhiro Yanagi
- 3P-2 Optical Properties of Perylene / Single-Walled Carbon Nanotubes Composites 139
○Takuya Tsunekawa, Takeshi Koyama, Koji Asaka, Yahachi Saito, Hideo Kishida, Arai Nakamura
- 3P-3 Difference in encapsulated AgBr lifetime between ¹²CNTs and ¹³CNTs under electron beam irradiation 140
○Keita Kobayashi, Takeshi Saito, Masaharu Kiyomiya, Hidehiro Yasuda
- 3P-4 ☆ Fabrication and characterization of structurally uniform conducting polymers within carbon nanotubes 141
○Kenshi Miyaura, Yasumitsu Miyata, Ryo Kitaura, Hisanori Shinohara
- 3P-5 Amphoteric Carrier Doping to Semiconducting Single-Wall Carbon Nanotubes by TTF and F₄TCNQ Encapsulation 142
○Yasuhiro Ito, Shunjiro Fujii, Maki Shimizu, Takeshi Tanaka, Hiromichi Kataura

Formation of Graphene

- 3P-6 Microwave-assisted exfoliation of graphite in organic solvents without using strong oxidants 143
○Haruya Okimoto, Ryota Tada, Masahito Sano
- 3P-7 Raman characterization of patterned graphene directly synthesized by alcohol chemical vapor deposition 144
○Yusuke Kito, Hiroya Yamauchi, Tomoya Kamizyukoku, Manabu Suzuki, Takahiro Maruyama, Shigeya Narituka
- 3P-8 Characterization of interface between hexagonal graphene domains grown on hetero-epitaxial Cu films 145
○Yui Ogawa, Kenji Kawahara, Masahiro Miyashita, Masaharu Tsuji, Hiroki Ago
- 3P-9 ☆ CVD Growth of Mono- and Bi-Layer Graphene from Ethanol 146
○Xiao Chen, Pei Zhao, Bo Hou, Shohei Chiashi, Shigeo Maruyama
- 3P-10 Direct growth of hexagonal domain graphene on SiO₂ substrate 147
○Toshiaki Kato, Rikizo Hatakeyama, Toshiro Kaneko

September 7, Fri.

Properties of Graphene

- 3P-11 First-Principles Study of Carbon-Impurity States in Hexagonal Boron-Nitride Monolayer 148
○Yoshitaka Fujimoto, Takashi Koretsune, Susumu Saito
- 3P-12 Electronic Structures of Bilayer Graphene under Electric Field 149
○Satoru Konabe, Susumu Okada
- 3P-13 Raman scattering study on the X-ray irradiation effect of graphene 150
○Toshiya Murakami, Kazuki Yamazaki, Susumu Kamo, Noriyuki Hasuiki, Hiroshi Harima, Kenji Kisoda, Chihiro Itoh
- 3P-14 Edge Effects on Thermoelectric Power of Graphene Nanoribbons : First-Principles Simulation 151
○Teppei Kato, Shinji Usui, Takahiro Yamamoto
- 3P-15 Wave Packet Dynamics Simulations on Electrical Conduction in Graphene Nanoribbons 152
Yukihiro Takada, ○Kengo Takashima, Takahiro Yamamoto
- 3P-16 Multiple Dirac points of graphene on a quasiperiodic superlattice 153
☆ ○Masayuki Tashima, Naomichi Hatano
- 3P-17 Sheet resistivity for nitrogen doped graphene film grown on Cu foil by sonication mist CVD 154
○Takahiro Mizuno, Morio Takizawa, Shunji Bandow
- 3P-18 Simulated Image of Suspended Graphene by Helium Ion Microscope 155
○Yoshiyuki Miyamoto
- 3P-19 Lattice matching and band gap opening in graphene and h-BN stacked thin films 156
☆ ○Yuki Sakai, Susumu Saito
- 3P-20 Synthesis and Optical Properties of Graphene Quantum Dots 157
☆ ○Naoto Fuyuno, Daichi Kozawa, Yuhei Miyauchi, Shinichiro Mouri, Kazunari Matsuda
- 3P-21 First-principles study on geometries and electronic structures of halogen-terminated armchair graphene nanoribbons 158
☆ ○Hideyuki Jippo, Mari Ohfuchi
- 3P-22 Novel spintronic phenomena arising from pore-edge polarized spins of ferromagnetic graphene nanomeshes 159
○Naoki Kosugi, Yasuki Hashimoto, Kenshi Sakuramoto, Keigo Takeuchi, Shota Kamikawa, Yuko Yagi, Junji Haruyama, Yoshiaki Hashimoto, Kazuhiro Fujita, Yuto Kato, Shingo Katsumoto, Yasuhiro Iye, Pei Zhao, Shigeo Maruyama, Apparao Rao
- 3P-23 Magnetic behaviors sensitive to foreign-atom termination of pore-edge in graphene nanomeshes 160
○Keigo Takeuchi, Kenshi Sakuramoto, Naoki Kosugi, Yasuki Hashimoto, Yuko Yagi, Junji Haruyama, Pei Zhao, Shigeo Maruyama, Apparao Rao

September 7, Fri.

Applications of Graphene

- 3P-24 Electronic structures of hexagonal boron nitride with topological line defects 161
○Yoko Tomita, Susumu Okada
- 3P-25 Hole-doping to CVD graphene induced by electron beam resist 162
○Yui Ogawa, Masaharu Tsuji, Hiroki Ago
- 3P-26 Fabrication of freestanding graphene nanoribbons devices for in-situ TEM 163
☆ characterization
○Shoji Suzuki, Ryo Kitaura, Yuki Sasaki, Keiichi Kamon, Yasumitsu Miyata, Hisanori Shinohara
- 3P-27 The effects of graphene-layer thickness on I - V characteristics of CNT-FETs with 164
graphene contacts
○Masato Tamaoki, Shigeru Kishimoto, Takashi Mizutani
- 3P-28 Synthesis of Nanocarbon Composites Based on Reduced Graphene Oxides 165
○Ellya Indahyanti, Hiroyuki Yokoi, Kazuto Hatakeyama, Yasumichi Matsumoto
- 3P-29 First-principles simulations of graphene dual-double gate transistors: implementation of 166
gate electric field
Mari Ohfuchi

Nanohorns

- 3P-30 Apoptotic Mechanism of RAW264.7 Induced by Carbon Nanohorns 167
○Mei Yang, Minfang Zhang, Yoshio Tahara, Sumio Iijima, Masako Yudasaka
- 3P-31 Synthesis of carbon nanohorns dispersed with metallic nanoparticles by gas-injected arc- 168
in-water method
○Noriaki Sano, Tatporn Suntornlohanakul, Chantamane Poonjarernsilp, Daisuke Hirama, Kosuke Taniguchi, Tatsuhiko Norimoto, Taiga Ishii, Hajime Tamon, Tawatchai Charinpanitkul

Nanowires

- 3P-32 Vibronic interaction in the forbidden electronic transition of polyynes and cyanopolynes 169
○Tomonari Wakabayashi, Yoriko Wada, Makiko Tomioka

Carbon Nanoparticles

- 3P-33 Methanol oxidation reaction characteristics of carbon nanomaterials with PtRu-support 170
○Masahiro Ozaki, Yoshiyuki Suda, Hirofumi Takikawa, Hideto Tanoue, Hitoshi Ue, Kazuki Shimizu
- 3P-34 IR spectra of polyyne-iodine complexes in nonpolar solvents 171
○Yoriko Wada, Yusuke Morisawa, Tomonari Wakabayashi
- 3P-35 Formation of carbon nanocapsules from silicon nanoparticles deposited on a carbon 172
☆ nanotube heater
○Tomohiro Terada, Koji Asaka, Hitoshi Nakahara, Yahachi Saito

September 7, Fri.

- 3P-36 Distribution of Lanthanum containing carbon nanocapsules in the DC arc cathode deposit 173
○Kazunori Yamamoto, Shin-ichi Shamoto, Takeshi Akasaka

Miscellaneous

- 3P-37 Dependence of carbon nanocoil length on sonication time 174
☆ ○Koji Maruyama, Yosiyuki Suda, Hideto Tanoue, Hirohumi Takikawa, Hitoshi Ue,
Kazuki Shimizu, Yoshito Umeda
- 3P-38 Doping of Fullerene to Iron Oxide Nanotubes 175
○Yuki Shiraki, Yuki Mishina, Shunji Bandow
- 3P-39 Supercooled and Glassy Water Confined in Zeolite Templated Carbon 176
○Haruka Kyakuno, Kazuyuki Matsuda, Yusuke Nakai, Tomoko Fukuoka, Yutaka
Maniwa, Hiroto Nishihara, Takashi Kyotani
- 3P-40 Microscopic study of Zeolite Templated Carbon (ZTC) by using ^{13}C NMR spectroscopy 177
○Kensuke Yamada, Yusuke Nakai, Kazuyuki Matsuda, Yutaka Maniwa, Hiroto
Nishihara, Takashi Kyotani
- 3P-41 Measurement of electric property of carbon nanocoil in scanning electron microscope 178
○Ryuji Kunimoto, Taiichiro Yonemura, Yoshiyuki Suda, Hideto Tanoue, Hirofumi
Takikawa, Hitoshi Ue, Kazuki Shimizu, Yoshito Umeda
- 3P-42 Development of CNT-based Polymer Electrolyte Fuel Cell Electrocatalyst 179
○Tsuyohiko Fujigaya, Mohamed Reda Berber, Naotoshi Nakashima

基調講演
Plenary Lecture

特別講演
Special Lecture

1S - 1 ~ 1S - 3

2S - 4

3S - 5 ~ 3S - 6

Synthesis and characterization of carbon-nanotube-based hybrid materials

○Toshiya Okazaki

Nanotube Research Center, AIST, Tsukuba 305-8565, Japan

One of the most characteristic features of single-walled carbon nanotubes (SWCNTs) is that they have an inner space with dimensions suitable for accommodating molecules and molecular materials. Doping molecules to the inner spaces instead of outside the SWCNTs is expected to be a useful technique for achieving realistic applications of SWCNTs to increase their stability and durability. For example, low-temperature scanning tunneling spectroscopy (LT-STTS) revealed that a band gap of ~ 0.5 eV is narrowed down to ~ 0.1 eV at the site where Gd@C₈₂ molecule is inserted in semiconducting (11, 9) SWCNT [1]. Although it provides possible design rules for proposing hybrid structures having a specific type of electronic functionality, it was yet unclear from either the experimental or theoretical point of view what is the effect of encapsulated fullerene molecules on the band gap modification of SWCNTs.

We have studied on the electronic and the phonon properties of fullerenes encapsulating SWCNTs (nanopeapods) by using spectroscopic techniques such as photoluminescence (PL) [2-5] and resonance Raman scattering [6-8]. The PL peak positions and the radial breathing mode (RBM) frequencies show characteristic changes upon fullerene encapsulations. For instance, the observed shifts in the optical transition energies and the RBM frequencies of SWCNTs show strong tube diameter dependence, which can be explained by the van der Waals type intermolecular interaction between SWCNTs and the encapsulated fullerenes.

The important finding from these studies is that SWCNTs are ideal templates for one-dimensional (1D) organic nanostructures. However, no other molecule has shown well-ordered arrangements in SWCNTs even though fullerenes form one-dimensional crystals inside SWCNTs. We recently demonstrated such 1D organization of coronenes, a class of planar π -conjugated molecules, by using SWCNTs as templates [9]. Interestingly, the assembling structure of the coronene columns is different from the crystal structure of bulk coronenes.

In this symposium, we will first review the spectroscopic studies on fullerene nanopeapods and then report several characteristic nanostructures formed inside SWCNTs including coronene. The basic properties of the produced 1D molecular crystal will be discussed.

[1] J. Lee *et al.*, *Nature*, **415**, 1005 (2002). [2] T. Okazaki *et al.*, *J. Am. Chem. Soc.*, **130**, 4122 (2008). [3] S. Okubo *et al.*, *J. Phys. Chem. C.*, **113**, 571 (2009). [4] Y. Iizumi *et al.*, *Chem. Commun.*, **46**, 1293 (2010). [5] S. Okubo *et al.*, *J. Am. Chem. Soc.*, **132**, 15252 (2010). [6] S.-K. Joung *et al.*, *Phys. Rev. Lett.*, **103**, 027403 (2009). [7] S.-K. Joung *et al.*, *Phys. Chem. Chem. Phys.*, **12**, 8118 (2010). [8] S.-K. Joung *et al.*, *Phys. Status Solidi B*, **247**, 2700 (2010). [9] T. Okazaki *et al.*, *Angew. Chem. Int. Ed.*, **50**, 4853 (2011).

Corresponding Author: T. Okazaki

Tel: +81-29-861-4173, Fax: +81-29-861-6241

E-mail: toshi.okazaki@aist.go.jp

Superconductivity proximate to antiferromagnetism in fullerene superconductors

○Kosmas Prassides

Department of Chemistry, Durham University, Durham DH1 3LE, UK

A_3C_{60} (A = alkali metal) superconductors were known to adopt face-centred cubic (fcc) structures with their superconducting T_c increasing monotonically with increasing interfullerene spacing, reaching a 33 K maximum for $RbCs_2C_{60}$ – this physical picture had remained unaltered since 1992. Trace superconductivity (s/c fraction < 0.1%) at 40 K under pressure was also reported in 1995 in multiphase samples with nominal composition Cs_3C_{60} . Despite numerous attempts by many groups worldwide, this remained unconfirmed and the structure and composition of the material responsible for superconductivity unidentified. Thus the possibility of enhancing fulleride superconductivity and understanding the structures and properties of these archetypal molecular solids had remained elusive.

Here I will present our recent progress in this field in accessing high-symmetry hyperexpanded alkali fullerides in the vicinity of the Mott-Hubbard metal-insulator boundary and at previously inaccessible intermolecular separations. The physical picture that emerges for the alkali fullerides is that, contrary to long-held beliefs, they are the simplest members of the high- T_c superconductivity family. We demonstrated this by showing that in the two hyperexpanded Cs_3C_{60} polymorphs (fcc- and A15-structured) [1,2], superconductivity emerges upon applied pressure out of an antiferromagnetic insulating state and displays an unconventional behaviour – a superconductivity dome – explicable by the prominent role of strong electron correlations (Fig. 1).

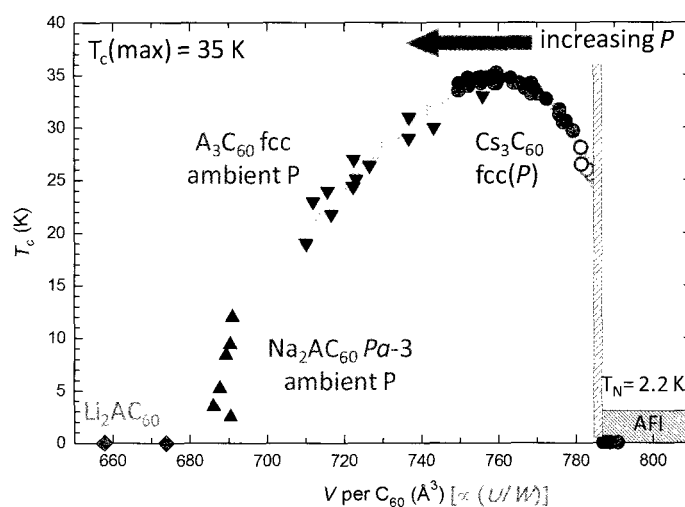


Fig. 1. Electronic phase diagram of fcc A_3C_{60} fullerides shown as a function of volume occupied per fulleride anion.

[1] Y. Takabayashi *et al.*, *Science* **323**, 1585 (2009).

[2] A. Y. Ganin *et al.*, *Nature* **466**, 221 (2010).

Corresponding Author: K. Prassides

Tel: +44-191-334-2063, Fax: +44-191-334-2051,

E-mail: K.Prassides@durham.ac.uk

Toward the Creation of Graphene Terahertz Lasers

○Taiichi Otsuji, Akira Satou, and Victor Ryzhii

Research Institute of Electrical Communication, Tohoku University, Sendai, 980-8579, Japan

Graphene, a monolayer carbon-atomic honeycomb crystal, has attracted attention due to its peculiar optoelectronic properties owing to the massless/gapless energy spectrum [1]. Optical or injection pumping of graphene can exhibit negative-dynamic conductivity in the terahertz (THz) spectral range [2, 3]. This paper reviews recent advances toward graphene THz lasers.

When the photogenerated electrons and holes are heated, collective excitations due to the carrier-carrier scattering take a dominant roll to perform an ultrafast carrier quasi-equilibration (see Fig. 1). Then carriers at high-energy tails of their distributions emit the optical phonons, cooling themselves and accumulating around the Dirac points (see Fig. 1). Due to a fast intraband relaxation (ps or less) and relatively slow interband recombination ($\gg 1$ ps) of photoelectrons/holes, the population inversion is obtainable. We also theoretically revealed the occurrence of negative dynamic conductivity in a wide THz frequency range [3, 4] (see Fig. 1). We conducted THz time domain spectroscopy for fs-laser pumped exfoliated monolayer graphene samples and showed that graphene amplifies an incoming THz field [5]. When the pumping intensity weakens below 1×10^7 W/cm² threshold behavior can be seen, testifying the occurrence of amplified stimulated THz emission.

Optical pumping with rather high photon energy of the order of “~eV” significantly heats the carriers, which dramatically increases the pumping threshold, preventing the population inversion [6]. Current injection pumping is a best of solution because electrical pumping can serve any pumping energy down under the order of “meV” when a p-i-n junction is formed like semiconductor laser diodes. Dual gate structure can make a p-i-n junction in the graphene channel [3] (see Fig. 2). Waveguiding the THz emitted waves with less attenuation is another key issue (see Fig. 2). We theoretically discover the amplification of surface plasmon-polariton when traveling along the graphene-channel waveguide under population inversion [7]. These new findings can lead to creation of a new type of room-temperature operating graphene THz lasers. This work is supported by JSPS GA-SPR and JST-CREST.

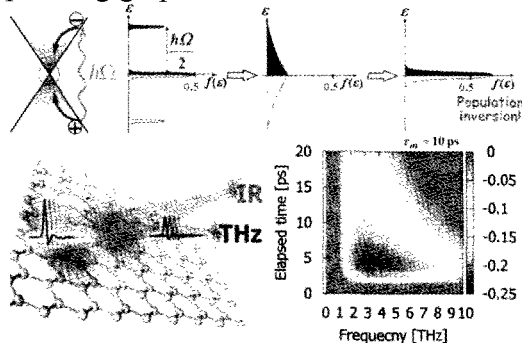


Fig. 1. Carrier dynamics and conductivity in graphene.

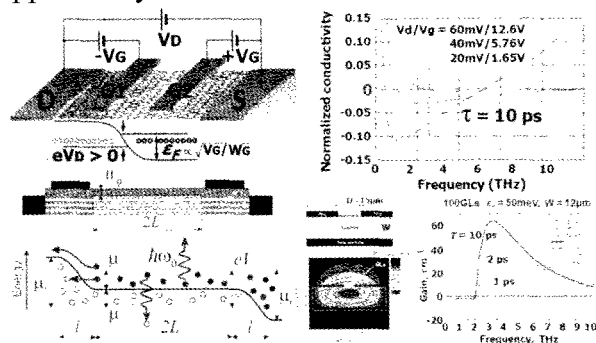


Fig. 2. A dual-gate graphene injection laser transistor.

- [1] A.K. Geim and K.S. Novoselov, *Nat. Mater.* **6**, 183 (2007).
 [2] V. Ryzhii et al., *J. Appl. Phys.* **101**, 083114 (2007).
 [3] V. Ryzhii et al., *J. Appl. Phys.* **110**, 094503 (2011).
 [4] A. Satou et al., *Jpn. J. Appl. Phys.* **50**, 070116 (2011).

- [5] S. Boubanga-Tombet et al., *Phys. Rev. B* **85**, 035443 (2012).
 [6] V. Ryzhii et al., *Jpn. J. Appl. Phys.* **50**, 094001 (2011).
 [7] A.A. Dubinov et al., *J. Phys.: Condens. Matter* **23**, 145302 (2011).

Corresponding Author: T. Otsuji

Tel: +81-22-217-6104, Fax: +81-22-217-6104,

E-mail: otsuji@riec.tohoku.ac.jp

Carbon nanotube field effect transistors with graphene contacts

Takashi Mizutani

Department of Quantum Engineering, Nagoya University, Nagoya, 464-8603, Japan

In order to apply carbon nanotube field-effect transistors (CNT-FETs) in electronics, it is important to address the issues such as the decrease of the contact resistance, control of the conduction type (n channel or p channel), and suppression of the ambipolar behavior. For this purpose, we have fabricated CNT-FETs with graphene contacts and studied the effects of the metal overlayer on the CNT channel.

The CNT-FETs with graphene contacts [1-2] were fabricated by depositing tri-layer structure of Au/Ni/a-C on the both ends of the CNT and the following graphitization annealing at 800°C. Graphene formation was confirmed by the TEM observation and the Raman scattering measurement. The devices showed p-channel behavior in air ambient with smaller contact resistances than the device with Au contacts. The conduction type changed to ambipolar in a vacuum after annealing at 200°C. The p-type conduction in air was attributed to the adsorbed oxygen on the device surface. The Fermi level of graphene contacts was found to be located at slightly below the midgap of the CNTs in a vacuum [2].

The conduction type of the CNTs with graphene contacts was controlled by the overlayer metal deposited on the CNT surface [3]. n-type conduction was realized by using Ti with a small work function as the overlayer metal, and p-type conduction by Pd with a large work function. The conduction type control was realized by employing the charge transfer from the overlayer metal to the CNT channel and the resultant band bending.

Ambipolar behavior was suppressed by introducing a floating gate which was placed on the CNT channel near the drain contact [4]. In the case of the n-channel devices, the metal with the small work function was suitable as the floating gate material because it forms the barrier against the holes which might be injected from the drain contact. In the case of the p-channel devices, Pd with the large work function was suitable as the floating gate material.

This work is partially supported by Grant-in-Aid for Scientific Research on Priority Areas from MEXT.

- [1] Y. Chai et al., IEEE Trans. ED. **59**, 12 (2012).
- [2] M. Tamaoki et al., Appl. Phys. Lett. (2012) (in print).
- [3] S. Ishii et al., 43rd FNTG Symposium (2012).
- [4] S. Ishii et al., (to be submitted).

Corresponding Author: T. Mizutani

Tel: +81-52-789-5230, Fax: +81-52-789-5232,

E-mail: tmizu@nuee.nagoya-u.ac.jp

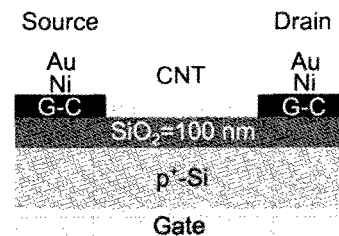


Fig. 1 Schematic cross section of the CNT-FET with graphene contacts.

Plasma processing of carbon-based nanomaterials

○R. Mohan Sankaran

*Department of Chemical Engineering, Case Western Reserve University, Cleveland, Ohio,
U.S.A.*

Low-temperature, low-pressure plasmas have played an essential role in the microelectronics industry. Generally, these plasmas are used to precisely etch and deposit Si-based materials. As new technologies emerge, recent trends have shifted from a focus on Si- to carbon-based materials. In particular, carbon-based nanomaterials such as carbon nanotubes and graphene are of great interest for nanoscale electronic devices. However, carbon is characterized by an enormous range of diversity that creates a significant synthetic challenge. A key challenge is therefore the development of processes that are capable of producing well-defined carbon-based nanomaterials. In this talk, I will present our recent efforts in this area based on our platform technology, atmospheric-pressure microplasmas. I will show that these novel plasma sources are capable of generating size- and compositionally-controlled metal nanoparticles for the catalytic growth of chirally-enriched single-walled carbon nanotubes.[1] Microplasmas can also serve as an atmospheric-pressure source of radicals such as atomic hydrogen to reduce graphene oxide at low temperatures.[2] Recently, we have discovered that hydrocarbon precursors can be dissociated in a microplasma to homogeneously nucleate carbon nanoparticles with diamond phase.[3] I will discuss these results in detail, highlighting the potential advantages of plasma processing for carbon nanomaterial synthesis and modification.

[1] W-H. Chiang and R. M. Sankaran, *Nat. Mater.* **8**, 882 (2009).

[2] S. W. Lee and R. M. Sankaran, *J. Phys. Chem. Lett.* **3**, 772 (2012).

[3] A. Kumar *et al.*, in preparation.

Corresponding Author: R. Mohan Sankaran

Tel: +1-216-368-4589

E-mail: mohan@case.edu

Epitaxial CVD Growth of Graphene

Hiroki Ago

Institute for Materials Chemistry and Engineering and Graduate School of Engineering Sciences, Kyushu University, Fukuoka 816-8580

Graphene is emerging as a new material for future applications in electronics, mechanics, optics, and energy. Recently, catalytic chemical vapor deposition (CVD) growth has attracted considerable interest as an effective means of producing large-area graphene films with relatively low cost. However, because most of the CVD growth has been done over polycrystalline metal films or foils, as-grown graphene has relatively small grain size and its orientation is not controlled.

Here, we present our recent studies on graphene growth using heteroepitaxial Cu and Co metal films deposited on sapphire c-plane and MgO(111) substrates [1-7]. We realized the CVD growth of uniform single-layer graphene not only on the Cu film with low C solubility but also on the Co film with high C solubility. These heteroepitaxial metal films enable the growth of orientation-controlled graphene consistent with the Cu and Co lattices [2,3].

Furthermore, low energy electron microscope (LEEM) analysis reveals that the graphene films grown on heteroepitaxial Cu(111) and Cu(100) planes have different domain structures, as illustrated in Figure 1 [7]. Square lattice of Cu(100) gives the single-layer graphene with two domain orientations rotated by 30°. On the other hand, uniform domain orientation is observed for the graphene grown on Cu(111). The growth mechanism of single-layer graphene on Cu surface is also discussed in terms of evolution of graphene domains [8]. Finally, our recent effort for the CVD growth of the graphene nanoribbons will be demonstrated [9]. We expect our epitaxial CVD approach paves the way for high-quality graphene with controlled structure applicable to graphene-based electronics and mechanics.

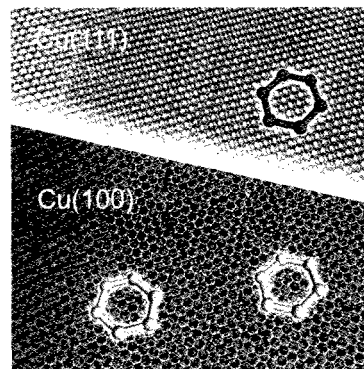


Figure 1. Illustration of graphene domains grown on two different Cu planes

References:

[1] H. Ago, *Small*, **6**, 1226 (2010). [2] H. Ago, *ACS Nano*, **4**, 7407 (2010). [3] B. Hu, *Carbon*, **50**, 57 (2012). [4] C. M. Orofeo, *Carbon*, **50**, 2189 (2012). [5] B. Hu, *New J. Chem.*, **36**, 73 (2012). [6] C. M. Orofeo, *Nano Res.*, **4**, 530 (2011). [7] Y. Ogawa, *J. Phys. Chem. Lett.*, **3**, 219 (2012). [8] H. Ago, *J. Phys. Chem. Lett.* (Perspective), in press. [9] H. Ago, *Nanoscale*, in press.

Acknowledgement:

This work was supported by JSPS Funding Program for Next Generation World-Leading Researchers (NEXT Program, GR075) and JST-PRESTO.

Corresponding Author: Hiroki Ago (Tel&Fax: +81-92-583-7817, E-mail: ago@cm.kyushu-u.ac.jp)

一般講演
General Lecture

1 - 1 ~ 1 - 16

2 - 1 ~ 2 - 6

3 - 1 ~ 3 - 18

Binary alloy effect on the chirality selection of carbon nanotubes

○Yohji Achiba¹⁾, Takeshi Kodama¹⁾, Kenro Hashimoto¹⁾, Haruo Shiromaru¹⁾ and Toshiya Okazaki²⁾

¹⁾ *Department of Chemistry, Tokyo Metropolitan University, Hachioji, 192-0397, Japan*

²⁾ *Advanced Industrial Science and Technology, Tsukuba, 305-8505, Japan*

Controlling size and chirality distributions in the production of single wall carbon nanotubes (SWNTs) is undoubtedly one of the most important issues in the potential applications of the SWNTs to nano-material science and technology. So far, many experimental attempts have been carried out on the selective production of specific (n,m) tubes by various kinds of the SWNT production methods. Among these trials, so called “CoMoCAT” and “Co-MCM-41” are typical successful examples in which the (6,5) tube formation has been demonstrated to be of fairly prominence. In these experiments, the selection of the (6,5) tube seems to be realized by combination of CO disproportionation reaction and Co metal catalyst.

On the other hand, the laser vaporization method combined with RhPd catalyst under some specific condition gives another good example for the realization of highly selective SWNT growth, in which over 80% selective growth of (6,5) species has clearly been shown, suggesting the presence of some special reasons for the favorable growth of (6,5) tube.

In the present work, we will demonstrate how the Rh/Pd binary metal catalyst system does work on the chirality selective growth of SWNTs on the basis of some experimental results revealed by systematical changes of Rh/Pd ratio in the laser vaporization SWNT synthesis system. The presence of the solid solution phase of Rh/Pd binary metal catalyst system seems to play an essential role on the highly chirality selective formation of particular (n,m) tubes.

Figure 1 shows the change of the chirality distribution upon adding Pd to the Rh mono-metallic catalyst system. All the samples shown in Fig. 1 were prepared at 975°C furnace temperature. It is clear that by increasing Pd concentration to the Rh system, not only the size distribution changes into the smaller diameter one but also the distribution of “near armchair” structure is significantly enhanced. It was also found that under the extreme condition such as low temperature and high concentration of Pd, over 90% carbon nanotubes in the soot consists of (6,5) tubes. We will discuss the reason why such a chirality-selective formation of carbon nanotube takes place by use of binary alloy catalyst system.

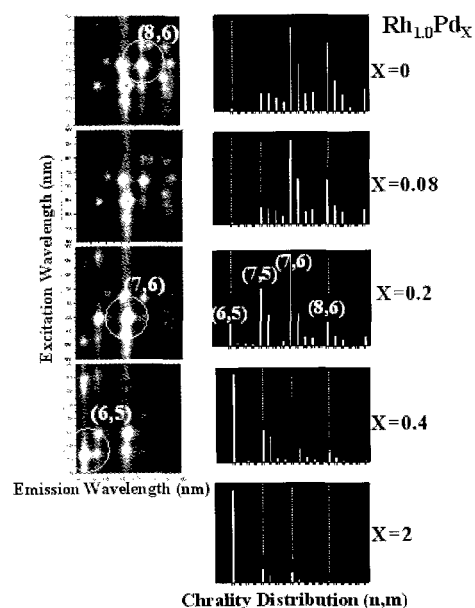


Fig. 1 The Pd addition effect on the chirality distribution of carbon nanotubes produced by a laser vaporization-furnace method

Corresponding Author: Y. Achiba

Tel: +81-42-677-2534, Fax: +81-42-677-2525,

E-mail: achiba-yohji@tmu.ac.jp

Raman study on defects induced double walled carbon nanotube by X-ray irradiation

○Toshiya Murakami¹, Yuki Yamamoto¹, Kenji Kisoda², Chihiro Itoh¹

¹Department of Material Science, Wakayama University, Wakayama, 640-8510, Japan

²Department of Physics, Wakayama University, Wakayama, 640-8510, Japan

Structural modification of carbon nanotube (CNT) results in change of its electronic property because of the strong correlation of the electronic structure with its diameter. For developing carbon-based nano-electronic devices, it is necessary to control CNT structures. X-ray irradiation has been shown to modify the structure of single walled carbon nanotube (SWNT).[1] DWNT is the simplest multi walled carbon nanotube and possesses common properties of SWNT. Therefore, the study on the X-ray irradiation effect in DWNT provides insights on interplay between carbon layers and X-ray induced atomic process in nanocarbons.

In this report, we show the results of the Raman scattering spectroscopy on the soft X-ray (277eV) irradiated DWNTs. After X-ray irradiation, the intensity ratio of D- to G-bands (D/G) was slightly enhanced compared to the irradiated SWNT with the same experimental condition.[1] This small enhancement of D/G in DWNT indicates that DWNTs are more stable under X-ray irradiation than SWNTs. In Fig. 1(b), we show the low-frequency Raman spectra of before and after the X-ray irradiation. The peaks at 158 cm⁻¹ and 266 cm⁻¹ are ascribed to RBMs of outer and inner tubes of DWNT, respectively. X-ray irradiation broadened the width of these peaks. However, the increase in FWHM of the outer tube is greater than that of the inner tube as shown in Fig. 1(c). The defects were recovered by annealing in the vacuum (not shown). Based on these results, we infer that the vacancy-interstitial pairs, Frenkel defects, are induced in DWNT by X-ray irradiation. The vacancy-interstitial separation of the Frenkel pairs on the outer tube is conceivably longer than that of the inner tube.

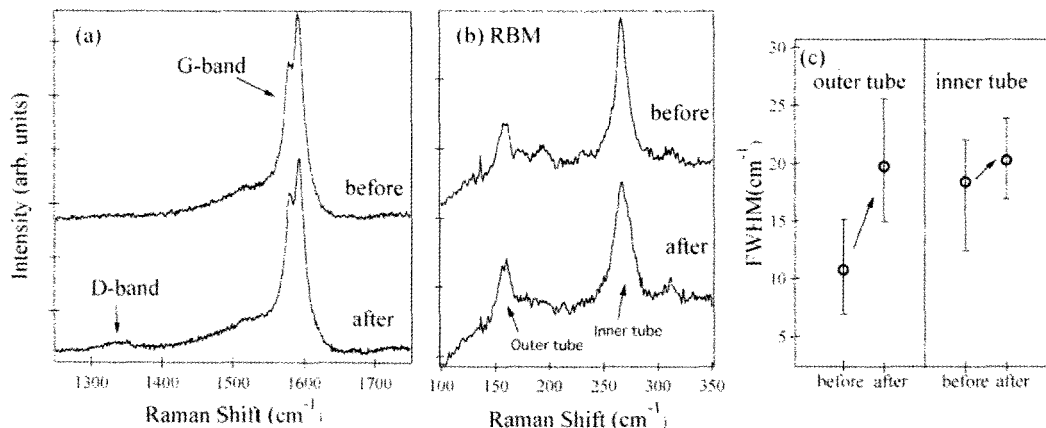


Fig.1. Raman spectra at $\lambda_{ex}=532$ nm for (a)G band, D band and (b)RBM before and after X-ray irradiation, and (c)FWHM estimated by RBM peaks.

[1] C. Itoh, et al., Nuclear Instruments and Methods in Physics Research Section, **266** (2008) 2772

Corresponding Author: T. Murakami

Tel: +81-73-457-8532

E-mail: murakami@sys.wakayama-u.ac.jp

Electrochemical Iodine Doping of SWCNTs

○Shinji Kawasaki, Song Ha Yong, Ayar Al-zubaidi, Yosuke Ishii
Nagoya Institute of Technology, Gokiso, Nagoya 466-8555, Japan

Takenobu Sakai
Toyota Motor Corporation, 1200, Mishuku, Susono 410-1193, Japan

The physical properties of single-walled carbon nanotube (SWNT) bundles doped with halogens and alkali metals exhibit large differences with respect to the undoped pristine material. Among the doped SWCNTs, iodine doped SWCNTs have attracted much interest because the electric conductivity of SWCNTs drastically increase by iodine doping and the I-doped SWCNTs are stable against air. Usually iodine doping of SWCNTs is carried out by immersing SWCNTs in iodine melt in a sealed glass tube. In the present paper, we will show a much easier doping method.

We fabricated a three electrode configuration cell consisting of a SWCNT bucky paper working electrode, an Ag/AgCl reference electrode and a Pt counter electrode. The test cell is immersed in a NaI aqueous solution. By applying 2 V for 1 h, highly iodine doped SWCNTs can be obtained as shown in Fig. 1. As shown in Fig. 1, an intense peak at about 172 cm^{-1} and its overtones are observed after the electrochemical doping treatment. The peak indicates the existence of polyiodine ions (probably I_5^- ion). We can easily control the content of iodine (the doping level) by changing electrolysis duration, electrolyte concentration and applying potential. It should be noted that the doped iodine molecules can be extracted by applying the opposite potential.

In the presentation, we will show very interesting physical properties of the iodine doped SWCNTs in water.

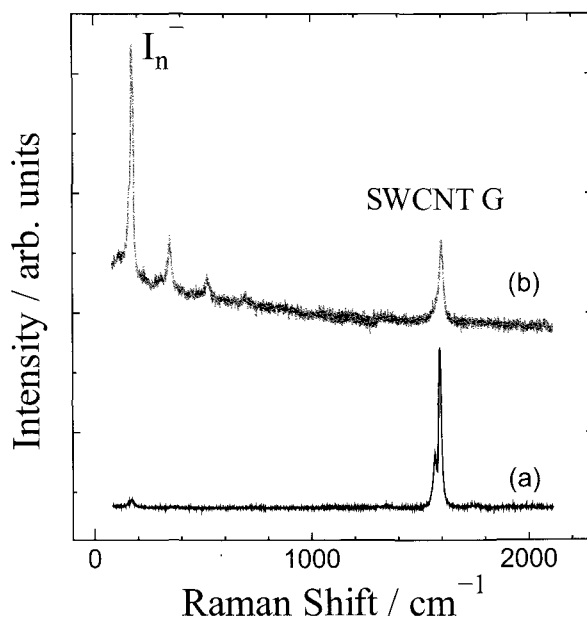


Fig. 1 Raman spectra of (a) pristine and (b) electrochemically I-doped SWCNTs.

Corresponding Author: S. Kawasaki

E-mail: kawasaki.shinji@nitech.ac.jp, Phone & Fax: +81-52-735-5221

Selective Functionalization of Single-Walled Carbon Nanotubes

○Yutaka Maeda¹, Yuri Amagai¹, Junki Higo¹, Jun Matsui², Michio Yamada¹, Tadashi Hasegawa¹, Jing Lu³, Shigeru Nagase⁴, Takeshi Akasaka⁵

¹ Department of Chemistry, Tokyo Gakugei University, Koganei, 184-8501, Japan

² Institute of Multidisciplinary Research for Advanced Materials, Tohoku University, Katahira, Sendai 980-8577, Japan

³ Department of Physics, Peking University, Beijing 100871, People Republic of China

⁴ Fukui Institute for Fundamental Chemistry, Kyoto University, Kyoto 606-8103, Japan

⁵ Life Science Center of Tsukuba Advanced Research Alliance, University of Tsukuba, Tsukuba 305-8577, Japan

The creation of new compounds involving main group elements is currently fascinating subject to discover the unique electronic properties that can be applied as new functional materials. The unique electronic structure of main group element moiety plays a crucial role in characteristic electronic properties and chemical reactivity of organic compounds. Recently, we studied the functionalization of single-walled carbon nanotubes (SWNTs) using organic compounds involving main group elements. Treatment of SWNTs using amine is effective for their individual dispersion and separation of metallic SWNTs. [1] The silylation of SWNTs is effective for the band-gap tuning of SWNTs, which increases field emission properties of SWNTs and enhances the n-type properties of field effect transistors. [2]

In the present work, we report a simple selective functionalization of SWNTs using organosulfur compounds. A THF solution of SWNTs containing organosulfur compound was sonicated in a bath type sonicator for 2 h. The suspension was irradiated under saturated oxygen with a 500W halogen lamp. As shown in Figure 1, characteristic Raman and absorption spectra assigned to metallic SWNTs was decreased after irradiation, which indicates a helicity selective reaction takes place. Prolonged photoreaction showed that not only electronic-type selectivity but also diameter selectivity takes place. In order to clarify the reaction details, the photoreaction of SWNTs with organosulfur compound under various conditions was conducted and these control experiments suggest that the oxygen atom transfer from thioperoxysulfate intermediate, [3] which generated via photoinduced electron transfer, to SWNTs takes place. The XPS spectra of the SWNTs before and after the photoreaction show no peaks attributable to sulfur, though the atomic ratio of C to O ([C]/[O]) in SWNTs is decreased, which supports the oxygenation of SWNTs.

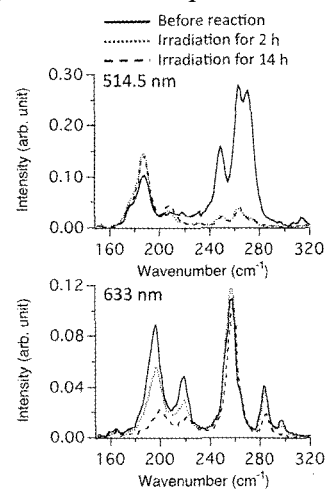


Fig.1 Raman spectra of SWNTs after photoreaction.

[1] Y. Maeda *et al.* J. Am. Chem. Soc. **127**, 10287 (2005). Nanoscale **3**, 1904 (2011). Nano. **7**, 1130001 (2012)

[2] Y. Maeda *et al.* Chem. Mater. **18**, 4205 (2006). R. Kumashiro *et al.* J. Phys. Chem. Solids. **69**, 1206 (2008).

[3] S. Lacombe *et al.* Photochem. Photobiol. Sci. **1**, 347 (2003). Y. Maeda *et al.* Chem. Lett. **40**, 1431 (2011).

Corresponding Author: Y. Maeda

Tel&Fax: +81-42-329-7512

E-mail: ymaeda@u-gakugei.ac.jp

Fabrication of nitrogen substituted single-walled carbon nanotubes by diffusion plasma reaction and their electrical transport properties

○Toshiaki Kato, Koshi Murakoshi, Makoto Akutsu, Rikizo Hatakeyama, Toshiro Kaneko

Department of Electronic Engineering, Tohoku University, Sendai 980-8579, Japan

Nitrogen doped nanocarbon materials such as single-walled carbon nanotubes (SWNTs) and graphene have attracted intense attentions due to their unique physical and chemical features. Up to now, there are many reports relating with the fabrication of nitrogen doped SWNTs and graphene. In the case of graphene, the electrical transport properties can be changed by doping nitrogen from p-type to n-type, which is consistent with the theoretical predictions. Interestingly, however, clear n-type electrical properties have not been observed for nitrogen doped SWNTs. To address this issue, we attempt to fabricate nitrogen doped SWNTs with diffusion plasma reaction and realize n-type SWNTs field effect transistors (FETs).

Nitrogen doping to SWNTs was carried out with in-situ or ex-situ plasma treatment. For the in-situ doping, nitrogen gas was mixed during the growth process of SWNTs under plasma CVD, whereas nitrogen plasma irradiation was performed to SWNTs as a post treatment for ex-situ doping. The properties of SWNTs were measured by Raman scattering spectroscopy, X-ray photoelectron spectroscopy (XPS), and a vacuum probe station under the FET configurations. In the case of ex-situ treatment, the 2D Raman peaks of nitrogen doped SWNTs tend to shift depending on the doping level of nitrogen. The multiple electrical measurements for the same SWNTs-FET device shows that the electrical transport property gradually changes from p-type to n-type with an increase in the post plasma treatment time and clear n-type features are observed after the long time nitrogen plasma treatment. This n-type feature is also observed for nitrogen doped SWNTs fabricated by in-situ doping process. These results indicate that diffusion plasma reaction might create the unique doping structures of nitrogen in SWNTs, which play a role as an electron donor to SWNTs as similar with the case of graphene.

Corresponding Author T. Kato

E-mail: kato12@eccei.tohoku.ac.jp

Tel&Fax: +81-22-795-7046 / +81-22-263-9225

Nucleophilic cycloadditions to C_{70} : Vibronic coupling density analysis for its reactivity

○Naoki Haruta¹, Tohru Sato¹, Kazuyoshi Tanaka¹

¹ Department of Molecular Engineering, Graduate School of Engineering,
Kyoto University, Kyoto, 615-8510, Japan

C_{70} is the second most abundant fullerene. Nucleophilic cycloadditions to C_{70} have been widely studied [1]. Since e_1'' LUMOs of C_{70} are low-lying, C_{70} is a good electron acceptor. According to experimental findings, cycloadditions occur at a-b and c-c bonds (Fig.1). The frontier orbital theory, however, encounters difficulty to predict its regioselectivity since its averaged LUMO density is delocalized over the molecule. In order to overcome this difficulty, we discuss vibronic (electron-vibration) coupling for a reaction mode.

We use the concept of vibronic coupling density (VCD) [2] η_s to explain its regioselectivity:

$$\eta_s(\mathbf{r}) = \Delta\rho(\mathbf{r}) \times v_s(\mathbf{r}),$$

where $\Delta\rho$ is the electron density difference between a neutral state and a charge-transfer (anionized) state, v_s the derivative of the potential acting on a single electron from all the nuclei with respect to the reaction mode s . The integration of η_s gives the strength of vibronic coupling. Based on the Parr and Yang's principle [3], we have proposed that η_s can be regarded as a reactivity index [2]. Recently, the VCD analysis has been shown to be effective to predict the reactivity of C_{60} [4]. Figs.2 (a) and (b) show the reaction mode s and η_s for the $E_1''\theta$ charge-transfer state of C_{70} . a-b and c-c bonds are strongly lengthened, while a-a bonds are strongly shortened. η_s has large distributions on these bonds. The large distributions of η_s on a-b and c-c bonds are similar to ethylene anion (Fig.2 (c)). This result indicates that the C_{70} cage has ethylene moieties as a functional group. On the other hand, η_s has the different type of distributions on a-a bonds since a-a bonds are shortened. This is the opposite direction of the reaction process.

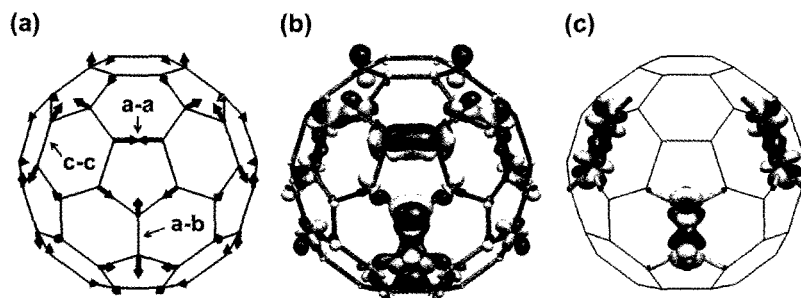


Fig.2 (a) the reaction mode s , (b) η_s for the $E_1''\theta$ anionized state of C_{70} , and (c) η_s for ethylene anion placed on the C_{70} cage.

[1] C. Thilgen, F. Diederich Chem. Rev. **106**, 5049 (2006).

[2] T. Sato *et al.* J. Phys. Chem. A **112**, 758 (2008).

[3] R. G. Parr, W. Yang J. Am. Chem. Soc. **106**, 4049 (1984).

[4] T. Sato *et al.* Chem. Phys. Lett. **531**, 257 (2012).

Corresponding Author: T. Sato

Tel: +81-75-383-2803, Fax: +81-75-383-2556, E-mail: tsato@scl.kyoto-u.ac.jp

Thermodynamic Stability and Exohedral Derivatization of Hepta-Fullerene

○W.-W. Wang, J.-S. Dang, and X. Zhao*

*Institute for Chemical Physics & Department of Chemistry, Faculty of Science,
Xi'an Jiaotong University, Xi'an 710049, China*

Heptagon in carbon sp^2 nano materials (fullerene, graphene, and nanotube) has been treated as an important defect because it can significantly alter the structure and properties of carbon allotropes. Very recently, a new C_{68} fullerene with a 7-membered ring has been captured in the form of chloride $C_{68}Cl_6$ from a carbon arc plasma *in situ* by Tan *et al.*¹ The exciting findings not only imply that the thermodynamically stable hepta-fullerene can be isolated and characterized by saturated with adatoms on reactive sites, but also provides direct and powerful evidence for demonstrating the rationality of the bottom-up growth mechanism in which fullerenes are derive from atomic carbon or small clusters in elevated temperature range.

Herein a systematic investigation² has been performed on the geometries, thermodynamic stabilities, and electronic properties of C_{68} species by using density functional theory (DFT) method. A total of 203435 structures (consist of 6332 classical C_{68} and 197103 hepta- C_{68}) come out from the GSW algorithm program and a hepta- C_{68} (namely by $C_{68_id146:C_7}$) was predicted to be the most thermodynamically favorable framework at elevated temperatures, which accord with the experimental results. In the case of the exohedral derivatives of $C_{68_id146:C_7}$, analyses on geometrical and electronic characteristics of $C_{68}X_6$ (exohedral derivatives of $C_{68_id146:C_7}$; X: H, F, and Cl) were preformed to clarify the stability and chemical properties of hepta-fullerene-based hydride and halogenides. The negative formation energies and rather large HOMO-LUMO gap of the compounds reveal that they are stable derivatives and hydrogenation, fluorination and chlorination are all feasible ways to stabilize the carbon cage. Furthermore, the regioselectivity and addition sequence of six chlorination sites towards $C_{68}Cl_6$ have been elucidated and an optimal pathway is proposed according to the analyses on structural and electronic properties of $C_{68}Cl_n$ ($n:0\sim5$).

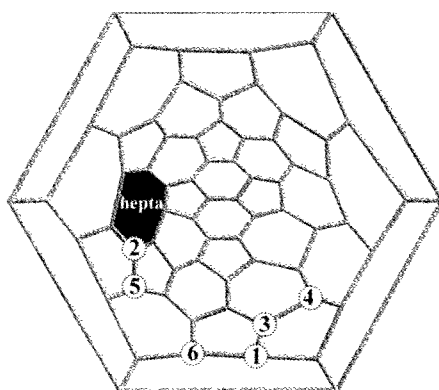


Figure 1. Structure and chlorination sites (numbered as 1-6) of $C_{68_id146:C_7}$.

Reference:

1. Y. Z. Tan, *et al. Nature Comm.* **2011**, 2, 420.
 2. W. W. Wang, J. S. Dang, J. J. Zheng, X. Zhao *J. Phys. Chem. C*, **2012**, 116, in press.
- * Corresponding author: X. Zhao; Email: x86zhao@yahoo.co.jp

Electron-Transfer Reduction of Li Ion Encapsulated Fullerene

○Kei Ohkubo, Yuki Kawashima, Shunichi Fukuzumi

Department of Material and Life Science, Graduate School of Engineering, Osaka University and ALCA, Japan Science and Technology Agency (JST), Suita, Osaka, 565-0871, Japan

Fullerene, which has a highly delocalized three-dimensional π -system, is suitable for efficient electron acceptor because the uptake or release of electrons results in minimal structural and solvation changes upon electron transfer. The reorganization energy of electron-transfer reduction of pristine I_h - C_{60} has been determined from the driving force dependence of electron-transfer reduction rate constants of C_{60} with various π -electron donors [1]. Endohedral fullerenes have recently gained increased attention with regard to the potential applicability due to the specific reactivities. However, there has been no report on the systematic comparison between reactivities of electron-transfer reduction of endohedral fullerene and C_{60} . We report herein the electron transfer reactivities between lithium encapsulated fullerene, $Li^+@C_{60}$, and electron donors.

Upon nanosecond laser excitation at 430 nm of a benzonitrile (PhCN) solution $Li^+@C_{60}$, a transient triplet-triplet (T-T) absorption spectrum is observed with $\lambda_{max} = 740$ nm. The T-T absorbance decays obeying first-order kinetics without T-T annihilation. The addition of 1,4-dimethoxybenzene to a solution of $Li^+@C_{60}$ in benzonitrile (PhCN) results in electron transfer from 1,4-dimethoxybenzene to the triplet excited state of $Li^+@C_{60}$ [$^3(Li^+@C_{60})^*$] to produce 1,4-dimethoxybenzene radical cation ($\lambda_{max} = 430$ nm) and $Li^+@C_{60}^{\cdot-}$ ($\lambda_{max} = 1035$ nm [2, 3]). The k_{et} values for electron transfer from electron donors to the triplet excited states of $Li^+@C_{60}$ and pristine C_{60} were determined by using various electron donors, (Fig. 1). The rate constants of photoinduced electron transfer of $Li^+@C_{60}$ are significantly larger than those of C_{60} when the rate constants less than the diffusion-limited value are compared at the same E_{ox} values of electron donors. Particularly, the k_{et} value of electron transfer from 1,4-dimethoxybenzene ($E_{ox} = 1.21$ V vs SCE) to $^3(Li^+@C_{60})^*$ ($2.7 \times 10^9 M^{-1} s^{-1}$) is 390 times faster than that to $^3C_{60}^*$ ($6.9 \times 10^6 M^{-1} s^{-1}$).

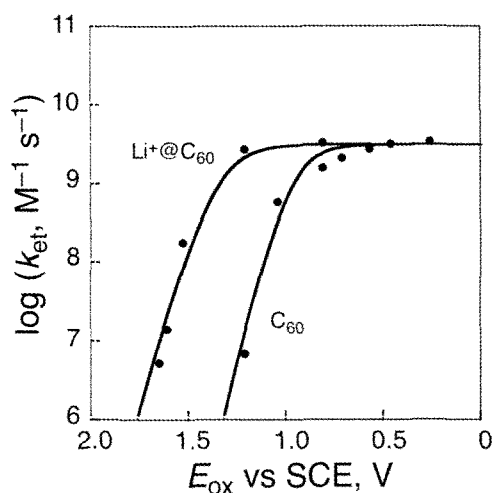


Fig. 1 Plots of $\log k_{et}$ vs the one-electron oxidation potentials of electron donors (E_{ox}) for electron transfer from various electron donors to $^3(Li^+@C_{60})^*$ and $^3C_{60}^*$ in PhCN.

[1] S. Fukuzumi and K. Ohkubo *et al. Chem. Eur. J.* **9**, 1585 (2003).

[2] S. Fukuzumi and K. Ohkubo *et al. J. Am. Chem. Soc.* **133**, 15938 (2011).

[3] K. Ohkubo, Y. Kawashima, S. Fukuzumi *Chem. Commun.* **48**, 4314 (2012).

Corresponding Author: K. Ohkubo

Tel: +81-6-6879-7369, Fax: +81-6-6879-7370,

E-mail: ookubo@chem.eng.osaka-u.ac.jp

Rapid Separation of Metallofullerenes by Titanium Chloride

○Kazuhiko Akiyama¹, Erina Takeuchi¹, Zhiyong Wang², Kazuki Chiba¹, Yusuke Nakanishi², Shoko Noda², and Hisanori Shinohara²

¹ Grad. School of Sci. and Eng., Tokyo Metropolitan Univ., Hachioji, 192-0397, Japan

² Dept. of Chem. & Inst. for Advanced Research, Nagoya Univ., Nagoya 464-8602, Japan

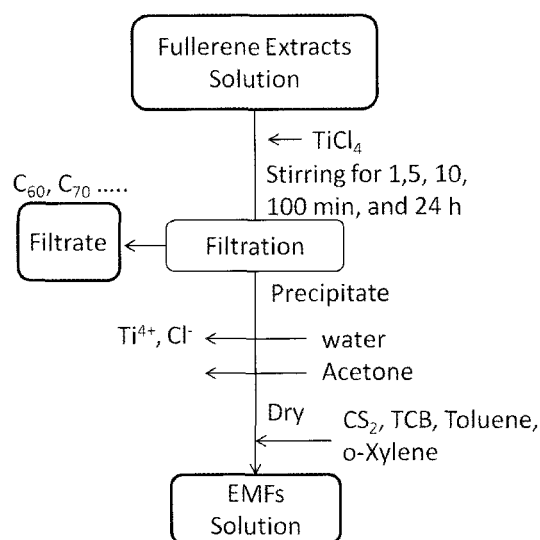
Endohedral Metallofullerenes (EMFs) are one of the promising materials for the applications in electronics and biomedicine due to their interesting electronic properties and novel molecular structures. However, the applications of EMFs have not sufficiently been developed because of the difficulties in the separation and purification of EMFs. To overcome these difficulties, several separation and purification techniques using the redox properties of EMFs have been reported. Recently, Bolsker and coworker reported that Gd metallofullerenes is effectively separated from empty fullerenes by using strong oxidant of AlCl_3 . [1] However, it was found that only about 60% of EMFs was recovered and remained 40% of metallofullerenes was lost. [2] Here, we report that TiCl_4 is more effective oxidant for the EMFs separation and EMFs can be rapidly separated from empty fullerenes, typically within 1 min by using TiCl_4 as oxidant.

Lanthanum (La) EMFs were prepared by arc discharge method. Crude fullerene extracts containing EMFs were extracted from generated soot by 1,2,4-trichlorobenzene (TCB). EMFs were separated by the manner as shown in scheme 1. The contents of La EMFs in the “filtrate” and “EMFs solution” were determined by the comparison of the HPLC peak intensities at the retention time of $\text{La}@C_{82}$ for each sample with those for original “fullerene extracts solution”.

Figure 1 shows the separation efficiency of La EMFs estimated from HPLC analysis for each solvent used for the separation and each reaction time. As shown in the figure, EMFs was effectively separated from empty fullerenes with less than 10 min of reaction time with TiCl_4 , but separation efficiency was decreased with increase of reaction time.

[1] J. W. Raebiger *et al.* *J. Phys. Chem. C*, **112**, 6605 (2008).

[2] a) T. Hamano *et al.* The 41st FNTG General Symposium, 2P-33 (2011). b) K. Akiyama *et al.* *J. Am. Chem. Soc.*, **134**, 9762 (2012). Corresponding Author: Kazuhiko Akiyama, E-mail: kakiyama@tmu.ac.jp



Scheme 1. Separation Scheme of EMFs

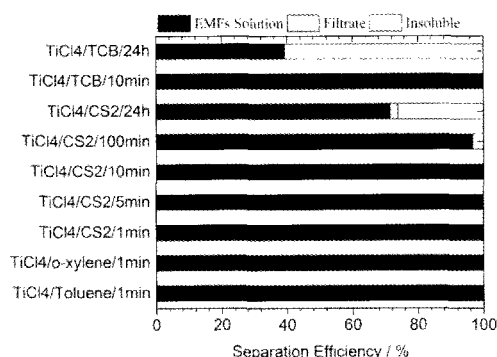


Figure 1. Separation Efficiency of La EMFs

Crystalline characteristics of fullerene doped GaAs layers grown by MBE

○Jiro Nishinaga^{1,2}, Yoshiji Horikoshi¹

¹ Waseda Institute for Advanced Study, Waseda University, 1-6-1 Nishiwaseda, Shinjuku, Tokyo 169-8050, Japan

² PRESTO, JST, 4-1-8 Honcho Kawaguchi, Saitama, 332-0012, Japan

Fullerene C₆₀ molecules crystallize into a face-centered cubic structure on crystalline substrates such as Si and GaAs, and C₆₀ molecules have a spherical structure with a diameter of 1.0 nm, which is much larger than those of Ga and As atoms. Nevertheless, we found that C₆₀ molecules are absorbed on specific sites of GaAs surfaces, and these sites are determined by a three-dimensional relationship between C₆₀ molecules and surface reconstruction of the substrates [1]. This finding implies that C₆₀ molecules are incorporated into GaAs lattices without deterioration of the crystalline quality, and C₆₀ molecules act as quantum dots with excellent size uniformity. Indeed, we have successfully fabricated C₆₀ uniformly doped and δ -doped GaAs layers by a migration enhanced epitaxy (MEE) method, and the layers are confirmed to have good crystalline quality by TEM measurements [2]. C₆₀ uniformly doped GaAs layers show highly resistive characteristics and Raman peaks from doped C₆₀ molecules are confirmed. These results suggest that C₆₀ molecules cannot be decomposed into isolated carbon atoms and they behave as if they were electron traps or distinct recombination centers.

In this study, to investigate the electron traps induced by incorporation of C₆₀, we fabricate C₆₀ uniformly doped GaAs layers by MEE method. The photoconductivity spectra are measured with illumination of wavelength range between 600 and 1100 nm.

Figure 1 shows photoconductivity spectra of the C₆₀ doped GaAs layer measured at 4.2 K. The photoconductivity peak appears around the GaAs bandgap energy (E_g, 820 nm). However, the signal also appears even when the below-bandgap excitation. The peak around 1000 nm is observed only in the C₆₀ doped GaAs layers, implying that the resonant excitation between C₆₀ trap level and GaAs occurs. Figure 2 shows the band structure profile of the C₆₀, Si codoped GaAs layer under illumination with energy below E_g. The electron transitions from the valence band to the C₆₀ trap levels and from the C₆₀ trap levels to the conduction band may occur simultaneously.

[1] J. Nishinaga *et al.* Jpn. J. Appl. Phys. **48**, 025502 (2009).

[2] J. Nishinaga *et al.* J. Cryst. Growth. **323**, 135 (2011)

Corresponding Author: J. Nishinaga

Tel: +81-3-5286-3797, Fax: +81-3-5286-3797,

E-mail: jiro247@aoni.waseda.jp

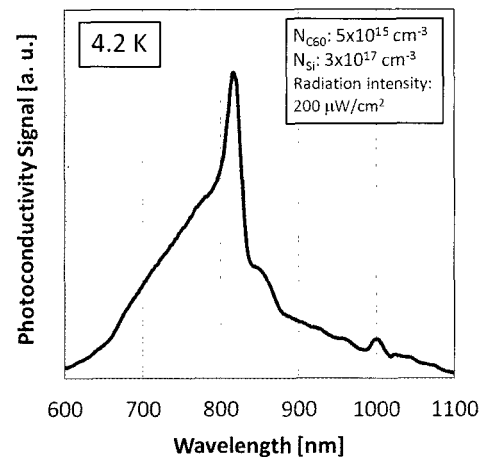


Fig.1 Photoconductivity spectra of C₆₀ doped GaAs.

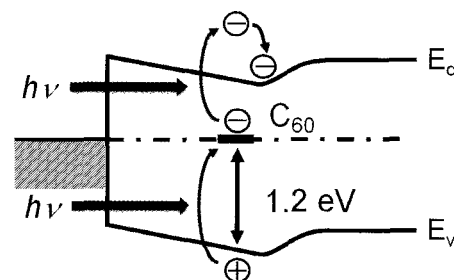


Fig.2 Band structure profile of C₆₀ doped GaAs.

Structural effect of fullerene derivatives with phosphonic ester in organic photovoltaic devices.

○Shogo Miura¹, Jaebuem Oh², Misun Ryu², Haeseong Lee^{2,3}, Jin Jang⁴,
Chyongjin Pac^{1,5}, and Hiroshi Moriyama*¹

¹Dept. of Chemistry, Toho University, Miyama 2-2-1, Funabashi 274-8510, Japan

²TAKOMA Technology Co., Ltd., Nosung-myeon, Nonsan-city, Chungnam, 320-922, Korea

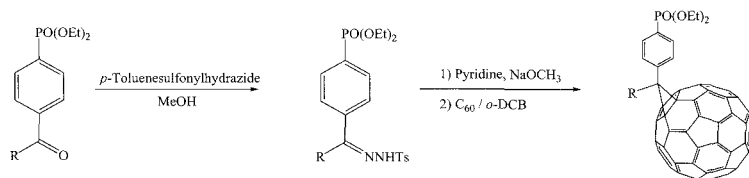
³Dept. of Advanced Materials Jeonju University, Wansangu Jeonju, 560-759, Korea

⁴Dept. of Information Display, Kyung Hee University, Dongdaemun-ku, Seoul, 130-171, Korea

⁵Dept. of Materials Chemistry, Korea University, Sejong Jochiwon, Chung-Nam 339-700, Korea

Bulk heterojunction (BHJ)-type organic photovoltaic (OPV) cells have attracted attention because they can be expected to be a promising next-generation solar cell. BHJs are composed of blends of conjugated polymer, such as poly-3-hexyl thiophene (P3HT) and fullerene derivatives. [6,6]Phenyl-C₆₁-butyric acid methyl ester (PCBM) is recognized as one of the most important electron acceptors so far used in OPVs. For the P3HT/PCBM system, high power conversion efficiency (PCE) has been achieved by device optimization.

In this study, we newly designed and synthesized three electron acceptors analogous to PCBM by considering solubility and morphology. The synthetic scheme for these fullerene derivatives with phosphonic ester is based on those of PCBM [1–3] as shown below.



The three electron acceptors, (MPPE, HPPE, and DPPE) have the same skeleton with different alkyl chains (R = CH₃, C₆H₁₃, and C₁₂H₂₅, respectively).

We fabricated OPV devices using the new electron acceptors and P3HT, and compared their PCEs with those of P3HT/PCBM. It can be noted that the fullerene derivative with the shorter alkyl chain showed higher J_{sc} , and it was shown that the shorter chain exhibited the higher PCE. The affinity between electron donor and electron acceptor seems to play an important role for higher PCE, judging from their parameters.

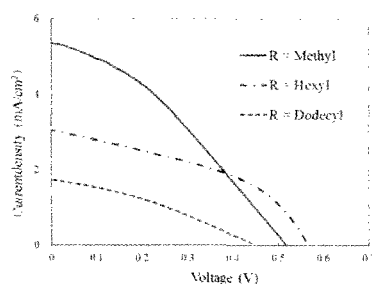


Table 1. Photovoltaic parameters using novel C₆₀ derivatives.

	J_{SC} (mA/cm ²)	V_{OC} (V)	FF	PCE (%)
MPPE (R = CH ₃)	5.47	0.528	33.8	0.98
HPPE (R = C ₆ H ₁₃)	3.07	0.557	42.5	0.74
DPPE (R = C ₁₂ H ₂₅)	1.75	0.453	32.7	0.26

Figure 1. J - V characteristics of the devices fabricated with P3HT and novel C₆₀ derivatives.

[1] J. C. Hummelen, B. W. Knight, F. LePeq, F. Wudl, J. Yao, C. L. Wilkins, *J. Org. Chem.* **1995**, *60*, 532–538. [2] L. J. Goossen, M. K.

Dezfuli, *Synlett.*, **2005**, *3*, 445–448. [3] B. Scheiper, M. Bonnekessel, H. Krause, A. Furstner, *J. Org. Chem.*, **2004**, *69*, 3943–3949.

Corresponding Author : Hiroshi Moriyama

TEL: +81-47-472-1211, FAX: +81-47-476-9449, E-mail: moriyama@chem.sci.toho-u.ac.jp

A New Generation of Cu–CMP Slurry using Water-Soluble Fullerenol

○Ken Kokubo¹, Terutake Hayashi², Hiroki Tanada², Hideyuki Tachika², Hirotaka Kishida², Kazumasa Kano², Ryota Murai², Masaki Michihata², Takumi Oshima¹, and Yasuhiro Takaya²

¹*Division of Applied Chemistry, Graduate School of Engineering, Osaka University*

²*Department of Mechanical Engineering, Graduate School of Engineering, Osaka University, Suita, Osaka 565-0871, Japan*

Polyhydroxylated fullerene, so-called fullerenol, has attracted much attention in the field of life science and materials chemistry in view of its high water solubility, high antioxidant activity, antimicrobial activity, anti-inflammatory, unique conductivity, and so on. To conduct these studies in a systematic way, a series of fullerenols having various numbers of hydroxyl groups has been desired, and thus we have synthesized novel highly hydroxylated fullerenols with 36–44 hydroxyl groups by a facile H₂O₂ method [1]. Interestingly, the particle size analysis of these fullerenols in water showed a narrow distribution at ca. 1 nm, suggesting the single dispersion with their molecular size.

In recent years, chemical mechanical polishing (CMP), a polishing technology in which both chemical reaction on the surface of wafer induced by chemical additives and the mechanical removal by abrasive grains in the slurry are involved, has become a key and the essential technology to achieve ultra-high-density integrated circuits, ULSI, on semiconductor devices with multilayer interconnections. However, the desirable continuing reduction in the design rule has necessitated abrasive grains having a smaller size than conventional ones.

In our study, the water-soluble fullerenol was employed as abrasive grains for use in the Cu–CMP slurry and indeed the slurry showed high planarization efficiency, which improved the roughness of copper wafer surface from ca. 10 nm RMS to less than 0.5 nm [2]. The role of fullerenol on copper removal in Cu–CMP process was also investigated to elucidate the removal mechanism. In this presentation, we will review our recent progress on a novel application of the fullerenols to Cu–CMP technology. The detailed results on Cu–CMP and the proposed mechanism of the nano-level planarization using water-soluble fullerenols will be presented.

[1] Kokubo, K. *et al. ACS Nano* **2008**, 2, 327; Kokubo, K. *et al. Nano Res.* **2011**, 4, 204.

[2] Takaya, Y. *et al. CIRP Ann-Manuf. Technol.* **2009**, 58, 45; Takaya Y. *et al. CIRP Ann-Manuf. Technol.* **2011**, 60, 567.

Corresponding Author: Ken Kokubo

TEL: +81-6-6879-4592, FAX: +81-6-6879-4593, E-mail: kokubo@chem.eng.osaka-u.ac.jp

Preparation and photophysical properties of chemically converted graphene covalently functionalized with porphyrins

○Tomokazu Umeyama^{1,2}, Junya Mihara¹, Hiroshi Imahori^{1,3}

¹ Graduate School of Engineering, Kyoto University, Kyoto, 615-8510, Japan

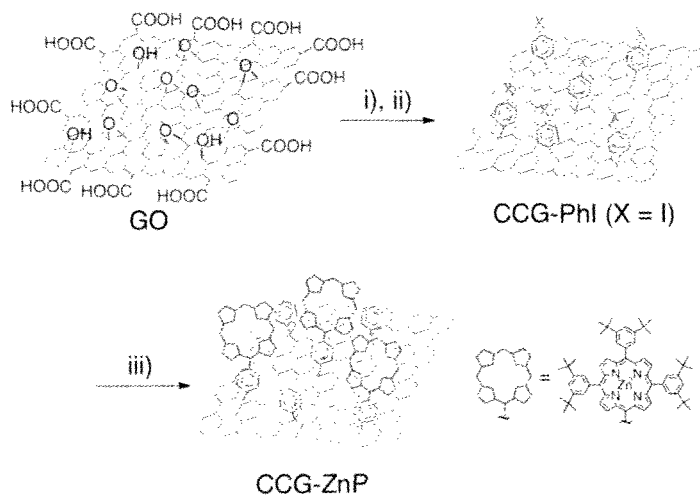
² PRESTO, Japan Science and Technology Agency (JST), Kawaguchi, 332-0012, Japan

³ Integrated Cell-Material Sciences (WPI-iCeMS), Kyoto University, Kyoto, 615-8510, Japan

The functionalization of graphenes with large aromatic molecules is expected to modulate the electronic and optical properties of graphenes by the interactions between the two components in the ground and excited states. In this study, we prepared chemically-converted graphene (CCG) covalently functionalized with porphyrins with a short rigid phenylene spacer (CCG-ZnP) and investigated the optical and photophysical properties in detail [1].

CCG-ZnP was synthesized according to the two-step functionalization procedure as shown in Scheme 1. First, surfactant-wrapped CCG was prepared by chemical reduction of graphene oxide (GO) and reacted with *p*-iodophenyl diazonium salt in aqueous solution to yield pre-functionalized CCG with *p*-iodophenyl groups (CCG-PhI). Then, Suzuki coupling reaction of CCG-PhI with porphyrin boronic ester gave CCG-ZnP. In steady-state photoluminescence spectra, the emission from the porphyrin linked to the CCG was quenched strongly relative to that of the porphyrin reference.

Fluorescence lifetime and femtosecond transient absorption measurements of the CCG-ZnP revealed short-lived porphyrin singlet excited state (38 ps) without yielding the porphyrin radical cation, substantiating the occurrence of energy transfer from the porphyrin excited state to the CCG and subsequent rapid decay of the CCG excited state to the ground state. Consistently, the photocurrent action spectrum of a photoelectrochemical device with a SnO₂ electrode coated by CCG-ZnP exhibited no photocurrent response from the porphyrin absorption.



Scheme 1. Preparation of CCG-ZnP. i) SDS, N₂H₄·H₂O, NH₃ aq., 95°C, 1h; ii) 4-iodobenzenediazonium tetrafluoroborate, H₂O, room temperature, 2h; iii) 5,10,15-tris(3,5-di-*t*-butylphenyl)-20-(4,4,5,5-tetramethyl[1,3,2]di-oxaborolan-2-yl)porphyrinatozinc(II), Pd(PPh₃)₄, Cs₂CO₃, DMF, 90 °C, 24h.

[1] T. Umeyama, J. Mihara, N. Tezuka, Y. Matano, K. Stranius, V. Chukharev, N. V. Tkachenko, H. Lemmetyinen, K. Noda, K. Matsushige, T. Shishido, Z. Liu, K. Hirose-Takai, K. Suenaga, H. Imahori, *Chem. Eur. J.* **18**, 4250 (2012).

Corresponding Author: T. Umeyama

Tel: +81-75-383-2568, Fax: +81-75-383-2571

E-mail: umeyama@scl.kyoto-u.ac.jp

Water-soluble graphene through polyglycerol grafting

○Toku Yasuda^{1,2}, Li Zhao², Liu Gang², Shuji Aonuma¹, Takahide Kimura², Naoki Komatsu²

¹ Department of Materials Chemistry, Osaka Electro-Communication University, Osaka, 572-8530, Japan

² Department of Chemistry, Shiga University of Medical Science, Otsu, 520-2192, Japan

For applications of nanocarbons in biology and medicine, such as imaging probe and drug carrier, they have to be well solubilized in a physiological environment. In this context, surface chemical functionalization has been extensively investigated to impart strong hydrophilicity to nanocarbons. We found recently that polyglycerol (PG) grafting on the surface of nanodiamond (ND) made the ND highly soluble in a phosphate buffer [1]. The aqueous solution is very stable for months and the solubility of the PG-functionalized ND (ND-PG) is as high as 16 mg/mL in phosphate buffer saline (PBS), which is 400 times larger than that of the PEG-functionalized ND [2]. In this paper, we will present our recent result of PG grafting of graphene through ring-opening polymerization of glycidol to prepare PG-functionalized graphene (PG-G) soluble in pure water. We carried out the PG-functionalization of graphene under similar reaction conditions to those of the ND-PG [1], but used commercial graphene as a starting material. The aqueous solution is also very stable for weeks and the solubility of PG-G is 1.4 mg/mL in pure water (Fig. 1). PG-G was characterized by UV, IR, and Raman spectroscopies, and scanning transmission electron microscopy (STEM, Fig. 2). As a result, few layer graphenes are found to be dominant in PG-G.

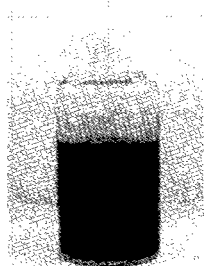


Fig. 1 polyglycerol-functionalized graphene in water



Fig. 2 STEM images of polyglycerol-functionalized graphene

- [1] L. Zhao, T. Takimoto, M. Ito, N. Kitagawa, T. Kimura, N. Komatsu, *Angew. Chem. Int. Ed.*, **50**, 1388 (2011).
 [2] T. Takimoto, T. Chano, S. Shimizu, H. Okabe, M. Ito, M. Morita, T. Kimura, T. Inubushi, N. Komatsu, *Chem. Mater.*, **22**, 3462 (2010).

Corresponding Author: Naoki Komatsu

Tel: +81-77-548-2102, Fax: +81-77-548-2405, E-mail: nkomatsu@shiga-med.ac.jp

Utilizing graphene FET device for GHz transport and THz detection

Akram Mahjoub¹, T. Abe¹, Y. Iso¹, T. Ouchi¹, S. Suzuki¹, H. Fukuda¹, N. Aoki¹,
K. Miyamoto¹, T. Omatsu¹, J. P. Bird², D. K. Ferry³, K. Ishibashi⁴, and Y. Ochiai¹

¹Graduate School of Advanced Integration Science, Chiba University, 263-8522, Japan

²Department of Electrical Engineering, University at Buffalo, SUNY, NY 14216, USA

³Department of Electrical Engineering, The Arizona State University, AZ 85287-5706, USA

⁴Advanced Device Laboratory, Institute of Physical and Chemical Research (RIKEN), Japan

The graphene had become one of the well-known carbon nanomaterials. With its unique structure and performance, a new way to look at quantum interference phenomena has become visible to us [1], thus makes it the ultimate two dimensional conductor. A single sheet of carbon atoms arranged into a hexagonal honeycomb crystal structure, with outstanding electrical, optical and thermal properties. The absolutely unique band structures that express the coexistence of band energies and massless Dirac fermions provides this material with quality to observe several new quantum coherent interference phenomena. With such properties, graphene material is showing a great tendency for microwave applications. The massless carrier's transport behavior, the thermal and optical properties combined together, makes this material as one of the great candidates for THz sensing devices. The terahertz (THz) region of the electromagnetic spectrum is of great interest for wide range of applications. The realization of THz spectral-imaging systems for applications of such devices requires frequency-tunable compact sources and detectors are needed the most. Alongside the associated massless carrier's transport properties of grapheme the unique band structure, make this material of an ideal interest for high frequency application and opens the means of utilizing this material as broadly tunable sensors [2], for specific application in the THz regime. The gap-less spectrum characteristic of single-layer graphene, as well as the small elusive gap that appears in the bi-layer grapheme, is ideally well matched to the low (meV) energy of photons in the THz regime [3], therefore it is in a high marked contrast to conventional semiconductors whose relevant band gaps are typically several orders of larger magnitudes.

Our experiment reveals the interplay of different photo-response mechanisms, primarily involving rectification of and due to THz radiation in the presence of non-linearity as well as bolometric effect. The study provides a valuable framework to analyze the photo-response of graphene THz sensor. The observation of another effect on bolometric responses shows a strong tendency for many applications.

[1] Y.Ujiiie, S. Motooka, T. Morimoto, N. Aoki, D. K. Ferry, J. P. Bird, and Y. Ochiai, *J. Phys.: Cond. Matt.*, 21, pp. 382202, (2009).

[2] A. Mahjoub, S. Motooka, N. Aoki, J. Song, J. P. Bird, Y. Kawano, D. K. Ferry, K. Ishibashi, and Y. Ochiai, *J. J. A. P.*, 50, pp. 070119, (2011).

[3] J. W. Song, G. R. Aizin, J. Mikalopas, Y. Kawano, K. Ishibashi, N. Aoki, J. L. Reno5, Y. Ochiai, and J. P. Bird, *Appl. Phys. Lett.*, 97, pp. 083109, (2010).

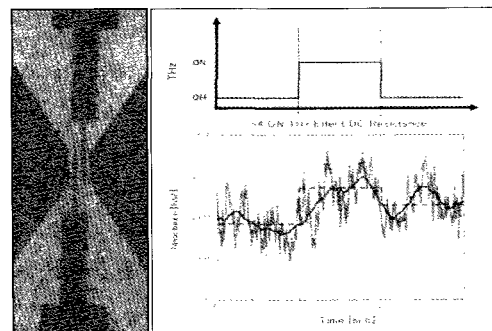


Fig.1: The observed response due to the THz .

Synthesis of carbon nanosheet films from a solid carbon source and their applications to solar cell

○Z. Wang¹, M. Shoji², T. Ito², H. Ogata^{1,2,3}

¹*Institute for Sustainability Research and Education, Hosei University, fujimi, 02-8160, Japan*

²*Graduate School of Engineering, Hosei University, koganei, 184-8584, Japan*

³*Research Center for Micro-Nano Technology, Hosei University, koganei, 184-0003, Japan*

Due to their excellent mechanical, physical, electronic properties, carbon materials, such as nanotubes and graphene, have attracted great attention in many fields of electronic devices, catalyst supports, lithium ion batteries, supercapacitors, biosensors, and solar cells. Especially, solar cell composing of carbon nanotubes (CNTs) or graphene have been extensively investigated. For instance, Wei et al. employed double-walled CNTs with n-type silicon to build conventional p-n junctions with a PCE of >1 % [1], and subsequently optimized the fabrication process of CNT-Si solar cells with the PCE of about 7 % [2]. Additionally, Jia et al. inserted a thin oxide layer into the CNT-Si interface to create a CNT-oxide-Si heterojunction solar cell with higher PCE of above 10 % [3]. Li et al. also deposited graphene sheets on n-Si wafer to form Schottky junction solar cell with the efficiencies up to 1.5 % [4]. Miao et al. further improve the PCE of graphene/n-Si Schottky junction solar cell to reach 8.6 % by chemical doping [5]. Besides CNTs and graphene, carbon nanosheets (CNSs), which consist of few-layer graphene sheets and vertically stand on the substrates, may be contributed to those heterojunction solar cells because of their controllability of the carrier type and concentration by doping [6]. Although the CNSs with porous structures have lower conductivity than graphene, they also possess higher transmittance and faster electron transfer due to their special structures.

Here, we explore the CNSs as the energy conversion material to construct heterojunction solar cell. The CNSs used in this study were grown on the permalloy (45 % Ni and 55 % Fe, 10 mm × 25 mm × 20 μm) foils by microwave plasma enhanced chemical vapor deposition (MPECVD) with a solid carbon source. From the observation of SEM and TEM images shown in Fig. 1a and b, the as-synthesized CNSs have thinner and more uniform layers than those previously obtained from a gaseous carbon source by MPECVD technique [7]. The CNSs on the permalloy foils can be easily transferred to any substrates, as shown in Fig. 1c. Fig. 1d shows the dark current-voltage characteristic of a CNS-Si diode. The detailed results will be presented in the coming conference.

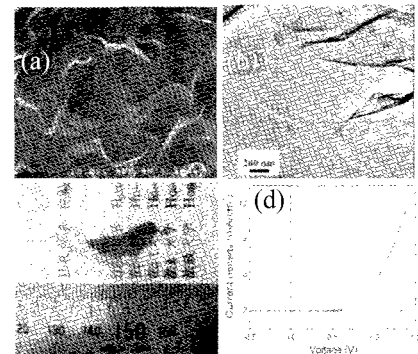


Fig. 1 Typical SEM (a) and TEM (b) images of the CNSs on the permalloy foil by MPECVD technique from a solid carbon source. (c) Optical image of CNSs on a glass dish. (d) Dark I-V characteristic of a CNS-Si diode.

[1] J. Wei *et al.*, *Nano Lett.* **7**, 2317 (2007). [2] Y. Jia *et al.*, *Adv. Mater.* **20**, 4594 (2008). [3] Y. Jia *et al.*, *Appl. Phys. Lett.* **98**, 133115 (2011). [4] M. Li *et al.*, *Adv. Mater.* **22**, 2743 (2010). [5] X. Miao *et al.*, *Nano Lett.* **12**, 2745 (2012). [6] W. Takeuchi *et al.*, *Appl. Phys. Lett.* **92**, 213103 (2008). [7] Z. Wang *et al.*, *Appl. Surf. Sci.* **257**, 9082 (2011).

Corresponding Author: H. Ogata. Tel/fax: +81-42-387-6229. E-mail: hogata@hosei.ac.jp.

Synthesis of Endohedral Fullerene C₆₀ Encapsulating a Single Molecule of Water

○Kei Kurotobi¹ and Yasujiro Murata²

¹*iCeMS, Kyotodaigaku-katsura, Nishikyo-ku, Kyoto 615-8510, Japan*

²*Institute for Chemical research, Kyoto University, Gokasho, Uji 611-0011, Japan*

A single water molecule within a confined subnano space is one of the important topics in both material and life sciences, in the point of a demonstration of its fundamental properties compared with bulk water. But water usually exists in hydrogen-bonded environments, so a single molecule of H₂O that is completely isolated is rare so far.

The inner space of the fullerene C₆₀ is suitable to entrap a water molecule. When atoms or molecules are encapsulated in fullerenes, it is often possible to control the properties of the outer carbon cage as well as to study the isolated species. Endohedral fullerenes encapsulating a wide variety of species, such as metal ions and rare gases, have been synthesized with physical methods under harsh conditions.[1] However, these methods are not suitable to obtain endohedral fullerenes encapsulating small molecules.

The molecular surgical approach,[2] involving creation of an opening on the empty fullerene cage, insertion of a small guest through the opening, and closure of the opening with retention of the guest, is a promising method to synthesize yet-unknown endohedral fullerenes.

In order to realize endohedral fullerenes encapsulating a water molecule, which is biggest molecule among such guests, creation as well as restoration of a larger orifice is needed. Herein we report the first organic synthesis of H₂O@C₆₀ with the dynamic control of the opening size under mild conditions. [3]

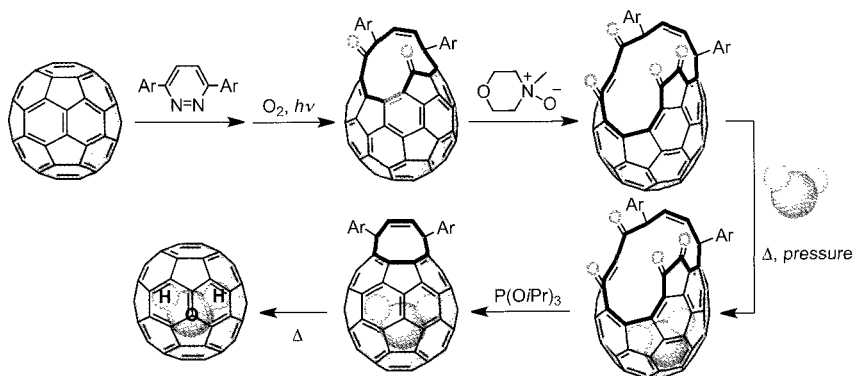


Fig.2 Synthetic route of H₂O@C₆₀.

References:

- [1] T. Akasaka and S. Nagase, Eds., *Endofullerenes: A New Family of Carbon Clusters* (Kluwer Academic, Dordrecht, 2002).
 [2] (a) K. Komatsu, *et al. Science*, **2005**, 307, 238. (b) M. Murata, *et al. J. Am. Chem. Soc.*, **2006**, 128, 8024.
 [3] K. Kurotobi, Y. Murata, *Science*, **2011**, 333, 613.

Corresponding Author: K. Kurotobi
 Tel: +81-75-383-2809, Fax: +81-75-383-2571,
 E-mail: kurotobi@scl.kyoto-u.ac.jp

Chemistry of Cation-Endohedral Fullerene: [Li⁺@C₆₀]

○Hiroshi Okada¹, Masashi Maruyama¹, Takashi Komuro², Takahito Watanabe²,
Yasuhiko Kasama³, Hiromi Tobita², Yutaka Matsuo¹

¹ Department of Chemistry, School of Science, The University of Tokyo,
Tokyo, 113-0033, Japan

² Department of Chemistry, Graduate School of Science, Tohoku University,
Sendai 980-8578, Japan

³ Idea International Corporation, Sendai 980-8579, Japan

Endohedral fullerenes are particularly attractive nanocarbon materials. One of the most intriguing points is a change of properties by encapsulating *something*. From this point of view, C₆₀-based endohedral metallofullerenes (M@C₆₀s) are the best materials to examine the contrasts between metal-encapsulated and empty fullerene, because of the generality of C₆₀. Several groups challenged to synthesize and isolate M@C₆₀s, but complete isolation and structure determination had not been reported until our group succeeded in the structural analysis of lithium endohedral C₆₀ (Li@C₆₀) as its cation salt [1, 2].

Li@C₆₀ was synthesized by ion-implantation technique in a vacuumed chamber. Complete separation from a mixture with empty C₆₀ by extraction or HPLC technique was unsuccessful. We presumed that the strong interaction caused by an electron transfer exists between Li@C₆₀ and C₆₀, and, thus, tried chemical oxidation of Li@C₆₀ by ammoniumyl cation, [(4-BrC₆H₄)₃N](SbCl₆). This approach successfully gave the cationic salt, [Li@C₆₀](SbCl₆). We were also able to purify the cation by electrolyte-added HPLC to obtain the PF₆ salt, [Li@C₆₀](PF₆). NMR and UV-vis spectra of Li@C₆₀ cation indicated that the cation consists of a neutral C₆₀ cage and an encapsulated Li cation, formulated by [Li⁺@C₆₀].

Next, we started chemical functionalizations of [Li⁺@C₆₀], and a targets was covalently modified [Li⁺@C₆₀]. One of the most popular fullerene derivatives, PCBM ([6,6]-phenyl-C61-butyric acid methyl ester) [3], was chosen as a container of Li⁺ ion. Thus, [Li⁺@C₆₀](PF₆)⁻ smoothly reacted with a diazoalkane (PhC(=N₂)CH₂CH₂CH₂COOMe) to afford 5,6-opened isomer, [5,6]-[Li@PCBM]PF₆⁻, which then thermally isomerized to 6,6-closed isomer, [6,6]-[Li@PCBM]PF₆⁻ [4]. Another target of chemical functionalizations was transition metal complexes of [Li⁺@C₆₀]. We found that [Li⁺@C₆₀] formed stable complexes with electron-rich metal fragments, IrCl(CO)(PPh₃)₂ or Pt(PPh₃)₂, which are also known to be coordinated by C₆₀ [5, 6]. In both chemical modifications, significant differences of reactivity between [Li⁺@C₆₀] and C₆₀ were observed.

[1] S. Aoyagi *et al.* Nature Chem. **2**, 678 (2010).

[2] S. Aoyagi *et al.* Angew. Chem. Int. Ed. **51**, 3377 (2012).

[3] J. C. Hummelen *et al.* J. Org. Chem. **60**, 532 (1995).

[4] Y. Matsuo *et al.* Org. Lett., in press.

[5] L. Balch *et al.* Inorg. Chem. **30**, 2940 (1991).

[6] P. J. Fagan *et al.* Science **252**, 1160 (1991).

Corresponding Author: H. Okada

Tel: +81-3-5841-1371, Fax: +81-3-5841-1371

E-mail: h_okada@chem.s.u-tokyo.ac.jp

Establishment of intra-molecular electron accepting and donating systems based on endohedral metallofullerenes

○Yuta Takano^{1,2}, Naomi Mizorogi², M. Angeles Herranz³, Nazario Martin³, Dirk M. Guldi⁴, Shigeru Nagase⁵ and Takeshi Akasaka²

¹ Institute for Integrated Cell-Material Sciences (WPI-iCeMS), Kyoto University, Kyoto, 615-8510, Japan

² Life Science Center of Tsukuba Advanced Research Alliance (TARA Center), University of Tsukuba, Tsukuba, 305-8577, Japan

³ Department of Organic Chemistry I, Complutense University of Madrid, E-28040, Spain

⁴ Department of Chemistry and Pharmacy, Friedrich-Alexander-University Erlangen-Nürnberg, Erlangen, 91058, Germany

⁵ Fukui Institute for Fundamental Chemistry, Kyoto University, Kyoto 606-8103, Japan

Endohedral metallofullerenes have attracted special interest as new spherical molecules because they possess unusual physical and chemical properties that are imparted by the encapsulated metal atoms.^[1] Although electron donor-acceptor (D-A) conjugates based on empty fullerenes have been well investigated as potential materials to be building blocks for electronic and optoelectronic devices, quite limited number of reports concerning metallofullerenes-based D-A molecules are available.^[2]

In this work, three types of D-A conjugates based on lanthanum-encapsulated fullerenes (La₂@C₈₀ and La@C₈₂) were synthesized and fully characterized (Figure). Their unique electronic properties involving intra-molecular electron transfer behavior were corroborated by UV-vis-NIR absorption spectrometry, electrochemistry and time-resolved spectrometry.

Characteristic intra-molecular charge-separation and recombination were observed in the case of the metallofulleropyrrolidines of La₂@C₈₀ which are linked with an electron donor, that is π -extended tetrathiafulvalene (exTTF).^[3] Utilizing the same addend and electron donor (i.e., pyrrolidine ring connected to exTTF), we achieved the observation on the intra-electron transfer in a paramagnetic endohedral metallofullerene, that is La@C₈₂.

It is worth mentioning that the D-A conjugates of La₂@C₈₀ and tetracyano-9,10-anthra-*p*-quinodimethane (TCAQ) demonstrated the unprecedented formation of the (La₂@C₈₀)⁺-(TCAQ)⁻ radical ion pair state in the photo-induced excited state, in which La₂@C₈₀ acts as an electron donor.

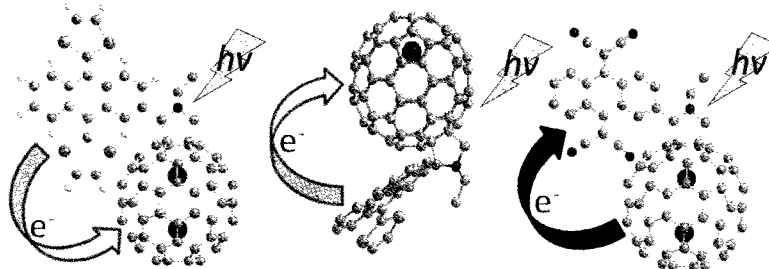


Figure. Schematic drawings of donor-acceptor conjugates based on lanthanum-encapsulated fullerenes in this work. (Left) La₂@C₈₀ with exTTF, (center) La@C₈₂ with exTTF and (right) La₂@C₈₀ with TCAQ.

[1] For recent review, see: *Chemistry of Nanocarbons*; T. Akasaka, F. Wudl, S. Nagase Eds.; Wiley-VCH; Chichester, 2010.

[2] For recent review, see: *Carbon Nanotubes and Related Structures: Synthesis, Characterization, Functionalization, and Applications*; D. M. Guldi, N. Martin Eds.; Wiley-VCH; Weinheim, Germany, 2009.

[3] Y. Takano *et al.* *J. Am. Chem. Soc.* **2010**, *132*, 8048-8055.

Corresponding Author: T. Akasaka

Tel&Fax: +81-29-853-6409

E-mail: akasaka@tara.tsukuba.ac.jp

Room Temperature Observation of Single-Electron Tunneling via Fullerene Quantum Dots in a Si-based Device Structure

○Ryoma Hayakawa, Chikyow Toyohiro, Yutaka Wakayama

International Center for Materials Nanoarchitectonics (WPI-MANA), National Institute for Materials Science, 1-1 Namiki, Tsukuba 305-0044, Japan

A single-electron memory, where Si and Ge nano-dots are adopted as floating gates, is a promising candidate for future Si-based memory devices [1,2]. Here, we have proposed to utilize organic molecules as quantum dots in the devices (Fig. 1) [3]. In particular, C_{60} molecules were considered to be excellent quantum dots. This reason is that each molecule has very uniform size on nanometer scale, leading to large-scale integration of quantum dots (10^{13}cm^{-2}) and stable operation at room temperature. Furthermore, the molecule possesses multiple ionized states, which would fulfill multi-level memory operation.

We successfully demonstrate single-electron tunneling (SET) through C_{60} molecules in a metal-insulator-semiconductor (MIS) structure which is a basic component of all single-electron memory devices (Fig.2). Note that, multiple staircases were observable in I-V curve and were seen up to 280 K that is almost room temperature. These results clearly exhibit that C_{60} molecules work as quantum dots and have a potential to realize multi-level memory operation in a practical device configuration. Additionally, the SETs were found to have originated from resonant tunneling via the energy levels of the embedded C_{60} molecules, *e.g.*, the highest occupied molecular orbital (HOMO) and the lowest unoccupied molecular orbital (LUMO). This finding indicates that the threshold voltages for SET are tunable according to the molecular orbital. Our results suggest that the incorporation of molecular dots into the Si-MIS structure has considerable potential for realizing novel memory devices and achieves large-scale integration of individual molecular functionalities.

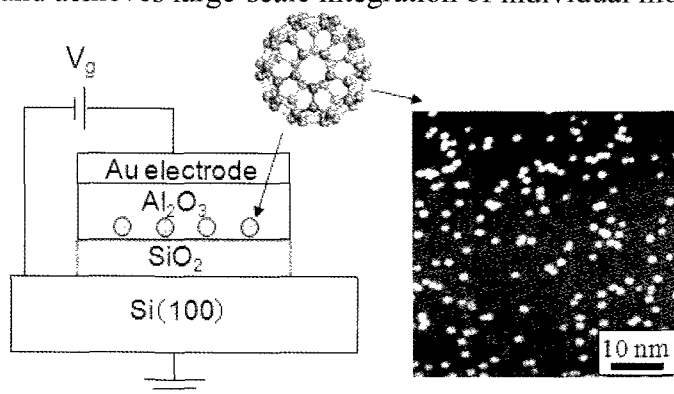


Fig. 1 A schematic illustration of the MIS structure with C_{60} molecules as quantum dots.

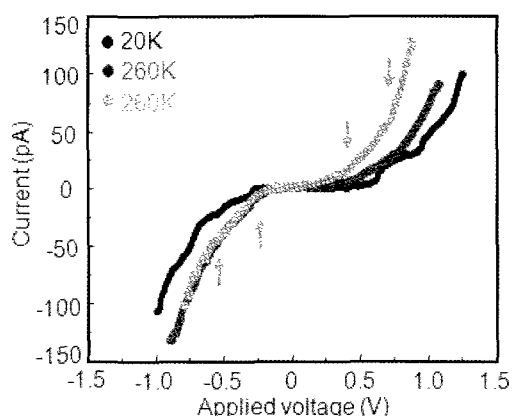


Fig. 2 Temperature dependence of I-V curves in the sample with C_{60} molecules.

- [1] S. Tiwari, F. Rana, H. Hanafi, H. Haratstein, E. F. Crabbe, K. Chan, *Appl. Phys. Lett.* **68**, 1377-1379 (1996).
- [2] C. Pace, F. Crupi, S. Lombardo, C. Gerardi, G. Cocorullo, *Appl. Phys. Lett.* **87**, 182106-1-182106-3 (2005).
- [3] R. Hayakawa, N. Hiroshiba, T. Chikyow, Y. Wakayama, *Adv. Funct. Mater.* **21**, 2933-2937 (2011).

Corresponding Author: R. Hayakawa

Tel: +81-29-851-3354 (ex. 8813), Fax: +81-29-860-4916,

E-mail: HAYAKAWA.Ryoma@nims.go.jp

A patternable CNT-Cu composite possessing hundred-times higher electrical current-carrying-capacity than metals

○ Chandramouli Subramaniam¹, Takeo Yamada^{1,2}, Don N. Futaba^{1,2}, Motoo Yumura^{1,2}, Kenji Hata^{1,2,3}

¹ Technology Research Association for Single Wall Carbon Nanotubes (TASC), Central 5, 1-1-1-Higashi, Tsukuba, Ibaraki, 305-8565, Japan.

² National Institute of Advanced Industrial Science and Technology (AIST), Central 5, 1-1-1-Higashi, Tsukuba, Ibaraki, 305-8565, Japan.

³ Japan Science and Technology Agency (JST), Honcho 4-1-8, Kawaguchi 332-0012, Japan.

Here, we present a unique carbon nanotube-copper (CNT-Cu) composite possessing 100 times higher current-carrying-capacity (ampacity) than any metal, while matching the electrical conductivity of Cu. Specifically, the CNT-Cu composite has an ampacity of 6×10^8 A/cm² (Cu: 5×10^6 A/cm²) and an electrical conductivity of 4.7×10^5 S/cm (Cu: 5.7×10^5 S/cm). Further, with a density of 5.2 g/cm³ (Cu: 8.9 g/cm³) this material is a light-weight, high-performance electrical conductor. The stand-out performance of CNT-Cu composite is clearly seen in a map of ampacity versus conductivity for all common materials (Fig. 1). In the map, metals (Cu, Au etc.) possess high conductivity yet low ampacity while nanocarbons (nanotubes, graphene) have high ampacity and low conductivity. CNT-Cu composite occupies a singular place with both high ampacity and high conductivity.

This result assumes significance in the context of progressive miniaturization of electrical devices and gadgets, with current densities limits of Cu and Au about to be surpassed in 2014[1].

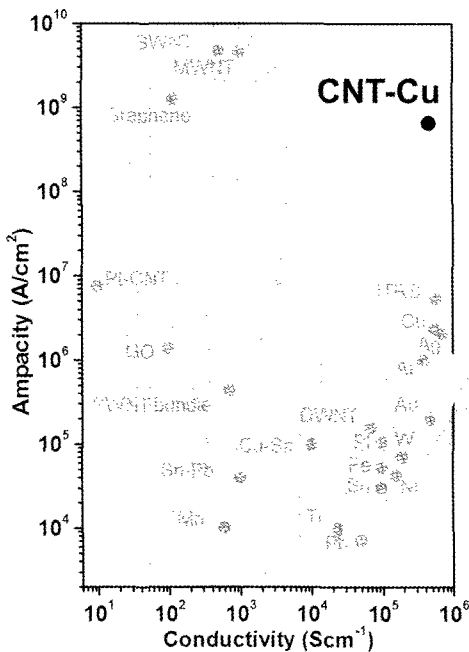


Fig.1 Map of ampacity versus electrical conductivity for materials including metals and nano-carbons.

Critically important to achieve these properties was to develop a process to deposit Cu uniformly throughout the long, aligned, bulk, pre-formed Super-growth CNT structure. This was done using a two-stage nucleation-growth strategy. Initial-stage electrodeposition of Cu seeds on CNT was done in organic medium to increase wettability of hydrophobic CNT surface. Subsequent growth by aqueous electroplating resulted in well-distributed CNT intertwined with continuous Cu. The large CNT-Cu interface area thus created, is vital for achieving high ampacity and conductivity.

Versatility of this strategy provides compatibility with solid-state micro-fabrication processes, enabling precise patterning of CNT-Cu into multi-dimensional, intricate geometries resembling back-end-of-line electronic circuits and interconnecting with identical electrical properties.

[1] International Technology Roadmap for Semiconductors, 2012 Ed.

Corresponding Author: Kenji Hata

Tel: +81-0298614654, Fax: +81-0298614851

E-mail: kenji-hata@aist.go.jp

Effect of Mechanical Strain on Polycrystalline Graphene

○Mark A. Bissett¹, Wataru Izumida², Riichiro Saito², Hiroki Ago^{1*}

¹ Institute of Materials Chemistry and Engineering, Kyushu University, Fukuoka, 816-8580

² Department of Physics, Tohoku University, Sendai, 980-8578

Since its discovery graphene has been the focus of a wide field of research aimed at understanding its unique properties and developing novel applications. These properties include high tensile strength, flexibility, transparency, and most importantly very high mobility. It has been shown previously that exfoliated graphene consists of large single domain areas, while CVD-grown graphene consists of a patchwork of smaller domains [1]. The presence of these smaller domains leads to the formation of domain boundaries due to the mis-orientation of adjacent lattices. Domain boundaries in graphene have been shown to have a significant effect on the carrier mobility, mechanical properties and electronic structure of CVD graphene [2]. Mechanical strain on graphene is also of interest for electronics applications, as it has the ability to alter the electronic structure. Previous studies of strained graphene have focused on exfoliated graphene in contact with various polymers [3]. However, for future device applications where large scale films are required CVD graphene is preferable. Thus, it is important to gain an understanding of what affect the presence of domain boundaries has on strained graphene. In this work we compare the behavior of both CVD-grown and mechanically exfoliated graphene while undergoing mechanical strain.

Raman spectroscopy provides a quick and versatile technique to investigate the structure of graphene. When mechanical strain is applied to graphene the characteristic Raman peaks (D, G, and G') each shift in frequency due to distortion of the lattice structure. Figure 1 shows the plots of Raman peak frequency with applied strain for both exfoliated and CVD grown graphene. The plot of exfoliated graphene peak shift matches literature [3]. However, the CVD graphene shows an opposite slope for the shift in G and G' peaks. This indicates that the CVD graphene is behaving differently when strain is applied. It is believed that the presence of domain boundaries affects the shifting of Dirac cones and phonon dispersion when strain is applied. Using Raman spectra calculation for the electronic structure of deformed graphene, we will propose possible explanation for different (same) behavior of G (G') band for CVD and exfoliated graphene sample. We also studied a more flexible polydimethylsiloxane (PDMS) substrate which is widely used for soft lithography and flexible devices. Unique dependence on the polymer substrate in terms of behavior of Raman G, D, G' bands is also demonstrated.

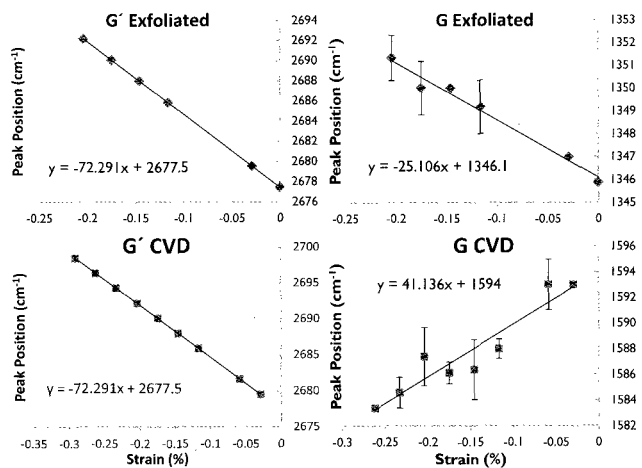


Fig. 1: Plots of Raman peak positions (G and G') for exfoliated and CVD-grown graphene

[1] Huang, P.Y. et al., Nature, **469**, 7330, (2011)

[2] Song, H.S. et al., Scientific Reports, **2**, 337, (2012)

[3] Ferralis, N., Journal of Materials Science, **45**, 19, (2010)

Corresponding Author: H. Ago, Tel: +81-92-583-7817, Fax: +81-92-583-7817, E-mail: Ago@cm.kyushu-u.ac.jp

Properties of Single Wall Carbon Nanotube Aggregates Formed by Vapor Diffusion Methods

○Kazuhiro Yanagi¹, Hideki Kawai¹, Hikaru Kudo¹, Kai Hasegawa, Hiromichi Kataura², Ryo Nakatzu³

¹ Department of Physics, Tokyo Metropolitan University

² AIST/CREST

³ Graduate School of Pharmaceutical Science, Kyoto University

Recent progress of purification techniques enables us to obtain high-purity metallic, semiconducting single wall carbon nanotubes (SWCNTs), and SWCNTs in a single-chiral state [1]. By using those purified SWCNTs, remarkable transport and optical characteristics reflecting intrinsic properties of SWCNTs have been reported in their networks [2], however, random orientations of SWCNTs have degraded transport performances. In our group, to solve this problem, we have tried to develop techniques to control orientations of SWCNTs during formation of their aggregates, and to make crystals of SWCNTs as our future goal. We applied a vapor diffusion method to form SWCNT-aggregates [3]. Vapor diffusion method is typically used for crystallizations of membrane protein. Membrane proteins are hydrophobic nano-materials, and thus surfactants are needed to mono-disperse them into water, which are similar to SWCNTs. Thus we applied this method to control aggregate formation of SWCNTs. After more than 800 screening tests, we found that needle-like crystals were formed in a proper condition. Micro Raman measurements revealed that SWCNTs were contained in the crystals and tended to be aligned along with the crystal axis, and also the purity of SWCNTs was improved through the formation of the crystals. However, surfactants were also sometimes crystallized in a proper condition, alignment ratio of SWCNTs was very low, and correct evaluation of the amount of SWCNTs contained in the crystals was difficult [3]. Thus we applied another approach to make SWCNT aggregates. In previous vapor diffusion processes, water vapor diffuses from a sample drop to a reservoir (Fig. 1(a)). We applied another approach using alcohol vapor diffusion (Fig. 1(b)). In this approach, alcohol vapor diffuses from the reservoir to the sample drop, increasing the concentration of alcohol in a controlled manner without reducing the amount of sample solution. This approach enabled us to obtain pure SWCNT-aggregates without forming aggregates of surfactants. Moreover, (6,5) purity was improved by this method (Fig. 1(c)).

[1] H. Liu et al., *Nature Commun.* **2**, 309 (2011), M. Kawai, K. Yanagi et al., *J. Am. Chem. Soc.* **134**, 9545 (2012).

[2] Yanagi et al., *ACS Nano* **4**, 4027 (2010), Yanagi et al., *Adv. Mater.* **23**, 2811 (2011)

[3] H. Kudo, K. Yanagi, et al., Abstract of The 42th Fullerene-Nanotubes General Symposium (2012).

Corresponding Author: K. Yanagi

Tel: +81-42-677-2494, Fax: +81-42-677-2483

E-mail: yanagi-kazuhiro@tmu.ac.jp

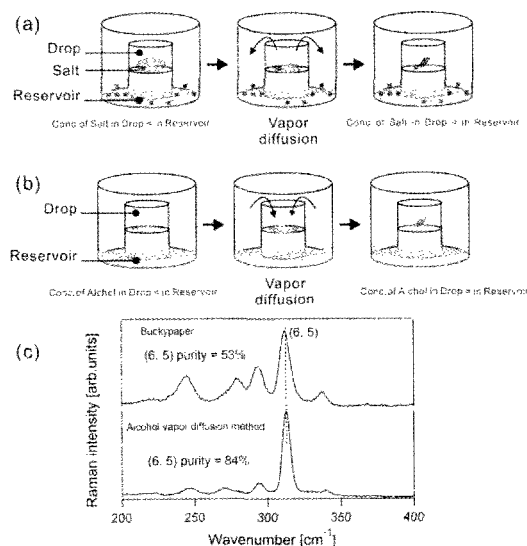


Fig. 1. Schematic illustrations of (a) previous vapor diffusion, and (b) alcohol vapor diffusion methods. (c) Improvement of purity by the alcohol vapor diffusion method.

Effects of the Defective Structures for Carbon Nanotube on the Antidegradation and Electrical Conductivity of Rubber Composites

○Tomoya Nagaoka, Koji Tsuchiya, Yoshiyuki Takahashi, Hirofumi Yajima*

*Department of Applied Chemistry, Faculty of Science, Tokyo University of Science
1-3 Kagurazaka, Shinjuku-ku, Tokyo 162-8601, Japan*

Carbon nanotubes (CNTs) have been expected to be effective as fillers in polymer matrices for their functionalization due to CNTs' outstanding electrical/mechanical properties and peculiar structures. However, because of the highly entangled agglomerates owing to strong *van der Waals* interaction, it is difficult to individually disperse CNTs in polymer matrices. In our previous study with respect to the fabrication of electrically conductive rubber-composite materials consisting of styrene-butadiene rubber (SBR) and CNTs, we demonstrated a novel mixing technique with the combination of ultrasonication and a rotation/revolution mixing without mechanical shear [1]. As a result, it has been found that the percolation threshold of the composites produced with our novel mixing method was significantly low (< 1 phr, phr : parts per hundred rubber), compared to that (ca. 10 phr) of the composites prepared with a conventional Banbury mixer. In the present study, we have reported the antidegradation functions of multi-walled carbon nanotubes (MWNTs) incorporated into isoprene rubber (IR). FT-IR spectra revealed that the intensity of the peak corresponding to carbonyl group ($-C=O$) for the MWNT/IR composite remained unchanged even after heat treatment, which suggested that the degradation of IR was suppressed by the addition of MWNTs. However, the antidegradation ability of MWNTs was strongly dependent on the difference in structural characteristics of MWNTs, in which some MWNT species had no antidegradation ability. Furthermore, the inhibition effect of MWNTs on the generation of radical owing to mechanical stretching for the MWNT/IR composite films was measured by means of ESR equipped with our-own making tensile test machine. The ESR results implied that the rate of radical elimination was increased with the defect degree of grapheme-like structures in MWNTs. Consequently, the disordered structure of MWNTs was suggested to give rise to the antidegradation, since there exist considerably high charge densities around the defects such as pentagons, heptagons and holes involved in a high affinity for radicals (polymer radicals or peroxy radicals) generated by the heat and mechanical-stretching treatments. The influence of the defects of MWNTs on percolation thresholds was also examined for the electrically conductive IR composite materials. The addition of MWNTs with a certain amount of the defects resulted in the percolation threshold with the lowest value, at the expense of the dispersion of MWNTs in rubber matrices. The foregoing results led us to the conclusion that a certain amount of defect of CNTs was significantly involved in the improvement of the properties of rubber/CNT composites.

[1] K. Tsuchiya et al., *Compos. Sci. Technol.* 71 (2011) 1098-1104

*Corresponding Author: Hirofumi Yajima

TEL: +81-3-3260-4272(ext.5760), FAX: +81-3-5261-4631, E-mail: yajima@rs.kagu.tus.ac.jp

Fabrication and applications of carbon nanotube-alumina composite

○Mamoru Omori, Go Yamamoto, Keiichi Shirasu, Toshiyuki Hashida

Graduate School of Engineering, Tohoku University, Sendai, 980-8579, Japan

Fabrications of carbon nanotube (CNT)-alumina composite have been done in many places. However, composites with enough mechanical properties for application have not been prepared because of agglomeration of CNTs. We tried two attempts, using aluminum hydroxide instead of alumina powder and selecting dispersive multi-walled carbon nanotubes (MWNTs). MWNTs are classified into two groups of thick and thin. Thick MWNTs consist of a large number of graphene and grows more than 30 nm in diameter, and they are produced at limited factories. Thin MWNTs of a small number of graphene are less than 30 nm in diameter and are dealt with many companies in the world. The stiffness of MWNTs depends on a number of graphene and diameter. Thick MWNTs are high stiffness and less agglomerated when they are mixed in water slurry. Thin MWNTs with low stiffness can not avoid agglomeration and differ from each other about it. The small size of agglomerated thin MWNTs may not greatly reduce strength of composite. There is a thin MWNT orderly agglomerated less than ten microns. The size of this agglomerated thin MWNT is expected to be less than several microns in composite and not to lower strength greatly. The composites were prepared from 0.3 to 5 mass% of these MWNTs by spark plasma sintering (SPS). Thick MWNTs were individualized in the composite consisted of less than 1 mass% of them. Thin MWNTs were not individualized and agglomerated less than 5 microns in the composite. The strength of all the composites was more than 400 MPa and the toughness was more than that of the alumina compact synthesized from a commercial alumina powder. The dispersed thick MWNT increased the strength and toughness of the composite by bridging and pullout of it. The composite was characterized by high strength and toughness, electric conductor, microwave absorption and low friction. To promote applications of the composite, it was coated with graphite film by rubbing graphite powder on its surface and turned into a low friction material, as shown in Fig. 1. The graphite film from 2 to 3 μm was bonded to the MWNTs exposed on the surface of the composite by van der Waals force and not peeled away by rubbing with paper or cloth.

Various industrial materials can be derived from this composite. 1. Electric conductive alumina: dust-free components for IC production and photocopy machine and plating substrate. 2. Microwave absorber. 3. Low friction: self lubricating bearing and acetabular cup in total hip joint replacement.

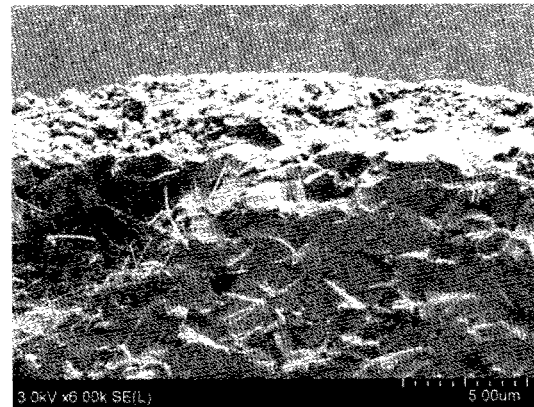


Fig. 1 SEM image of fractured surface of the 5% thick MWNT (2600°C) composite coated with graphite film.

Corresponding Author: M. Omori

Tel: +81-22-795-7524, Fax: +81-22-795-4311,

E-mail: m-omori@rift.mech.tohoku.ac.jp

Fabrication of flexible bulk-heterojunction organic solar cells using single-wall carbon nanotube thin films as transparent conducting anodes

○Shunjiro Fujii^{1,2,3}, Takeshi Tanaka^{1,3}, Satoko Nishiyama³, Hiromichi Kataura^{1,2,3}

¹*Nanosystem Research Institute, National Institute of Advanced Industrial Science and Technology (AIST), Tsukuba, Ibaraki 305-8562, Japan*

²*JST, CREST, Kawaguchi 330-0012, Japan*

³*Technology Research Association for Single Wall Carbon Nanotubes (TASC), Tsukuba, Ibaraki 305-8565, Japan*

Organic solar cells (OSCs) are of special interest owing to their advantages of low-cost and solution-processable fabrications in addition to their compatibility with flexible plastic substrates. OSCs are often built on indium tin oxide (ITO) coated substrates because ITO offers high transparency in the visible region as well as good electrical conductivity. However, the poor mechanical stability of ITO can cause device failures when an ITO-coated flexible substrate is bent [1]. In addition, the limited supply of indium will increase the cost of ITO in future. Recently there are some reports on OSCs using single-wall carbon nanotube (SWCNT) films as anode instead of ITO electrode [2,3]. However, most of the OSCs were fabricated on glass substrates, and those on flexible substrates have not yet been developed. In this study, we fabricated bulk-heterojunction (BHJ) OSCs using SWCNT films as transparent conducting anodes on flexible plastic substrates.

The BHJ OSCs were fabricated based on poly(3-hexylthiophene) (P3HT) and (6,6)-phenyl C61 butyric acid methyl ester (PCBM) on conducting polyethylene terephthalate (PET) by spin-coating technique. We firstly fabricated the OSCs on ITO-coated PET substrate to optimize thermal annealing conditions with minimal deformation of the PET substrate. Next, we fabricated OSCs on SWCNT film/PET substrates. SWCNT film on PET substrate was fabricated by bar-coating. By replacing ITO electrode with SWCNT film, a power conversion efficiency of the OSC was improved from 1.3% to 1.7% (30% increase). In this presentation, detailed characteristics of the OSC will be discussed.



Figure 1 Photograph of the OSC in the configuration of PET/SWCNT film/ PEDOT:PSS/P3HT:PCBM/Al.

[1] T. Z. Chen et al., *Thin Solid Films*, 394, 202 (2001).

[2] T. M. Barnes et al. *Appl. Phys. Lett.* 96, 243309 (2009)

[3] T. P. Tyler et al. *Adv. Energy Mater.* 1, 785 (2010)

Corresponding Author: Hiromichi Kataura

E-mail: h-kataura@aist.go.jp

Thin single-walled boron nitride nanotubes synthesized in single-wall carbon nanotubes

○Ryo Nakanishi¹, Ryo Kitaura¹, Yuta Yamamoto², Shigeo Arai², Jamie H Warner³,
Yasumitsu Miyata¹ and Hisanori Shinohara¹

¹*Department of Chemistry & Institute for Advanced Research, Nagoya University, Nagoya, 464-8602, Japan*

²*Ecotopia Science Institute, Nagoya University, Nagoya, 464-8603, Japan*

³*Department of Materials, University of Oxford, Oxford, OX1 3PH, UK*

Due to the cylindrical structure, single-wall carbon nanotubes (SWCNTs) can be used as nano-scale test tubes to synthesize a new class of one-dimensional nanomaterials such as atomic wires [1]. However, the small band gap of SWCNTs causes charge transfer between CNTs and atomic wires, which modulate properties of atomic wires. Boron nitride nanotubes (BNNTs) are also nano-scale cylindrical tubes consisting of hexagonal boron nitride sheets. One of the most important features of BNNTs is that BNNTs possess a large band gap (~ 6.0 eV) irrespective of the chiralities [2]. Therefore, single-walled BNNTs (SWBNNTs) with narrow diameters are the ideal nano-scale vessel to explore physical properties of atomic wires encapsulated. Selective and bulk synthesis of narrow diameter SWBNNTs is, however, still in its infancy. Here, we have focused on a development of a novel synthesis method of SWBNNTs using SWCNTs as nano-reactor.

We selected Meijo-SO type SWCNTs, which have a narrow diameter distribution (1.4 ± 0.1 nm) as a template, and ammonia-borane complex (AB) as a precursor of SWBNNTs. AB was sealed into a glass tube with cap-opened SWCNTs under high vacuum (10^{-6} Torr), and was encapsulated into them with heating at 823 K for 3 days. After capped those ends with C_{60} and washed with deionized water for 1 hour, AB encapsulated SWCNTs (AB@SWCNTs) were annealed at 1673 K for 3 days. Transmission electron microscopy (TEM) image (Fig. 1(a)) shows tubular possessing honeycomb structure inside SWCNT, which is almost identical to that of double-wall CNTs. Scanning TEM (STEM) - high-angle annular dark-field (HAADF) image (Fig. 1(b)) shows that there is a white line-shaped contrast inside SWCNTs, which is consistent with the TEM observation. Electron energy-loss spectroscopy (EELS) spectrum shown in Fig. 1(c) displays clear features arising both from carbon K-edge and boron K-edge. We have also observed peaks arising from nitrogen K-edge. These results clearly demonstrate that SWBNNTs are successfully fabricated inside SWCNTs.

[1] R. Kitaura *et al.*, *Angew. Chem. Int. Ed.* 48, 8298 (2009).

[2] N. G. Chopra *et al.*, *Science* 269, 966 (1995).

Corresponding Author: Ryo Kitaura and Hisanori Shinohara

Tel: +81-52-789-2483, Fax: +81-52-747-6442, E-mail: r.kitaura@nagoya-u.jp, noris@nagoya-u.jp

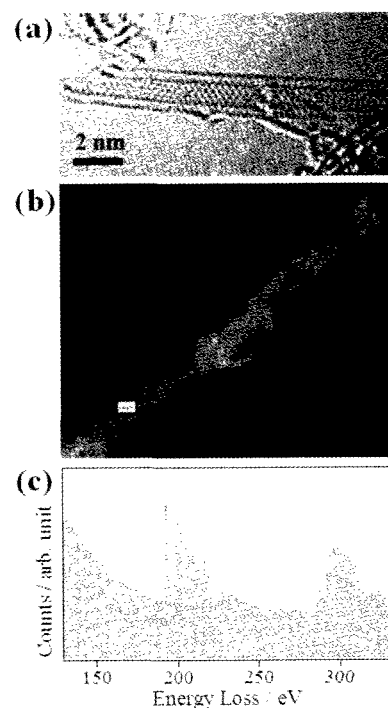


Fig. 1 (a) TEM image, (b) STEM-HAADF image, and (c) EELS analysis result of SWBNNT synthesized in SWCNT.

Optical properties of small-diameter carbon nanotubes

○Takashi Koretsune and Susumu Saito

Department of Physics, Tokyo Institute of Technology, Tokyo, 152-8551, Japan

The optical properties for most of carbon nanotubes have been well understood based on the band structure of graphene with some curvature effects. In the small-diameter nanotubes, however, it is well known that the curvature drastically affects the electronic structures[1,2]; for example, (5,0) tube should be semiconducting in the naïve cutting line picture while density-functional theory (DFT) predicts that it is metallic. Since it is now possible to synthesize such small-diameter nanotubes experimentally, it is of great importance to reconsider the optical properties of these small-diameter tubes from first principle. Thus, we theoretically study most of small-diameter nanotubes including chiral ones using the DFT, and predict the radial breathing mode and the absorption and emission properties within the single-particle picture.

In this paper, we focus on all kinds of nanotubes with diameters of $3.5 \text{ \AA} < d < 7 \text{ \AA}$ and perform electronic structure calculations within local density approximation in the framework of DFT. We use norm-conserved pseudopotential and a plane wave basis set with a cutoff energy of 60 Ry. The supercell approach is adopted to calculate isolated nanotubes and the geometry is fully optimized by keeping a sufficiently large interwall distance.

Figs. 1(a)-(c) show the electronic band structures of (4,3), (6,2) and (7,0) tubes, respectively. In (4,3) tube, there is a large band gap of 1.33 eV, which is almost as large as that expected from the cutting line picture, indicating that the electronic structure and the optical properties of (4,3) tube can be understood as in larger tubes. On the contrary, in (6,2) and (7,0) tubes, band gaps are 0.69 eV and 0.22 eV, respectively, which are considerably smaller than those from the cutting line picture and the band structures are qualitatively different. We discuss that this is due to the M-point wavefunction in the Brillouin zone of graphene, and that as a result, the luminescence should be suppressed significantly.

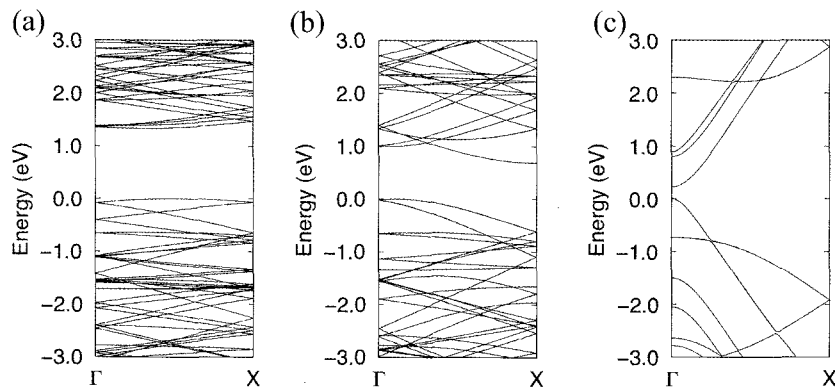


Fig. 1 Electronic band structures of (a) (4,3), (b) (6,2), and (c) (7,0) nanotubes.

[1] X. Blase, L. X. Benedict, E. L. Shirley, and S. G. Louie, Phys. Rev. Lett. 72, 1878 (1994).

[2] K. Kato and S. Saito, Physica E 43, 669 (2011).

Corresponding Author: T. Koretsune

E-mail: koretune@stat.phys.titech.ac.jp

Photoluminescence Spectroscopy of Oxygen-Doped Carbon Nanotubes

○Munehiyo Iwamura¹, Yuhei Miyauchi^{1,2}, Shinichiro Mouri¹, Tadashi Kawazoe³,
Motoichi Ohtsu³, Kazunari Matsuda¹

¹ Institute of Advanced Energy, Kyoto University, Uji, Kyoto, 611-0011, Japan

² PRESTO, Japan Science and Technology Agency, Kawaguchi, Saitama, 332-0012, Japan

³ Department of Electrical Engineering and Information Systems, Tokyo University, Bunkyo,
Tokyo, 113-8656, Japan

Single-walled carbon nanotubes (SWNTs) are attractive as quasi-one dimensional (1D) materials not only for the fundamental 1D physics researches [1,2] but also various optoelectronics applications such as nanosized light emitters. However, their typically low luminescence quantum yield (QY) [3] has limited the performance of nanotube-based light emitting devices.

Here we report that the localized electronic states generated by oxygen doping in (6, 5) SWNTs (E_{11}^*) have much larger QY than that of the E_{11} excitons in the same SWNTs. Oxygen-doped SWNTs were prepared based on the procedure developed by Ghosh *et al.* [4]. Figure 1 shows typical photoluminescence (PL) spectra of pristine and oxygen-doped SWNTs. By comparing PL spectra of various samples with different oxygen-doping conditions, the QY of the E_{11}^* exciton is determined to be more than one-order larger than that of the E_{11} exciton, based on the exciton diffusion model.

In order to clarify the origin of the enhanced QY, we conducted time-resolved PL measurements. The effective PL lifetime of about 100 ps was observed for the E_{11}^* excitons, while the intrinsic E_{11} excitons exhibited the lifetimes of only less than 20 ps. From these results of the effective PL lifetime and the QY, we found that the radiative recombination lifetime of the E_{11}^* exciton is 2-3 times shorter than the intrinsic E_{11} exciton. The enhanced QY of the E_{11}^* state is therefore attributed to the two main factors, the longer PL lifetime and the shorter radiative recombination lifetime.

Furthermore, we observed temperature dependence of PL intensities of both E_{11} and E_{11}^* states. The integrated PL intensity of E_{11}^* peak slightly decreased with decreasing temperature, while the E_{11} intensity behaved like 1D state being proportional to $T^{-1/2}$. These results are attributed to different dimensionality of E_{11} (quasi-1D) and E_{11}^* (quasi-0D) excitons.

[1] P. Avouris, M. Freitag, and V. Perebeinos, *Nature Photon.* **2**, 341 (2008).

[2] Y. Miyauchi, H. Hirori, K. Matsuda, and Y. Kanemitsu, *Phys. Rev. B* **80**, 081410(R) (2009).

[3] J. Lefebvre, D. G. Austing, J. Bond, and P. Finnie, *Nano Lett.* **6**, 1603 (2006).

[4] S. Ghosh, S. M. Bachilo, R. A. Simonette, K. M. Beckingham, and R. B. Weisman, *Science* **330**, 1656 (2010).

Corresponding Author: M. Iwamura

Tel: +81-774-38-3465,

E-mail: m.i.0812@iae.kyoto-u.ac.jp

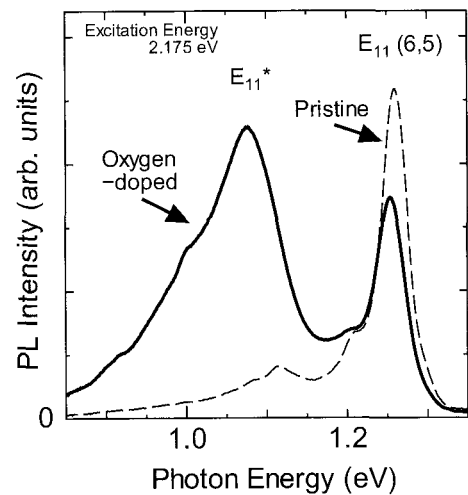


Fig.1. PL spectra of pristine and oxygen-doped SWNTs (2.175 eV excitation).

Photocurrents with multiple exciton generation in single-walled carbon nanotubes

○Satoru Konabe^{1,2} and Susumu Okada^{1,2}

¹*Graduate School of Pure and Applied Sciences, University of Tsukuba, Tsukuba, Ibaraki 305-8571, Japan*

²*Japan Science and Technology Agency, CREST, 5 Sanbancho, Chiyoda, Tokyo 102-0075, Japan*

Multiple exciton generation (MEG) could boost the power conversion efficiency of photovoltaic devices by creating multiple excitons from a single photon. It has been demonstrated that MEG has been realized in the system with low-dimension and nanometer scale, such as semiconductor nanocrystal and carbon nanotubes [1,2,3,4]. However, even though MEG occurs, it does not necessarily mean that the photocurrents increases since the neutral exciton itself does not directly contribute to photocurrents. Therefore, it is important to investigate the amount of carriers or photocurrents that are generated by dissociating excitons to discuss the power conversion. This is particularly important for carbon nanotubes since excitons in carbon nanotube have huge binding energy that becomes up to several hundred of meV. For the exciton dissociation, there are two mechanisms: an electric field generated by a p-n junction and the Auger ionization [5] which is peculiar to nano-scaled materials that have a strong Coulomb interaction between excitons.

In the present paper, we performed numerical simulations of photocurrents in single-walled carbon nanotubes. Our simulation is based on simple kinetic equations for the number of excitons and carriers. The simulation properly includes the MEG process [6] and the Auger ionization process [5], in addition to the exciton generation by absorbing photons, radiative recombination, and exciton dissociation by an electric field. From our simulation results, we found that the photocurrent strongly depends on parameter, such as excitation energy, laser intensity, and electric field that dissociates an exciton.

References:

- [1] A. Ueda *et al.* Appl. Phys. Lett. **92**, 233105 (2008).
- [2] N. M. Gabor *et al.* Science **325**, 1367 (2009).
- [3] S. Wang *et al.*, Nano Lett. **10**, 2381 (2010).
- [4] Y. Li *et al.*, APEX **4**, 065101 (2011).
- [5] S. Konabe *et al.*, APEX. **2**, 092202 (2009).
- [6] S. Konabe and S. Okada Phys. Rev. Lett. **108**, 227401 (2012).

Corresponding Author: Satoru Konabe

E-mail: konabe@comas.frsc.tsukuba.ac.jp

Tel: +81-2-9853-5600 ext.8233

Diameter reduction of SWNTs by nitrogen incorporation and encapsulation of a one-dimensional nitrogen gas

○ Theerapol Thurakitseree¹, Christian Kramberger², Heeyuen Koh¹, Yudai Izumi³, Toyohiko Kinoshita³, Takayuki Muro³, Shohei Chiashi¹, Erik Einarsson^{1,4}, Shigeo Maruyama¹

¹Department of Mechanical Engineering, The University of Tokyo, Tokyo 113-8656, Japan

²Faculty of Physics, University of Vienna, Vienna, A-1090, Austria

³Japan Synchrotron Radiation Research Institute, Hyogo 679-5198, Japan

⁴Global Center of Excellence for Mechanical Systems Innovation, The University of Tokyo, Tokyo 113-8656, Japan

Direct structure-controlled synthesis of single-walled carbon nanotubes (SWNTs) is desirable in order to obtain homogeneous SWNT properties. By incorporating nitrogen during synthesis, the nanotube structure can be modified. Here we report a significant *reduction* in SWNT diameter once N was introduced during no-flow chemical vapor deposition (CVD) process [1, 2]. Synthesis was performed using ethanol feedstock containing varying concentrations of acetonitrile (CH₃CN). Based on analysis of optical absorption spectra, the mean diameter of vertically aligned SWNTs decreased from 2.1 nm to less than 1 nm with the addition of less than 3 vol.% of acetonitrile in the ethanol feedstock. Notably, the small-diameter SWNTs remained vertically aligned [3].

X-ray photoelectron spectroscopy and X-ray absorption spectroscopy were used to investigate the incorporation into the SWNTs and the bonding configuration. The total N content was found to saturate at 1.2 at.%. Interestingly, the majority of the incorporation (approximately 1 at.%) was found to be from N₂ molecules contained inside the small-diameter SWNT containers, with only minor contributions from sp² and pyridinic configurations [4].

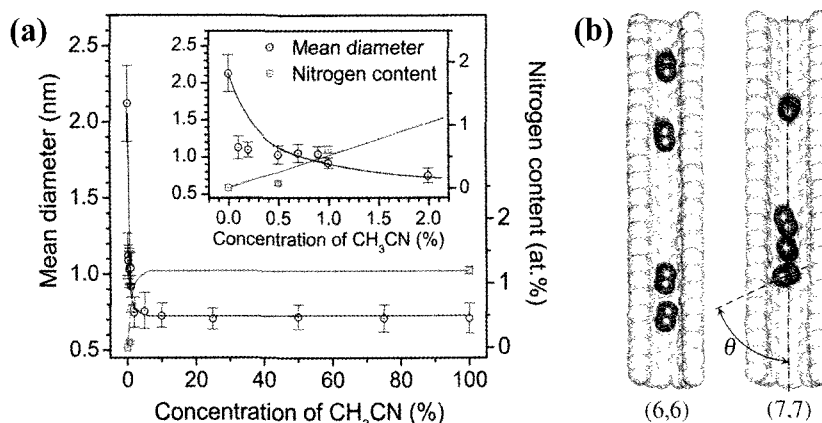


Fig. 1. (a). A plot between mean diameters and N content of VA-SWNTs synthesized using different concentration of CH₃CN in ethanol, and (b) molecular dynamics simulation of N₂ inside small-diameter SWNTs.

[1] S. Maruyama *et al.*, Chem. Phys. Lett. **360**, 229 (2002).

[2] H. Oshima *et al.*, Jpn. J. Appl. Phys. **47**, 1982 (2008).

[3] T. Thurakitseree *et al.*, Carbon **50**, 2635 (2012).

[4] C. Kramberger *et al.*, submitted.

Corresponding Author: Shigeo Maruyama

TEL: +81-3-5841-6421, FAX: +81-3-5800-6983, E-mail: maruyama@photon.t.u-tokyo.ac.jp

Numerical Study of Edge States in Zigzag BC₂N Nanoribbons

○Kikuo Harigaya¹ and Tomoaki Kaneko²

¹*Nanosystem Research Institute, AIST, Tsukuba 305-8565, Japan*

²*Computational Materials Science Unit, NIMS, Tsukuba, 305-0047, Japan*

Graphene nanoribbon (GNR) is a finite width graphene sheet. The electronic properties of GNRs strongly depend on the edge structures [1]. GNRs with zigzag edges have the so-called edge states. Recently, graphene nanoribbons were fabricated by several ways [2]. Quite recently, the edge states in GNRs were confirmed by STM/STS measurement [3]. On the other hand, BC₂N sheet is organic analogous of graphene. The electronic properties of nanoribbons made with BC₂N were investigated by several authors [4]. However, there are no reports on the presence of the flat bands and edge states in BC₂N nanoribbons. In this paper, we investigate the electronic properties of BC₂N nanoribbons with zigzag edges as shown in the left part of Fig. 1 (a) using a tight binding model. In this figure, B and N atoms are indicated by the black and gray circles, and C atoms are located the empty vertices.

Figure 1 (b) shows calculated band structure of BC₂N nanoribbon. We observed the flat bands. The calculated local density of states at $E=0$ is presented in the right part of Fig. 1 (a). We observed the of the edge state but the charge distribution at both edges are different each other, i.e., the charge distribution at the edge where the outermost sites are occupied with C atoms is similar to that at the conventional zigzag edge, while the charge of the edge states at the edge where the outermost sites are occupied with B and N atoms distributes the both sublattice sites. The former is similar to the edge state at the conventional graphene zigzag edge but the latter is similar to the edge states at the zigzag where the outermost C atoms are replaced with B and N alternately [5].

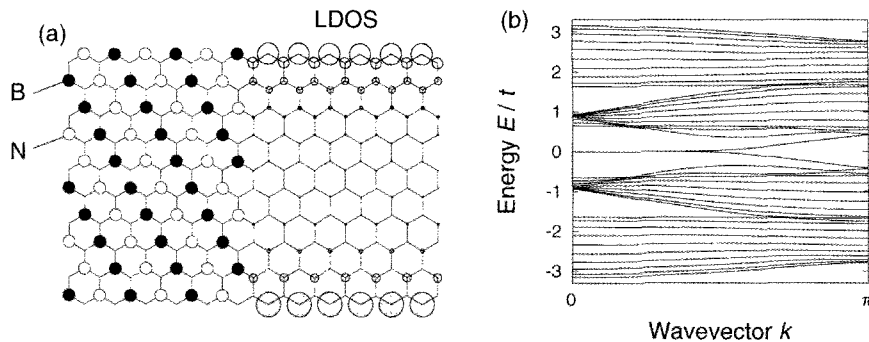


Fig.1 Schematic illustration of BC₂N nanoribbon treated in this paper (left side) and calculated LDOS (right side). (b) The band structure of BC₂N nanoribbon.

[1] M. Fujita *et al.*, J. Phys. Soc. Jpn. **65**, 1920 (1996); K. Nakada *et al.*, Phys. Rev. B **54**, 17954 (1996).

[2] M. Y. Han *et al.*, Phys. Rev. Lett. **98**, 206805 (2007); D. V. Kosynkin *et al.*, Nature **458**, 872 (2009); L. Y. Jiao *et al.*, Nature Nanotech. **5**, 321 (2010); J. M. Cai *et al.*, Nature **466**, 470 (2010).

[3] C. Tao *et al.*, Nature Nanotech. **7**, 616 (2011).

[4] P. Lu, *et al.*, J. Phys. Chem. C **115**, 3572 (2011); Appl. Phys. Lett. **96**, 133103 (2010); B. Xu, *et al.*, Phys. Rev. B **81**, 205419 (2010); L. Lai and J. Lu, Nanoscale **3**, 2583 (2011).

[5] T. Kaneko, K. Harigaya and H. Imamura, (in preparation)

Corresponding Author: K. Harigaya

Tel: +81-29-861-5151, Fax: +81-29-861-6236,

E-mail: k.harigaya@aist.go.jp

G band intensity and joint density of states of twisted bilayer graphene

○Kentaro Sato ¹, Riichiro Saito ¹, Chunxiao Cong ², Ting Yu ^{2,3}, Mildred S. Dresselhaus ^{4,5}

¹ *Department of Physics, Tohoku University, Sendai, 980-8578, Japan*

² *Division of Physics and Applied Physics, School of Physical and Mathematical Sciences, Nanyang Technological University, 637371, Singapore*

³ *Department of Physics, Faculty of Science, National University of Singapore, 117542, Singapore*

⁴ *Department of Electrical Engineering and Computer Sciences, Massachusetts Institute of Technology, Cambridge, MA 02139-4307, USA.*

⁵ *Department of Physics, Massachusetts Institute of Technology, Cambridge, Massachusetts 02139-4307, USA*

When the first layer of AB stacked bilayer graphene rotates about an axis perpendicular to the second layer of bilayer graphene, a commensurate structure with a much larger unit cell than that of monolayer graphene appears at a specific rotation angle. Such a bilayer graphene, which is called twisted bilayer graphene, has interesting physical properties. For example, the Fermi velocity of twisted bilayer graphene decreases with decreasing twisting angle relative to that for monolayer graphene [1]. Thus it is important to know the twisting angle of twisted bilayer graphene to understand its physical properties.

Resonance Raman spectroscopy has been used to study optical properties of graphene related systems [2]. The resonance Raman spectra give us rich information to characterize not only the number of graphene layers but also the stacking structure. Several groups reported that the G band intensity of twisted bilayer graphene is enhanced at a specific twisting angle for a given laser excitation energy (E_{laser}) [3-5]. It is considered that such a behavior gives us information to help evaluate the twisting angle of a twisted bilayer graphene sample using only resonance Raman spectroscopy.

In this presentation, we calculate the G band Raman intensity of twisted bilayer graphene as a function of E_{laser} and twisting angle. Raman intensity is given by calculating electron-photon and electron-phonon matrix elements based on the extended tight binding (ETB) scheme. The electronic structure of twisted bilayer graphene is calculated by using the ETB method. The calculated results show that the G band intensity enhancement occurs at the energy gap that the joint density of states is singular. Here, we call such the energy gap E_{ii} like single wall carbon nanotubes. To estimate twisting angle, we show a relation between the lattice constant of twisted bilayer graphene and E_{11} [6]. We compare our calculations with experiments.

[1] G. Trambly de Laissardiere *et al.*, Nano Lett. 10, 804 (2010).

[2] A. Jorio *et al.*, Raman Spectroscopy in Graphene Related Systems, Wiley-VCH (2011).

[3] Z. Ni *et al.*, Phys. Rev. B 80, 125404 (2009).

[4] R. W. Havener *et al.*, Nano Lett. 12, 3162 (2012).

[5] K. Kim *et al.*, Phys. Rev. Lett. 108, 246103 (2012).

[6] K. Sato *et al.*, submitted (2012).

Corresponding Author: Kentaro Sato

Tel: +81-22-795-6442, Fax: +81-22-795-6447

E-mail: kentaro@flex.phys.tohoku.ac.jp

Production of Nanopores and Proton Conduction in Graphene Oxide Nanosheets Prepared by Photoreaction

○Michio Koinuma^{1,2}, Chikako Ogata^{1,2}, Yuki Kamei^{1,2}, Kazuto Hatakeyama^{1,2}, Hikaru Tateishi^{1,2}, Kengo Gezuhara^{1,2}, Takaaki Taniguchi^{1,2}, Yasumichi Matsumoto^{1,2}

¹ Graduate School of Science and Technology, Kumamoto University, 2-39-1 Kurokami, Kumamoto, 860-8555, Japan

² JST, CREST, K's Gobancho 6F, 7 Gobancho, Chiyoda-ku, Tokyo, 102-0076, Japan

Graphene Oxide (GO) nanosheets have interesting properties such as photoluminescence, ferromagnetism, electrodes, and water permeation. Reduced graphene oxide (rGO) nanosheets are highly conductive and can be used in various electrical devices. They are prepared from GO nanosheets by various reduction methods, such as thermal and hydrazine treatments. Simple photoreduction methods using UV light at room temperature have also been developed.^[1] Irradiation in water produces many nanopores and results in ferromagnetic properties, which arise from the edges of the pores and small broken pieces of rGO.^[2]

The GO was prepared using Hummers' method. The suspension was diluted with pure water, placed on mica, and then dried under vacuum. The surfaces morphology and the composition of the oxygenated groups of the GO single nanosheets were observed using AFM and XPS. The DC current and the AC resistance of the GO were measured with a comb electrode. Products, such as CO₂ and H₂, were analyzed using online gas chromatography.

Many unique properties of graphene oxide (GO) strongly depend on the oxygenated functional groups and morphologies. Here, the photoreaction process is demonstrated to be very useful to control these factors. We report the fast, simple production of nanopores in porous GO via photoreaction in O₂ under UV irradiation at room temperature as shown in Fig.1. Quantitative analysis using X-ray photoelectron spectroscopy showed that nanopores were produced in areas of oxygenated groups (sp³ carbon bonds) creating porous reduced graphene oxide (rGO). The photoreaction mechanism was proposed based on changes in the number of oxygenated groups. Proton conduction occurred at the basal plane of epoxide groups in virgin GO, even at low humidity, and at carboxyl groups for porous rGO at high humidity. Thus, GO and rGO samples with various morphologies, oxygenated functional groups, and conduction types can be easily fabricated by controlling the photoreaction conditions.

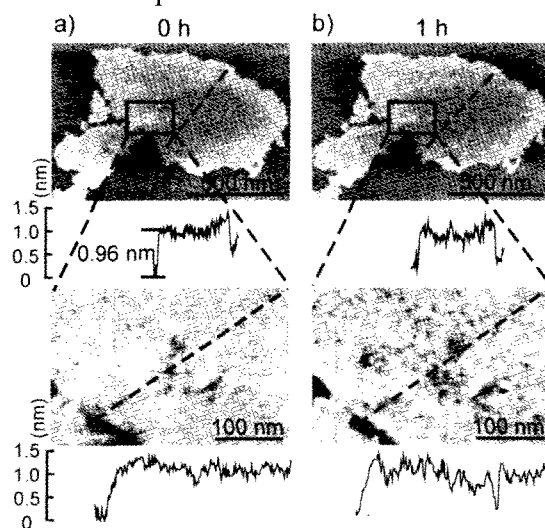


Fig. 1 AFM images of the GO nanosheet after the photoreaction in O₂. The images are for the same sheet after irradiation for (a) 0 h, (b) 1 h

[1] Y. Matsumoto *et al.* *Chem. Lett.* **39**, 750 (2010), *ACS Appl. Mater. & Interfaces* **2**, 3461 (2010).

[2] Y. Matsumoto *et al.* *J. Phys. Chem. C* **115**, 19280 (2011).

Corresponding Author: M.Koinuma

Tel: +81-96-342-3660, Fax: +81-96-342-3659,

E-mail: koinuma@chem.kumamoto-u.ac.jp

Photoluminescence Kinetics of Monolayer Epitaxial Graphene in the Near-Infrared Region

○ Takeshi Koyama,¹ Yoshito Ito,² Kazuma Yoshida,² Hiroki Ago,^{2,3} Hideo Kishida,¹ and Arao Nakamura^{1,4}

¹Department of Applied Physics, Nagoya University, Nagoya, 464-8603, Japan

²Graduate School of Engineering Sciences, Kyushu University, Fukuoka, 816-8500, Japan

³Institute for Materials Chemistry and Engineering, Kyushu University, Fukuoka, Japan

⁴Toyota Physical and Chemical Research Institute, Nagakute, 480-1192, Japan

Graphene is a zero band-gap semiconductor showing unique electronic and optical properties owing to its linear dispersion band. The linear dispersion band also characterizes the dynamics of photoexcited carriers. Recent time-resolved measurements [1] and theoretical studies [2] have shown that photoexcitation between the linear dispersion bands initially creates nonequilibrium carriers which experience ultrafast thermalization via electron-electron and electron-phonon scatterings followed by cooling via the electron-phonon scatterings. In this study, we investigate the dynamics of photoexcited carriers in monolayer graphene on a SiO₂ substrate by time-resolved luminescence measurements.

The monolayer graphene used in this study was epitaxially grown over Cu(111)/sapphire by chemical vapor deposition [3], and then transferred onto a SiO₂ substrate. Raman spectra were measured for characterization of the obtained graphene: The number of layer was identified to be one from the spectral shape of 2D band, and the Fermi energy shift due to the hole doping in air was determined to be -0.225 eV by the peak position of G band. Photoluminescence (PL) kinetics were observed using femtosecond time-resolved luminescence spectroscopy based on the frequency up-conversion technique [4]. The light source was a mode-locked Ti:sapphire laser (82 MHz, 800 nm, and 100 fs), and the excitation density was 3.8×10^{-2} J m⁻² per pulse. The absorbed pulse energy was estimated to be 8.7×10^{-4} J m⁻². All measurements were conducted at room temperature in air.

Figure 1 shows PL decay kinetics at 0.9 eV in the sample. The observed PL kinetics is analyzed based on the carrier cooling model taking into account the electron-phonon interaction. When the Fermi energy shift due to the hole doping is considered, the observed kinetics can be well reproduced (solid line). In contrast, the kinetics cannot be reproduced, when the doping effect is neglected (dashed line). This indicates that the doped carriers play an important role in the cooling dynamics of photoexcited carriers. The model analysis shows that the maximum electron temperature is ~ 450 K. It is found that, even at such a low temperature, the carrier cooling is governed by the coupling with optical phonons.

[1] M. Breusing *et al.*, Phys. Rev. B **83**, 153410 (2011). [2] R. Kim *et al.*, Phys. Rev. B **84**, 075449 (2011); E. Malic *et al.*, Phys. Rev. B **84**, 205406 (2011). [3] B. Hu *et al.*, Carbon **50**, 57 (2012); C. M. Orofeo *et al.*, Carbon **50**, 2189 (2012). [4] T. Koyama *et al.*, Phys. Chem. Chem. Phys. **14**, 1070 (2012).

Corresponding Author: Takeshi Koyama

E-mail: koyama@nuap.nagoya-u.ac.jp

Tel: 052-789-4452, **Fax:** 052-789-5316

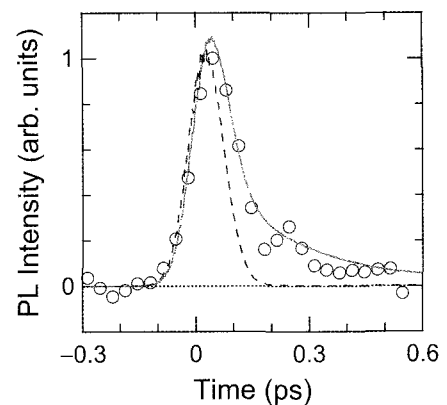


Fig. 1. PL decay kinetics at 0.9 eV.

Bilayer graphene sandwiched by ionic molecules: Band-gap and carrier type engineering

○Nguyen Thanh Cuong^{1,3}, Minoru Otani^{1,3}, Susumu Okada^{2,3}

¹*Nanosystem Research Institute, National Institute of Advanced Industrial Science and Technology (AIST), Tsukuba 305-8568, Japan*

²*Graduate school of Pure and Applied Sciences, University of Tsukuba, Tsukuba 305-8571, Japan*

³*Japan Science and Technology Agency, CREST, 7 Gobancho, Chiyoda-ku, Tokyo 102-0076, Japan*

Graphene has been keeping a premier position not only in the field of the low-dimensional sciences but also in the semiconductor device engineering due to its unique structural and electronic properties. However, graphene is a metal with a pair of linear dispersion bands at the Fermi level, so that they are not utilized in logical electronic devices [1]. Therefore, it is important to tune the electronic structure and to get a semiconducting graphene. Several efforts have been made to control the band-gap of graphene, such as chemical doping [2] and an electric field [3]. In this work, we propose the new and easy procedure how to control the electronic structure and conducting properties of graphene by adsorbing ionic materials to two surfaces of bilayer graphene. Our first-principles calculations show that bilayer graphene sandwiched by the anion and cation ionic molecules is a semiconductor with 0.28 eV band-gap due to the strong local dipole field induced by cation-anion pair. Furthermore, we can control the semiconducting carrier type of a bilayer graphene sandwiched by ionic molecules: *i*-type (intrinsic), *n*-type or *p*-type by changing cation and anion molecule species. These findings open a possibility for realizing the graphene-based semiconducting devices by using the hybrid structure comprising graphene and ionic molecules.

[1] F. Schwierz, *Nature Nanotech.* 5, 487 (2010).

[2] X. Tian, J. Xu, X. Wang, *J. Phys. Chem. B* 114, 11377 (2010).

[3] H. Miyazaki, K. Tsukagoshi, A. Kanda, M. Otani, and S. Okada, *Nano Letters* 10 (2010) 3888.

Corresponding Author: Nguyen Thanh Cuong

E-mail: cuong-nguyen@aist.go.jp

Tel: +81-29-861-6067, Fax: +81-29-861-3171

Photochemical modification of graphene surfaces with water molecules

○Ryo Nouchi^{1,2}, Nobuhiko Mitoma³, Katsumi Tanigaki^{2,3}

¹ *Nanoscience and Nanotechnology Research Center, Osaka Prefecture University, Sakai 599-8570, Japan*

² *WPI Advanced Institute for Materials Research, Tohoku University, Sendai, 980-8577, Japan*

³ *Department of Physics, Tohoku University, Sendai, 980-8578, Japan*

Graphene is a single layer of graphite, indicating that all carbon atoms constructing graphene belong to its surface. Thus, graphene is known to be sensitive to various surface/interface phenomena. We have investigated interfaces with metallic electrodes [1-4] and chemical modification of graphene surfaces [5,6], which has exemplified that the surface/interface phenomena exert a significant influence on electrical properties of graphene. In this presentation, we will focus on our recent finding that microscopic Raman spectroscopy measurements with a high power laser irradiation can cause a structural change of graphene [7-9].

Single layer graphene flakes were formed onto a highly-doped Si substrate with a 300-nm-thick thermal oxide layer on top of it by a conventional mechanical exfoliation. Two types of substrates were prepared; one type of substrate was hydrophilically treated so that the substrate surface is covered with water molecules. As shown in Fig. 1, graphene deposited on the “wet” substrate exhibited an increase in the *D* band intensity. On the other hand, graphene on a substrate without the hydrophilic treatment did not show such evolution of the *D* band. The necessity of

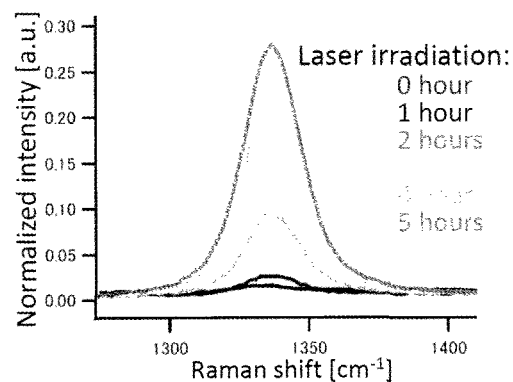


Fig.1 Evolution of the Raman *D* band of graphene formed on a hydrophilically-treated substrate. The peaks are normalized to the peak intensity of the *G* band.

water molecules suggests a photochemical modification of graphene surfaces with water molecules, which is triggered by the microscopic Raman measurement itself [7-9].

[1] R. Nouchi, M. Shiraishi and Y. Suzuki, *Appl. Phys. Lett.* **93**, 152104 (2008).

[2] R. Nouchi and K. Tanigaki, *Appl. Phys. Lett.* **96**, 253503 (2010).

[3] R. Nouchi, T. Saito and K. Tanigaki, *Appl. Phys. Express* **4**, 035101 (2011).

[4] R. Nouchi, T. Saito and K. Tanigaki, *J. Appl. Phys.* **111**, 084314 (2012).

[5] X.-Y. Fan, R. Nouchi, L.-C. Yin and K. Tanigaki, *Nanotechnology* **21**, 475208 (2010).

[6] X.-Y. Fan, R. Nouchi and K. Tanigaki, *J. Phys. Chem. C* **115**, 12960 (2011).

[7] N. Mitoma, R. Nouchi and K. Tanigaki, The 72nd JSAP Autumn Meeting, 1a-E-2 (2011).

[8] N. Mitoma, R. Nouchi and K. Tanigaki, The 59th JSAP Spring Meeting, 16a-B2-2 (2012).

[9] N. Mitoma, R. Nouchi and K. Tanigaki, submitted.

Corresponding Author: R. Nouchi

Tel: +81-72-254-8394, Fax: +81-72-254-8394,

E-mail: r-nouchi@21c.osakafu-u.ac.jp

Structure and electronic properties of carbon nanohorn aggregates prepared under nitrogen atmosphere

○Ryota Yuge¹, Takashi Manako¹, Masako Yudasaka², Kiyohiko Toyama¹, Takashi Yamaguchi³, Sumio Iijima⁴, and Kaichiro Nakano¹

¹ *Smart Energy Research Laboratories, NEC Corporation, Tsukuba 305-8501, Japan*

² *Nanotube Research Center, National Institute of Advanced Science and Technology (AIST), Tsukuba, 305-8565, Japan*

³ *Institute for Advanced Research, Nagoya University, Nagoya, 464-8602, Japan*

⁴ *Department of Materials Science and Engineering, Meijo University, Nagoya 468-8502, Japan*

Single-wall carbon nanohorns (SWNHs) are single-graphene tubules with nanometer-scale diameters, and about 2000 of them gather and form a spherical aggregate with diameters of 50-200 nm. Many fundamental and application studies have been done since its discovery in 1998 [1]. SWNHs with high purity are usually produced by CO₂ laser ablation of graphite without using a catalyst at a high production rate of 1 kg/day [2]. Here, we tried to synthesize SWNHs under N₂ atmosphere for achieving the low cost and investigated thoroughly the structures and electronic properties.

The CO₂ laser ablation was operated at 3.5 kW. During 30 seconds laser ablation, the target was rotated at 2 rpm. The buffer gases were N₂, or Ar. The gas flow rate and pressure were 10 L/min and 760 Torr, respectively. The obtained samples are denoted as N₂-SWNHs or Ar-SWNHs.

Shapes of N₂-SWNHs observed by a scanning electron microscopy and scanning transmission electron microscopy were quite similar to those of Ar-SWNHs. However, X-ray photoelectron spectroscopy results of N₂-SWNHs showed that the binding energy of N1s peak was 398 eV and that of C1s peak shifted to lower binding energy. Electron spin resonance spectra also indicated that localized spins and free electrons of N₂-SWNHs became about two times more than those of Ar-SWNHs. Therefore, we believe that the nitrogen atoms were incorporated into graphene lattice of SWNHs and carrier densities increased when SWNHs was synthesized under N₂ atmosphere. The details are shown in the presentation.

[1] S. Iijima *et al.* Chem. Phys. Lett. **309**, 165 (1999).

[2] T. Azami *et al.* J. Phys. Chem. C, **112**, 1330 (2008).

Corresponding Author: R. Yuge

Tel: +81-29-850-1566, Fax: +81-29-856-6137

E-mail: r-yuge@bk.jp.nec.com

Gastrointestinal behavior of orally-administered single-walled carbon nanohorns

○Maki Nakamura¹, Yoshio Tahara¹, Tatsuya Murakami², Sumio Iijima^{1,3}, Masako Yudasaka¹

¹ Nanotube Research Center, AIST, 1-1-1 Higashi, Tsukuba 305-8565, Japan

² Institute for Integrated Cell-Material Sciences (WPI-iCeMS), Kyoto University, Kyoto 606-8501, Japan

³ Meijo University, 1-501 Shiogamaguchi, Nagoya 468-8502, Japan

Single-walled carbon nanohorns (SWNHs) are expected to be applicable to drug carriers of drug delivery systems. We previously demonstrated that local injection of prednisolone-loaded SWNHs into the tarsal joint of rats with collagen-induced arthritis showed an anti-inflammatory effect [1]. The use of SWNHs as drug carriers by oral administration assumes to be useful, since graphitic SWNHs would tolerate acidic and alkaline environment in a gastrointestinal tract (e.g., stomach acid and digestive enzyme). However, such study has not been conducted yet. We show in this report the gastrointestinal behavior of orally-administered SWNHs and discuss the possibility of SWNHs as oral drug carriers:

For the quantity measurement of SWNHs, Gd₂O₃-embedded SWNHs (Gd-NHs) [2] were used in this study. Gd-NHs (2 mg per mouse) were administered orally into 8- to 9-week-old female mice (BALB/cA). After 4, 8, 16, 24 and 48 h, the mice were sacrificed by rapid collection of blood from the inferior vena cava, and removed liver, spleen, stomach, small intestine, cecum, and colon. Feces were also collected. After the combustion and acid dissolution treatment of blood, organs, and feces, the quantities of Gd from Gd-NHs in these samples were measured by inductively coupled plasma atomic emission spectroscopy.

The Gd in Gd-NHs was detected from gastrointestinal tract (i.e., stomach, small intestine, cecum, and colon), and feces; but not from liver, spleen, and blood. Almost 98% of SWNHs were excreted within 24 h, and over 99% after 48 h (Fig. 1). These results indicated that orally-administered SWNHs were not absorbed into the body through the gastrointestinal tract, and excreted in feces, suggesting that neither accumulation of orally-administered SWNHs in the body nor associated toxicity would be observed. SWNHs could be riskless oral drug carriers in drug therapy of gastrointestinal diseases, such as ulcerative colitis, colon cancer, and so on.

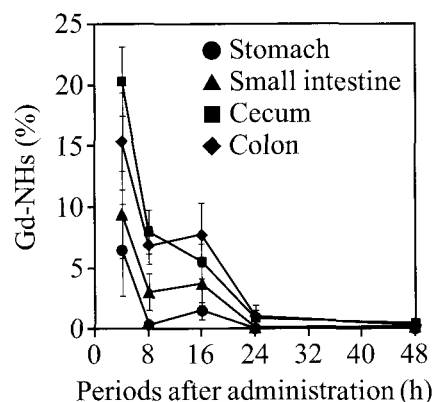


Fig. 1 Gastrointestinal behavior of Gd-NHs in mice. Quantities of Gd-NHs are plotted as percentages of the total quantity of administered Gd-NHs.

[1] M. Nakamura *et al.* *Nanotechnology* **22**, 465102 (2011).

[2] J. Miyawaki *et al.* *ACS Nano* **3**, 1399 (2009).

Corresponding Author: M. Nakamura, M. Yudasaka

Tel&Fax: +81-29-861-6290

E-mail: ma-ki-nakamura@aist.go.jp, m-yudasaka@aist.go.jp

Improvement in energy density of electric double-layer capacitors by mixture of AcB and CNB

○Y. Okabe¹, H. Izumi¹, Y. Suda¹, H. Takikawa¹, H. Tanoue¹, H. Ue², K. Shimizu³

¹*Department of Electrical and Electronic Information Engineering,
Toyohashi University of Technology,*

²*Tokai Carbon Co., Ltd.,*

³*Shonan Plastic Mfg. Co., Ltd.*

Electric double layer capacitors (EDLC) use carbon nano materials as electrode. It performs charge and discharge by the electric double layer which arises in the interface of an electrode and an electrolysis solution. In order to use EDLC for hybrid cars or electric vehicles, we have to increase energy density. In this research, to raise the energy density of EDLC, carbon nano materials which have different structures were mixed. We used two kinds of carbon materials. One is the arc black (AcB), and the other is the carbon nano balloon (CNB). AcB includes an amorphous ingredient mostly and has a large specific surface area. Then AcB has larger specific capacity than CNB. On the other hand, surface of CNB is graphitic and it has high conductivity. In order to utilize each characteristic of AcB and CNB, they were used for the main material of the electrode by the ratio of 1:1. Fig.1 shows that the specific capacity became higher than capacitors which used each alone at the rate from 100 mV/s to 500 mV/s, and the characteristic at a high rate was improved. Furthermore, Fig.2 shows a Ragon plot of EDLC and that exhibited a high energy density by mixing AcB and CNB.

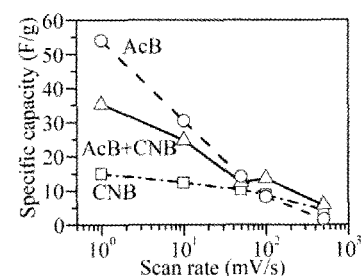


Fig.1 Specific capacitance

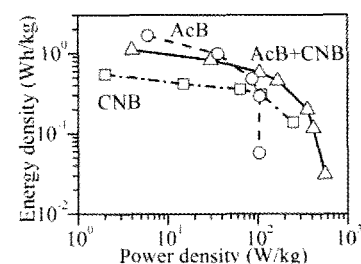


Fig.2 Ragon plot

This work has been partly supported by the Research Project of the Venture Business Laboratory from Toyohashi University of Technology (TUT); the Core University Programs (JSPS-CAS program in the field of "Plasma and Nuclear Fusion") from the Japan Society for the Promotion of Science (JSPS); and a Grand-in-Aid for Scientific Research from the JSPS.

[1] Cheng Zheng, *et al.*: *J. Power Sources*, 195, 4406-4409 (2010)

Corresponding Author: Yoshiyuki Suda

E-mail: suda@ee.tut.ac.jp, Tel: 0532-44-6726

ポスター発表
Poster Preview

1P - 1 ~ 1P - 50

2P - 1 ~ 2P - 41

3P - 1 ~ 3P - 42

Growth investigation of C₆₀-C₇₀ two-component fullerene nanowhiskers

○Chika Hirata, Shuichi Shimomura¹, Takatsugu Wakahara and Kun'ichi Miyazawa

*Fullerene Engineering Group, Carbon Composite Materials Group¹,
Materials Processing Unit, National Institute for Materials Science(NIMS),
1-1 Namiki, Tsukuba 305-0044, Japan*

The liquid-liquid interfacial precipitation simple method (LLIP method) has been used to synthesize various fullerene nanowhiskers. Since it is very important to study the size control of fullerene nanowhiskers for their practical application, we have been developing various methods by modifying the original LLIP method proposed in 2002 [1].

The factors that influence the growth of C₆₀NWs are light, temperature, growth time, water, and the kind and composition of solvent.

It is reported that the diameter control of C₆₀NWs is possible by controlling the area of liquid-liquid interface [2]. Additionally, we synthesized C₆₀NWs using several bottles of different inner diameters, and measured the length and diameter of C₆₀NWs [Fig.1, Fig2]. It is found that the length and diameter of C₆₀NWs increase with increasing the size of glass bottle. Although we reported the fabrication of C₆₀-C₇₀ two-component nanowhiskers [3], the influence of composition on the growth of C₆₀-C₇₀ nanowhiskers have not been clarified. Hence we investigate how the powder composition influences the growth of fullerene nanowhiskers.

In preparing the C₆₀-C₇₀NWs, toluene was used as a good solvent and isopropyl alcohol (IPA) as a poor solvent of C₆₀. C₆₀ powders containing C₇₀ were dissolved in toluene (2.8 mg/ml) and the C₆₀-C₇₀-toluene solutions were ultrasonicated for 30 minutes to obtain C₆₀-C₇₀-saturated toluene solutions. The solutions were filtered to remove undissolved residuals of C₆₀ and C₇₀. IPA was gently added to the C₆₀-C₇₀-saturated toluene solutions, and manually mixed 30 times. The synthesis temperature was 15°C. It has been found that the growth rate of C₆₀-C₇₀ nanowhiskers varies depending on the composition of C₆₀ and C₇₀.

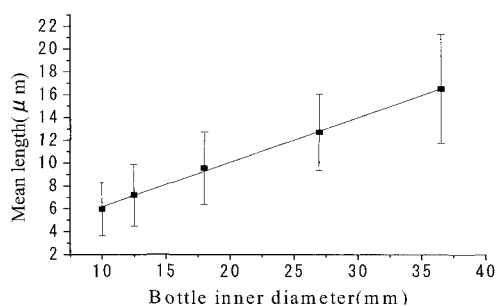


Fig.1 Relationship between the mean length of C₆₀NWs and the inner diameter of glass bottle.

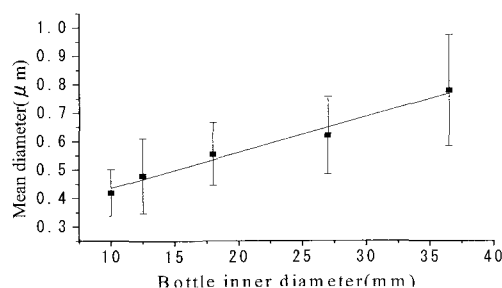


Fig.2 Relationship between the mean diameter of C₆₀NWs and the inner diameter of glass bottle.

[1] Fullerene Nanowhiskers, Kun'ichi Miyazawa (Ed.) (Pan Stanford Publishing, 2011).

[2] T.Wakahara, K.Miyazawa, Y.Nemoto, O.Ito, Carbon⁴⁹ (2011) 4644-4649

[3]K. Miyazawa, J. Minato, T. Mashino, T. Yoshii and T. Suga, Trans. Mat. Res. Soc. Japan **30** (2005) 967-970

Corresponding Author: K.Miyazawa

Tel: +81-29-860-4528, Fax: +81-29-860-4667,

E-mail: miyazawa.kunichi@nims.go.jp

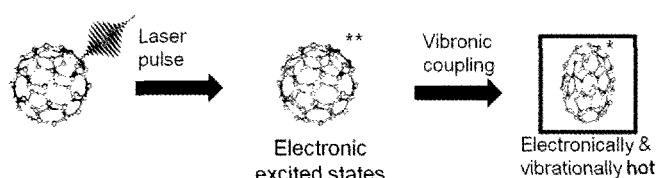
Simulation of Near-Infrared Excitation of Raman Active Modes in Fullerene C₆₀ by a Time-Dependent Adiabatic State Approach

○Kaoru Yamazaki, Takashi Nakamura, Naoyuki Niitsu, Manabu Kanno, and Hirohiko Kono

*Department of Chemistry, Graduate School of Science,
Tohoku University, Sendai, 980-8578, Japan*

Intense near-IR laser pulse with femtosecond (fs, 10^{-15} s) order duration is a prominent tool to fabricate nanoscale electronic devices made from nanocarbons [1]. The interaction with near-IR fs laser pulses induces coherent vibration of nanocarbons which leads to structural transformation (e.g., fragmentation and rearrangement) [2] in the range from picoseconds to microseconds as illustrated in Fig. 1. Recently, we reported a molecular dynamics (MD) study on the fragmentation of C₆₀ fullerene induced by near-IR fs laser pulses based on density functional theory and density-functional based tight-binding (DFTB) theory [3,4]. We showed that the fragmentation patterns and dynamics of C₆₀ depend on the vibrational mode initially excited by the laser pulses, even though the fragmentations occur in nanoseconds (ns, 10^{-9} s) after laser irradiation [5].

(1) Laser-molecule interactions ($t \approx 100$ fs) → Energy capturing



(2) Structural transformations ($t = \text{ps}-\mu\text{s}$)

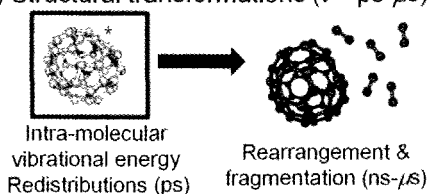


Fig. 1 Laser induced processes of nanocarbons

Toward efficient simulations of laser induced structural dynamics in larger nanocarbons such as carbon nanotube and graphene, we developed a new theoretical method, which enables the calculation of laser-induced dynamics of nanocarbons in the nanosecond (ns) time-scale. In this method, we combined the time-dependent adiabatic state approach, which can properly describe the distortion of potential energy surfaces of nanocarbons by near-IR laser fields [6], and the DFTB theory [4] which can treat ns-scale reaction dynamics of nanocarbon semi-quantatively [5]. In this presentation we discuss the dynamics of near-IR excitation of Raman active modes in fullerene C₆₀ as a test case.

[1] R. Stöhr *et al.*, ACS Nano **5**, 5141–5150 (2011).

[2] T. Laarmann *et al.*, Phys. Rev. Lett. **98**, 058302 (2007).

[3] D. Porezag, *et al.*, Phys. Rev. B **51**, 12947–12957 (1995).

[4] M. Elstner, *et al.*, Phys. Rev. B **58**, 7260–7268 (1998).

[5] N. Niitsu, K. Yamazaki *et al.*, J. Chem. Phys. **136**, 164304 (2012).

[6] Y. Sato, H. Kono, S. Koseki, and Y. Fujimura, J. Am. Chem. Soc. **125**, 8019–8031 (2003).

Corresponding Author: H. Kono

Tel & Fax: +81-22-795-7720

E-mail: hirohiko-kono@m.tohoku.ac.jp

Theoretical investigation of the fragmentation dynamics of photoexcited C_{60} fullerene

○Takashi Nakamura¹, Naoyuki Niitsu¹, Manabu Kanno¹, Hirohiko Kono¹, Kiyoshi Ueda²

¹Graduate School of Science, Tohoku University, Sendai 980-8578, Japan

²Institute of Multidisciplinary Research for Advanced Materials, Tohoku University, Sendai 980-8577, Japan

【Introduction】 It is experimentally known that ionization competes with fragmentation when C_{60} fullerene is irradiated by intense laser pulses. The ratio between ionization and fragmentation can be controlled by changing the photon energy and pulse width. For instance, using near infrared laser pulses ($\lambda = 800$ nm), fragmentation is promoted by a pulse with 5 ps duration. For a shorter pulse with 25 fs duration, multiply charged cations are created and fragmentation is relatively suppressed [1]. On the other hand, irradiation of X-ray free electron lasers (XFELs) is expected to produce multiply charged cations C_{60}^{n+} up to $n = 12$ via the different process consisting of inner shell ionization, rearrangement of electrons, and Auger ionization. The multiply charged C_{60} cations are considered to dissociate due to its excess vibrational energy, which can be estimated from the energy of emitted electrons. The information on the dynamics of C_{60}^{n+} can be obtained from the observation of its fragments. We theoretically investigated the vibrational and fragmentation dynamics of C_{60}^{n+} with high excess energy.

【Method】 On the assumption of irradiating C_{60} with XFEL, we optimized the structures of C_{60}^{n+} ($n = 8, 10, 12$) and added 40~120 eV of energy. We investigated the dynamics of C_{60}^{n+} such as fragmentation time and fragmentation patterns using molecular dynamics (MD) calculations based on a density-functional tight-binding method.

【Results and Discussion】 Various fragmentation patterns were observed depending on energy. For lower energies of 40~60 eV, C_2 evaporation proceeds after Stone-Wales rearrangement shown in Fig.1 [2]. The activation barriers for Stone-Wales rearrangement of C_{60}^{n+} are less than 10 eV. The excess energy is therefore high enough to cause Stone-Wales rearrangement. For higher energies of 80~120 eV, two types of fragmentation shown in Fig.2 are observed, as in the case of neutral C_{60} [3]. In Process 2, the cage cleaves first and then small fragments are ejected. The lifetime of C_{60}^{n+} for fragmentation becomes shorter as the charge and energy increase. In the poster, we report the dependence of fragmentation on the charge and energy of C_{60}^{n+} .

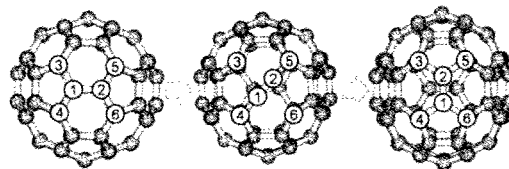


Fig. 1 Stone-Wales rearrangements for lower initial energy (40~60 eV)

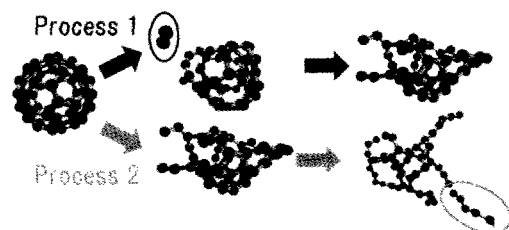


Fig. 2 Two fragmentation processes of C_{60}^{n+} ($n = 8, 10, 12$) for higher energy (80~120 eV).

[1] I. V. Hertel et al., *Adv. At.Mol. Opt. Phys.* **50**, 219 (2005).

[2] A. J. Stone and D. J. Wales, *Chem. Phys. Lett.* **128**, 501(1986)

[3] N. Niitsu et al., *J. Chem. Phys.* **136**, 164304(2012)

Geometric and electronic structures of two-dimensional networks of fused C_{26} fullerenes

○Mina Maruyama and Susumu Okada

Graduate School of Pure and Applied Sciences, University of Tsukuba, Tennodai, Tsukuba 305-8577, Japan

Hollow-cage carbon clusters, fullerenes, are known to form condensed phases in which the fullerene is a constituent unit as in the case of atoms in the conventional solids. Since fullerenes have moderate chemical reactivity, various new carbon network materials derived from fullerenes have been synthesized and studied intensively. For instance, C_{60} molecules form covalent bonds with its adjacents leading to interesting forms of one-, two-, and three-dimensional carbon allotropes with three-fold and four-fold coordinated C atoms. Electronic structures of these novel carbon allotropes derived from C_{60} strongly depend on their dimensionality and morphologies. Small fullerenes, C_n where $n < 60$, are possible candidates as a constituent unit for such new forms of C allotropes with mixed coordination. Indeed, geometric and electronic structures of such smaller fullerenes, such as C_{20} and C_{36} , were studied in theoretically. Here, we design a novel two-dimensional covalent network with hexagonal symmetry comprising of small fullerene C_{26} . Since C_{26} has D_{3h} symmetry, we can construct a two-dimensional hexagonal covalent network of C atoms generated by a fused C_{26} unit. To examine stability, stable geometries, and electronic structures of condensed phase C_{26} , we perform the first-principles total-energy calculations in the framework of the density functional theory..

Figure 1 shows an optimized structure of two-dimensionally polymerized C_{26} . As shown in figure, the condensed phase of C_{26} forms a two-dimensional hexagonal network as in the case of graphene sheet. Therefore, the resultant material is the candidate for novel layered materials with large interstitial sites and the host materials for foreign atoms and molecules. By focusing on the bonding network of this material, the polymer comprises two-fold and three-fold coordinated C atoms. Furthermore, according to the structural relaxation, C_{26} unit no longer is a polyhedron consisting of pentagons and hexagons but it contains octagonal rings besides pentagons and hexagons.

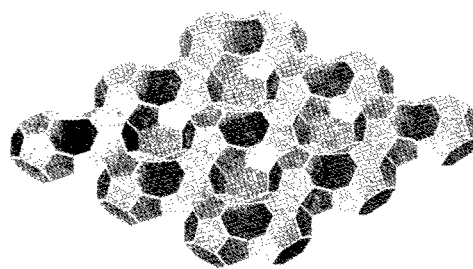


Fig. 1 Optimized structure of C_{26} polymer.

Corresponding Author: M.Maruyama
Tel: +81-29-853-5600, Fax: +81-29-853-5924,
E-mail: mmaruyama@comas.frsc.tsukuba.ac.jp

Charge density distribution of water molecule encapsulated in fullerene C₆₀

○Shinobu Aoyagi¹, Yuki Sado², Ryo Kitaura², Hisanori Shinohara²,
Tomoko Nishida³, Yasujiro Murata³

¹ *Department of Information and Biological Sciences, Nagoya City University,
Nagoya 467-8501, Japan*

² *Department of Chemistry and Institute for Advanced Research, Nagoya University,
Nagoya 464-8602, Japan*

³ *Institute for Chemical Research, Kyoto University, Uji, Kyoto 611-0011, Japan*

An endohedral fullerene with a dipole moment will be achieved by an encapsulation of a polar molecule such as water molecule. Recently, fullerene C₆₀ with a water molecule inside, H₂O@C₆₀ (Fig.1) has been synthesized by the molecular surgical method [1]. The effective dipole moment of H₂O@C₆₀ should depend on the orientation and dynamics of the encapsulated water molecule. The X-ray structure analysis of a co-crystal of H₂O@C₆₀ and octaethylporphyrin nickel (Ni(OEP)) has revealed that the OH bonds of the water molecule located at the cage center direct toward the Ni atoms of the Ni(OEP) ligands outside the carbon cage [1]. The molecular orientation would be changed in a pure H₂O@C₆₀ crystal without any ligand and solvent molecules. Indeed it has been found that the endohedral structure of Li⁺@C₆₀ depends on the specie and arrangement of coordinated counter anions [2,3]. In order to reveal the molecular orientation and thermal motion of the encapsulated water molecule in the pure H₂O@C₆₀ crystal, the crystal structure analysis was carried out by means of the synchrotron radiation X-ray diffraction at SPring-8 (Hyogo, Japan).

The structure of pure H₂O@C₆₀ crystal is very similar to that of pristine C₆₀ crystal. The crystal has a cubic structure and undergoes a phase transition due to a freezing of free rotation of the carbon cage at around 260 K. The carbon cage in the low temperature phase has a disordered structure in which two kinds of cage orientation coexist. The molecular structure of H₂O@C₆₀ at 20 K was successfully determined except the position of hydrogen atoms.

To visualize the hydrogen atoms, the charge density distribution of the encapsulated water molecule was obtained by the maximum entropy method (MEM). Charge density peaks for hydrogen atoms were not clearly observed, while a peak for an oxygen atom was observed at the cage center. This result demonstrates that the orientation of the encapsulated water molecule is disordered even at 20 K. Broad charge density distribution for the disordered hydrogen atoms was observed in the difference MEM charge densities which are obtained by subtracting model charge densities without hydrogen atoms from the experimental one. Possible orientations of the encapsulated water molecule are discussed based on the difference MEM charge densities.

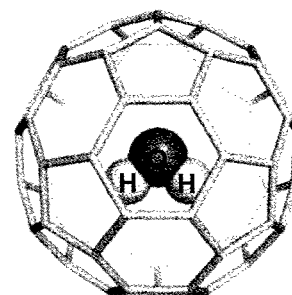


Fig.1 Schematic molecular structure
of H₂O@C₆₀.

[1] K Kurotobi and Y. Murata *Science* **333**, 613 (2011).

[2] S. Aoyagi *et al.* *Angew. Chem. Int. Ed.* **51**, 3377 (2012).

[3] S. Aoyagi *et al.* *Nature Chem.* **2**, 678 (2010).

Corresponding Author: S. Aoyagi

Tel: +81-52-872-5061, Fax: +81-52-872-3495,

E-mail: aoyagi@nsc.nagoya-cu.ac.jp

Growth Mechanism of Fullerenes Revisited

○ Susumu Saito

*Department of Physics, and
Research Center for Nanometer-Scale Quantum Physics
Tokyo Institute of Technology
2-12-1 Oh-okayama, Meguro-ku, Tokyo 152-8551, Japan*

Ever since the macroscopic production of C_{60} fullerenes more than two decades ago [1], C_{60} and other fullerenes have been intensively studied in many fields of science and technology. On the other hand, the origin of the extreme abundance of C_{60} in soot as well as the microscopic formation process of C_{60} and other fullerenes still remains to be revealed. In our previous work addressing the formation process of carbon clusters and fullerenes using the transferable tight-binding Hamiltonian with long-range interatomic interaction [2], it has been revealed that carbon clusters should take closed-cage geometries with mainly hexagons and pentagons from the size of C_{40} [3]. Also, from the first-principles density-functional study we have confirmed that the reactivity of C_{60} with the C atom is smaller than that of C_{70} although the C_{70} is energetically more stable than C_{60} [4]. In the present work we discuss the growth mechanism of fullerenes and the time evolution of the abundance of carbon clusters using the statistical analysis [5]. In addition to the “growth reactions” of carbon clusters, the C_2 loss process, which has been confirmed to be more “popular” process in fullerenes larger than C_{60} , is taken into account. It is revealed that in certain conditions the carbon-cluster system considered can possess extremely abundant C_{60} fullerenes (Fig. 1).

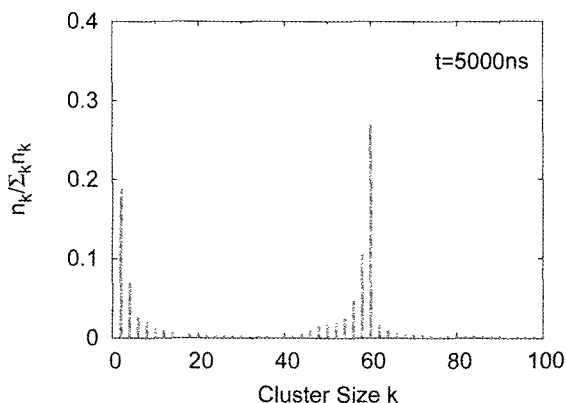


Figure 1 Population densities after 5ms [5].

[1] W. Krätschmer, L. D. Lamb, K. Fostiropoulos, and D. R. Huffman, *Nature* **347**, 354 (1990).

[2] Y. Omata, Y. Yamagami, K. Tadano, T. Miyake, and S. Saito, *Physica E* **29**, 454 (2005).

[3] Y. Ueno and S. Saito, *Phys. Rev. B* **77**, 085403 (2008).

[4] Y. Ueno and S. Saito, *Physica E* **40**, 285 (2007).

[5] Y. Ueno and S. Saito, to be published.

Corresponding Author: S. Saito

Tel: 03-5734-2070, Fax: 03-5734-2739

E-mail: saito@stat.phys.titech.ac.jp

Fullerene Growth Mechanism and Regioselectivity of Dimeric Carbon Addition

O.J.-S. Dang, W.-W. Wang, and Xiang Zhao*

*Institute for Chemical Physics & Department of Chemistry, Faculty of Science,
Xi'an Jiaotong University, Xi'an 710049, China*

Ever since the discovery and macroscopic scale synthesis of I_h -symmetric C_{60} , several hypothetical models have been established to elucidate the formation process of fullerenes from graphite or amorphous carbon. Based on mass spectrometry information elicited from previous experiments, fullerenes are believed to derive from atomic carbon or small clusters. Such a growth model is defined as a bottom-up mechanism. A heptagon-corporation chlorinated C_{68} species was captured and isolated recently from carbon arc plasma *in situ*,¹ which provides important evidence for the rationality of the formation modeling.

In the present work, a bottom-up topological pathway was established to elucidate the growth of small fullerenes and the generation of I_h -symmetric C_{60} . In contrast to countless growth mechanisms, the model described herein has two distinctive features. First, each fullerene on the route possesses the lowest potential energy or exhibits a predominant molar fraction at elevated temperatures in the corresponding series. Second, a C_2 insertion without any high-barrier rearrangement process (such as Stone–Wales transformation) can connect two adjacent molecules on the route directly. These two characteristics imply that the fullerene stability can be inherited through continuous insertion of a C_2 cluster during carbon-cage enlargement. Furthermore, an investigation of the regioselectivity of C_2 addition using density functional theory (DFT) is reported and the kinetic calculation results² demonstrate that the reaction to the most stable product exhibits the highest chemical reactivity, indicating that the proposed growth route is favorable both thermodynamically and kinetically.

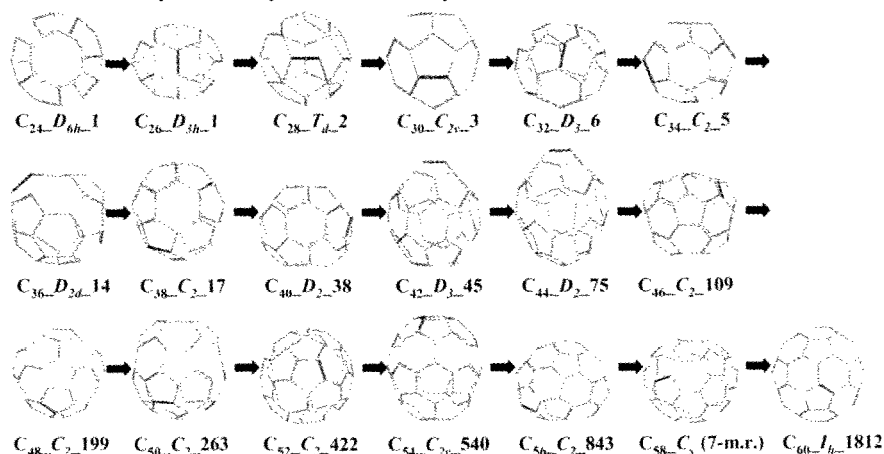


Figure 1. Growth pathway from C_{24} to C_{60} .

Reference:

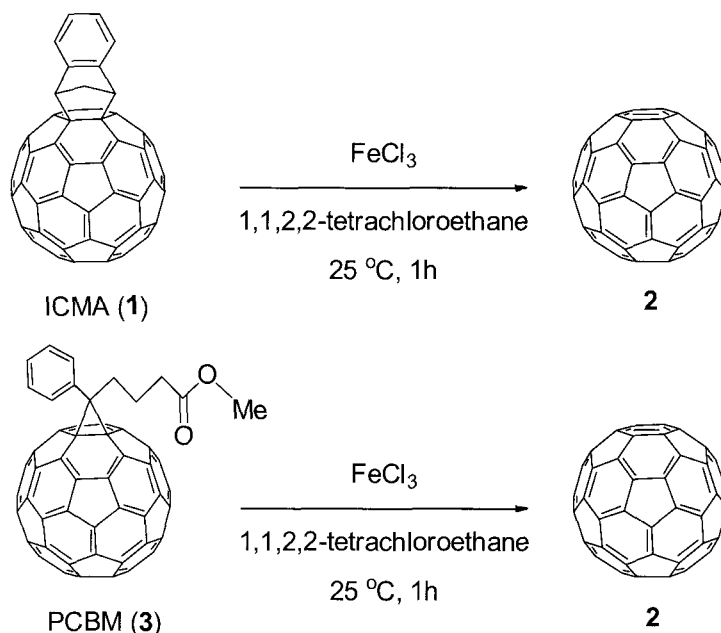
1. Y. Z. Tan, *et al. Nature Comm.* **2011**, 2, 420.
2. J. S. Dang, W. W. Wang, J. J. Zheng, X. Zhao, *et al. J. Phys. Chem. C*, **2012**, 116, in press.

* Corresponding author: X. Zhao; Email: x86zhao@yahoo.co.jp

FeCl₃-mediated retro-reaction of fullerene derivatives○Masahiko Hashiguchi¹, Takao Ueno¹, Yutaka Matsuo²¹ Fullerene Development Group, Performance Products Division, Mitsubishi Chemical Corporation, Kitakyushu, 806-0004, Japan² Department of Chemistry, The University of Tokyo, Tokyo, 113-0033, Japan

We have reported facile synthetic methods of fullerene derivatives (polyarylated fullerenes and fullerenyl esters) using inexpensive iron trichloride (FeCl₃)^[1,2]. Herein we report a new retro-reaction of fullerene derivatives by using FeCl₃.

ICMA (indene-C₆₀ monoadduct) and PCBM (phenyl-C₆₁-butyric acid methyl ester) are commonly used n-type component in organic photovoltaics, therefore the retro-reaction cannot occur simply by heating at 150°C in 1,1,2,2-tetrachloroethane. However, FeCl₃-mediated retro-reaction of their fullerene derivatives proceeded at 25°C with approximately 100% conversion, yielded an unsubstituted C₆₀ (up to 37% yield).

**Scheme 1.** Retro-reaction of fullerene derivatives

Other Lewis acids and a Brønsted acid were tested; FeCl₂, AlCl₃, BF₃·Et₂O, RuCl₃, NiCl₂, CoCl₂, ZnCl₂, and *p*-toluenesulfonic acid all gave poor results. We surmise that strong electron accepting ability to oxidize the fullerene unit is necessary for this retro-reaction. The detail will be shown in the poster presentation.

[1] M. Hashiguchi, K. Watanabe, Y. Matsuo, *Org. Biomol. Chem.* **9**, 6417 (2011).[2] M. Hashiguchi, N. Obata, M. Maruyama, K. S. Yeo, T. Ueno, T. Ikebe, I. Takahashi, Y. Matsuo, *Org. Lett.* **14**, 3276 (2012).

Corresponding Author: Masahiko Hashiguchi

Tel: +81-93-643-4402, Fax: +81-93-643-4401

E-mail: 6206530@cc.m-kagaku.co.jp

Dual reactivity of azafulleroid due to its ambident n/π -basicity

○Naohiko Ikuma, Yuta Doi, Tsubasa Mikie, Koji Nakagawa,
Ken Kokubo and Takumi Oshima

*Division of Applied Chemistry, Graduate School of Engineering,
Osaka University, Suita 565-0871, Japan*

Azafulleroid, derived from 1,3-dipolar cycloaddition of azide with C_{60} and nitrogen evolution, behaves as an ambident nucleophile containing one basic nitrogen and two reactive bridgehead double bonds with larger HOMO-coefficients (Figure 1). Thus, azafulleroid can be useful synthetic precursor for various fullerene derivatives, depending on its electronic and/or steric effects around the reaction sites.

Here, we report the acid-promoted arylation of variously substituted azafulleroids. This reaction was prompted by excess amount of CF_3SO_3H , while no reaction occurred with CH_3SO_3H . It was found that the products depended on the substituents of the bridged nitrogen atom; the alkyl-substituted azafulleroid provided 1,4-arylamino fullerene, while the aryl-substituted azafulleroid gave tetrakis- or pentakis-adducts. The difference in the reactivity would be ascribed to which site of the enamino moiety the protonation initially occurred, as illustrated in Scheme 1.

bridged nitrogen

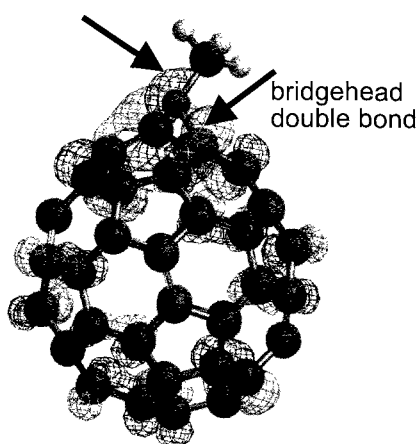
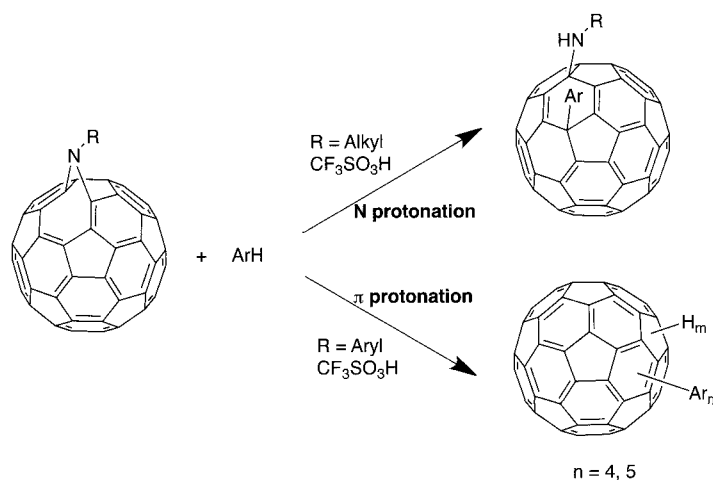


Figure 1. HOMO of azafulleroid (R = Me)



Scheme 1.

Corresponding Author: Takumi Oshima

E-mail: oshima@chem.eng.osaka-u.ac.jp Tel: +81-6-6879-4591 Fax: +81-6-6879-4591

Theoretical investigation on vibrational excitation and reaction dynamics of polyhydroxy fullerene induced by a near-infrared laser

○Akinobu Ikeda¹, Naoyuki Niitsu¹, Manabu Kanno¹, Stephan Irle², Hirohiko Kono¹

¹Graduate School of Science, Tohoku University, Sendai 980-8578, Japan

²Graduate School of Science, Nagoya University, Nagoya 464-8602, Japan

【Introduction】 Polyhydroxy fullerenes ($C_{60}(OH)_{24}$) are rapidly heated when irradiated even by a low-intensity laser ($<10^3$ W/cm²), and then energetic fullerene cages collide, leading to disintegration or coalescence into various larger nanocarbons. (Fig. 1) [1]. This type of reaction does not occur in the case of fullerenes or their derivatives with other functional groups. To reveal the mechanism of this reaction, we investigated the behavior of polyhydroxy fullerenes in a continuous-wave (CW) laser and the subsequent reaction dynamics of the heated polyhydroxy fullerene.

【Method】 We calculated the nanosecond dynamics of $C_{60}(OH)_{24}$ irradiated by a near-IR pulse (10^3 W/cm², 785 nm, 5 ns) with a rectangular pulse shape as well as the subsequent dynamics of vibrationally excited $C_{60}(OH)_{24}$ and $C_{60}(OH)_4$ with the density-functional tight-binding method. The dipole interaction with laser fields was described in the time-dependent adiabatic state approach [2].

【Results】 We found that after the laser field is turned on ($t = 0$), O-H stretching vibration is first excited. This indicates that hydroxyl groups can be easily heated by a low-intensity laser. At $t > 2$ ns, the skeletal vibrations of the fullerene cage are also observed. As a result, the kinetic energy of $C_{60}(OH)_{24}$ was rapidly increased by 140 K at $t \sim 5$ ns (Fig. 2). This indicates that enormous rise in temperature is expected for a CW laser excitation. In addition, the subsequent dynamics of highly heated $C_{60}(OH)_{24}$ and $C_{60}(OH)_4$ suggests that dehydration reactions tend to occur between adjacent hydroxyl groups. Both the electronic structure calculation of the transition state (B3LYP/6-31G**) and the Arrhenius plot for the dynamics of $C_{60}(OH)_4$ showed that the activation energy of the dehydration reaction is about 2 eV.

[1] V. Krishna, N. Stevens, B. Koopman, and B. Moudgil, *Nature Nanotechnology* **5**, 330 (2010).

[2] Y. Sato, H. Kono, S. Koseki, and Y. Fujimura, *J. Am. Chem. Soc.* **125**, 8020 (2003).

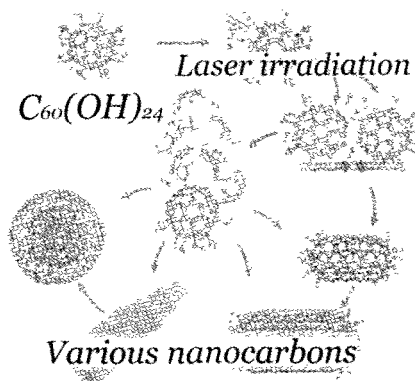


Fig. 1: Proposed mechanism for laser-induced transformation of $C_{60}(OH)_{24}$ [1].

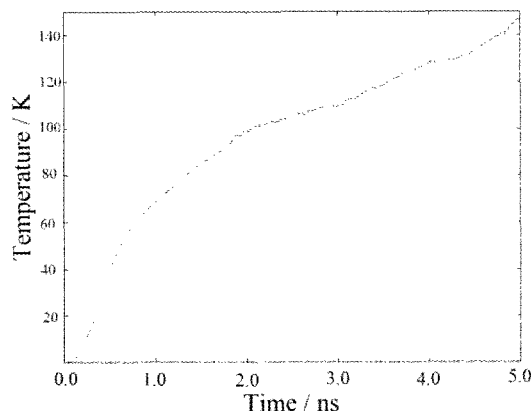


Fig. 2: Temporal change in the temperature of $C_{60}(OH)_{24}$ for near-IR laser excitation.

Highly Hydrophilic Non-Surface-Active Conical Fullerene Amphiphiles for Dispersion of Solid Materials

○ Hirohisa Nitta, Koji Harano, Eiichi Nakamura

*Department of Chemistry, The University of Tokyo, Hongo, Bunkyo-ku,
Tokyo 113-0033, Japan*

Surfactants are amphiphilic molecules that have been widely used in daily life and industries as detergents and dispersion agents, and the functions are determined by critical micelle concentration (CMC). Surfactants preferably adsorb onto air-water interface, and it is only after full coverage of the surface or above CMC that they start to self-assemble in bulk. Lowering CMC while retaining enough water solubility is necessary because the performance of surfactants become sufficient at concentrations above their CMC.

Considering the self-assembly process, we envisaged that non-surface-active amphiphiles would serve as good dispersion agents. Because non-surface active amphiphiles do not adsorb onto an air-water interface, they can directly assemble in water, resulting in low CMC. Matsuoka and his co-workers have proposed a theory of non-surface activity of amphiphilic block copolymers [1]. They say that a charged amphiphilic molecule generates image charge in air when it approaches water surface. If the molecules have multiple charged groups, strong electrostatic repulsion between the original charges and the image charges inhibits adsorption onto water surface.

Here we developed non-surface active conical fullerene amphiphiles, and applied them for dispersion of solid materials (Fig. 1). The molecules are designed to have multiple charged groups so that they have high water solubility, and were expected to show non-surface-active character due to the multiple charges getting closer to air phase upon approaching to water surface. As expected, the amphiphiles did not show surface activity, and as a result, showed significantly low CMC. The ability of the amphiphiles for dispersion of solid materials was demonstrated by dispersion of nanocarbons (single-wall carbon nanotubes (SWNTs), carbon nanohorns (CNHs), and graphene). The newly developed fullerene amphiphiles dispersed the nanocarbons successfully with higher efficiency compared to conventional surfactants. In addition, the dispersion efficiency was better than $\text{KC}_{60}\text{Ph}_5$ [2], a similar conical fullerene derivative with a single hydrophilic group and lower CMC, highlighting the advantage of the molecular design with both high hydrophilicity and non-surface activity.

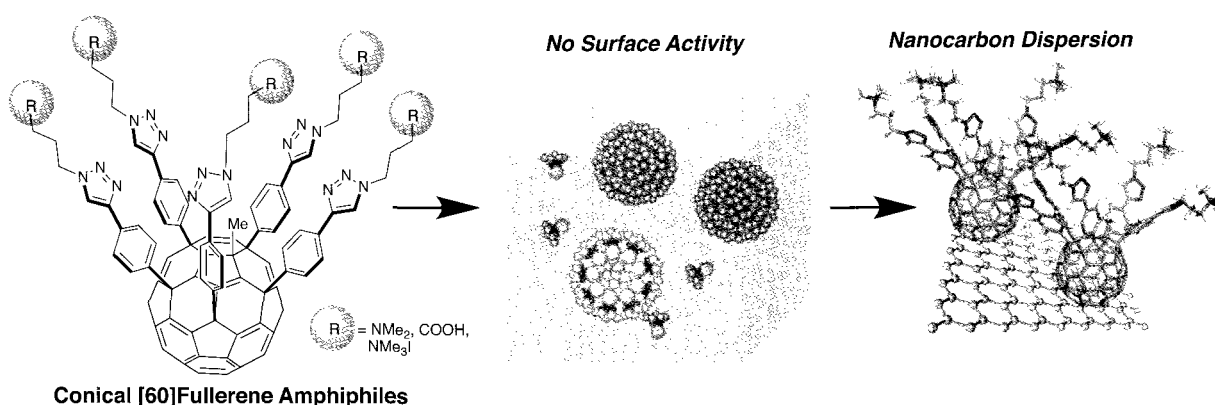


Fig. 1 Structure, self-assembly, and function of conical [60]fullerene amphiphiles.

[1] A. Ghosh, S. Yusa, H. Matsuoka, Y. Saruwatari *Langmuir* **27**, 9237 (2011).

[2] S. Zhou, C. Burger, B. Chu, M. Sawamura, N. Nagahama, M. Toganoh, U. E. Hackler, H. Isobe, E. Nakamura *Science* **291**, 1944 (2001).

Corresponding Author: Eiichi. Nakamura, Tel/FAX: +81-3-5841-4356, E-mail: nakamura@chem.s.u-tokyo.ac.jp

Magic number effects on aggregation of polyhydroxylated fullerenes in alcohol–water binary solvent

○Yuji Nakamura, Hiroshi Ueno, Naohiko Ikuma, Ken Kokubo, Takumi Oshima
*Division of Applied Chemistry, Graduate School of Engineering, Osaka University,
 Suita, 565-0871, Japan*

As the size of nanoparticles decreases, property of the surface becomes more dominant than that in the bulk. We have developed the facile synthesis of highly hydroxylated fullerenes, so-called fullerrenols $C_{60}(OH)_{36}$ and $C_{60}(OH)_{44}$, and have found their particle sizes in water are only ca. 1 nm as small as the molecular size [1]. The property of hydroxylated surface of the fullerrenol is very interesting in view of the aggregation manner because of the attractive intermolecular hydrogen bond. Herein, we report the notable aggregation behavior of fullerrenols by changing the solvent polarity.

The particle size of two types of fullerrenols, water-insoluble $C_{60}(OH)_{10}$ and water-soluble $C_{60}(OH)_{36}$, in a binary polar solution was measured using Induced Grating (IG) method [2]. By increasing the ratio of alcohols in aqueous $C_{60}(OH)_{36}$ solution, the highly dispersing $C_{60}(OH)_{36}$ molecule (ca. 1 nm) sharply aggregated up to ca. 6–7 nm (Fig. 1). Then the further addition of alcohols brought about the secondary gradual aggregation. Such an appreciable two-step aggregation implied the formation of “magic number” cluster, as exemplified for the $(C_{60})_n$ clusters (e.g., $n = 13, 19, 39$, and so on) in gas-phase [3]. This cluster formation may be caused by the characteristic solute–solvent interaction between the fullerrenol and the solvent molecules mainly due to the hydrogen bond of hydroxyl groups. By contrast, DMSO–water binary solvent did not show the similar two-step aggregation behavior.

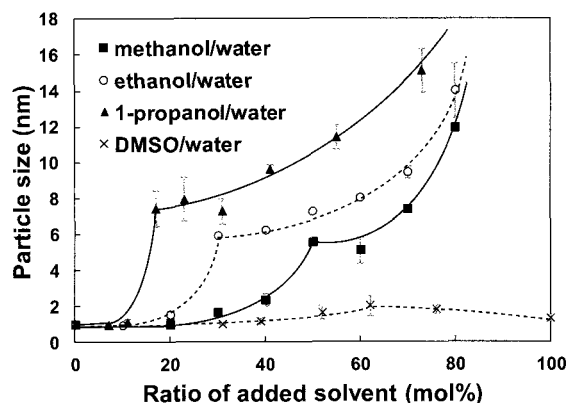


Figure 1. Particle sizes of polyhydroxylated fullerene $C_{60}(OH)_{36}$ aggregate in binary solvent (1 mM) measured by IG method on varying molar ratio of methanol (■), ethanol (○), 1-propanol (▲), and DMSO (×).

[1] K. Kokubo *et al.* *ACS Nano* **2**, 327 (2008); K. Kokubo *et al.* *Nano Res.* **4**, 204 (2011).

[2] Y. Wada *et al.* *Opt. Exp.* **14**, 5755 (2006).

[3] W. Branz *et al.* *Chem. Phys. Lett.* **328**, 245 (2000).

Corresponding Author: K. Kokubo

Tel: +81-6-6879-4592, Fax: +81-6-6879-4593, E-mail: kokubo@chem.eng.osaka-u.ac.jp

Synthesis and Photophysical Properties of [60]Fullerene–Cobalt Dyads and Triads

○Masashi Maruyama¹, Dirk M. Guldi², Eiichi Nakamura¹, Yutaka Matsuo¹

¹ Department of Chemistry, School of Science, The University of Tokyo, Hongo, Bunkyo-ku, Tokyo 113-0033, Japan

² Department of Chemistry and Pharmacy and Interdisciplinary Center for Molecular Materials, Friedrich-Alexander-Universität, Erlangen-Nürnberg, Germany

Connection of [60]fullerene moieties and chromophores is a widely known methodology for creation of photo-induced charge or energy transfer systems. Aiming at utilization of a wide range of regions in sunlight, dyad or triad systems bearing chromophores with complementary absorptions have been intensely studied.[1] Especially, efficient uses of long-wavelength light are of great importance in artificial photosynthesis, photovoltaic systems, and so on.

Penta-aryl [60]fullerene derivatives are known as highly functionalized [60]fullerene derivatives, which are capable of affording columnar liquid crystals, self-assembled monolayers, various metal complexes, photovoltaic materials, and so on.[2] Photophysical properties, especially time-dependent behaviors, have been studied in some cases, and their potentials in photo-functional systems were elucidated.[3] However, charge or energy transfer dynamics of penta-aryl [60]fullerene derivatives upon long-wavelength light irradiation have long remained unknown because of the synthetic limitations of such systems.

Thus, we developed several synthetic methods to obtain a variety of [60]fullerene–cobalt dyad and triad materials, which can be represented as A'–A (acceptor–acceptor), A–D (acceptor–donor), and A–D–A (acceptor–donor–acceptor) systems (Figure 1). Their photophysical properties were investigated with time-dependent spectroscopic measurements. Details of the dynamics in excited states are to be discussed in the poster session.[4]

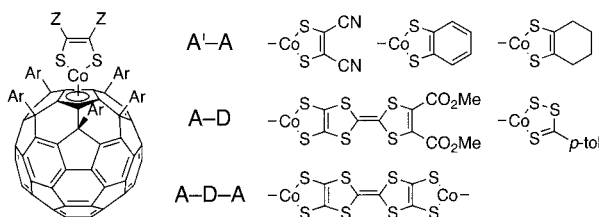


Figure 1. Structures of [60]fullerene dyads and triads investigated in this work.

[1] For reviews, (a) D. M. Guldi, *Chem. Soc. Rev.* **31**, 22–36 (2003) (b) I. Beletskaya, *et al. Chem. Rev.* **109**, 1659–1713 (2009).

[2] (a) M. Sawamura, *et al. Nature*, **419**, 702–705 (2002). (b) Y. Matsuo, *et al. J. Am. Chem. Soc.*, **130**, 5016–5017 (2008). (c) Y. Matsuo *et al. Chem. Rev.*, **108**, 3016–3028 (2008). (d) T. Niinomi, *et al. J. Mater. Chem.*, **19**, 5804–5811 (2009).

[3] (a) D. M. Guldi, *et al. J. Am. Chem. Soc.*, **128**, 9420–9427 (2006). (b) M. Renata, *et al. J. Am. Chem. Soc.*, **130**, 16207–16215 (2008). (c) Y. Matsuo, *et al. J. Am. Chem. Soc.*, **132**, 6342–6348 (2010).

[4] (a) Y. Matsuo, *et al. J. Am. Chem. Soc.*, **131**, 12643–12649 (2009). (b) Y. Matsuo, *et al. J. Nanosci. Nanotech. in press.* (c) M. Maruyama, *et al. CSJ Annual Meeting* (2012)

Corresponding Author: Y. Matsuo

Tel: +81-03-5841-1476, Fax: +81-03-5841-1476

E-mail: matsuo@chem.s.u-tokyo.ac.jp

Selective synthesis and molecular structure of alkoxyfullerenes: substitution reaction of octabromofullerene with alcohol

○Kouya Uchiyama ¹, Hiroshi Moriyama ^{*1}, Kenji Yoza ²

¹ Department of Chemistry, Toho University, Funabashi, 274-8510, Japan

² Bruker AXS, Yokohama, 221-0022, Japan

Regioselective synthesis of fullerene derivatives with multiple addends is still a challenging issue because of the inevitable formation of many isomers. In view of further application of fullerene derivatives, it is important to establish synthetic methods for multifunctionalized fullerene derivatives without any isomers.

Halofullerenes $C_{60}X_n$, such as chlorofullerene and bromofullerene, can be obtained quantitatively and easily without any isomers. They have relatively weak C–X bonds; therefore, substitution reactions with various nucleophiles can occur. Such reactions make it possible to prepare not only fullerene derivatives that cannot be prepared by the direct addition reaction to fullerene but also multifunctionalized fullerene derivatives selectively. In particular, $C_{60}Cl_6$ reacts with nucleophiles such as MeLi and NaOR to form isostructural $C_{60}Me_6$ [1] and $C_{60}(OR)_5Cl$ [2], respectively. While the substitution reaction of $C_{60}Cl_6$ is a powerful selective synthetic method for multifunctionalized fullerene derivatives, substitution reaction of bromofullerenes has not been studied intensively compared with $C_{60}Cl_6$ because of their low solubility in organic solvents, although selective replacement of bromine has been achieved in a partially brominated fullerene derivative [3].

Here, we report a selective substitution reaction of octabromofullerene $C_{60}Br_8$ [4] with methanol and ethanol in the presence of a silver salt, which facilitates the substitution reaction of bromine. The products, alkoxyfullerenes $C_{60}(OR)_8$ ($R = CH_3, C_2H_5$), were shown to have C_{2v} symmetry, the same as $C_{60}Br_8$ by 1H and ^{13}C NMR spectroscopy, in which ^{13}C NMR spectra exhibited 17 signals for a fullerene skeleton. The single-crystal X-ray crystal structure (Fig. 1) was totally consistent with the 1H and ^{13}C NMR spectra and the addition pattern for alkoxyfullerenes was found to remain as shown in the scheme.

This work was supported by a MEXT-Supported Program for the Strategic Research Foundation at Private Universities.

[1] H. Al-Matar, A. K. Abdul-Sada, A. G. Avent, P. W. Fowler, P. B. Hitchcock, K. M. Rogers, R. Taylor, *J. Chem. Soc., Perkin Trans.* **2002**, 2, 53–58. [2] A. G. Avent, P. R. Birkett, A. D. Darwish, S. Houlton, R. Taylor, K. S. T. Thomson, X.-W. Wei, *J. Chem. Soc., Perkin Trans.* **2001**, 5, 782–786. [3] Z. Jia, Q. Zhang, Y. Li, L. Gan, B. Zheng, G. Yuan, S. Zhang, D. Zhu, *Tetrahedron* **2007**, 63, 9120–9123. [4] P. R. Birkett, P. B. Hitchcock, H.W. Kroto, R. Taylor, D. R. M. Walton, *Nature* **1992**, 357, 479–481.

Corresponding Author: Hiroshi Moriyama

TEL: +81-47-472-1211, FAX: +81-47-476-9449, E-mail: moriyama@chem.sci.toho-u.ac.jp

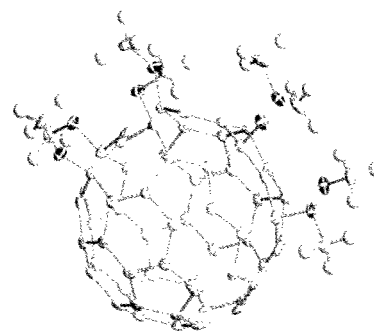
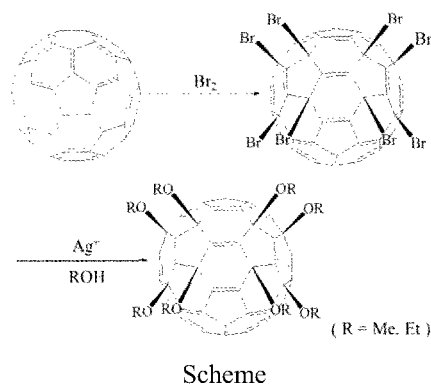


Figure 1. Crystal structure of $C_{60}(OMe)_8$.

What causes the selectivity of the metallofullerene formation?

○Yohji Achiba, Takeshi Kodama, Kenro Hashimoto and Haruo Shiromaru

Department of Chemistry, Tokyo Metropolitan University, Hachioji, 192-0397, Japan

Since 1985, the discovery of fullerene molecule, the isolation and characterization of metallofullerenes has been one of the biggest issues in the fullerene science and technology. Actually, after the first isolation and purification work of La@C₈₂ with a bulk quantity in 1993¹⁾, a lot of isolation works on metallofullerenes have been appeared in the literatures, and historically, some of their cage structures have been well characterized by ¹³C NMR in solution. Furthermore, during the last 10 years, a single crystal X-ray diffraction method has been successfully introduced to carry out the crystallographic identification of a particular isomer for a particular size of metallofullerene, and so far, over 36 different cage structures have been examined and identified²⁾. On the basis of these experimental progresses in determining cage structures, in the present work, we are intended to clarify “*what causes the selection of a particular cage structure in the metallofullerene growth process*”.

In order to construct a growth model for such a selective formation of a particular isomer structure, first, we have to consider the reason why a particular isomer structure is experimentally isolated and stabilized. There might be at least four key-factors by which some of metallofullerene isomers formed in the soot are actually experimentally isolated: 1) energetics (stability of “a particular charged state” of the π cage network with a particular size), 2) chemical stability of the particular charged state (large HOMO-LUMO gap is better, preventing from polymerization or other reactions), 3) 5/6 network structure superiority (closely related to network growth rate), and 4) cage size (non IPR cage structure becomes to be much more important in the smaller size range). These four factors are definitely more or less related with each other even on the way of network forming process, but in the present work we will emphasize the important role of specific network structures of intermediate precursors for the isolated fullerenes.

Figure 1 shows four different cap structures (5/6 network with 6 pentagons) which commonly appear in the cage structures of the experimentally identified metallofullerenes with a single metal atom inside. For example, three cage structures of four identified M@C₈₂ molecules consist of the cap C, and the remaining one's cap is B. Furthermore, it should be quite interesting to note that all these four cap structures also possess only one common structure with in their 5/6 network as shown in Fig. 1 (top). More detailed discussion will be done in the symposium.

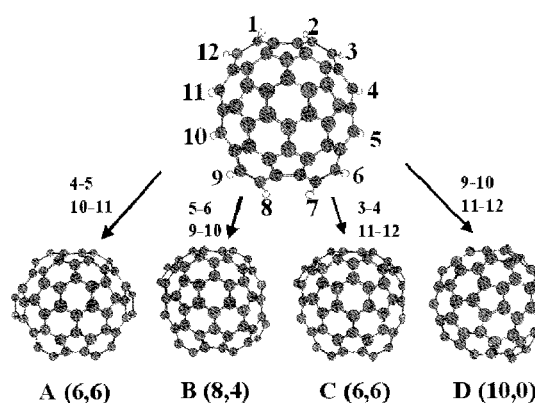


Fig. 1. The cap structures commonly appeared among 36 structurally identified metallofullerenes.

[1] K. Kikuchi et al., Chem. Phys. Lett., 216, 67 (1993).

[2] see recent published literatures by Prof. T. Akasaka and Prof. A. Balch research group.

Corresponding Author: Y. Achiba

Tel: +81-42-677-2534, Fax: +81-42-677-2525,

E-mail: achiba-yohji@tmu.ac.jp

Synthesis of Carboxy Metallofullerenes for Medical Application

○Erina Takeuchi, Kazuhiko Akiyama, Youhei Kawabata, and Shiro Kubuki

Department of Chemistry, Tokyo Metropolitan University, Hachioji, 192-0397, Japan

Water-soluble endohedral metallofullerenes (EMFs) are expected to use for the medical applications. For example, water-soluble Gd EMFs are applicable for high sensitive magnetic resonance imaging (MRI) contrast reagent [1] and neutron capture therapy [2]. In these water-soluble EMFs, carboxy EMFs are one of the promising reagent for the drug delivery system (DDS), because these are conjugated with desired peptide of morbidity parts by amide bond. We had reported that synthesis of carboxy EMFs encapsulating La by radiochemical approach for radioimmunotherapy [3]. However, this method wasn't suitable for synthesis of carboxy EMFs encapsulating short-half-life radionuclide because it takes 48 hour to synthesize carboxy EMFs. In this study, we report rapid synthesis of carboxy EMFs and properties of these synthesized carboxy EMFs with this method.

La@C₈₂ was separated from crude fullerene extracts by TiCl₄ [4] and then purified by HPLC. After that, purified La@C₈₂ was dissolved to *o*-dichlorobenzene (DCB). Succinic acid peroxide (SAP) was added to La@C₈₂/DCB solution under Ar gas flow and sealed in the PTFE bottle. This solution was heated by microwave oven for few minutes. Products were extracted by 0.2 M NaOH solution. Extracted products was separated by gel filtration chromatography (column: TSKgel G3000PW_{XL}, eluent: 0.1 M phosphate buffer solution/ acetonitrile = 8/2). Molecular weight of these products were estimated from the retention time of GFC with Sodium Polystyrene Sulfonate (PSS-Na) as the molecular weight standard. Addition of ethylenecarboxy group was confirmed by the addition of fluorescent reagent (9-anthryldiazo methane (ADAM)) to fraction. UV/vis absorption spectra and small angle X-ray scattering (SAXS) was also measured.

Elution peaks derived from carboxy EMFs were observed at 19.0 min, 19.7 min, 20.9 min, and 23.0 min. Fig.1 shows the correlation between observed retention time and molecular weight of PSS-Na. Estimated molecular weight of produced carboxy EMFs from this calibration curve were about 3700, 3000, 2000, and 1100, respectively. Particle diameter determined by SAXS was about 2-3 nm. These results indicate that carboxy EMFs are dispersed in aqueous phase as a single molecule.

[1] M.Mikawa *et al. Bioconjugate Chem.* **12**, 510-514 (2001).

[2] Y.Horiguchi *et al. Sci.Technol.Adv.Mater.* **12**, 044607 (2011).

[3] E.Takeuchi *et al. The 41nd Fullerenes-Nanotubes-Graphene General Symposium*, 2P-32 (2011).

[4] K.Akiyama *et al. J.Am.Chem.Soc.* **134**, 9762-9767 (2012).

Corresponding Author: K.Akiyama

Tel: +81-42-677-1111(ext. 3587), Fax: +81-42-677-2430, E-mail:kakiyama@tmu.ac.jp

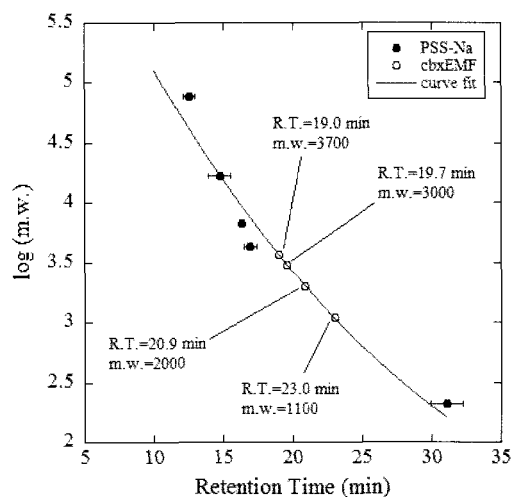


Fig.1 The calibration curve between observed retention peaks and PSS-Na.

Synthesis of Lithium-Encapsulated Fullerenol as “Cation-Encapsulated Anion Nanoparticle”

○Hiroshi Ueno, Yuji Nakamura, Naohiko Ikuma, Ken Kokubo, Takumi Oshima

*Division of Applied Chemistry, Graduate School of Engineering,
Osaka University, Suita, 565-0871, Japan*

Lithium-encapsulated fullerene $\text{Li}^+\text{@C}_{60}$, as SbCl_6^- salt [1], has attracted a growing attention in the field of organic electronics because of its strong electron accepting ability and great ionicity due to the encapsulated lithium cation. On the other hand, hydroxylated fullerenes, so-called fullerenols $\text{C}_{60}(\text{OH})_n$, have also attracted a considerable attention owing to their prominent hydrophilicity, bioactivity, and unique conductivity. Thus, the combination of these properties will lead to a new class of nanocarbons which can play a significant role in the field of materials chemistry. In our previous paper [2], we reported the synthesis of $\text{Li@C}_{60}(\text{OH})_{18}$ along with $\text{C}_{60}(\text{OH})_{18}$ by the hydroxylation of Li@C_{60} cluster (as a mixture with C_{60}) and its physicochemical properties. However, the amount of Li^+ encapsulated fullerenol was too low (12%) to discuss the details of properties [2]. Here, we report the synthesis of lithium-encapsulated fullerenol $\text{Li}^+\text{@C}_{60}\text{O}^-(\text{OH})_{11}$ by hydroxylation of pure $[\text{Li}^+\text{@C}_{60}](\text{PF}_6^-)$ and its notable properties induced by the lithium cation and the outer hydroxyl groups.

The hydroxylation of $[\text{Li}^+\text{@C}_{60}](\text{PF}_6^-)$ was carried out by the reported fuming sulfuric acid method under the optimized reaction conditions [3]. The spectral data by IR, NMR, MALDI-TOF-MS, and elemental analysis clearly suggested the formation of lithium encapsulated fullerenol with eleven $-\text{OH}$ groups and one fullerenoxide anion (C_{60}O^-) moiety. Very interestingly, each of the hydroxyl protons resonated separately on ^1H NMR, whereas the reference empty fullerenol synthesized by the same procedure showed the highly broadened OH signal probably because of the presence of a wide variety of isomers. Furthermore, it is noteworthy that a counter anion PF_6^- completely disappeared as indicated by both the ^{31}P and ^{19}F NMR analyses. In ^7Li NMR spectrum (Figure 1), the encapsulated Li^+ was found to be more shielded (ca. -15 to -19 ppm) than the previously reported value of -10.5 ppm for $[\text{Li}^+\text{@C}_{60}](\text{SbCl}_6^-)$ salt. This abnormal upfield shift may be caused by the increased diamagnetic shielding by the attractive negative fullerenoxide moiety.

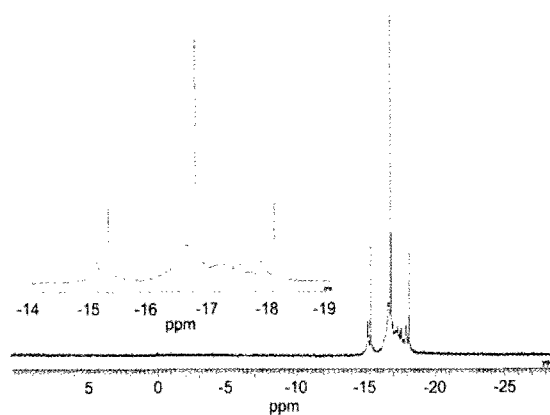


Figure 1. ^7Li NMR spectrum of Li^+ encapsulated fullerenol in $\text{DMSO}-d_6$. The D_2O solution of LiCl was used as an external standard.

[1] Sawa, H.; Tobita, H. *et al.*, *Nature Chem.* **2010**, *2*, 678-683.

[2] Ueno, H. *et al.*, *Nano Res.* **2012**, in press.

[3] Chiang, L. Y. *et al.*, *J. Org. Chem.* **1994**, *59*, 3960-3968.

Corresponding Author: Ken Kokubo

TEL: +81-6-6879-4592, FAX: +81-6-6879-4593, E-mail: kokubo@chem.eng.osaka-u.ac.jp

The Origin and Mechanism of Non-HPLC Rapid Purification of Metallofullerenes with TiCl_4

○Zhiyong Wang¹, Yusuke Nakanishi¹, Shoko Noda¹, Kazuhiko Akiyama²,
Hisanori Shinohara¹

¹ Department of Chemistry and Institute for Advanced Research, Nagoya University, Nagoya
464-8602, Japan

² Graduate School of Science and Engineering, Tokyo Metropolitan University, Hachioji
192-0397, Japan

Large scale separation/purification of metallofullerenes is a critical step towards the practical applications of metallofullerenes. Unfortunately, the isolation of metallofullerenes with high performance liquid chromatography (HPLC) is quite time consuming and expensive, and usually only milligram scale of metallofullerenes can be obtained and purified by using HPLC. Very recently, to circumvent the drawbacks of the HPLC separation/purification, we have developed an extremely efficient non-chromatographic method based on reactions with TiCl_4 Lewis acid [1]. We have found that metallofullerenes react very quickly, typically within several minutes, with TiCl_4 to form insoluble complex in such solvents, for example, as carbon disulfide and toluene, whereas most of the empty fullerenes are almost completely non-reactive towards TiCl_4 .

Here, we report our findings on the origin and mechanism of non-HPLC rapid purification of metallofullerenes with TiCl_4 . The reactivity of metallofullerenes has been found to be critically dependent on their first oxidation potentials. A lower oxidation potential leads to a higher reactivity. The threshold in the first oxidation potential for reaction with TiCl_4 is determined to be 0.62-0.72 V vs. Fc/Fc^+ (Fig. 1). All types of metallofullerenes with first oxidation potentials lower than this threshold can be separated from inert empty fullerenes. Electron transfer from metallofullerenes to TiCl_4 , evidenced by the change in absorption spectrum, offers an interpretation of the relation between reactivity and oxidation potential. This study provides a fundamental principle for the future quantitative work on separation/purification of metallofullerenes with TiCl_4 .

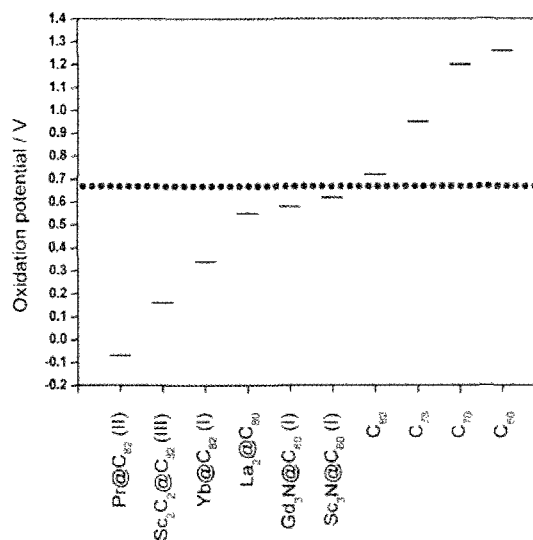


Fig.1 Plot of first oxidation potentials (vs. Fc/Fc^+) of fullerenes/metallofullerenes that we have examined. The dashed line indicates the position of threshold for reaction with TiCl_4 .

[1] K. Akiyama *et al.* *J. Am. Chem. Soc.* **134**, 9762 (2012).

Corresponding Author: Hisanori Shinohara
Tel: +81-52-789-2482, Fax: +81-52-747-6442,
E-mail: noris@nagoya-u.jp

Single-crystal X-ray structural analyses of a series of divalent Yb@C₈₂ isomers: Yb@C_s(6)-C₈₂, Yb@C₂(5)-C₈₂, Yb@C_{2v}(9)-C₈₂

○Mitsuaki Suzuki¹, Xing Lu^{1,2}, Zdenek Slanina¹, Naomi Mizorogi¹, Shigeru Nagase³, Marilyn M. Olmstead⁴, Alan L. Balch⁴, and Takeshi Akasaka¹

¹*Life Science Center of Tsukuba Advanced Research Alliance, University of Tsukuba, Tsukuba, Ibaraki 305-8577, Japan*

²*College of Materials Science and Technology, Huazhong University of Science and Technology, 1037 Luoyu Road, Wuhan 430074, China*

³*Fukui Institute for Fundamental Chemistry, Kyoto University, Kyoto 606-8103, Japan*

⁴*Department of Chemistry, University of California, One Shields Avenue, Davis, California 95616, United States*

Endohedral metallofullerenes (EMFs) have attracted great attention because of their novel structures and fascinating properties resulted from the electron transfer from the metallic species to the cage. M@C₈₂ species (M = Sc, Y, and lanthanides) are among the most popular EMFs because they are normally more abundantly synthesized using the arc discharge method. It has been revealed that in these species the internal metal transfers three electrons to the fullerene cage, and thus the formed EMFs are called trivalent EMFs. However, when a divalent metal is encapsulated, the yield of the corresponding divalent EMFs is extremely low, which has hindered further characterization dramatically¹.

Molecular structures of M@C₈₂ determined by single crystal X-ray diffraction study are confined to La@C_{2v}(9)-C₈₂² and Gd@C_{2v}(9)-C₈₂³, although ¹³C-NMR studies of M@C_{2v}(9)-C₈₂ (M = La⁴, Y⁵, Ce⁶, and Pr⁷) and La@C_s(6)-C₈₂⁸ have also shown great success in establishing their cage structures. In all these cases, the internal takes a trivalent valence state. We report here for the first time the molecular structures of Yb@C₂(5)-C₈₂, Yb@C_s(6)-C₈₂, and Yb@C_{2v}(9)-C₈₂ that have been revealed by single crystal X-ray crystallographic analyses performed on cocrystals with Ni^{II} octaethylporphyrin [Ni^{II}(OEP)]. In these EMFs, the Yb is divalent.

References

- [1] (a) *Endofullerenes: A New Family of Carbon Clusters*, T. Akasaka, S. Nagase, Eds.; Kluwer: Dordrecht, The Netherlands, 2002, (b) *Chemistry of Nanocarbons*, T. Akasaka, F. Wudl, S. Nagase, Eds.; Wiley-Blackwell: Chichester, 2010.
- [2] S. Sato, *et al.* *Angew. Chem. Int. Ed.* **51**, 1589 (2012).
- [3] M. Suzuki, *et al.* *Inorg. Chem.* **51**, 5270 (2012).
- [4] T. Akasaka, *et al.* *J. Am. Chem. Soc.* **122**, 9316 (2000).
- [5] L. Feng, *et al.* *Chem. Phys. Lett.* **405**, 274 (2005).
- [6] T. Wakahara, *et al.* *J. Am. Chem. Soc.* **126**, 4883 (2004).
- [7] T. Wakahara, *et al.* *Chem. Phys. Lett.* **360**, 235 (2002).
- [8] T. Akasaka, *et al.* *J. Phys. Chem. B* **105**, 2971 (2001).

Corresponding Author: T. Akasaka

Tel: +81-29-853-6409, Fax: +81-29-853-6409,

E-mail: akasaka@tara.tsukuba.ac.jp

Enhancement of nitrogen encapsulation into fullerene under control of plasma potential

○Soon Cheon Cho, Rikizo Hatakeyama, Toshiro Kaneko

Department of Electronic Engineering, Tohoku University, Sendai, 980-8579, Japan

The nitrogen-atom endohedral fullerene ($N@C_{60}$) attracts interest because $N@C_{60}$ could have some unique advantages in isolating the atom from its environment, thereby providing a building block for the qubits of the quantum computer [1]. However, one of the problems of probing the properties of this $N@C_{60}$ is the difficulty in producing them in large amounts and high purity. Therefore, the purpose of this study is to adjust the plasma structure for $N@C_{60}$ synthesis using the energetic nitrogen ion irradiation in order to improve the yield [2]. We examine the effects of end-plate voltage (V_{ep}) for control of plasma space-potential (ϕ_s) with increasing RF-power (P_{RF}) in order to maintain the suitable ion irradiation-energy E_i [$= e(\phi_s - V_{sub})$] for the high purity $N@C_{60}$ synthesis. Here, grid voltage ($V_g = -90$ V), substrate voltage ($V_{sub} = -90$ V), gas pressure ($P_{N_2} = 25$ Pa) is fixed.

Figure 1 shows the purity and ϕ_s as a function of P_{RF} for (a) $V_{ep} = \text{floating}$ and (b) $V_{ep} = 0$ V under the conditions of an oven temperature $T_{ov} = 850$ °C. For $V_{ep} = \text{floating}$, the purity increases with P_{RF} but changes to decrease for $P_{RF} > 500$ W, because ϕ_s decreases with an increase in P_{RF} , resulting in the decrease in E_i . In order to keep the suitable E_i , we apply the V_{ep} which can control the ϕ_s . As shown in Fig. 1(b), the ϕ_s is almost kept constant even when the P_{RF} increases up to 900 W, and thus, the purity increases with increasing P_{RF} . In addition, as shown in Fig. (2), it is found that the purity increases with an increase in T_{ov} because sublimation of C_{60} with dispersed form as T_{ov} increases. We proved that there is an optimum condition of the nitrogen plasma for the high-purity synthesis of $N@C_{60}$, which consists of the high plasma density with suitable E_i from 70 to 80 eV and control of C_{60} behaviors. As a result, the $N@C_{60}$ is synthesized in high purity of 0.83 %, which is the highest in the world.

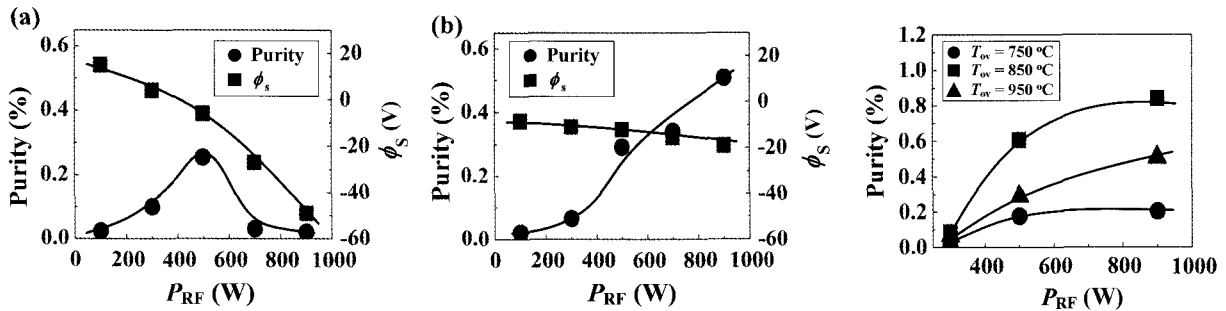


Fig. 1. Purity and ϕ_s as a function of P_{RF} for (a) $V_{ep} = \text{floating}$ and (b) $V_{ep} = 0$ V $T_{ov} = 850$ °C.

Fig. 2. Dependence of purity on P_{RF} and T_{ov} for $V_{ep} = 0$ V.

[1] L. Franco, S. Ceola, C. Corvaja, S. Bolzonella, W. Harnett, and M. Maggini, *Chem. Phys. Lett.* **422**, 100 (2006).

[2] S. C. Cho, T. Kaneko, H. Ishida, and R. Hatakeyama, *Appl. Phys. Exp.* **5**, 026202 (2012).

Corresponding Author: Soon Cheon Cho

Tel: +81-22-795-7046, Fax: +81-22-263-9225,

E-mail: cho10@ecei.tohoku.ac.jp

Application of MCD Spectroscopy and TD-DFT to Endohedral Metallofullerenes. New Insights into Characterization of Their Electronic Transitions

○Michio Yamada,¹ Zdenek Slanina,² Naomi Mizorogi,² Atsuya Muranaka,³ Yutaka Maeda,¹ Shigeru Nagase,⁴ Takeshi Akasaka,² and Nagao Kobayashi⁵

¹ Department of Chemistry, Tokyo Gakugei University, Tokyo, 184-8501, Japan

² Life Science Center of Tsukuba Advanced Research Alliance, University of Tsukuba, Ibaraki 305-8577, Japan

³ Advanced Elements Chemistry Laboratory, Advanced Science Institute, RIKEN, Saitama 351-0198, Japan

⁴ Fukui Institute for Fundamental Chemistry, Kyoto University, Kyoto 606-8103, Japan

⁵ Department of Chemistry, Graduate School of Science, Tohoku University, Miyagi 980-8578, Japan

We describe, for the first time, the application of magnetic circular dichroism (MCD) spectroscopy and time-dependent density functional theory (TD-DFT) calculations using B3LYP and M06-2X functionals to characterize the electronic transitions of endohedral metallofullerenes (EMFs).¹ Results revealed that the electronic transitions of La@C_{2v}-C₈₂, La₂@I_h-C₈₀, and Sc₃N@I_h-C₈₀ can be assigned using these techniques. Particularly, a difference in the electronic transitions between La₂@I_h-C₈₀ and Sc₃N@I_h-C₈₀, which is invisible in the absorption spectra, was observed clearly in MCD spectra. The observed MCD bands agree well with the oscillator strengths calculated using B3LYP functional. In addition, the MCD bands of La₂@I_h-C₈₀ were altered upon [5,6]-addition, demonstrating that the MCD spectroscopy is sensitive to chemical functionalization of EMFs, and that it is therefore powerful to distinguish the [5,6]-adducts from pristine La₂@I_h-C₈₀ although no marked difference exists in their absorption spectra.



Magnetic Circular Dichroism & Time-Dependent DFT

[1] M. Yamada *et al.* submitted.

Corresponding Author: T. Tohoku
Tel & Fax: +81-29-853-6409
E-mail: akasaka@tara.tsukuba.ac.jp

Fabrication of Li@C₆₀ Monolayer from [Li@C₆₀](PF₆) Salt

○Yoichi Yamada¹, Ken Tanaka¹, Masahiro Sasaki¹, Yasuhiko Kasama², Kazuhiko Kawachi², and Seiji Sakai³

¹ Institute of Applied Physics, Tsukuba University, Tsukuba, 305-8573, Japan

² Idea International Inc., Sendai, 980-8579, Japan

³ Japan Atomic Energy Agency, Tokai, 319-1195, Japan

Although the endohedral doping of metal atom in the C₆₀ cage is promising way to modify the electronic orbitals of C₆₀, purification of the metallofullerene has been challenging due to its high reactivity. Recently, a stable salt of Li@C₆₀ and anionic counterpart (PF₆, SbCl₆) has been realized with good crystallinity and high Li@C₆₀ concentration up to 95% [1]. Here we demonstrated the vacuum evaporation of the [Li@C₆₀](PF₆) salt to form a monolayer of Li@C₆₀ on the metal substrates.

Two distinct evaporations from the [Li@C₆₀](PF₆) salt were seen at different temperatures of about 200 °C and 400 °C, monitored by quartz microbalance (Fig.1). XPS measurements suggested that the former evaporation is due to PF₆-related materials and the latter is due to Li@C₆₀-related materials. SIMS measurements of the latter products revealed that the Li concentration became approximately 1/3 of the original [Li@C₆₀](PF₆) salt. It is thus speculated that Li atoms desorb from the C₆₀ cage during the evaporation. It is also found that the latter products contains small amount of F atoms. This may be as a result of the desorption of PF₅ at the first stage of the evaporation, which should leave one F atom per one Li@C₆₀ molecule.

STM measurements of the evaporated film on the Cu(111) or HOPG substrates revealed the formation of a well-ordered monolayer which consists of Li@C₆₀ and C₆₀ molecules (Fig.2). Two molecules exhibit different contrast in the STM image and the contrast depends strongly on the applied bias voltage. The observation reflects significant difference in the electronic states of Li@C₆₀ and C₆₀ molecules. It is noted that a random aggregation of molecules was not found in spite of the high reactivity of Li@C₆₀. This should be owing to significant molecule-substrate interaction preventing the molecular aggregation. In addition, passivation of Li@C₆₀ by residual F atoms should also be a key to hinder the aggregation.

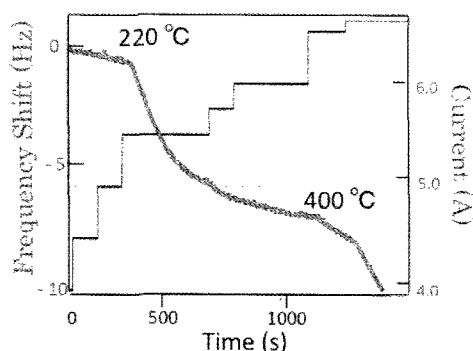


Fig.1 Change in frequency of QCM during evaporation of [Li@C₆₀](PF₆) salt.

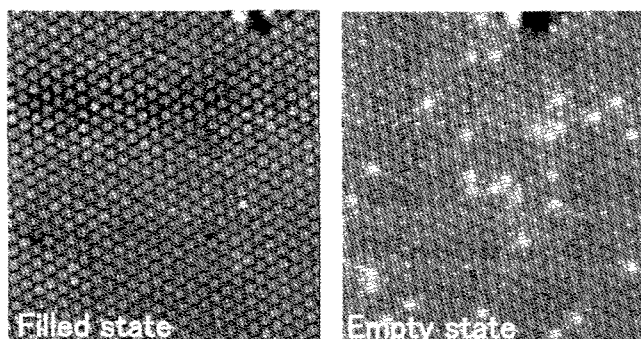


Fig.2 Filled and empty state STM images of Li@C₆₀-C₆₀ mixed monolayer, taken with bias of -2.8 and +2.8 V, respectively.

[1] S. Aoyagi, *et al.* Nature Chemistry 2, 678 (2010).

Corresponding Author: Y. Yamada

Tel, Fax: +81-29-853-5038

E-mail: yamada@bk.tsukuba.ac.jp

Characterization of Endohedral Lithium Metallofullerene Clusters

○Eunsang Kwon¹, Ken-ichirou Komatsu², Shin-ichi Okuda², Kazuhiko Kawachi²,
Yasuhiko Kasama², Tomoaki Endo³

¹ *Research and Analytical center for Giant Molecules, Graduate School of Science, Tohoku University, Sendai, 980-8578, Japan*

² *Idea International Co., Ltd, 981-0922, Japan*

³ *Sendai National College of Technology, 981-1239, Japan*

Metallofullerenes are expected to have novel potential applications in material science.

Since the highest symmetry and the most stable fullerene cage, C₆₀, doped with alkali-metal are interesting particularly because of their superconducting properties [1], analogous to the series of the endohedral metallofullerenes, alkali-metal@C₆₀, has also attracted considerable attention in the field of novel material development. Although only the isolation and characterization of lithium@C₆₀ have been reported [2] among the series of the alkali metal@C₆₀, the structure of the precursor cluster which was generated in the process of the low energy ion bombardment method [3] is still unclear.

In the present work, we studied the characterization of the cluster by high-resolution NMR spectroscopy combined with theoretical calculations and other analytical techniques. As shown in Fig. 1 (a), the solid-state ⁷Li NMR spectrum of the crude products exhibit two main signals at -14.9 and 0.9 ppm (relative to the external LiCl reference). The signal at -14.9 ppm can be assigned to the Li⁺ in C₆₀, and the one at 0.9 ppm to the lithium of the LiOR (R = alkyl group) with the support of theoretical calculations using gauge-independent atomic orbital (GIAO) method at the level of density functional theory (DFT B3LYP/6-311++G(d,p) level of theory). The peak at -14.9 ppm was significantly increased after treatment with excess gamma-cyclodextrin, followed by washing with water and drying (Fig.1 (b)). The mean particle size of the cluster after desorption of C₆₀ using gamma-cyclodextrin from the crude products was determined by DLS to be about 120 nm with narrow size distribution. The positive ion mode LDI-TOF mass spectra of the resulting cluster showed a molecular ion peak of Li@C₆₀ as a base peak. These results indicated that the structure of the cluster should be surrounded by C₆₀ which could combine by LiOR species.

[1] A. F. Herbard, *et al.* Nature, **350**, 600 (1991). [2] S. Aoyagi *et al.* Nature Chemistry, **2**, 678 (2010). [3] R. Tellgmann *et al.* Nature, **382**, 407 (1996).

Corresponding Author: E. Kwon

Tel: +81-22-795-6752, Fax: +81-22-795-6752,

E-mail: ekwon@m.tohoku.ac.jp

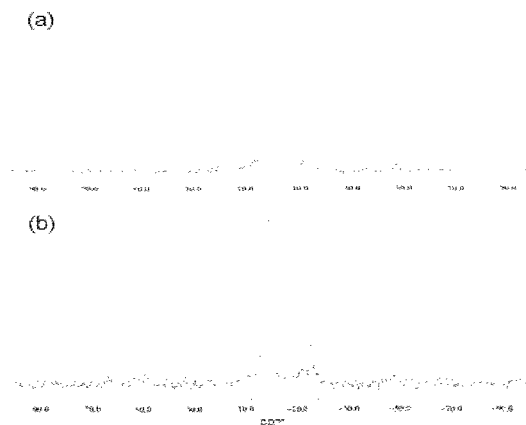


Fig.1 Solid-state ⁷Li NMR spectra of the cluster (a) before treatment with gamma-cyclodextrin and (b) after treatment with gamma-cyclodextrin, followed by washing with water and drying.

Fabrication and Solid State Properties of Fullerenol Nanostructures

○Keisuke Baba¹, Toshiyuki Ito¹, Hironori Ogata^{1,2}

¹ Department of Chemical Science and Technology, Hosei University, Koganei 184-8584, Japan

² Research Center for Micro-Nano Technology, Hosei University, Koganei 184-0003, Japan

Fullerenol (Polyhydroxylated Fullerene: $C_{60}(OH)_x$) have been thought to have potential application in a variety of areas, including optoelectronics, medical therapeutics, biotechnology, chemical mechanical polishing, and fuel cells, owing to their high solubility in a large variety of solvents (depending on the number of hydroxyl groups, x). The study of nanomaterials is one of the most active areas due to their interesting properties that differ from those of bulk substances, and their wide possibilities of applications.

We previously reported the fabrication of both nanosheets and nanocrystals consist of water-insoluble fullerenol($C_{60}(OH)_{7.8}$) by the liquid phase growth method using both good and poor solvents. In this study, we prepared and fabricated water-soluble fullerenol nanostructures by the liquid phase growth methods. Fig.1. shows the SEM(a) and TEM(b) images of water-soluble fullerenol crumpled sheet fabricated by reprecipitation method. From TEM image, one can see that nanocrystals are on the sheet. Average diameter and coefficient of variation were estimated to be 8.1 nm and 12%, respectively. These values are similar to those of $C_{60}(OH)_{7.8}$ nanocrystals previously reported.

In this presentation, solid state properties and molecular dynamics of fullerenols will be reported.

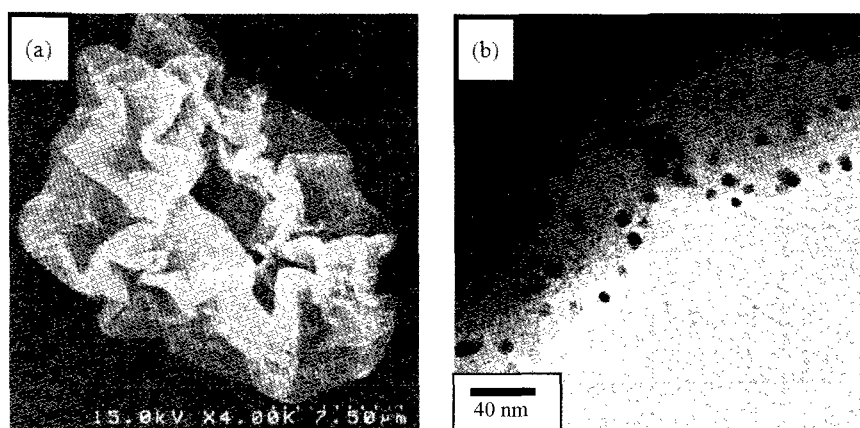


Fig.1. SEM image(a) of water-soluble fullerenol Crumpled sheet.
And TEM image(b) of nano-crystals on the sheet.

[1] Akito M. *et al.*, Jpn. J. Appl. Phys. **48**, 050206 (2009)

[2] Chiang *et al.* J. Org. Chem., **59**, 3960 (1994)

[3] K. Kokubo, *et al.*, ACS Nano, **2**, 327 (2008)

[4] K. Baba, *et al.*, The 42nd Fullerenes-Nanotubes-Graphene General Symposium, 2-5 (2012)

Corresponding Author: Hironori Ogata

Tel: +81-42-387-6229, Fax: +81-42-387-6229,

E-mail: hogata@hosei.ac.jp

Templated Synthesis of Polymer Nanocapsules on Water-Soluble Fullerene Vesicles

○Ricardo Mizoguchi Gorgoll, Koji Harano, Eiichi Nakamura

*Department of Chemistry, The University of Tokyo,
Hongo, Bunkyo-ku, Tokyo, 113-0033, Japan*

The controlled synthesis of polymer nanocapsules, vital for their effective biological application, is a challenging task. Nanocapsules can be obtained from the polymerization in template structures; however size and shape control comes with a trade-off for template removability.

Our group reported the preparation of nanometer-sized bilayer vesicles from self-assembly of nonpolar/polar/nonpolar fullerene amphiphiles (Figure 1a). In this vesicle, para-substituted phenyl groups are exposed on the surface creating a nanosized hydrophobic environment in water.¹ We applied the unique surface of fullerene vesicles as a confined space for olefin metathesis and synthesis of polymer nanocapsules.

Catalyst-embedded vesicles were prepared by the introduction of a fluorous-tagged Grubbs' catalyst to the vesicle solution (Figure 1b). Reactivity of the catalyst was confirmed in olefin metathesis reactions. Confinement of the catalyst in the rigid and hydrophobic fullerene membrane resulted in size selectivity of the substrate.

We demonstrated the fullerene vesicles as a novel soft template with rigid framework for nanocapsule synthesis. Polymer nanocapsules with uniform size were obtained by polymerization on the vesicle surface and extraction from the template solution (Figure 1c).

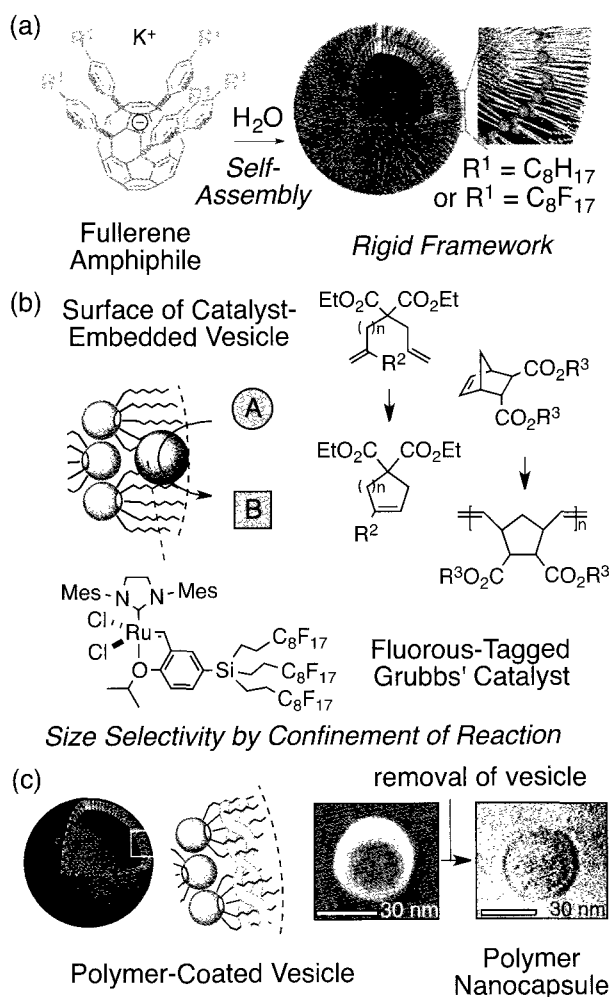


Figure 1. (a) Self-assembly of fullerene amphiphiles into bilayer vesicles in water. (b) Olefin metathesis on catalyst-embedded fullerene vesicles. (c) Schematic and SEM images of polymer-coated vesicle and STEM image of polymer nanocapsule after removal of template.

[1] Homma, T.; Harano, K.; Isobe, H.; Nakamura, E. *Angew. Chem. Int. Ed.* **2010**, *49*, 1665–1668. Homma T.; Harano, K.; Isobe, H.; Nakamura, E. *J. Am. Chem. Soc.* **2011**, *133*, 6364–6370.

Corresponding Author: Eiichi Nakamura

Tel&Fax: +81-3-5841-4356

E-mail: nakamura@chem.s.u-tokyo.ac.jp

Photo Polymerization of C₆₀ Thin Film Using Focused Optical Vortex

○Naoto Toriumi¹, Tatsuya Doi¹, Daiki Momiyama¹, Wataru Akiyama¹, Katsuhiko Miyamoto¹, Takashige Omatsu¹, Jonathan P. Bird², Nobuyuki Aoki¹, and Yuichi Ochiai¹

¹ Graduate School of Advanced Integration Science, Chiba University, Chiba, 263-8522 Japan

² Department of Electrical Engineering, University at Buffalo, SUNY, Buffalo, NY 14260-1920, USA

Recently, a state of the art photo-polymerization of a C₆₀ thin film has been realized by irradiation of topological laser beam namely optical vortex (OV). Since the beam has a helical wavefront and a torque appears along the tangential direction, a confinement force can be expected along the peripheral direction of the beam and the polymerization takes a progress with a compressive photon-pressure under a high-beam-power density. Therefore, it can be expected to achieve a highly-packed and uniform photo-polymerization in a C₆₀ thin film. Moreover, combining with circular polarization, total angular momentum of light can be controlled [1].

In our study, thermally evaporated C₆₀ thin film was deposited 50 nm on a SiO₂ layer on top of a heavily doped Si substrate. A continuous-wave 532 nm laser beam was used for the optical source. The OV was produced by using a spiral phase plate and irradiated onto the sample through an objective lens. After the irradiation, the sample was soaked in toluene for 3 minutes to remove non-polymerized C₆₀ films on the sample surface.

In our trial of irradiation of a focused OV beam on a C₆₀ thin film, circular patterns have successfully resolved after the irradiations for a few minutes. A peak shift of Raman spectrum corresponding to A_g(2) mode suggests a polymerization of the C₆₀ molecule [2]. Moreover, the photo-polymer shows a metallic characteristic, a linear current-voltage characteristic and almost no gate voltage dependences as shown in Fig. 1. It is completely difference from the *n*-type semiconductor characteristics observed in a C₆₀ thin film polymerized by UV light irradiation [3]. Moreover, no significant cracking cracks were confirmed in the polymerized region by OV. Therefore, non-conventional polymerization regime can be expected in the photo-polymer by OV irradiation.

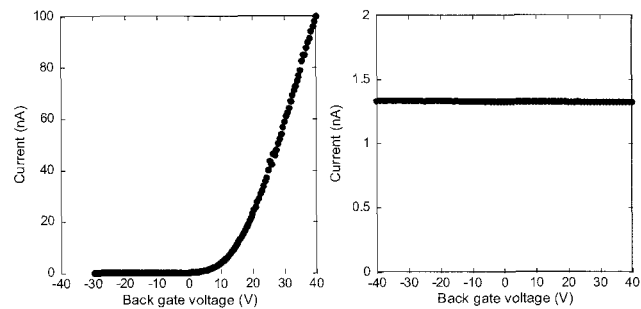


Fig. 1. Gate voltage dependence of C₆₀ photo-polymer by UV (left) and OV (right) irradiation.

[1] T. Omatsu *et al.*, Opt. Express **18** (2010) 17967.

[2] S. J. Duclos *et al.*, Solid State Commun. **80** (1991) 481.

[3] Y. Chiba *et al.*, J. Phys.: Conf. Ser. **159** (2009) 012017.

Corresponding Author: N. Aoki

Tel: +81-43-290-3430, Fax: +81-43-290-3427,

E-mail: n-aoki@faculty.chiba-u.jp

siRNA Delivery System Using Water-Soluble Amino-Fullerene Derivative

○Kosuke Minami¹, Koji Okamoto², Eisei Noiri², Koji Harano¹, Eiichi Nakamura¹

¹ Department of Chemistry, The University of Tokyo, Tokyo, 113-0033, Japan

² Department of Hemodialysis and Apheresis, University Hospital, The University of Tokyo, Tokyo, 113-0033, Japan

RNA interference (RNAi)¹ has gained significant attention as an alternative method to traditional gene therapy using DNA. However, RNA including siRNA is unstable and rapidly degraded in physiological environment. In addition, siRNA is highly soluble in water, so it is difficult to permeate through hydrophobic cell membranes. Therefore, the transfection reagents to protect and deliver siRNA into cells are required. Cationic liposomes or polymers are commonly studied as the transfection reagents, but they have significant dose-dependent cytotoxicity, which makes the therapeutic application difficult.

We focused on a water-soluble cationic amino-fullerene, (Tetrapiperazino)fullerene epoxide (TPFE, Figure 1), which had been reported as the DNA transfection reagent *in vitro*² and *in vivo*.³ TPFE has no cytotoxicity, effectively stabilized DNA and delivered DNA into cells. In this presentation, we reported the application of TPFE for the siRNA delivery system.

TPFE dissolved into acidic buffer and mixed with siRNA to form siRNA-TPFE complex as a 100 nm-ordered globules, derived from the electrostatic interaction between cationic amines and anionic phosphate RNA backbone, and hydrophobic effect of fullerene core. The siRNA-TPFE complex showed significant resistance of degradation under the simulated biological condition. In addition, we carried out the siRNA transfection analysis in cultured cells. Lipofectamine2000, which is commercially available transfection reagent and consist of cationic liposomes, was used as a positive control. The knockdown efficiency of TPFE was higher than that of lipofectamine2000, when we used not only chemically stabilized siRNA (Stealth RNA, invitrogen) but also free siRNA (Figure 2). Importantly, siRNA-TPFE complexes showed no cytotoxicity. Therefore, it is expected that TPFE has the potential to apply the siRNA delivery systems.

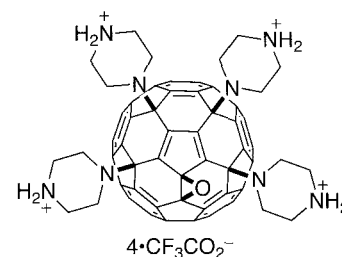


Figure 1. Structure of TPFE.

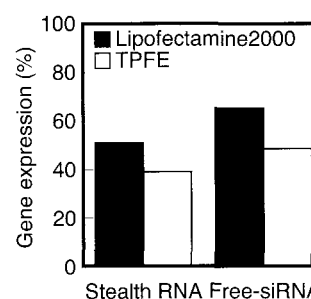


Figure 2. Transfection *in vitro*.

[1] Fire, A.; Xu, S.; Montgomery, M. K.; Kostas, S. A.; Driver, S. E.; Mello, C. C. *Nature* **1998**, *391*, 806–811.

[2] Isobe, H.; Nakanishi, W.; Tomita, N.; Jinno, S.; Okayama, H.; Nakamura, E. *Chem.-Asian J.* **2006**, *1*–2, 167–175.

[3] Maeda-Mamiya, R.; Noiri, E.; Isobe, H.; Okamoto, K.; Doi, K.; Sugaya, T.; Izumi, T.; Homma, T.; Nakamura, E. *Proc. Natl. Acad. Sci. U.S.A.*, **2010**, *107*, 5339–5344.

Corresponding Author: Eiichi Nakamura

Tel: +81-3-5841-4356, Fax: +81-3-5841-4356,

E-mail: nakamura@chem.s.u-tokyo.ac.jp

From nanotweezers to nanocalipers: Selective extraction of SWNTs with larger diameters

○Naoki Komatsu, Gang Liu, Takahide Kimura

Department of Chemistry, Shiga University of Medical Science, Seta, Otsu 520-2192, Japan.

We have been working on separation of SWNTs through molecular recognition. Tweezer-shape molecules have been employed as a host to realize diameter-based separation of SWNTs [1]. Although SWNTs with smaller diameters such as (6,5) were separated in high purity [2], the selectivity toward larger diameters was relatively low. Therefore, we change the molecular design of the host from nanotweezers to nanocalipers shown in Fig. 1. In this paper, we report on large enrichment of (10,5)-SWNTs through the extraction of HiPco with the nanocalipers **1**.

After bath-sonication of the suspension of HiPco and **1**, the extracted SWNTs were concentrated, washed, and dissolved in

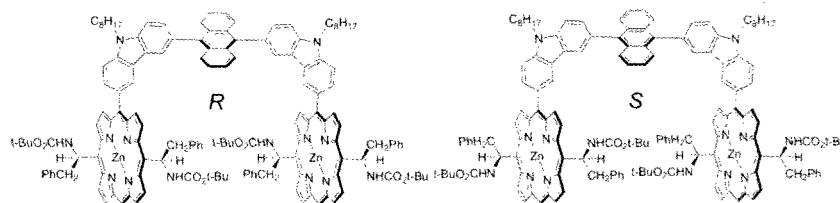


Fig 1. Structures of chiral diporphyrin nanocalipers, (*R*)- and (*S*)-**1**.

D₂O/SDBS by use of a rosette cooling cell [3]. The absorption spectra of the solution were measured as shown in Fig. 2. While SWNTs with smaller diameters (0.90 – 1.03 nm), such as (7,6), (9,4), (8,6), and (8,7), decreased significantly in their absorbance, only (10,5) and (11,3) were enriched by the extraction. In particular, (10,5)-SWNTs having 1.05 nm in diameter are found to be a dominant component from the absorption spectra. The Raman spectra also support the selective extraction of SWNTs with the above diameter range by use of the nanocalipers.

[1] G. Liu, N. Komatsu, in *Handbook of carbon nano materials* (Eds.: F. D'Souza, K. M. Kadish), World Scientific, **2012**, vol. 3, pp. 203-232; X. Peng, F. Wang, A. F. M. M. Rahman, A. Bauri, and N. Komatsu, *Chem. Lett.*, **2010**, 39, 1022.

[2] F. Wang, K. Matsuda, N. Komatsu, *J. Am. Chem. Soc.* **2010**, 132, 10876.

[3] T. Yasumitsu, G. Liu, J.-M. Levêque, S. Aonuma, L. Duclaux, T. Kimura, N. Komatsu, *Ultrason. Sonochem.*, in press (10.1016/j.ultsonch.2012.06.009).

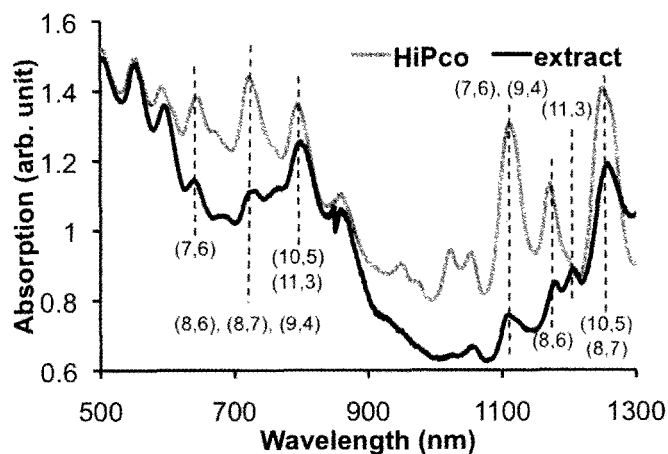


Fig. 2 Absorption spectra of HiPco and SWNTs extracted with (*R*)-**1**.

Corresponding Author: Naoki Komatsu

Tel: +81-77-548-2102, Fax: +81-77-548-2405. E-mail: nkomatsu@belle.shiga-med.ac.jp

A molecular dynamics simulation of SWNT growth by CVD method: Octopus and VLS modes

○Shigeo Maruyama, Kaoru Hisama, Takuya Noguchi, Tomoya Kawasuzuki, Yuki Takaki,
Junichiro Shiomi, Shohei Chiashi

Department of Mechanical Engineering, The University of Tokyo, Tokyo 113-8656, Japan

In order to explore the possible chirality-controlled growth process, the growth mechanism of single-walled carbon nanotubes (SWNTs) was studied by molecular dynamics simulations. We adopted a newly developed Tersoff-type classical potential for carbon and several metal atoms, such as Co, Ni, Pt, Fe and Ti. We used a genetic algorithm to optimize the potential functions for various solid structures and graphene-metal model predicted by density functional theory [1].

A metal cluster of certain size and at certain temperature is prepared and is exposed to carbon vapor at certain vapor density (pressure) [2]. We can observe the nucleation and growth of SWNTs at certain temperature range and pressure range depending on metal species (as shown in Fig. 1). In general, higher temperature and lower pressure are preferred for all metal species tested (Co, Fe, Ni, Pt). Higher pressure below the threshold pressure results faster growth simply proportional to the pressure. With the higher pressure beyond the threshold pressure, carbon coating of metal cluster with fullerene-like structure prohibited the growth of SWNTs. Lower temperature than the threshold temperature also results this carbon-coating. Higher temperature simply increased the growth rate with the pseudo-Arrhenius type dependence with an activation energy of about 0.4 eV for Fe. This activation energy is ascribed to the surface or sub-surface diffusion of carbon atoms on a metal cluster.

The threshold temperature is strongly dependent on metal species; much lower for Fe compared to Co. Furthermore, carbon structure interacting to metal cluster during the growth can be classified to two apparently different modes. A preferred structure at lower temperature is "Octopus" mode where several carbon chains are wrapping the metal cluster. Another structure appeared at higher temperature is "VLS" mode where carbon atoms are dissolved in metal cluster. The diameter of nanotube is similar to the metal cluster size for Octopus mode in contract to the VLS mode where the diameter is determined in the nucleated cap structure. The chirality of nanotubes grown in different MD conditions will be discussed.

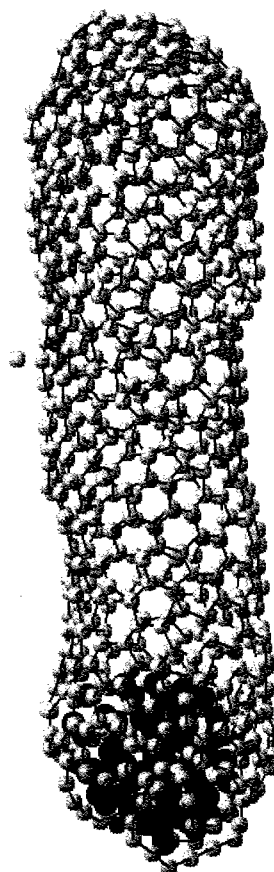


Fig. 1. Octopus mode growth from a Co_{60} cluster at 1600K. Carbon density corresponds to about atmospheric pressure.

[1] T. Matsuo, master thesis, <http://www.photon.t.u-tokyo.ac.jp/thesis/2011/2011matsuo.pdf>

[2] Y. Shibuta and S. Maruyama, Chem. Phys. Lett., 382 (2003) 381.

Corresponding Author: Shigeo Maruyama

Tel: +81-3-5841-6421, Fax: +81-3-5800-6983,

E-mail: maruyama@photon.t.u-tokyo.ac.jp

Catalyst Particle Array Formation Process Adjusted for Growth of Single-Walled Carbon Nanotube Forest with Different Structures

○Shunsuke Sakurai^{1,2}, Masayasu Inaguma¹, Don N Futaba^{1,2}, Motoo Yumura^{1,2},
and Kenji Hata^{1,2}

¹*Nanotube Research Center, National Institute of Advanced Industrial Science and Technology (AIST), Tsukuba 305-8565, Japan*

²*Technology Research Association for Single Wall Carbon Nanotubes (TASC), Tsukuba 305-8565, Japan*

Catalyst particle array for single-walled nanotube (SWNT) forest growth should achieve strict requirements, such as small particle sizes (< 3 nm) and high particle density (spacing below 20 nm) at the growth temperature typically above 700 °C. The most common method to satisfy the above requirements is to use an AlO_x layer to support the Fe catalysts. In this method, annealing in H₂ immediately prior to CNT growth (denoted as catalyst formation process), invoke the diffusion of Fe into AlO_x layer (subsurface diffusion), and transform the Fe thin film into a very high density array of small Fe catalysts array suited for SWNT forest growth. We have proposed that the offsetting effects of surface diffusion of Fe (Ostwald ripening effect) and subsurface diffusion is playing an important role to control the catalyst particle size [1].

In this study, we investigated the impact of independent control of the experimental conditions during catalyst formation process and CNT growth process. Since catalyst formation process continues until immediately prior to CNT growth, we build up the infrared lamp furnace system enabling us to heat up and cool down the furnace temperature very fast. Catalyst formation processes were conducted in different temperature, H₂ concentration, and total gas flow, though conditions during CNT growth process was fixed to conventional water-assisted CVD condition to synthesize SWNT forest.

The diameter of SWNT forest can be reduced from 3.2 nm to 1.9 nm by decreasing temperature and increasing gas flow rate during catalyst formation process. We also have found the strong correlation between diameter and density. Density of forest (ρ) goes up to 0.12 g/cm³ and estimated number of SWNT per area (area density) reached to 2.5×10^{12} cm⁻² with decreasing SWNT diameter. The mechanism of diameter control and correlation between diameter and density is discussed from the view point of catalyst formation process.

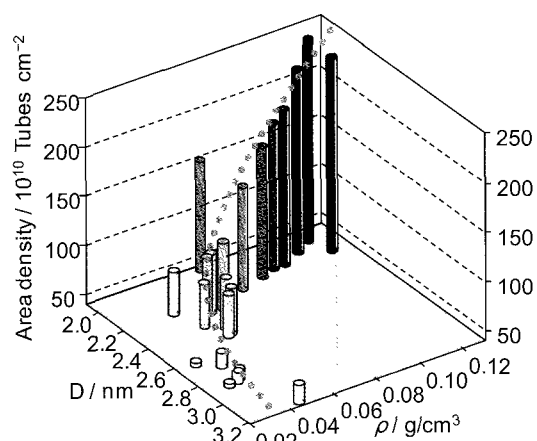


Figure: SWNT diameters, densities, and area densities of the SWNT forest synthesized after catalyst formation with different conditions.

[1] S. Sakurai, H. Nishino, D. N. Futaba, S. Yasuda, T. Yamada, A. Maigne, Y. Matsuo, E. Nakamura, M. Yumura, and K. Hata *J. Am. Chem. Soc.*, **134**, 2148 (2012).

Corresponding Author: Kenji Hata

TEL: +81-29-861-6205, FAX: +81-29-861-1169, E-mail: kenji-hata@aist.go.jp

Bottom-up synthesis of finite models of helical (*n,m*)-single-wall carbon nanotubes

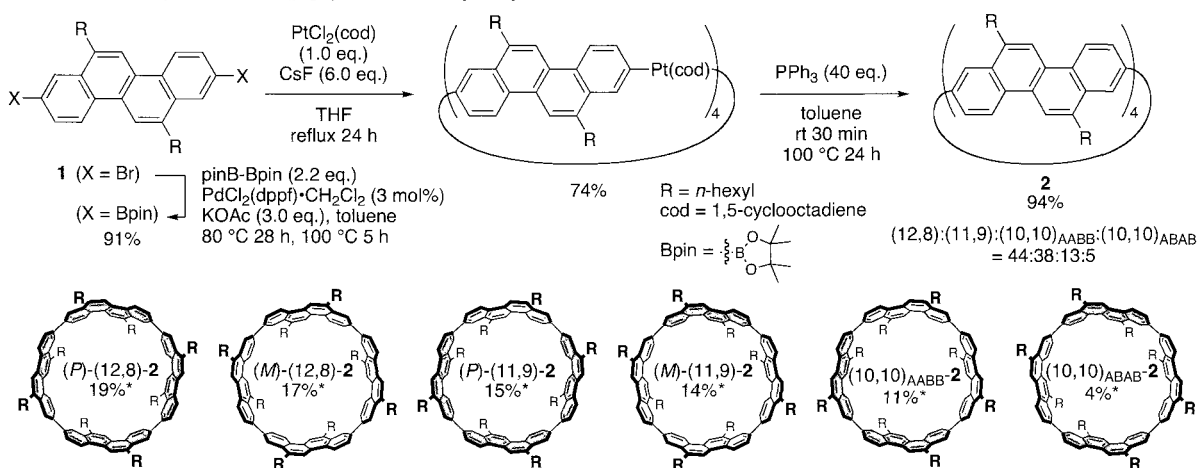
○Shunpei Hitosugi, Waka Nakanishi, Takashi Yamasaki, Hiroyuki Isobe

Department of Chemistry, Tohoku University, Sendai, 980-8578, Japan

Bottom-up synthesis of hoop-shaped aromatic hydrocarbons is currently attracting great interest because of both the difficulty with which these compounds are synthesized and the fact that they contain tubular structures that can serve as finite models of single-wall carbon nanotubes (SWNTs). Although the synthesis of finite models for armchair (*n,n*)-SWNTs has been intensely investigated with cycloparaphenylenes (CPP) over the past few years,¹ the synthesis and isolation of models for chiral (*n,m*)-SWNTs ($n \neq m$), particularly those bearing persistent structures with optical activity, has not been achieved.

We found that model compounds of helical (*n,m*)-SWNT ($n \neq m$) were synthetically accessible by using chrysenylene unit as a building block.² Thus, a stepwise macrocyclization of dibromochrysenylene derivative **1** afforded [4]cyclo-2,8-chrysenylene **2** ([4]CC) in high yield (Scheme 1).³ Although we used a strategy similar to that of the pioneering studies of Yamago for the synthesis of [8]CPP,^{1c} we found that the arylated Pt-complex could be obtained straightforwardly through the reaction of boronate ester with divalent platinum. Unlike the previous examples of CPP,⁴ the chrysenylene unit in [4]CC did not rotate under ambient temperature to give six rotational isomers. We succeeded complete isolation and identification of six isomers and achieved synthesis of the first optically active helical SWNT models ((*P*)/(*M*)-(12,8)-**2**, (*P*)/(*M*)-(12,8)-**2**). Finally, we examined enantioenrichment in the synthesis and obtained the (*P*)-helical isomer in up to 17% *ee*, by using cholesterol derivative as a chiral source.

Scheme 1. Synthesis of [4]cyclo-2,8-chrysenylene **2**



* Isolated yield after HPLC separation.

[1] (a) C. R. Bertozzi *et al.* *J. Am. Chem. Soc.* **130**, 17646 (2008). (b) K. Itami *et al.* *Angew. Chem. Int. Ed.* **48**, 6112 (2009). (c) S. Yamago *et al.* *Angew. Chem. Int. Ed.* **49**, 757 (2010).

[2] H. Isobe, S. Hitosugi, T. Matsuno, T. Iwamoto, J. Ichikawa, *Org. Lett.* **11**, 4026 (2009).

[3] S. Hitosugi, W. Nakanishi, T. Yamasaki, H. Isobe, *Nat. Commun.* **2**, doi: 10.1038/ncomms1505 (2011).

[4] K. Itami *et al.* *Org. Lett.* **13**, 2480 (2011).

Corresponding Author: H. Isobe

Tel: +81-22-795-6585, Fax: +81-22-795-6586,

E-mail: isobe@m.tohoku.ac.jp

Purification of Single Wall Carbon Nanotubes by Formation of Aggregates Caused by Control of Alcohol Concentration

○H. Kawai¹, K. Hasegawa¹, M. Fujiwara², S. Takeuchi², H. Kataura³, R. Nakatsu⁴,
K. Yanagi^{1*}

¹Tokyo Metropolitan Univ., ²Hokkaido Univ. & Osaka Univ., ³AIST/JST-CREST,
⁴Kyoto Univ.

Single wall carbon nanotubes (SWCNTs) show various properties depending on their chiralities. Recently, it becomes possible to obtain high-purity SWCNTs with a single chirality by density gradient ultracentrifugation and gel chromatography and so on [1]. Those techniques enable us to investigate the physical properties of SWCNTs with uniform electronic structure, but those techniques can't control orientations of SWCNTs in their network. In our group, we applied vapor diffusion method (VD method) to control orientations of (6, 5) chiral SWCNTs [2]. We found that content ratio of (6, 5) SWCNTs was significantly increased by VD method. Figs. 1(a) and (c) show Raman spectra of buckypaper and SWCNT-aggregates produced by VD method, respectively. We estimated (6,5) purity by comparing RBM peak intensities. VD method improved purity from 53% to 84%. Furthermore, we found that the aggregates formed by addition of alcohol in a proper concentration could improve the purity. Fig. 1(b) shows Raman spectra of this method using isopropyl alcohol (IPA). This method improved purity from 53% to 76%. This is very simple, but can improve chirality purity.

This work was performed under the Cooperative Research Program of "Network Joint Research Center for Materials and Devices"

[1] H. Liu et al., *Nature Commun.* **2**, 309 (2011), M. Kawai et al., *J. Am. Chem. Soc.* **134**, 9545 (2012).

[2]H. Kudo et al., Abstract of The 42th Fullerene-Nanotubes General Symposium.

Corresponding Author: K. Yanagi

Tel: +81-42-677-2494,

Fax: +81-42-677-2483,

E-mail: yanagi-kazuhiro@tmu.ac.jp

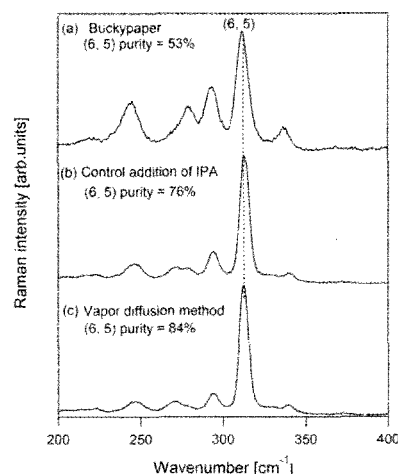


Fig1. Radial breathing modes of (a) Buckypaper, aggregates caused by (b) addition of IPA in a proper concentration, and (c) VD methods, respectively.

Dispersion of single-walled carbon nanotubes made by using ACCVD technique with porous glass

Yosuke Ito¹, ○Shinzo Suzuki¹, Hiroshi Nagasawa², Akira Ono³, Yohji Achiba⁴

¹*Department of Physics, Kyoto Sangyo University, Kyoto 603-8555, Japan*

²*Nano-support Co., Ltd., Kanagawa 251-0024, Japan*

³*Department of Engineering, Kanagawa University, Yokohama 221-8686, Japan*

⁴*Department of Chemistry, Tokyo Metropolitan University, Tokyo 192-0397, Japan*

Abstract:

Single-walled carbon nanotubes (SWNTs) made by using alcohol CVD (ACCVD) technique combined with porous glass (PG) were tested for dispersion in DNA and SDS solution. SWNTs in dispersed solution and residue were investigated by Raman spectroscopy. The experimental condition for making SWNTs by using this PG-ACCVD technique was similar to the condition described in the previous work [1].

Briefly, 3.0 wt% of Co (as cobalt acetate) was introduced in PG (30 nm pore size) in ethanol solution. This solution was then sonicated for 30 min, centrifuged at 2000G for 30 seconds. After removing ethanol, the resultant PG was placed in a quartz tube (i.d. 20 mm), heated at 80°C for 12 hours in air, and was further used for ACCVD treatment [2] using ethanol as carbon supply. The ambient temperature condition was varied between 700 °C and 800 °C, and the temperature dependence of SWNTs for the dispersion was investigated.

It was found that, although SWNTs can be made at each different temperature, almost no SWNTs were dispersed in the solution at 800 °C, where SWNTs were found to be still on PG after strong sonication and ultracentrifugation process. On the other hand, most of SWNTs made at 700 °C were destructed and dispersed in the solution. The different behaviors of SWNTs made at different temperature, and comparison with the purification process using acid/base treatment [3], are presented and discussed.

References:

- [1] S. Maruyama, R. Kojima, Y. Miyauchi, S. Chiashi, and M. Kohno, *Chem. Phys. Lett.*, **360**, 229(2002).
- [2] Y. Aoki, S. Suzuki, S. Okubo, H. Kataura, H. Nagasawa, and Y. Achiba, *Chem. Lett.*, **34**, 562(2005).
- [3] S. Okubo, T. Sekine, S. Suzuki, Y. Achiba, K. Tsukagoshi, Y. Aoyagi, and H. Kataura, *Jpn. J. Appl. Phys.*, **43**, L396(2004).

Corresponding Author: Shinzo Suzuki

TEL: +81-75-705-1631, **FAX:** +81-75-705-1640

E-mail: suzukish@cc.kyoto-su.ac.jp

***In situ* NEXAFS Study on Carbon Nanotube Growth Process by Surface Decomposition of SiC**

○Takahiro Maruyama¹, Yuki Ishiguro¹, Satoshi Sakakibara¹, Shigeya Naritsuka¹,
Kenta Amemiya²

¹ *Department of Materials Science and Engineering, Meijo University, Nagoya 468-8502,
Japan*

² *Photon Factory, Tsukuba 305-0801, Japan*

Carbon nanotube (CNT) growth by surface decomposition of SiC is a unique growth method, since zigzag-type CNTs are selectively formed only by heating SiC crystals in a vacuum without any catalyst. At the initial stage of CNT formation, nanosized hemispherical structures composed of carbon atoms are formed on SiC surface [1]. These “carbon nanocaps” determine the structure of CNTs, therefore, it is important to clarify the formation process of carbon nanocaps. In this study, we carried out *in situ* NEXAFS measurements at high temperature to investigate the formation mechanism of the carbon nanocap.

After HF etching, 6H-SiC(000-1) substrates were placed in a high vacuum chamber and gradually heated to an intended temperature. C K edge NEXAFS spectra were measured at BL-7A in Auger electron yield mode, keeping the sample at the heating temperature. For all temperature, the NEXAFS measurements were carried out with two different incident angles (θ), 30° and 90°, to investigate the orientation of the C-C bond.

Fig. 1 shows NEXAFS difference spectra of SiC(000-1) at 960 and 1380°C, where the spectral component of SiC was subtracted. π^* resonance peaks of C-C bond were clearly observed for the two incident angles for each temperature. In contrast to the spectra at 960°C, the π^* resonance peak at normal incidence was stronger than that for $\theta=30^\circ$ at 1380 °C. This indicates that the orientation of C-C bond changed as temperature rose. Based on the QM/MD calculation [2], we will discuss the formation process of the carbon nanocaps.

A part of this work was supported by the JSPS, a Grant-in-Aid for Scientific Research (c) 21510119. The NEXAFS measurements were performed under the approval of Photon Factory Program Advisory Committee (Proposal No. 2011G539).

References

[1] T. Maruyama et al. Chem. Phys. Lett. **423** (2006) 317.

[2] Z. Wang et al. J. Phys. **C111** (2007) 12960.

Corresponding author: Takahiro Maruyama

Phone: +81-52-838-2386, Fax: +81-52-832-1172

E-mail: takamaru@meijo-u.ac.jp

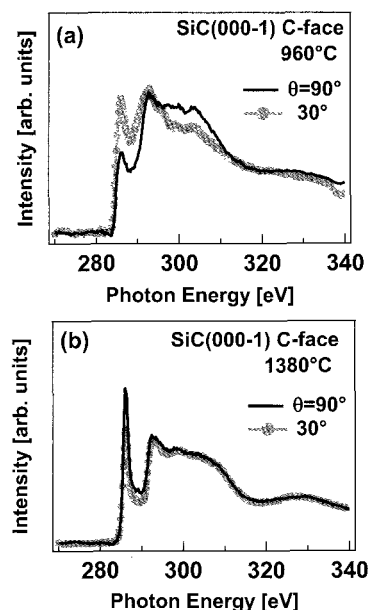


Fig. 1 *In situ* NEXAFS spectra for 6H-SiC(000-1) at 960 and 1380 °C.

Carbon Nanotube Growth on ZnO(0001) Zn-face using Gas Source Method in High Vacuum

○Takeshi Kawai, Shigeoya Naritsuka, Takahiro Maruyama

*Department of Materials Science and Engineering, Meijo University, Nagoya 468-8502,
Japan*

For fabrication of carbon nanotube (CNT) devices, growth of CNTs on semiconductor materials has been desirable. However, only few studies have been reported about direct growth of CNTs on semiconductor surfaces. Among compound semiconductor materials, ZnO has a direct wide band gap of 3.3 eV and shows a wide variation in resistivity, therefore, it has been anticipated as transparent conducting materials. In this study, using the gas source method [1], we attempted to grow CNTs on ZnO(0001) surfaces.

ZnO(0001) (Zn-face) substrates (Tokyo Denpa Co. Ltd.) and Fe and Pt catalysts were used for the CNT growth. After metal catalysts were deposited on the ZnO(0001) surfaces, they were transferred into a vacuum chamber and heated to the growth temperature in a hydrogen atmosphere. Then, CNT growth was carried out by the gas source method using methane. The growth temperature was set to be 700°C. The samples were characterized by SEM observation and Raman spectroscopy.

Fig. 1 shows the sample surface in which the growth was carried out from Fe catalyst at a methane pressure of 1.0×10^{-1} Pa. Entangled fiber-like products were observed on some portions of the sample surface. Taking into account the Raman results, there was a possibility that multi-walled CNTs grew. When the methane pressure was reduced below 1.0×10^{-2} Pa, the amount of products were fairly reduced. On the other hand, when the Pt catalyst was used, no products were observed, irrespective of the methane pressure.

This work was partially supported by the JSPS, Grant-in-aid for Scientific Research (c) 21510119 and the Instrument Center of the Institute for Molecular Science (IMS).

References

[1] T. Maruyama et al., *J. Nanosci. Nanotechnol.* **10** (2010) 1.

Corresponding author: Takahiro Maruyama

Phone: +81-52-838-2386, Fax: +81-52-832-1172

E-mail: takamaru@meijo-u.ac.jp

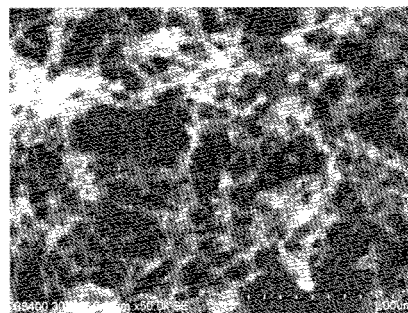


Fig. 1 SEM image of the sample surface from Fe catalyst after the growth at 700°C, 1.0×10^{-1} Pa.

Low Temperature Growth of SWNTs on Pt catalyst by Alcohol Gas Source Method in High Vacuum

○Hiroki Kondo¹, Naoya Fukuoka¹, Yoshihiro Mizutani¹, Ranajit Ghosh¹, Shigeya Naritsuka¹,
Takahiro Maruyama¹, Sumio Iijima^{1,2}

¹*Department of Materials Science and Engineering, Meijo University, Nagoya 468-8502,
Japan*

²*AIST, Tsukuba, Ibaraki 305-8565, Japan*

Single-walled carbon nanotubes (SWNTs) have been anticipated for applications in a lot of future nanodevices. To fabricate SWNT devices in a conventional LSI process, it is important to grow SWNTs at low temperature under high vacuum. In this study, using Pt catalyst, we carried out SWNT growth on SiO₂/Si substrates under various growth conditions and succeeded in SWNT growth at 400°C under an ethanol pressure of 1×10^{-4} Pa.

After deposition of Pt catalyst on the SiO₂/Si substrates using a pulsed arc plasma gun, the SWNT growth was carried out using alcohol gas source method in a high vacuum [1, 2]. The growth temperature was set between 400°C and 800°C, and the ethanol pressure was varied between 1×10^{-5} Pa and 1×10^{-1} Pa. The grown SWNTs were characterized by SEM, TEM and Raman spectroscopy.

When the growth temperature was decreased to 400°C, the G band intensity was reduced, but the RBM peaks were still observed. The diameter distributions estimated from RBM peaks of SWNTs grown with Pt at 400 and 700°C are shown in Fig. 1. Compared to the SWNTs grown at 700°C, both average diameter and diameter distribution decreased drastically at 400°C. In addition, in the SWNT growth at 400°C, the average diameter of the SWNTs grown with Pt was much smaller than that grown with Co. These results showed that Pt catalyst is suitable for the growth of SWNTs with the smaller-diameter and the narrower diameter distributions. Based on the Raman results, we will discuss the chirality of SWNTs grown from Pt catalyst and show that Pt catalyst is suitable for the growth of semiconductor SWNTs.

This work was partially supported by the Japan Society for the Promotion of Science (JSPS), Grant-in-aid for Scientific Research (c) 21510119 and the Instrument Center of the Institute for Molecular Science (IMS).

References

[1] T. Maruyama et al., *J. Nanosci. Nanotechnol.* **10** (2010) 1.

[2] T. Maruyama et al. *Mater. Express* **1** (2011) 267.

Corresponding author: Takahiro Maruyama

Phone: +81-52-838-2386, Fax: +81-52-832-1172

E-mail: takamaru@meijo-u.ac.jp

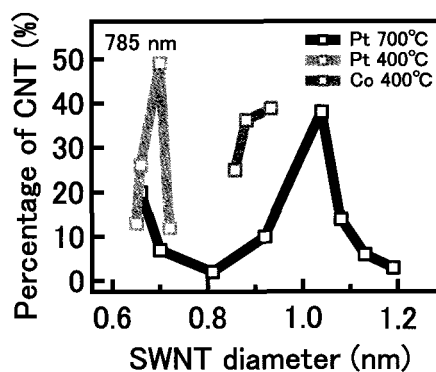


Fig. 1 The diameter distributions of SWNTs grown with Pt and Co. (Excitation wavelength: 785 nm)

Effect of Growth Temperature on Growth Rate in Carbon Nanotube Formation by Surface Decomposition of SiC

°Takatoshi Yajima, Satoshi Sakakibara, Shigeya Naritsuka, Takahiro Maruyama
Department of Materials Science and Engineering, Meijo University, Nagoya 468-8502, Japan

Carbon nanotube (CNT) growth by surface decomposition of SiC is a synthesis method to obtain vertically aligned, high-density CNTs only by heating SiC single crystal at high temperature ($>1300^{\circ}\text{C}$) in a vacuum. In addition, CNTs grown by this method are atomically bonded to SiC at the interface [1], which is desirable for device applications. In order to realize CNT devices, it is important to control the CNT length accurately. In this study, we investigated the effect of the growth condition on the growth rate in the surface decomposition method to control the CNT length.

6H-SiC(0001)(n-type) (CREE) was used for the CNT growth. After the substrates were cleaned with acetone and methanol by the ultrasonic cleaning, they were etched by immersing in 10% HF for 10 min. Then, the substrates were heated in a high vacuum (base pressure $\sim 1.0 \times 10^{-5}\text{Pa}$) to grow CNTs. The samples were characterized by SEM and Raman spectroscopy.

Figure 1 shows the relationship between the growth time and the length of CNTs for various growth temperatures ((a) : 1580°C , (b) : 1650°C , (c) : 1780°C). Up to 30 min, the CNT length increased linearly with the growth time, irrespective of the temperature. After the growth for 30-60 min, the growth rate became slower and the CNT length seemed to be saturated at 1580°C . These results showed that the decomposition of SiC and the sublimation of Si atoms strongly depend on the temperature. The effects of the growth temperature on the CNT growth will be discussed.

This work was partially supported by the Japan Society for the Promotion of Science (JSPS), Grant-in-aid for Scientific Research (c) 21510119 and the Instrument Center of the Institute for Molecular Science (IMS).

References

[1] M. Kusunoki et al. Chem. Phys. Lett. **366** (2002) 458.

Corresponding author: Takahiro Maruyama

Phone: +81-52-838-2386, Fax: +81-52-832-1172

E-mail: takamaru@meijo-u.ac.jp

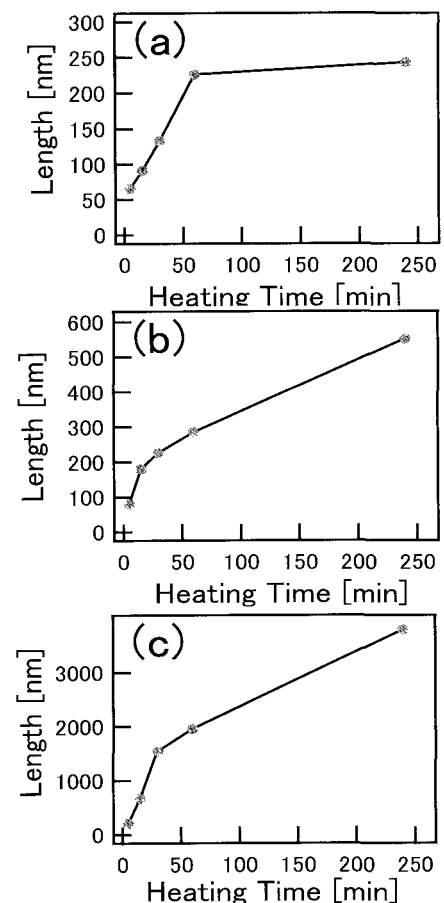


Fig.1 The relationship between the growth time and the CNT length for various temperatures (a) 1580°C , (b) 1650°C , and (c) 1780°C .

Thermodynamics of the interaction of carbon nanotubes with hydrogels in SDS solutions: Toward understanding metal/semiconductor separation

○Atsushi Hirano^{1,2}, Takeshi Tanaka¹, Hiromichi Kataura^{1,2}

¹ *Nanosystem Research Institute, National Institute of Advanced Industrial Science and Technology, Tsukuba, Ibaraki 305-8562, Japan*

² *JST, CREST, Kawaguchi, Saitama, 332-0012, Japan*

One of key technologies for the industrialization of single-wall carbon nanotubes (SWCNTs) is separation of SWCNTs into metallic and semiconducting species. We have previously developed the separation of SWCNTs using hydrogel columns.^[1,2] However, the mechanism is still unclear. In this study, we found that the interaction of SWCNTs with hydrogels in sodium dodecyl sulfate (SDS) solutions follows the Langmuir isotherm. The hydrogels used here were agarose gel and Sephacryl, both of which are effective in the separation.^[1-3] Metallic and semiconducting SWCNTs were found to be different in the adsorption constant. Thermodynamic analysis showed for the first time that the adsorption is endothermal reaction, i.e. entropy-driven. These results suggest the separation of SWCNTs using the hydrogels is accounted for by structural changes of coexisting SDS.

Figure 1 shows a model for the adsorption of SWCNTs onto the hydrogels based on the Langmuir isotherm that is expressed by one adsorption constant (K). Using this model, the adsorption constant was obtained from measurement of the amount of adsorbed SWCNTs onto the hydrogels. For both agarose gel and Sephacryl, the constants for semiconducting SWCNTs were larger than that for metallic SWCNTs (Figure 2), indicating that the semiconducting species interact more strongly with the hydrogels in equilibrium. Importantly, the constants increased with increasing temperature so that the adsorption was appeared to be endothermal reaction. In other words, enthalpy for the adsorption is positive ($\Delta H > 0$). Because adsorption reaction has ordinarily negative enthalpy, coexisting SDS should compensate the potential negative enthalpy with large positive entropy through its structural changes such as desorption or rearrangement. This is the first report of the thermodynamic analysis that provided new mechanistic insight into the interaction of SWCNTs with the hydrogels in SDS solutions. Such mechanism should work not only in the separation but also in the purification using the hydrogel columns.^[4]

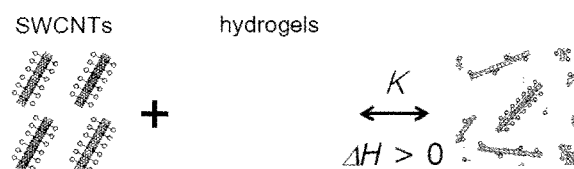


Fig. 1. Model for the adsorption of SWCNTs onto hydrogels. K depicts the adsorption constant.

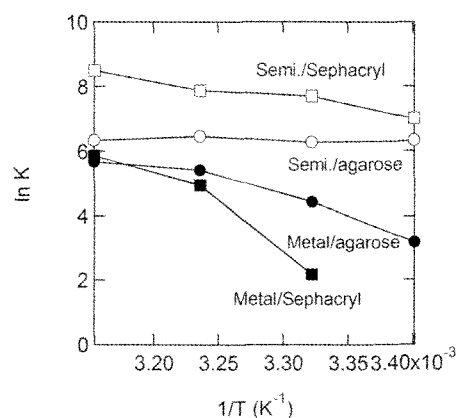


Fig. 2. Adsorption constants of metallic and semiconducting SWCNTs onto the hydrogels at various temperatures.

[1] T. Tanaka *et al.* Appl. Phys. Express **2**, 125002 (2009). [2] A. Hirano *et al.* J. Phys. Chem. C **115**, 21723 (2011). [3] H. Liu *et al.* Nat. Commun. **2**, 309 (2011). [4] A. Hirano *et al.* J. Phys. Chem. C **116**, 9816 (2012). Corresponding Author: H. Kataura, Tel: +81-29-861-2551, Fax: +81-29-861-2786, E-mail: h-kataura@aist.go.jp

Highly pure semiconducting single-wall carbon nanotubes obtained by stable electric-field-induced layer formation

°Fusako Sasaki¹, Kazuki Ihara^{1,2}, Takeshi Saito³, Fumiya Nihey^{1,2}

¹Technology Research Association for Single Wall Carbon Nanotubes (TASC), Tsukuba, 305-8565, Japan

²Smart Energy Research Laboratories, NEC Corporation, Tsukuba, 305-8501, Japan

³National Institute of Advanced Industrial Science and Technology (AIST), Tsukuba, 305-8565, Japan

Since single-wall carbon nanotubes (SWCNTs) are produced as a mixture of metallic and semiconducting ones by commonly-used synthesis methods, they have to be separated for electronic applications such as thin-film transistors. Furthermore, ion-free separation processes are preferable to enable the stable operation of electronic devices. We have proposed a method to separate metallic and semiconducting SWCNTs by electric-field-induced layer formation (ELF) with a nonionic surfactant as a dispersing agent [1]. Previously, repeated ELF treatments have been required to obtain semiconducting SWCNTs (sc-SWCNTs) with a purity > 98 % [2]. In this paper, we report the purification of sc-SWCNTs by using a modified separation cell. Highly pure (up to 98%) sc-SWCNTs were obtained by a single step of ELF treatment.

SWCNTs synthesized by chemical vapor deposition (diameter $d = 1.0, 1.3$ and 1.7 nm) were dispersed in D_2O with 1 wt % of polyoxyethylene (100) stearyl ether (Brij700) by sonication and ultracentrifugation. The solution was introduced into a vertical glass cell with a pair of electrodes. The cell has an anode column and a cooling jacket to stabilize the formation of SWCNT layers. Samples were fractionated after the application of voltage at 120 V for 190 hours. UV-Vis-NIR spectroscopy and Raman spectroscopy were conducted for each fraction. Photographs in Fig. 1 show the evolution of SWCNT solution ($d = 1.3$ nm). Lower (semiconductor-rich) and upper (metal-rich) layers were created and concentrated as time proceeded. Raman spectra of separated samples ($d = 1.3$ nm) are shown in Fig. 2. Relative RBM intensities suggest that the purity of sc-SWCNTs (F1) is 98 %. Similar results were obtained for the samples with $d = 1.0$ and 1.7 nm.

This work was supported by New Energy and Industrial Technology Development Organization (NEDO).

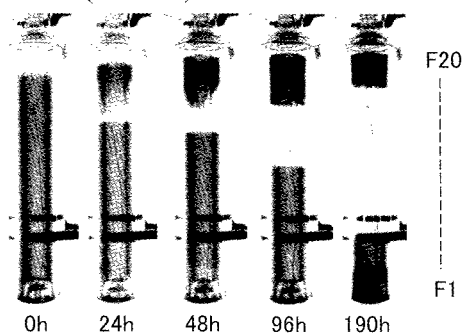


Fig. 1 Evolution of SWCNT solution

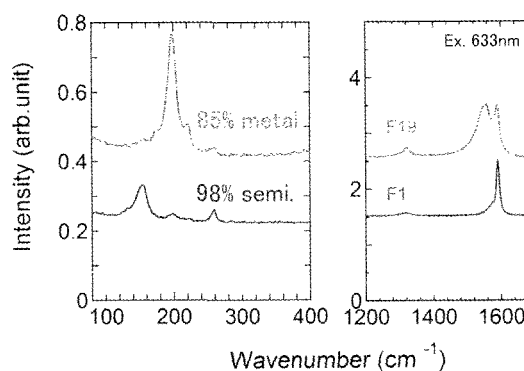


Fig. 2 Raman spectra of separated samples

References:

- [1] K. Ihara, H. Endoh, T. Saito, and F. Nihey, *J. Phys. Chem. C* **115**, 22827 (2011).
 [2] K. Ihara, T. Saito, and F. Nihey, The 40th Symposium Abstract, p.23 (2011).

Corresponding Author: Fusako Sasaki

E-mail: f_sasaki@tasc-nt.or.jp, **Tel:** +81-29-861-3778, **Fax:** +81-29-858-6330

A rosette cooling cell: more effective container for solubilization of single-walled carbon nanotubes under probe-type ultrasonic irradiation

○Yuta Kurabuchi^{1,2}, Tatsuki Yasumitsu^{1,2}, Gang Liu¹, Jean-Marc Levêque³, Shuji Aonuma², Laurent Duclaux³, Takahide Kimura¹, Naoki Komatsu¹

¹ Department of Chemistry, Shiga University of Medical Science, Seta, Otsu 520-2192, Japan.

² Department of Applied Chemistry, Osaka Electro-Communication University, Neyagawa, Osaka 572-8530, Japan.

³ Laboratory of Molecular Chemistry and Environment, University of Savoie, 73376, Le Bourget du Lac Cedex, France.

Sonochemical process plays an essential role to manipulate nanomaterial in liquid phase in terms of deagglomeration and dissolution. In spite of its importance, the sonochemical processing of SWNTs has not been considered seriously. Herein, we report on a more efficient cooling cell for probe-type ultrasonication. As compared with a conventional cylindrical cell, the concentration of the SWNTs solubilized in water was found to be almost double in a rosette cooling cell after ultracentrifugation [1].

When the aqueous suspensions of HiPco were probe-sonicated in the presence of SC (sodium cholate) or SDBS (sodium dodecylbenzenesulfonate), the supernatant from a rosette cell gave larger intensity of absorption than that from a cylindrical cell after ultracentrifugation as shown in Fig. 1. From the peak intensity in E_{11}^S and E_{22}^S regions, the concentration of SWNTs in a rosette cell is estimated to be twice as large as that in a cylindrical cell. Upon dissolution of other kinds of SWNTs such as CoMoCAT, a rosette cooling cell also showed much higher efficiency than a conventional cylindrical cell under probe-type sonication.

[1] T. Yasumitsu, G. Liu, J.-M. Levêque, S. Aonuma, L. Duclaux, T. Kimura, N. Komatsu, *Ultrason. Sonochem.*, in press (10.1016/j.ultsonch.2012.06.009).

Corresponding Author: N. Komatsu

Tel: +81-77-548-2102, Fax: +81-77-548-2405.

E-mail: nkomatsu@belle.shiga-med.ac.jp

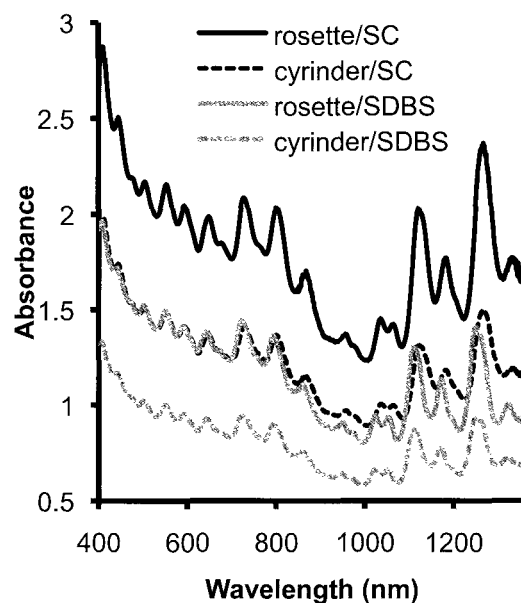


Fig. 1. Absorption spectra of HiPco dissolved in the presence of SC or SDBS in the rosette or cylindrical cell.

The simplest separation of single-chirality carbon nanotubes by temperature-controlled gel chromatography

○Huaping Liu^{1,2}, Yasuko Urabe^{1,2}, Takeshi Tanaka¹, Hiromichi Kataura^{1,2}

¹ *Nanosystem Research Institute, National Institute of Advanced Industrial Science and Technology (AIST), Tsukuba, Ibaraki 305-8562, Japan*

² *Japan Science and Technology Agency, CREST, Kawaguchi, Saitama 330-0012, Japan*

Utilizing single-wall carbon nanotubes (SWCNTs) in the fields of electronics and optoelectronics requires single-chirality SWCNTs with well-defined electronic properties, which drives scientists to pursue single-chirality carbon nanotube materials. Recently, we developed a novel multi-stage gel chromatography and realized large-scale single-chirality SWCNT separation [1, 2], but this technique usually requires repeated separation to achieve high-purity single-chirality nanotubes, which is time-consuming and costly.

Most recently, we found that temperature could chirality-dependently tailor the interaction strength between the SDS-wrapped SWCNTs and allyl dextran-based gel. According to this new finding, we developed temperature-controlled gel chromatography, allowing the extraction of (n, m) -enriched fraction in a single-step separation process [3]. Lowering the separation temperature chirality-dependently decreases the interaction between the SDS-wrapped SWCNTs and gel. When the separation temperature is set at a low degree at which only (n_1, m_1) SWCNTs having the strongest interaction with the gel can be adsorbed, pouring SWCNT dispersion into the gel columns directly leads to the separation of the high-purity single species. Similarly, another (n_2, m_2) SWCNTs having the second strongest interaction with the gel could be sorted out at a slightly higher temperature. In this manner, we sorted out seven (n, m) single-chiralities from the HiPco-SWCNTs at a series of temperatures (Fig. 1). The main feature of this temperature-controlled gel chromatography is that temperatures resolve (n, m) single-species, which dramatically simplifies the separation process of single-chirality SWCNTs. In this report, we will present additional interesting results on single-chirality separation of carbon nanotubes by temperature-controlled gel chromatography and also will propose a chirality-separation mechanism.

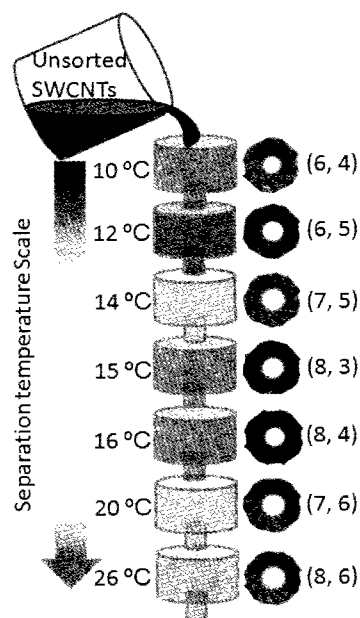


Fig. 1 Schematic diagram of single-chirality separation of SWCNTs by temperature-controlled gel chromatography.

[1] H. Liu *et al.* Nat. Commun. **2**, 309 (2011).

[2] H. Liu *et al.* Phys. Status Solidi B **248**, 2524 (2011).

[3] H. Liu *et al.* The 41st Fullerenes-Nanotubes-Graphene General Symp. p 27 (2011).

Corresponding Author: H. Kataura

Tel: +81-29-861-2551, Fax: +81-29-861-2786,

E-mail: h-kataura@aist.go.jp

Evaluation of damage to SWCNTs during dispersion process in casein aqueous solution by using a wet-type super atomizer

○Tadashi Takashima¹, Daisuke Inoue², Yasushi Maeda³, Shin Ono²

¹*Nano-tech Division, Yoshida Kikai Co. Ltd., Tokyo 146-0093, Japan*

²*Nano and Functional Materials and Science, Graduate School of Science and Engineering, University of Toyama, Toyama 930-8555, Japan*

³*Graduate School of Engineering, University of Fukui, Fukui 910-8507, Japan*

Single-walled carbon nanotubes (SWNTs) have received much attention as promising materials due to their mechanical and electronic properties. For their industrial application, dispersion of SWNTs in water and organic media is important. For dispersing SWNTs, ultrasonication has been widely used. Since ultrasonication is too strong to disperse SWNTs without destruction and shortening of SWNTs, development of a method for dispersing SWNTs in water and organic media without destructive damages has been needed.

In our previous work, we examined whether SWNTs can be dispersed in water containing proteins, casein and bovine serum albumin (BSA), by using a wet-type atomizer “NanoVater” (Yoshida Kikai Co. Ltd.). Since the Nanovater uses collision of solution under ultra-high pressure (max. 200 MPa) to disperse CNTs, the destruction of CNTs during dispersion process is expected to be reduced. Although casein was found to act as a good dispersant for SWNTs, the destructive damages of SWNTs in the dispersion process was not evaluated. In this work, we prepared casein-SWNTs dispersion solutions by using Nanovater and measured the Raman spectra of them to evaluate the destructive damages of SWNTs.

HiPco and CoMoCAT SWNTs (each 20 mg) were mixed with 40 ml of casein solution (5 mg/ml) and the mixtures were treated by the NanoVater under pressures around 180 MPa. These treatments were repeated 500 times and 1 ml samples at 100 times intervals were withdrawn. The sample suspensions were centrifuged and the supernatant was subjected to the Raman spectroscopic analysis. In the case of CoMoCAT SWNTs, no significant change in the G/D ratio of their spectra was observed during 500 times-repeated treatment. A comparison of the G/D ratio between the dispersion solutions prepared with the NanoVater and the Sonifier (Branson) showed that the dispersion process with NanoVater can reduce the destructive damage to SWNTs. We will also report the influence of the treatment with the NanoVater on HiPco SWNTs and discuss a usefulness of the NanoVater for dispersing not only SWNTs but also MWNTs in aqueous media.

Corresponding Author: Tadashi Takashima

Tel&Fax: +81-594-49-2255/+81-594-49-2277

E-mail: takasima@yoshidakikai.co.jp

Stability of Nano-Diamonds as the Catalyst for CVD Growth of Single-Walled Carbon Nanotubes

○Takanori Umino¹, Kenta Nakamura¹, Taiki Inoue¹, Norihiro Hiramatsu¹,
Shohei Chiashi¹, Yoshikazu Homma² and Shigeo Maruyama¹

¹Department of Mechanical Engineering, University of Tokyo, Tokyo 113-8656, Japan

²Department of Physics, Tokyo University of Science, Tokyo 162-8601, Japan

Structure control is still challenging topic in the research of SWNT growth. Controlling catalyst structure is one of the expected methods for structure control of SWNTs, and controllable and stable catalyst particles at even high temperature are needed. Here, we perform CVD by using nano-diamond particles as the catalyst [1] and investigate the stability of nano-diamond. To decrease diameter, nano-diamond particles were oxidized on silicon substrates in air at 600 or 800 °C before CVD. For comparison, Co/Mo catalyst prepared by using dip-coat process [2] was used. The catalyst stability was investigated by annealing treatment: one was annealed in Ar/H₂ gas for 2 hours at 900 °C before CVD and the other was not annealed.

SWNTs were characterized by using TEM and Raman scattering spectroscopy. TEM image and RBM peaks of SWNTs from nano-diamond are shown in Fig. 1. The G-band intensities of SWNTs from annealed Co/Mo catalysts were significantly smaller than those from non-annealed Co/Mo catalysts. In contrast, in the case of nano-diamond catalysts, the annealing treatment effect did not appear in Raman scattering spectrum. It indicates that the diameter distribution of nano-diamond did not change after the annealing treatment, while Co/Mo catalysts aggregated and became larger particles. Unlike Co/Mo catalysts, nano-diamond particles are quite stable at high temperature, which would suggest that it is possible to control the detail structure of SWNTs by controlling nano-diamond structure in advance.

References:

[1] D. Takagi, et al., J. Am. Chem. Soc., 131 (2009) 6922.

[2] Y. Murakami, et al., Chem. Phys. Lett., 377 (2003) 49.

Corresponding Author: Shigeo Maruyama

E-mail: maruyama@photon.t.u-tokyo.ac.jp

TEL: +81-3-5841-6421, FAX: +81-3-5800-6983

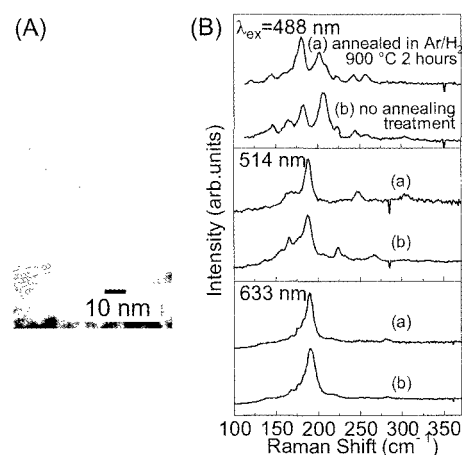


Fig. 1 (A) TEM image of SWNTs grown from nano-diamond. (B) Raman scattering spectra (RBM peaks) of SWNTs grown from nano-diamond particles. The oxidization treatment was performed at (A) 600 °C (B) 800 °C and the CVD temperature was 800 °C.

Reaction analysis on CNT growth mechanism by eDIPS method using ^{13}C carbon source

○Takayoshi Hirai¹, Kazuaki Hoshi¹, Yuki Kuwahara^{1,2}, Rena Shibata¹, Masaharu Kiyomiya¹, Shun Nakano¹, Takeshi Saito^{1,2}

¹Technical Research Association for Single Wall Carbon Nanotube, Higashi 1-1-1, Tsukuba, Japan

²Nanotube Research Center, National Institute of Advanced Industrial Science and Technology, Higashi 1-1-1, Tsukuba, Japan

Among the various chemical vapor deposition (CVD) techniques, the direct-injection-pyrolytic-synthesis (DIPS) method is excellent for the growth of carbon nanotubes (CNTs) in terms of its high yield and low production costs. Our group has reported various synthetic techniques with DIPS method, and then proposed enhanced DIPS (eDIPS) method where the tube diameter distribution can be controlled gradually and selectively by simple tuning of injected two carbon source (liquid organic solvent and gaseous hydrocarbon)[1]. In order to further optimization of the CNT production, the clarification of the growth mechanism is extremely important. Recently we have reported the reaction analysis of the eDIPS growth in which efficient carbon precursors for the SWCNT growth has been investigated by the analysis of the gas-phase decomposition products from various carbon sources [2, 3], laser ionization time-of-flight mass spectroscopy (TOF-MS) and CEMKIN simulation [3]. In this study, we report the results of the novel reaction analysis using carbon isotopes, that is, ^{13}C labeled gaseous hydrocarbon and liquid organic solvent.

Typical experimental procedures were carried out as reported; feedstocks were prepared by dissolving ferrocene into suitable ^{13}C -labeled or non-labeled organic solvents and adding the appropriate amount of sulfur source as a catalytic promoter. Those feedstocks were injected into the reactor through the spray nozzle under H_2/Ar atmospheres. And as a second carbon source, the appropriate amount of ^{13}C -labeled or non-labeled gaseous hydrocarbon was injected. Under a reaction condition using natural toluene (as a primary carbon source) and ^{13}C -labeled ethylene (as a secondary carbon source) at the ratio of $^{13}\text{C}/^{12}\text{C} = 0.36$, the percentage of ^{13}C in produced CNTs was evaluated to be 67% by the shift amount of G-band in the resonant Raman spectrum [4]. This result means that the preferential carbon source consumed for CNT growth is ethylene rather than toluene. The result of laser ionization TOF-MS in the gas-phase decomposition products also supported the preferential consumption of ethylene as the carbon source in the eDIPS growth of CNTs.

This work has been supported by New Energy and Industrial Technology Development Organization (NEDO) project.

[1] T. Saito *et al.*, *Appl. Phys. Express*, **2** (2009) 095006.

[2] B. Shukla *et al.*, *Chem. Commun.*, (2009) 3422.

[3] B. Shukla *et al.*, *Chem. Mater.*, **22** (2010) 6035.

[4] S. D. Costa *et al.*, *Carbon*, **49** (2011) 4719.

Corresponding Author: T. Saito, Tel: +81-29-861-4863, Fax: +81-29-861-4413, E-mail: takeshi-saito@aist.go.jp

Growth of Horizontally Aligned Single Walled Carbon Nanotubes: Effect of Catalyst Preparation and Crystal Quartz Surface

○Taiki Inoue¹, Grace Meikle^{1,2}, Saifullah Badar¹, Daisuke Hasegawa¹, Shohei Chiashi¹,
Shigeo Maruyama¹

¹ *Department of Mechanical Engineering, The University of Tokyo, 7-3-1 Hongo, Bunkyo-ku, Tokyo, Japan*

² *Department of Physics, University of Notre Dame, Notre Dame 46556, Indiana, United States*

Horizontally aligned single walled carbon nanotubes (HA-SWNTs) have been grown along a particular lattice direction on crystal quartz substrates [1-3]. High-density arrays of HA-SWNTs are desired for the fabrication of high-performance electronic devices. In this study, we examined the effect of surface structure of quartz substrates and catalyst preparation methods on the growth of HA-SWNTs.

Several types of quartz substrates polished by different procedures were prepared and surface structures of the substrates were investigated by atomic force microscopy (AFM). We observed marks (or defects) caused by polishing processes on substrate surfaces and found that the number density of the polishing marks varied with different polishing procedures. Then HA-SWNTs were grown on the quartz substrates by the alcohol chemical vapor deposition method [4]. Scanning electron microscopy (SEM) observation showed that misalignment of HA-SWNTs occurred more frequently on the quartz substrates with more polishing marks. This revealed that surface structures of quartz substrates due to different polishing procedures had a significant effect on the degree of alignment of HA-SWNTs.

Furthermore, we investigated the effect of catalyst preparation methods. Catalysts with stripe patterns were deposited on quartz substrates either by a dry process (vacuum deposition of cobalt) or a wet process (drop casting of cobalt acetate solution). It was found that the density of HA-SWNTs grown from the wet process catalysts was reproducibly higher than that from the dry process catalysts. Figure 1 shows an SEM image of HA-SWNTs with a density of ~20 tubes/ μm grown from the wet process catalysts. AFM observation revealed that the number density of nanoparticles from the wet process was lower and the diameter distribution of that was broader than those from the dry process. Low density of catalysts is considered to reduce the possibility that adjacent SWNTs will form bundles in the catalyst area, causing their alignment to be disturbed. Additionally, we believe that the broad distribution of catalyst particle size allows for reproducible formation of nanoparticles with the appropriate size for SWNT nucleation independent of slight changes in the catalyst deposition condition.

[1] C. Kocabas *et al.* J. Phys. Chem. C **111**, 17879 (2007).

[2] L. Ding *et al.* J. Am. Chem. Soc. **130**, 5428 (2008).

[3] S. Chiashi *et al.* J. Phys. Chem. C **116**, 6805 (2012).

[4] S. Maruyama *et al.* Chem. Phys. Lett. **360**, 229 (2002).

Corresponding Author: S. Maruyama

Tel: +81-3-5841-6421, Fax: +81-3-5800-6983

E-mail: maruyama@photon.t.u-tokyo.ac.jp

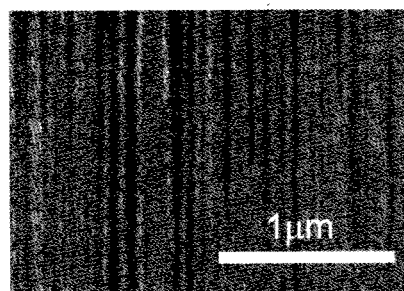


Fig.1 SEM image of HA-SWNTs grown from cobalt catalysts prepared by the wet process on the quartz substrate with less polishing marks.

Pulse plasma CVD for mass production of narrow-chirality distributed single-walled carbon nanotubes

○Koshi Murakoshi, Toshiaki Kato, Rikizo Hatakeyama, Toshiro Kaneko

Department of Electronic Engineering, Tohoku University, Sendai, 980-8579 Japan

One dimensional single-walled carbon nanotubes (SWNTs) are potential materials for future nanoelectronics. Since the electronic and optical properties of SWNTs strongly depend on their diameter and chirality, the selective synthesis of SWNTs with desired chiralities is one of the major challenges in nanotube science and applications. Recently, we have demonstrated a narrow-chirality distributed growth of SWNTs by time-programmed plasma CVD [1]. In this method, we used very short time growth of SWNTs. Based on the systematic investigations, it has been revealed that there is a close correlation between incubation time (t_i) and SWNT structures. Since t_i of the small diameter (or specific chirality) SWNTs is shorter than that of the larger (or other chiralities) one, selective growth of narrow-chirality distributed SWNTs has been realized by adjusting the growth time during plasma CVD. Due to the short growth time, however, only the small amount of narrow-chirality distributed SWNTs can be grown with this method.

In this study, we improve the previous time-programmed plasma CVD and establish a new strategy to realize the mass production of narrow-chirality distributed SWNTs using pulse plasma CVD. In the pulse plasma CVD, multiple short time growth of SWNTs can be possible by repeating the plasma generation. We used Co catalyst on SiO_2 / Si substrate and made the inductively-coupled plasma from mixture of CH_4 and H_2 . In this system, we can easily control the time-programmed plasma generation. In order to analyze the diameter and chirality, we used the Raman scattering spectroscopy. The amount of SWNTs was also estimated by the intensity of G-band, which was normalized by the intensity of Si.

When we carried out the pulse plasma CVD for SWNTs growth, it is found that the amount of SWNTs increases with an increase in the total growth time. Interestingly, it is also revealed that the initial narrow-diameter distribution of SWNTs can be maintained even after the pulse plasma CVD. We think this is because that only specific diameter or chirality SWNTs can be grown during each pulse of plasma CVD due to their very short t_i . This result indicates that it should be possible to realize the mass production of narrow-chirality distributed SWNTs with our established novel approach.

[1] T. Kato and R. Hatakeyama, ACS Nano **4**, 7395 (2010).

Corresponding Author: K. Murakoshi

Tel: +81-22-795-7046, Fax: +81-22-263-9225,

E-mail: murakoshi10@ecei.tohoku.ac.jp

Separation of ultra-long single-wall carbon nanotubes using glass beads filtration

○Hiromichi Kataura, Mayumi Tsuzuki, Shunjiro Fujii, Takeshi Tanaka

Nanosystem Research Institute (NRI), National Institute of Advanced Industrial Science and Technology (AIST), Tsukuba, Ibaraki 305-8562, Japan

Safety test of nanomaterial is very important for its practical use in the industrial products. Especially in the case of single-wall carbon nanotubes (SWCNTs), possible toxicity of SWCNTs longer than 10 μm is now hot issue, because macrophage cannot eat long SWCNTs. To see how the length affects the toxicity of SWCNTs, we have to prepare “long” and “short” SWCNT samples for experiments. It is well known that the short SWCNTs can be easily prepared by strong ultrasonic treatment that can cut SWCNTs into short pieces. On the other hand, preparation of long SWCNTs is not easy because raw SWCNTs contain both short and long pieces. To get only long SWCNTs, we need to separate SWCNTs into short and long pieces. To date, however, there was no good way to separate SWCNTs longer than 10 μm .

We have developed a new column filtration method to extract ultra-long SWCNTs majority of which is longer than 10 μm . In this study, eDIPS-SWCNTs (Nikkiso) were used as a long SWCNT source and natural deoxyribonucleic acid (DNA) was used as a dispersant. After a mild dispersion, SWCNT/DNA aqueous solution was introduced into a column filled with glass beads with 100 μm in average diameter. Some SWCNTs were trapped in glass beads column while the other SWCNTs flowed through the column. After washing the column with water, glass beads were recovered with trapped SWCNTs. Figure 1 shows the length distributions of trapped and the flow through SWCNTs measured by atomic force microscopy. For the trapped portion, SWCNTs longer than 10 μm were highly enriched up to 65.8 % and short SWCNTs were almost removed. On the other hand, the flow through SWCNTs shows similar length distribution to the raw SWCNTs but the abundance of long SWCNTs was considerably decreased. These results clearly indicate that the ultra-long SWCNTs were selectively trapped in the column. This selective filtration probably originated from attractive interaction between DNA and glass beads, which is often used to collect DNAs in the field of biology.

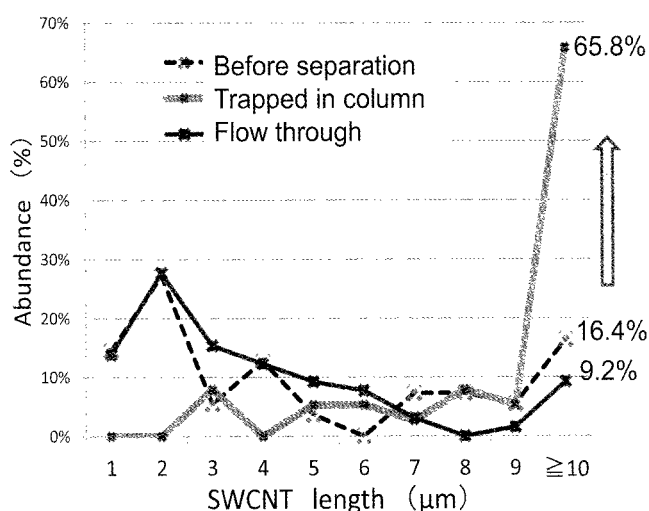


Figure 1. Length distribution of SWCNTs before and after the separation.

Corresponding Author: Hiromichi Kataura

E-mail: h-kataura@aist.go.jp **Tel:** +81-29-861-2551, **Fax:** +81-29-861-2786

Synthesis of Carbon Nanomaterials Using Metallic Nanoparticles as Catalysts

○Balachandran Jeyadevan¹, Yukihiro Osada¹, Yoshinori Sato² and Yuuki Sunayama¹

¹ *Department of Materials Science, The University of Shiga Prefecture, Hikone, 522-8533, Japan*

² *Graduate School of Environmental Studies, Tohoku University, Sendai, 980-8579, Japan*

Though sputtered metallic or alloy films with controlled grain size and composition have been used in CVD technique to synthesize carbon nanomaterials, they undergo morphological change during the reaction and the degree of change depends on the reaction conditions and cannot be controlled easily. As a consequence, the properties of the carbon materials, which depend on the properties of the catalyst, cannot be designed. On the other hand, if metallic nanoparticles can be used as catalyst, the control over their size during carbon nanomaterials synthesis can be controlled and would lead to the production of designed carbon material. Thus the feasibility of using iron nanoparticles for the synthesis of MWCNTs and also the effect of particle size on their morphology has been examined.

The synthesis of carbon nanomaterial was attempted using iron nanoparticles with different diameters as catalyst. The control over their diameters was attempted using iron particle dispersions with varying solid concentrations and treating the spin-coated iron particle monolayer on a silicon substrate at different reaction temperatures. And the products were characterized using SEM, TEM and Raman spectroscopy. The solid concentration of nanoparticle suspension and the reaction temperature influenced the ultimate size of the catalyst that assisted the growth of MWCNTs. The diameter of the particles increased for any increase in solid concentration (Fig. 1 (a)) and reaction temperature (Fig. 1 (b)). Consequently, the morphology of the nanotubes was influenced very much by the size of the nanoparticles and the diameter of the nanotubes increased with any increase in the particle diameter (Fig. 1 (c)). The syntheses of magnetite nanoparticles, which were used as the source for the preparation of iron nanoparticle catalyst and also their influence on the morphological change in carbon nanomaterials will also be discussed in detail.

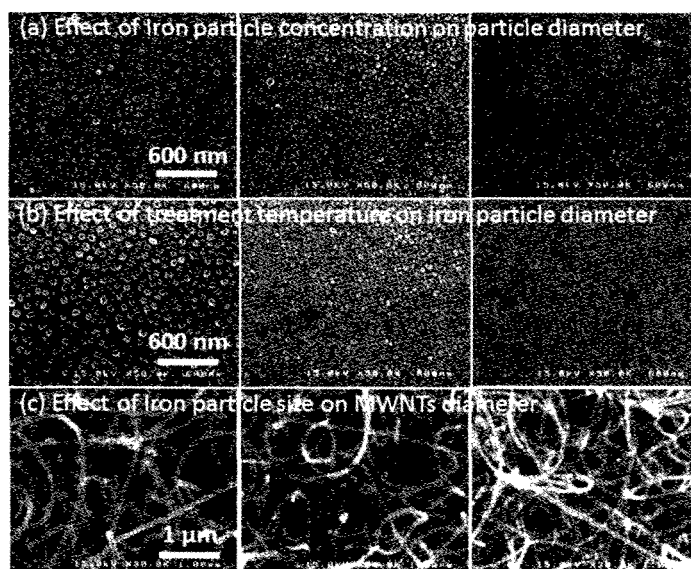


Fig. 1 The influence of particle concentration and reaction time on particle diameter and subsequent effect on MWNT diameter.

The effect of CNHs adsorbed simvastatin on bone regeneration

○Akiko Yamauchi¹, Sachiko Matsumura², Tadashi Iizuka¹, Kiyotaka Shiba²,
Masako Yudasaka³, Sumio Iijima^{3,4}, Atsuro Yokoyama¹

¹ Graduate School of Dental Medicine, Hokkaido University, Sapporo, 060-8586, Japan

² Division of Protein Engineering, Cancer Institute, Japanese Foundation for Cancer Research, Tokyo 135-8550, Japan

³ Nanotube Research Center, National Institute of Advanced Industrial Science and Technology, Tsukuba, 305-8565, Japan

⁴ Faculty of Science and Technology, Meijo University, Nagoya, 468-8502, Japan

Purpose: Previously we reported that application of carbon nanohorns (CNHs) for guided bone regeneration (GBR) technique was effective on bone regeneration¹⁾. The purpose of this study is to evaluate the effect of CNHs adsorbed simvastatin on bone regeneration.

Materials and Methods: One milligram of CNHs was dispersed in 5 ml of 50% ethanol solution. Simvastatin was dissolved in CNHs suspension, and it was fixed on porous polytetrafluoroethylene (PTFE) membrane by vacuum filtration (S-CNHs/PTFE). CNHs without simvastatin was also fixed on PTFE membrane (CNHs/PTFE)¹⁾. Bone defects of 7 mm diameter were created in calvarial bone of male Wistar rats (10-week-old). The animals were randomly assigned to 3 groups. The defects were covered with CNHs/PTFE membrane (NH groups) and S-CNHs/PTFE membrane (S-NH groups), or left untreated for control (C groups). The rats were sacrificed at 2 and 8 weeks after the surgery, and soft x-ray radiographic and histological evaluation were carried out.

Results & Discussion: In soft x-ray, NH and S-NH groups showed more radiopacity than those of C groups at 2 weeks. The radiopacity of S-NH groups was the most extensive among the three groups at 8 weeks. In histological evaluation, new bone was formed in the center area in NH and S-NH groups, while bone formation from the only marginal area of the bone defects was observed in C group at 2 weeks. At 8 weeks, newly formed bone in S-NH groups was larger than those in the other groups. The results suggested that CNHs might be the excellent carrier of simvastatin.

Conclusions: It was concluded that CNHs adsorbed simvastatin was effective on bone regeneration for GBR technique.

[1]Kasai T, Matsumura S, Iizuka T et al. Carbon nanohorns accelerate bone regeneration in rat calvarial bone defect. *Nanotechnology* 22, 065102, 2011

Corresponding Author: A. Yamauchi

Tel: +81-11-706-4270, Fax: +81-11-706-4903,

E-mail: yama-aki@den.hokudai.ac.jp

Biodistribution and biocompatibility of water-soluble carbon nanotubes

○Shigeaki Abe¹, Sachiko Itoh¹, Toshihisa Kobayashi², Takayuki Kiba³, Tsukasa Akasaka¹, Yasutaka Yawaka¹, Shin-Ichiro Sato², Motohiro Uo⁴, Fumio Watari¹, Daisuke Hayashi⁵, and Tomoya Takada⁵

¹ Graduate School of Dentai Medicine, Hokkaido University, Sapporo, 060-8586, Japan

² Graduate School of Chemical Science and Engineering, Hokkaido University, Sapporo, 060-8628, Japan

³ Graduate School of Information Science and Technology, Hokkaido University, Sapporo, 060-8628, Japan

⁴ Graduate School of Medical and Dental Sciences, Tokyo Medical and Dental University, Tokyo, 113-8510, Japan

⁵ Department of Material Chemistry, Asahikawa National College of Technology, Asahikawa, 071-8241, Japan

Recently, carbon nanotubes have received much attention for their potential applications to electric, mechanical, chemical and biotechnological fields. In particular, many researchers have paid attention to the interactions of CNTs with living organisms or the environment. The assessment of the effects on the human body is an important problem facing the potential use of CNTs for biomedical applications, such as drug or gene delivery systems, cancer tracking, and tissue engineering scaffolds. However, the effects of CNTs on animals, living organisms or cells have not been investigated enough. Some of the numerous materials considered biocompatible at the macrolevel have shown toxicity *in vitro* when the particle size reaches the micro-/nano-level. In this study, we prepared two-types of water-soluble carbon nanotubes (CNTs) and investigated their biodistribution in mice as well as biocompatibility. After administration, their organs were excised at various post-injection times, then observed using both optical and transmission electron microscopy (TEM). The color of the liver and lung markedly darkened, suggesting that administered CNTs reached these organs. By TEM observation, the CNTs were found in the liver and lung. They were observed even in the kidney and spleen, though their distributions in those organs were accumulated in the liver and lung. However, the time profile of the body weight of CNT-administered mice was close to that of control group. In addition, we estimated the cytocompatibility of the water-soluble CNTs for hepatocytes and XXX. According to a TNF- α assay of the cells cultured with CNTs, the expression level was almost the same as that of the control. These results suggested that the water-soluble CNTs have good bio-/cyto-compatibility under this condition at least.

- S.Abe *et al.* Nano Biomed. **1**, 143 (2009)
- S.Abe *et al.* J. Australian Ceram. Soc. **46**, 48 (2010)
- T. Takada, D. Santida and S. Abe, Nano Biomed. **2**, 147 (2010)
- S.Abe *et al.* Jpn J. Appl. Phys. **50**, 01BJ021 (2011)
- S.Abe *et al.* Physics Procedia, **14**, 147 (2011)
- S.Abe *et al.* Mol. Cryst. Liq. Cryst., **538**, 258 (2011)
- S.Abe *et al.* J. Surf. Sci. Nanotechnol. **9**, 80 (2011)
- S.Abe *et al.* J. Nanosci. Nanotechnol. **12**, 700 (2012).

Corresponding Author: S. Abe

Tel: +81-11-706-4252, Fax: +81-11-706-4252,

E-mail: sabe@den.hokudai.ac.jp

Temperature Dependence of Photoluminescence Spectra in Hole-Doped Single-Walled Carbon Nanotubes

○Shinichiro Mouri¹, Munechiyo Iwamura¹, Naoto Akizuki¹, Yuhei Miyauchi^{1,2},
Kazunari Matsuda¹

¹*Institute of Advanced Energy, Kyoto University, Uji, Kyoto 611-0011, Japan*

²*Japan Science and Technology Agency, PRESTO, 4-1-8 Honcho Kawaguchi, Saitama 332-0012, Japan*

Dimensionality is one of the important factors to understand the optical properties of materials. The temperature dependence of photoluminescence (PL) intensity in single-walled carbon nanotubes (SWNTs) has been explained by characteristic temperature dependence ($T^{-1/2}$) of one dimensional (1D) excitons radiative decay rate [1]. In hole-doped SWNTs, not only the excitons but also the trions (charged exciton) play important roles to determine optical properties [2]. However, the dimensionality of trions, i.e. localized or delocalized is under discussion. In this study, we measured the temperature dependence of PL spectra of hole-doped SWNTs and discussed the dimensionality of trions and excitons.

The PFO dispersed CoMoCAT sample with efficient *p*-type dopant F₄TCNQ, was used for hole-doped SWNTs [3]. Inset of Fig. 1 shows the PL spectra of hole-doped SWNTs at 5, 150, and 250 K. The trion PL peak around 1 eV almost does not change, while the exciton PL peak around 1.16 eV increases drastically below 100 K. Figure 1 shows the temperature dependence of PL intensity of trions (black filled squares) and excitons (gray open circles). The behavior of temperature dependence of the PL intensity is much different between the excitons and trions. The invariable behavior of trion PL intensity is explained associated with the radiative decay rate of localized (0D) states that is independent of temperature [4]. On the other hand, the increase of exciton PL intensity at low temperature reflects 1D nature. These results strongly indicate the different dimensionality of excitons and trions in the hole-doped SWNTs.

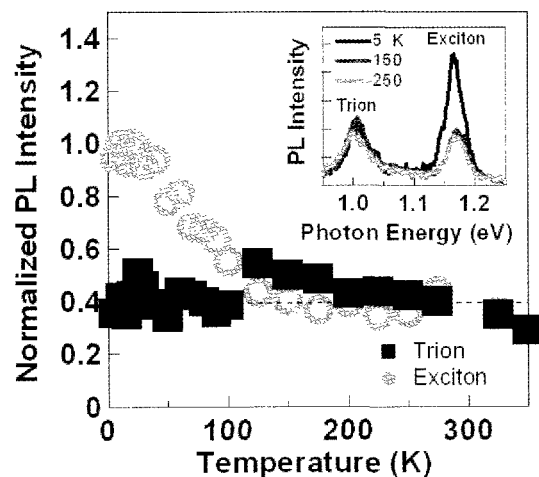


Fig. 1 Temperature dependence of normalized PL intensities of trions and excitons. Inset shows the PL spectra at 5, 150, and 250K.

[1] I. B. Mortimer and R. J. Nicholas, *Phys. Rev. Lett.* **98**, 027404 (2007).

[2] R. Matsunaga, K. Matsuda, and Y. Kanemitsu, *Phys. Rev. Lett.* **106**, 037404. (2011).

[3] S. Mouri and K. Matsuda, *J. Appl. Phys.* **111**, 094309 (2012).

[4] J. Feldmann, G. Peter, E. O. Gobel, P. Dawson, K. Moore, C. Foxon, and R. J. Elliott, *Phys. Rev. Lett.* **59**, 2337 (1987).

Corresponding Author: Shinichiro Mouri

Tel: +81-774-38-3463,

Fax: +81-774-38-3467,

E-mail: iguchan@iae.kyoto-u.ac.jp

Aggregation and agglomeration evaluation of dispersed carbon nanotubes

○Takeshi Eitoku¹, Masayoshi Tange¹, Haruhisa Kato², Toshiya Okazaki¹

¹ Nanotube Research Center, AIST, Tsukuba, Ibaraki 305-8565, Japan

² National Metrology Institute of Japan, AIST, Tsukuba, Ibaraki 305-8565, Japan

The evaluation of aggregation and agglomeration of CNT solution has been one of a serious problem in the CNT community. Currently, direct-imaging techniques such as transmission electron microscopy (TEM), scanning electron microscopy (SEM), and atomic force microscopy (AFM) are most commonly used to characterize the average dimensions of CNT. However, these methods can often suffer from certain disadvantages originated from the conditions of samples, since samples should be dried and fixed on a substrate or grid in the most case of these techniques. The results obtained thus do not necessarily reflect the in situ morphology and state of aggregation of CNT in solution. Moreover, there is a strong possibility of interaction between the sample and the substrate (grid) that can affect aggregation and resolvability. For these reasons, the establishment of bulk evaluation protocols in solution phase by spectroscopy or other techniques is strongly required.

Here we introduced a simple method based on depolarized dynamic light scattering (DDLS) performed at multiple scattering angles to characterize the size and morphology by monitoring the rotational diffusion and the translational diffusion, and compared results with the statistics obtained by TEM image analysis. We examined three types of multiwall carbon nanotube; MWNT made by arc-discharge method, MWNT made by CVD method, and tangled MWNT made by CVD method. It was found that we can easily estimate the shape, aspect ratio, and size of dispersed CNT by DDLS method, and that the results were almost consistent with the TEM image analysis. We also employed laser light scattering (Mie scattering) and Coulter counter techniques. The detailed analysis will be discussed in the symposium.

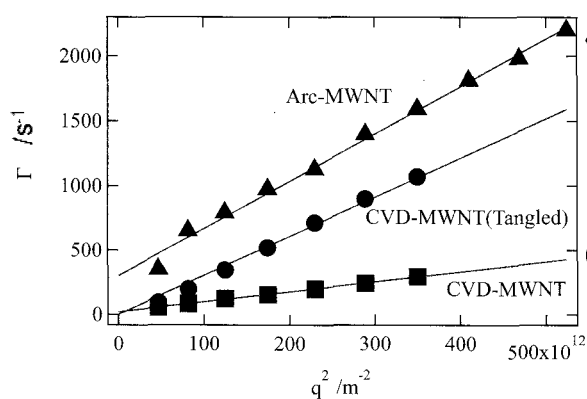


Fig.1. DDLS results of three different type of MWNTs.

Extracted aspect ratio and shape are illustrated (right side).

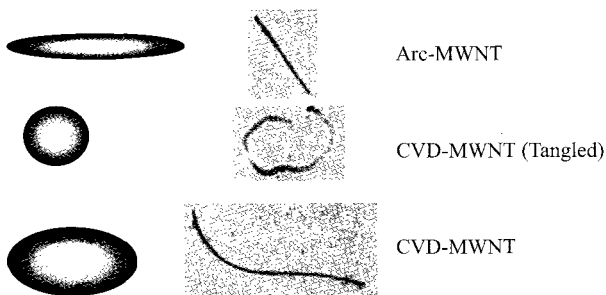


Fig.2. Typical TEM image of

examined three types of MWNTs

Corresponding Author: T. Okazaki

Tel: +81-29-861-4173, Fax: +81-29-861-6241,

E-mail: toshi.okazaki@aist.go.jp

Effects of Water Vapor on RBM of Single-Walled Carbon Nanotubes: Molecular Dynamics Simulation

○N. Homma¹, S. Sato¹, S. Chiashi², Y. Homma¹, and T. Yamamoto³

¹*Dept. of Physics, Tokyo Univ. of Science, Shinjuku, Tokyo 102-0073, Japan*

²*Dept. of Mechanical Engineering, The Univ. of Tokyo, Bunkyo, Tokyo 113-8656, Japan*

³*Dept. of Liberal Arts, Tokyo Univ. of Science, Chiyoda, Tokyo 102-0073, Japan*

Radial breathing mode (RBM) is one of the most important vibrational modes of an SWNT, because it is possible to uniquely assign the chirality to an individual SWNT by determining its frequency ω_{RBM} and intensity, and by comparing with theoretical calculations. It is known that ω_{RBM} does depend on local environment around a tube [1], but the nature of interaction between an SWNT and the environment remains to be elucidated.

In this study, we investigate effects of water vapor on RBM of SWNTs using molecular-dynamics (MD) simulation in the NVT ensemble. Figure 1A shows the simulated RBM of the (a) (13,0) SWNT in vacuum and (b) (13,0) SWNTs wrapped by water molecules. The RBM frequency of the (13,0) SWNT in vacuum was $f=222 \text{ cm}^{-1}$, and it up-shifted by $\Delta f \approx +7 \text{ cm}^{-1}$ in the water vapor. Our MD result is in excellent agreement with the experimental result in Fig.1B. Moreover, we revealed that the blue shift of RBM is caused by forming a condensed state of water on the “hydrophobic” carbon nanotube surface at room temperature. The condensed state consists of lateral hydrogen bonding of water molecules confined in the weak van der Waals potential. Details of the structure and underlying physics of the condensed state of water on an SWNT surface will be discussed in the presentation.

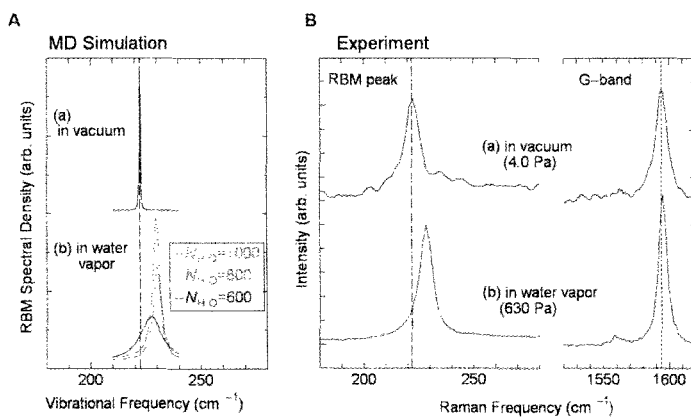


Fig.1 Effects of water vapor on the vibrational properties of SWNTs. (A) Calculated frequency of the RBM based on MD simulation for (13,0) SWNT (with a diameter $d=1.02 \text{ nm}$) in vacuum and water vapor. (B) Experimental Raman scattering spectra (G-band and RBM peak) from (10,5) SWNT ($d=1.05 \text{ nm}$) measured in vacuum (4.0 Pa) and water vapor (630 Pa).

Corresponding Author: Takahiro Yamamoto,
Tel&FAX: +81-3-5213-0990,
E-mail: takahiro@rs.tus.ac.jp

Evaluation of Functionalized Single-Walled Carbon Nanotubes by X-ray Photoelectron Spectroscopy

○Hiroyuki Nii, Syunsuke Noguchi, Ken-ichi Hongyou, and Hamazo Nakagawa

UBE Scientific Analysis Laboratory, Inc., Ube, Yamaguchi 755-8633, Japan

Chemical functionalization of carbon nanotubes (CNTs) has been studied by many researchers to improve their solubility and electrochemical properties. Although X-ray photoelectron spectroscopy (XPS) is one of the suitable tools for quantitative analysis of the surface composition and functional groups, it is difficult to evaluate the functional groups of the CNTs quantitatively because C 1s spectrum of CNTs shows an asymmetric line shape [1]. In this study, we conducted a quantitative evaluation of functionalized single-walled carbon nanotubes (SWNTs) by XPS using a peak fitting procedure.

Figure 1 shows the (a) C 1s and (b) O 1s spectra of a SWNT functionalized with carboxylic acid groups, purchased from sigma-aldrich, together with the results of the curve fitting. A pseudo Voigt function (a sum of a Lorentzian and a Gaussian) was used for the curve fitting, while a C-C peak of a highly oriented pyrolytic graphite (HOPG) was used to reproduce the C-C(CNT) peak because C 1s peak of the HOPG composed of graphene sheets also shows asymmetric line shape. A narrow main peak observed at 284.2 eV is assigned to C-C of the SWNT and the peaks observed at 290.8, 288.6, 286.3, 532.9, and 531.4 eV were assigned to a shake-up satellite, O=C-O, C-O, O-C, and O=C groups, respectively [2]. Results of a quantitative analysis of all elements are reported in Table 1. This indicates that the SWNT functionalized with carboxylic acid groups contains about 4 % of the O=C-O bonds and about 3 % of the C-O bonds. This is in good agreement with the compositions of O.

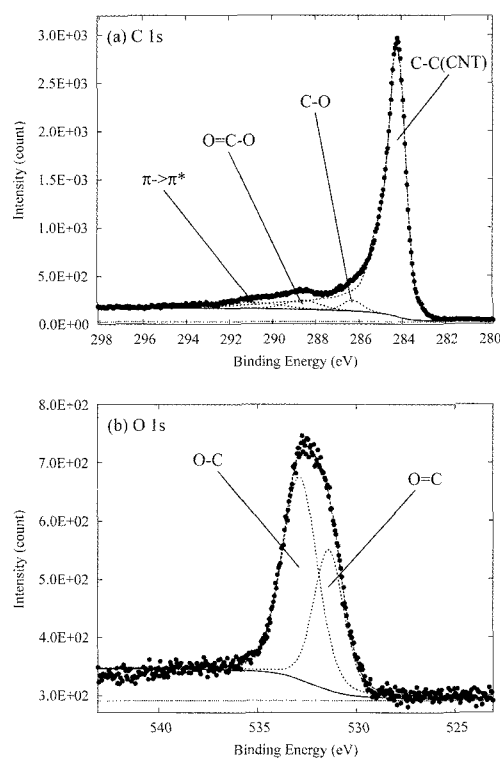


Fig. 1 XPS (a) C 1s and (b) O 1s spectra of the carboxylic acid functionalized SWNT.

Table 1 Atomic percentages (%) of all elements of the functionalized SWNT.

	C				O	
	$\pi \rightarrow \pi^*$	O=C-O	C-O	C-C(CNT)	O-C	O=C
Carboxylic acid		89.5			10.5	
functionalized SWNT	1.5	3.9	2.7	81.4	6.6	3.9

[1] A. Goldoni *et al.*: Appl. Phys. Lett. **80** (2002) 2165.

[2] S. Kundu *et al.*: J. Phys. Chem. C **112** (2008) 16869.

Corresponding Author: Hiroyuki Nii

Tel: +81-836-31-0987, Fax: +81-836-31-0956

E-mail: hiroyuki.nii@ube-ind.co.jp

Tilting of Dirac cones and vernier spectrum in finite-length metallic single-wall carbon nanotubes

○Wataru Izumida, Yuki Tatsumi, Riichiro Saito

Department of Physics, Tohoku University, Sendai, 980-8578, Japan

A metallic single-wall carbon nanotube (M-SWNT) exhibits linear energy bands near the Fermi energy. The linear bands describe left- and right-going massless Dirac particles with the same velocity. Many transport measurements have been interpreted based on the above picture, such as the fourfold shell structure of electrons in the nanotube quantum dot, reflecting the valley degeneracy of the K and K' points in the two-dimensional Brillouin zone as well as the spin degeneracy. It is shown that, with the exception of zigzag nanotubes, the left- and right-going Dirac particles have different velocities due to the curvature of the nanotube [1], which has been overlooked in the last two decades of nanotube research. The asymmetric velocities give an observable vernier spectrum of two different sequences of equal-interval levels in finite-length M-SWNTs, which could give a relevant interpretation for the experiments showing both two- and fourfold shells in a wide energy range.

Energy bands around the Fermi energy for M-SWNTs of $(n,m)=(4,4)$, $(6,6)$, $(7,1)$, and $(9,0)$ near the K and K' points are shown in the figure. The origin of the horizontal axis is shifted for each M-SWNT for comparing several SWNTs. The $(7,1)$ chiral and $(9,0)$ zigzag nanotubes show a finite energy gap because of the curvature. The armchair nanotubes, $(4,4)$ and $(6,6)$, are gapless. It is clear that *linear band tilting* is seen especially for the $(4,4)$ armchair SWNT but not for the $(9,0)$ zigzag SWNT. The linear band tilting is explained by the tilting of the Dirac cones within the effective mass theory.

An effect of the linear band tilting would appear as a vernier-like spectrum in a finite-length M-SWNT quantum dot. A standing wave as a linear combination of a right- (left-) going particle in the K valley and a left- (right-) going particle in the K' valley would be an eigenfunction. The wave number is quantized because of the finite length. Therefore the linear bands are quantized and there are two level separations reflecting the two different velocities [Fig. (c)]. The vernier spectrum is checked by a calculation for a finite-length SWNTs.

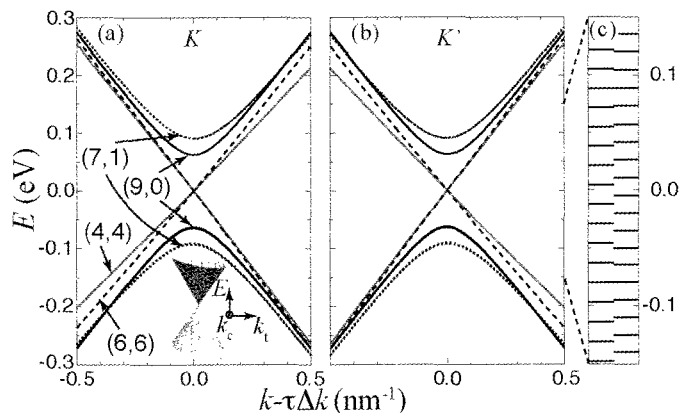


Fig. 1 (a), (b) Energy bands for M-SWNTs around the Fermi energy. Inset in (a) shows tilted Dirac cones near the K point for $(4,4)$ SWNT. (c) Vernier structure of quantized energies with two different level spacings peaks from left and right sides, for $L_{\text{NT}}=100$ nm $(6,6)$ SWNT.

[1] W. Izumida *et al.* Phys. Rev. B **85**, 165430 (2012).

Corresponding Author: W. Izumida

Tel: +81-22-795-6475, Fax: +81-22-795-6447,

E-mail: izumida@cmt.phys.tohoku.ac.jp

Theory of electronic Raman scattering in metallic single wall carbon nanotubes

○ Eddwi H. Hasdeo, Ahmad R.T. Nugraha, Kentaro Sato, and Riichiro Saito
Department of Physics, Tohoku University, Sendai 980-8578, Japan

Inelastic (Raman) scattering of light is a remarkable tool for studying elementary excitations in condensed matter systems. Although a lot of features that appear in the Raman spectra of carbon nanotubes are mostly related to the phonon Raman scattering process, there have been some studies which showed that electronic Raman scattering could also give a significant contribution to the Raman spectra [1]. Recently Farhat *et al.* [2] reported the first observation of the ERS feature in metallic single wall carbon nanotubes (M-SWNT). The ERS feature with a broad shape (100cm^{-1}) is observed at the transition energy M_i (i^{th} van Hove singularity energy of a M-SWNT), which is independent of the incident laser energy and the ERS feature does not observed for semiconductor SWNTs. The low-energy Raman shift indicates that the incident laser light is scattered by excitation of electron-hole pair within the linear energy band, which is confirmed by changing the Fermi energy [2]. However, the electron-hole pair creation in the metallic linear band is optically forbidden due to the vanishing electron-photon matrix element [3]. The electron-hole pair can be excited by electron-phonon interaction which is known as the Kohn anomaly effect [4], but the electron-phonon interaction can be ruled out since the ERS feature has no corresponding phonon mode. Thus, the reasonable candidate to explain ERS is by an energy-momentum transfer between the photo-excited carrier and the electron-hole pair at the linear energy band via the Coulomb interaction. In order to describe the ERS spectra, we calculate the exciton-exciton matrix elements, which describe the transition probability of the excitation of the electron-hole pair creation, using the tight-binding approximation [5]. From this calculation, we found that the first-order ERS process vanished for $q = 0$ momentum though the electron-electron interaction as a function of q becomes the maximum at $q = 0$. We argue that the vanishing exciton-exciton matrix element at $q = 0$ is due to the wave function symmetry. Therefore, we now have to consider second-order process which may contribute to the ERS feature in MSWNTs.

[1] T. P. Devereaux and R. Hackl, *Rev. Mod. Phys.* 79, 175–233 (2007).

[2] H. Farhat *et al.*, *Phys. Rev. Lett.* 107, 157401 (2011).

[3] A. Grüneis *et al.*, *Phys. Rev. B* 67, 165402 (2003).

[4] K. Sasaki *et al.*, *Phys. Rev. B* 78, 235405 (2008).

[5] J. Jiang *et al.*, *Phys. Rev. B* 75, 035407 (2007).

Corresponding Author: E. H. Hasdeo

TEL: +81-22-795-6442, FAX: +81-22-795-6447, E-mail: hasdeo@flex.phys.tohoku.ac.jp

Excitonic effects on coherent phonons in single wall carbon nanotubes

○ Ahmad R.T. Nugraha¹, Gary D. Sanders², Christopher J. Stanton², Riichiro Saito¹

¹*Department of Physics, Tohoku University, Sendai 980-8578, Japan*

²*Department of Physics, University of Florida, Florida 32611-8440, USA*

Ultrashort laser pulse pumped to a single wall carbon nanotube (SWNT) sample can induce photo-excited carriers which appear at the same time in the excited states of the SWNT. Before recombination of the electron-hole pairs, the lattice starts vibrating coherently in the same phase, which is known as coherent phonon spectroscopy. The most easily observed coherent phonon modes in SWNTs are the so-called radial breathing mode, in which the tube diameter and the ribbon width can initially expand or contract depending on their types and excitation energies [1-2]. Previously we have developed a microscopic theory for the generation and detection of coherent phonons in SWNTs within an extended tight binding model and effective mass theory [3-5]. We found that such expansion and contraction simply originate from k -dependent electron-phonon interaction in SWNTs. However, although the coherent phonon theory within electronic picture already described some features of the coherent phonon phenomena in SWNTs, we still neglected the presence of excitons in SWNTs which have a strong binding energy even at room temperature [6]. Due to this fact, the previous work could not explain the coherent phonon spectra lineshape which shows symmetric double peaks at the transition energies [1]. Instead, the calculation shows asymmetric double-peaked spectra [3]. Furthermore, excitonic effects should also give the Gaussian-like driving force in the real space instead of the constant driving force considered previously. Therefore, we modify the coherent phonon equation motion by including the spatial dependence based on a periodic Gaussian structure. The equation of motion now becomes a wave equation with a defined driving force, from which we can solve for the oscillations amplitudes. We then suggest that the generation of coherent phonons in SWNTs is actually due to the coupling of excitons and phonons with all wavevectors along the tube cutting line, not only a single zero phonon wavevector as considered in the previous work [3].

[1] J.-H. Kim et al., Phys. Rev. Lett. **102**, 037402 (2009).

[2] Y.-S. Lim et al., ACS Nano **4**, 3222-3226 (2010).

[3] G. D. Sanders et al., Phys. Rev. B **79**, 205434 (2009).

[4] A. R. T. Nugraha, G. D. Sanders, et al., Phys. Rev. B **84**, 174302 (2011).

[5] G. D. Sanders, A. R. T. Nugraha, R. Saito, C. J. Stanton, Phys. Rev. B **85**, 205401(2012).

[6] J. Jiang et al., Phys. Rev. B **75**, 035405 (2007).

Corresponding Author: A. R. T. Nugraha

TEL: +81-22-795-6442, FAX: +81-22-795-6447, E-mail: nugraha@flex.phys.tohoku.ac.jp

Thermoelectric Power of Metallic and Semiconducting Single-Wall Carbon Nanotube Buckypaper

○Kazuya Honda¹, Yusuke Nakai¹, Kazuhiro Yanagi¹, Yutaka Maniwa^{1,2}

¹*Department of Physics, Graduate School of Science and Engineering,
Tokyo Metropolitan University, Tokyo 192-0397, Japan*

²*JST, CREST, Kawaguchi, 332-0012, Japan*

Thermoelectric power (TEP) is very sensitive to band structure at the Fermi energy and can in principle distinguish a metal or semiconductor. Previous studies on TEP of single-wall carbon nanotubes (SWCNTs) were mainly performed in buckypaper and indicate unusual behavior such as a large value (~ 50 $\mu\text{V}/\text{K}$) at room temperature, metallic temperature dependence, and great influence of oxygen molecules [1][2]. However, these TEP studies have been done on buckypaper with an uncontrolled mixture of metallic and semiconducting SWCNTs. TEP of separately-prepared high-purity metallic and semiconducting SWCNTs thus remains unclear.

Recent progress of separation techniques by using density gradient ultracentrifugation enables us to obtain buckypaper of separated metallic and semiconducting SWCNTs [3][4]. We measured TEP of three sheets of buckypaper with different metallic-semiconducting SWCNT ratios. These samples with an average diameter of ~ 1.4 nm were made by an arc discharge method. We confirmed the good separation between metallic and semiconducting SWCNTs by means of optical absorption as shown in Fig. 1.

We found that TEP of semiconducting SWCNTs is 10 times larger than that of metallic SWCNTs at room temperature. Details on our experimental results as well as discussion on possible origin of the large TEP will be shown.

[1] J. Hone *et al.*, Phys. Rev. Lett. **80**, 1042 (1998).

[2] K. Bradley *et al.*, Phys. Rev. Lett. **85**, 4361 (2000).

[3] M. S. Arnold *et al.*, Nat. Nanotechnol. **1**, 60 (2006).

[4] K. Yanagi *et al.*, Appl. Phys. Express. **1**, 034003 (2008).

Corresponding Author: Yutaka Maniwa

Tel: +81-42-677-2490, E-mail: maniwa@phys.se.tmu.ac.jp

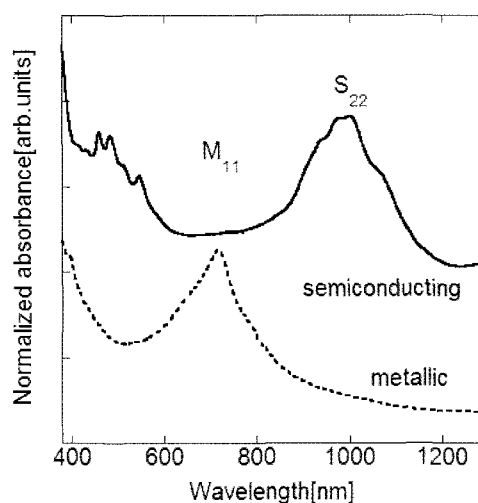


Fig. 1 Optical absorption spectra of measured samples. M_{11} and S_{22} indicate the optical transition of the metallic and semiconducting SWCNTs, respectively.

Electrostatic Potential of Hydrogenated Finite-length Carbon Nanotubes under an Electric Field

○Ayaka Yamanaka, Susumu Okada

Graduate School of Pure and Applied Sciences, University of Tsukuba, Tennodai, Tsukuba 305-8577, Japan

In this decade, carbon nanotubes are attracting much attention due to its possible application for semiconductor electronic devices in the next generation. Therefore it is urging us to unravel fundamental properties of carbon nanotubes under an electric field for designing and fabricating nanotube-based electronic devices. In our previous work, we elucidate that capped carbon nanotubes nonuniformly screen the external electric field. The screening strongly depends on the local atomic arrangement due to the inhomogeneous charge distribution arising from the bond alternation induced by the pentagonal ring at caps of nanotubes. In the present work, we study the electronic structure of finite-length carbon nanotubes with the open ends which are terminated by hydrogen atoms to unravel the effects of the caps of nanotubes.

All calculations are performed by using the density functional theory. To express the exchange correlation potential between interacting electrons, we apply the local density approximation. We use an ultrasoft pseudopotential to describe the interaction between valence electrons and ions. The effective screening medium (ESM) method is applied to investigate behaviors of carbon nanotubes under the electric field in the framework of the first-principles calculations.

We study the electronic properties of hydrogen-terminated finite-length armchair and zigzag nanotubes with 7-angstrom diameter under an electric field of which direction is parallel to the tube axis. We analyze the electrostatic potential on each C atomic site to uncover how the electric field affects on the electronic properties of the carbon nanotubes. Although the pentagonal rings associated with the nanotube-cap are absent, we find that the electrostatic potential also strongly depends on the atomic site as in the case of capped nanotubes (Fig. 1). The fact indicates that the structure-dependent screening against the external electric field is essential for any carbon nanotubes irrespective to their edge morphology. Furthermore, in the zigzag nanotubes, we find that the unusual screening against the external field associated with the peculiar edge localized state.

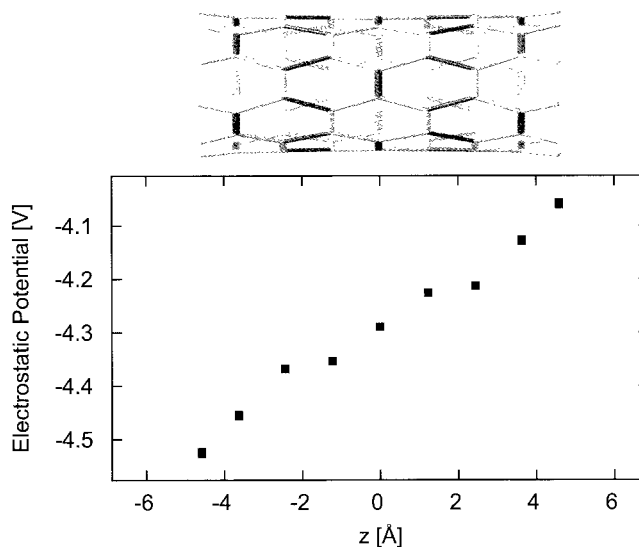


Fig.1 Electrostatic potential in armchair carbon nanotubes.

Corresponding Author: A. Yamanaka

Tel: +81-29-853-5600 (ext. 8233), Fax: +81-29-853-5924,

E-mail: ayamanaka@comas.frsc.tsukuba.ac.jp

Analysis of Operation Mechanisms of SWNT Network Field-Effect Transistors Studied via Scanning Gate Microscopy

○Masahiro Matsunaga¹, Xiaojun Wei¹, Kenji Maeda¹, Tatsuro Yahagi¹, Kazuaki Tanaka¹,
Jonathan P. Bird², Koji Ishibashi³, Yuichi Ochiai¹ and Nobuyuki Aoki¹

¹*Graduate School of Advanced Integration Science, Chiba University
1-33 Yayoi, Inage, Chiba 263-8522, Japan*

²*Department of Electrical Engineering, University at Buffalo, SUNY
Buffalo, New York 14260-1920, USA*

³*Advanced Device Laboratory, RIKEN, 2-1 Hirosawa, Wako, Saitama 351-0198, Japan*

Carbon nanotubes (CNTs) have been regarded as one of the most fascinating materials for scientific researches and industrial applications because of their potential for high-speed electronics due to the high electron velocity in CNTs and for flexible electronics due to their elasticity [1]. Field effect transistors (FETs) whose channel is composed of a network of single wall carbon nanotubes (SWNTs) have also been studied for the practical applications. Scanning gate microscopy (SGM) is one of techniques for local transport characteristics in semiconductor nano-structures and it has also been applied for SWNT FETs [2]. In the SGM, a tip of atomic force microscope (AFM) is used as “a mobile point gate” and a change of the source-drain current is stored as the SGM image [3].

In our study, we have applied the technique for the study of SWNT network FET to determine the mechanism of the FET operation in the channel. Two kinds of SWNTs, synthesized by CoMoCAT[®] process and semiconductor enriched ones by density gradient ultra-centrifuge separation method (DGU), were used in this study. Clear SGM responses are observed at inter-tube junctions in a network of CoMoCAT SWNTs. This would be corresponds to that the Schottky junctions formed with metallic and semiconducting SWNTs in the network and they would play an important role in the FET operation. In case of a network using semiconductor enriched SWNTs by DGU, multiple rings are observed in the SGM images suggesting an existence of discrete energy levels at room temperature. We will discuss on the difference of the operation regimes in these SWNT networks and on a realization of high-performance FETs.

[1] Q. Cao *et al.*, Nature **454** 495 (2008).

[2] D. Bozovic *et al.*, Phys. Rev B **67**, 033407, (2003).

[3] X. Wei *et al.*, Jpn. J. Appl. Phys. **51**.04DN05 (2012).

Corresponding Author: N. Aoki

Tel: +81-43-290-3430, Fax: +81-43-290-3427,

E-mail: n-aoki@faculty.chiba-u.jp

Photoluminescence Excitation Spectroscopy of Carrier-Doped Single-Walled Carbon Nanotubes

○Naoto Akizuki¹, Munechiyo Iwamura¹, Shinichiro Mouri¹, Yuhei Miyauchi^{1,2}, and Kazunari Matsuda¹

¹*Institute of Advanced Energy, Kyoto University, Uji, Kyoto 611-0011, Japan*

²*Japan Science and Technology Agency, PRESTO, 4-1-8 Honcho, Kawaguchi, Saitama 332-0012, Japan*

Carrier-doped single-walled carbon nanotubes (SWNTs) have been of great interest as nearly ideal one-dimensional (1D) electronic systems for the investigation of 1D many body physics and optoelectronics applications including LED and photovoltaic cells. Especially, stable charged excitons called as trions have been recently discovered in hole-doped SWNTs [1]. The application of trions for spin manipulation has been expected because of their non-zero spin and charge. However, the formation mechanism of trions has not been clarified yet. It is therefore important to clarify the mechanism and efficiency of trion formation in hole-doped SWNTs.

Here we studied photoluminescence (PL) excitation (PLE) spectra of hole-doped (7,5) SWNTs probed at the trion PL. SWNTs (CoMoCAT) were dispersed with PFO in toluene. Hole-doped SWNTs were prepared using F₄TCNQ as *p*-type dopant. The inset in Fig. 1 shows PL spectra of pristine and hole-doped SWNTs. The peaks around 1.01eV indicated by arrows have been assigned to trions [1]. Figure 1 compares the PLE spectrum probed at the trion PL with the absorption spectrum. We found that the intensity ratio of the E₂₂ peak to the E₁₁ peak in the PLE spectrum is smaller than that in absorption spectrum, indicating that the quantum yield of the trion PL depends on the excitation energy. Based on these observations, the trion formation mechanism will be discussed.

[1] R. Matsunaga *et al.*, Phys. Rev. Lett. **106**, 037404 (2011).

Corresponding Author: N. Akizuki

Tel: +81-774-38-3465,

E-mail: akizuki.naoto.88x@st.kyoto-u.ac.jp

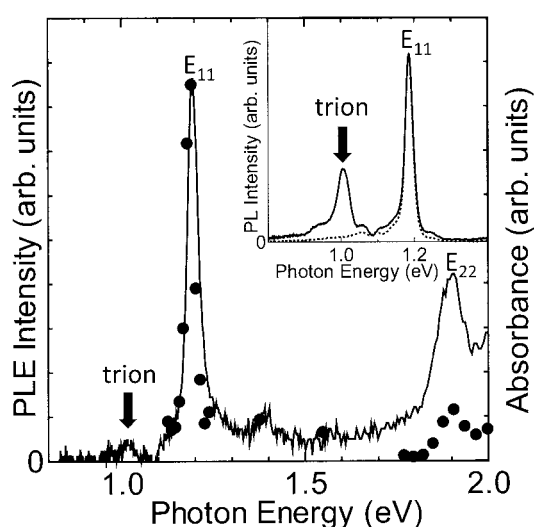


Fig. 1. Normalized absorption (solid curve) and PLE (solid circles) spectra of hole-doped SWNTs. The inset shows normalized PL spectra of pristine (dotted curve) and hole-doped (solid curve) SWNTs.

Coherent AC Transport in Metallic Carbon Nanotubes with Disorder

○Daisuke Hirai¹, Takahiro Yamamoto², Satoshi Watanabe¹

¹Department of Materials Engineering, The University of Tokyo

²Department of Electrical Engineering and Liberal Arts, Tokyo University of Science

Metallic carbon nanotubes (M-CNTs) are potential candidates for interconnects in next-generation ultra-high-frequency electronic devices, owing to their larger allowable current density and higher carrier mobility than those of conventional materials. Recent theoretical research on the AC response exhibited that inductive response become prominent with the CNT length [1]. In order to clarify the influence of defect, we analyzed the AC response of M-CNTs with a single atomic vacancy, and found that capacitive response is induced by electron scattering by the vacancy level [2,3]. However, we have not yet understood the influence of disorder on the AC response, which is known to affect significantly the DC transport properties [4].

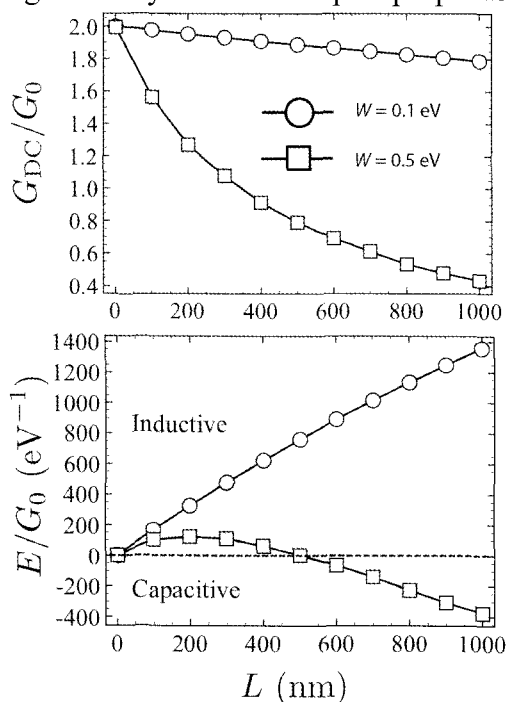


Fig. 1. CNT-length dependence of the DC conductance (upper panel) and emittance (lower panel) of a (10,10) M-CNT. $G_0 = e^2/h$ is the conductance quantum.

In this study, we analyzed influence of disorder on the AC response of M-CNTs. For calculating admittance, we used nonequilibrium Green's function method within the nearest-neighbor π -orbital tight-binding approximation and wide-band limit approximation [1-3]. We focused on sub-THz frequency regime, where the admittance, $Y(\omega)$, can be expanded as $Y(\omega) \simeq G_{DC} + iE\hbar\omega$. Here G_{DC} , E , and ω are the DC conductance, the emittance, and the frequency of AC bias voltage, respectively. In our simulation, the disorder potential is described as $V = \sum_i^{\text{all atoms}} V_i$, $|V_i| \leq W$, where V_i and W are localized potential at i th carbon atom in M-CNT and strength of disorder, respectively. Figure 1 shows CNT-length dependence of the DC conductance and emittance at the Fermi level averaged over 10,000 samples. The DC conductance drastically decreases with CNT length in the case of $W = 0.5$ eV. This is because of Anderson localization, and the estimated localization length is 597 nm. The emittance behavior, on the other hand, changes drastically with the strength of disorder. This phenomenon is

attributed to the competition between the inductive response related to the kinetic inductance [1] and the capacitive response induced by the electron scattering by the potential [2,3].

[1] T. Yamamoto *et al.*, Phys. Rev. B **81**, 115448 (2010).

[2] D. Hirai *et al.*, Appl. Phys. Express, **4**, 075103 (2011).

[3] D. Hirai *et al.*, Jpn. J. Appl. Phys., **51**, 04DN01 (2012).

[4] M. P. Anantram *et al.*, Phys. Rev. B **58**, 4882 (1998).

Corresponding Author: Daisuke Hirai

Tel: +81-3-5841-7136, Fax: +81-3-5841-1286,

E-mail: daisuke.hirai@cello.t.u-tokyo.ac.jp

Electronic States in Flattened Carbon Nanotubes with Effective-Mass Approximation

○ Takeshi Nakanishi¹, and Tsuneya Ando²

¹*Nanosystem Research Institute, AIST, Japan*

²*Department of Physics, Tokyo Institute of Technology, Japan*

Flattened carbon nanotubes are new kinds of quantum wires topologically different from the conventional wires fabricated at semiconductor heterostructures. The flattened carbon nanotubes are distinguished from single wall carbon nanotubes by inter-layer couplings in a collapsed region. The purpose of this study is to show electronic states of the flattened carbon nanotubes with symmetry considerations.

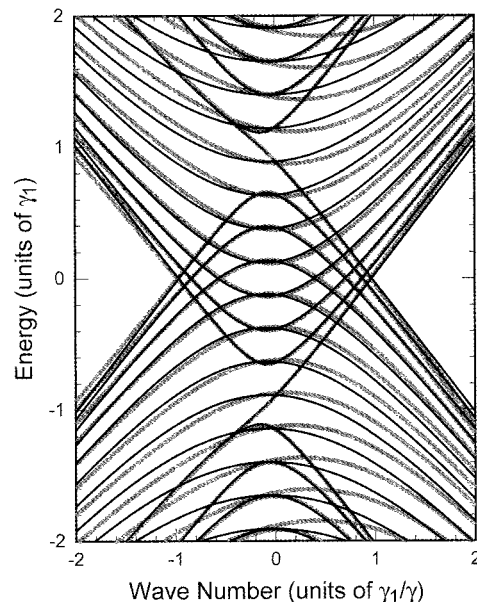
The flattened carbon nanotubes consist of fully collapsed region with layer spacing of 3.3\AA and curved regions. The fully collapsed region is a bilayer graphene, whereas one of the curved regions is a part of a carbon nanotube or a mono-layer graphene. The flattened carbon nanotubes are obtained through such way that inner tubes are extracted from multi-wall carbon nanotubes by vigorous sonication with water containing surfactants. TEM observation of thermally treated graphite show that the zigzag and armchair edges are mostly closed between adjacent graphene layer and the bilayer graphene often exhibits AA stacking.

Both ends of the bilayer graphene is continuously connected to the mono-layer graphenes at straight boundaries with zigzag and armchair atomic structure in a model of the flattened carbon nanotubes. We consider AA and AB stacking in the bilayer graphene. Boundary conditions between the mono-layer and bilayer graphene are derived in an effective-mass scheme. The results show that the envelope function in the lower layer of the bilayer graphene is continuously connected to mono-layer graphene, as expected, but the condition in upper layer sensitively depends on the edge structure and mixes the K and K' valleys at the armchair structure and does not at the zigzag structure.

Double Dirac cones repulse each other due to the inter-layer interaction in the bilayer graphene with AA stacking and are corresponding to bonding and anti-bonding bands. The inversion symmetry of the bilayer graphene with AA stacking holds in the presence of the curved regions of the flattened carbon nanotubes.

Thus, the bonding and anti-bonding bands does not mix in the flattened carbon nanotubes, as shown in Fig. 1. Finite width of the flattened carbon nanotube should possess discrete wave vector corresponding to standing waves typical of a confined quantum particle as the case of graphene ribbons. Edge states are shown by blue lines, and are qualitatively different from that in the graphene ribbons.

Fig. 1: Calculated energy dispersion of AA stacking graphene with zigzag boundary in tight-binding model (red lines) and in effective-mass scheme (black and blue lines).



Optical properties of ultrathin single-wall carbon nanotubes

○Toshiya Nakamura¹, Yasumitsu Miyata¹, Eri Inukai¹, Ryo Kitaura¹,
Hiromichi Kataura^{2,3}, Hisanori Shinohara¹

¹Department of Chemistry, Nagoya University & Institute for Advanced Research,
Nagoya 464-8602, Japan

²Nanosystem Research Institute, AIST, Tsukuba 305-8562, Japan, ³JST-CREST

The curvature of C-C bonds in single-wall carbon nanotubes (SWCNTs) plays an important role in their electronic structure. The recent calculation results based on the density function theory show that the band gaps of ultrathin nanotubes with high curvature tend to possess much narrower values than these based on the zone-folding approximation [1]. However, this prediction has not clarified yet experimentally so far due to the lack of available samples of ultrathin nanotubes. To overcome this issue, we have developed an efficient process to prepare samples containing SWCNTs with diameter around 0.5 nm [2].

Here, we report the spectroscopic characterization of ultrathin SWCNTs by using optical absorption, Raman, photoluminescence (PL) spectroscopy. In the present samples, PL peaks appear at 701 and 723 nm under light excitations at 412 and 539 nm, respectively, as shown in Fig.1. These peaks are unambiguously assigned to the PL of (4, 3) and (5, 3) SWCNTs from the resonance Raman spectra (Fig. 1b) together with the empirical Kataura plot [3]. Resonance Raman spectra also indicate the presence of another ultrathin nanotubes with a chiral index of (7, 2) in the present samples. Interestingly, an emission peak of (7, 2) tubes has never been seen at the predicted energies even under resonance excitation. In the presentation, we will discuss the optical properties of these ultrathin semiconducting SWCNTs.

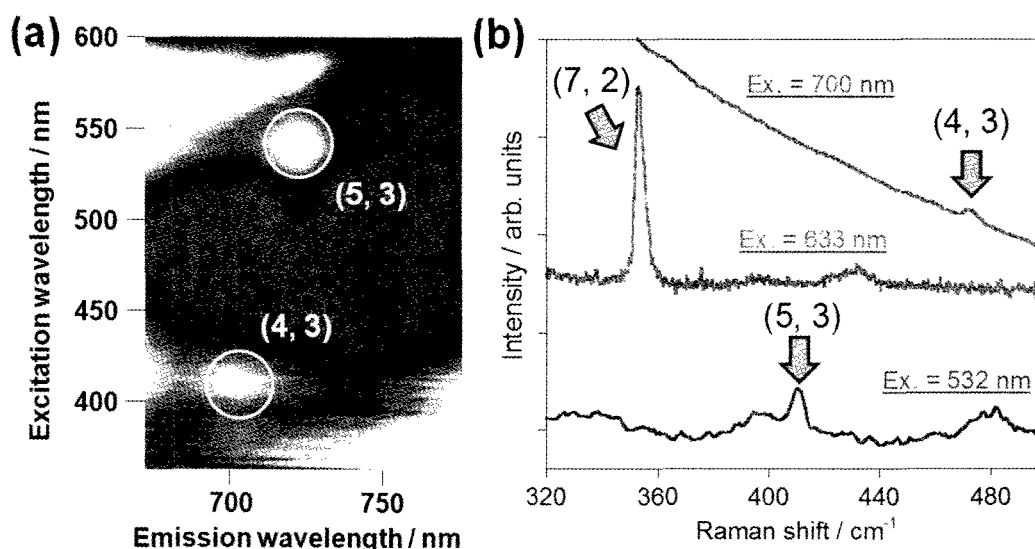


Figure 1. (a) A photoluminescence counter map and (b) resonance Raman spectra at 700 nm, 633 nm and 532 nm excitations of separated samples.

[1] K. Kato and S. Susumu, *Physica E*, 43, 669 (2011).

[2] T. Nakamura *et al.*, *The 42th FNTG General Symposium*.

[3] R. Weisman *et al.*, *Nano Lett.* 3, 1235 (2003).

Corresponding Author: Hisanori Shinohara

TEL: +81-52-789-2482, FAX: +81-52-747-6442, E-mail: noris@nagoya-u.ac.jp

Non-linear and Non-planar Free Thermal Vibration of Single-walled Carbon Nanotubes in Molecular Dynamic Simulation

Heeyuen Koh, James Cannon, Shohei Chiashi, Junichiro Shiomi and Shigeo Maruyama

Department of Mechanical Engineering, The University of Tokyo
7-3-1 Hongo, Bunkyo-ku, Tokyo 113-8656, Japan
Phone: +81-3-5841-6421 E-mail: maruyama@photon.t.u-tokyo.ac.jp

Vibration of suspended and cantilevered carbon nanotubes has been studied for electronic circuits such as transistor, mixer and sensors and in mesoscopic quantum theory. Recently, it is reported that the power spectrum of the free thermal vibration of cantilevered single walled carbon nanotubes (SWNT) can be well expressed by Euler beam and Timoshenko beam theory and the portion of the energy which can be explained by the continuum mechanics among the total thermal energy is about 97 percent [1, 2].

We observed that the cantilever beam motion is non planar and has beating and bifurcation in NVE condition using molecular dynamics (MD) calculation. As the reason of this nonlinear motion, we found constant strain along the tube axis in both armchair and zigzag SWNTs at 50K and 300K. Based on this condition, we can apply the nonlinear continuum beam equation [3] which can consider the mode coupling in different direction. The analytical solutions of this nonlinear equation are integrated using Galerkin method and Krylov-Bogoliubov-Mitropolski (KBM) method. Some similarities of MD calculation and nonlinear continuum theory in Poincare map are found as shown in Fig. 1, and this theory shows having couple of beating frequency around 1st mode cantilever motion is unavoidable.

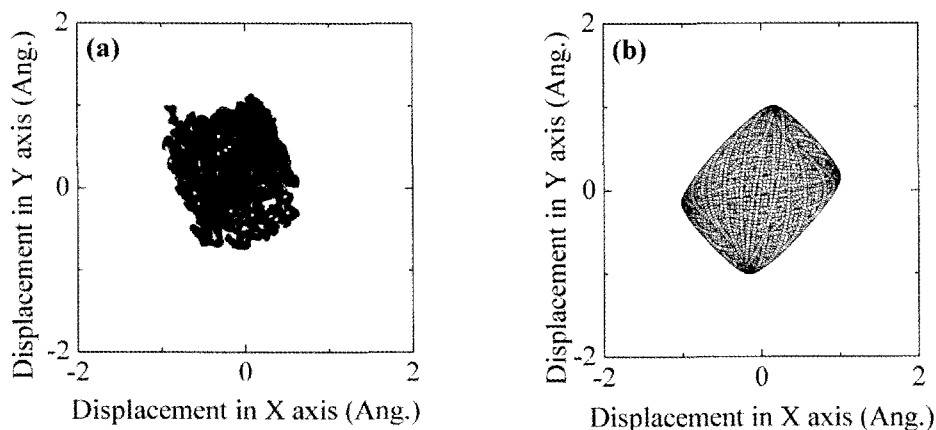


Fig. 1. Poincaré map of the cantilevered 8 nm (5,5) SWNT at 50 K. The trajectory is come from the tip location. (a) MD calculation and (b) Nonlinear Continuum theory.

Reference

- [1] E. H. Feng and R. E. Jones, *Phy. Rev. B*, **81**, 125436 (2010).
- [2] E. H. Feng and R. E. Jones, *Phy. Rev. B*, **83**, 195412 (2011).
- [3] C.-H. Ho, R. A. Scott and J. G. Easley, *Joun. Soun. Vib.*, **47**, 333 (1976).

Corresponding Author: Shigeo Maruyama

TEL: +81-3-5841-6421, FAX: +81-3-5800-6983, E-mail: maruyama@photon.t.u-tokyo.ac.jp

Electrical current behavior at CNT-SiC interface

○Masafumi Inaba¹, Megumi Shibuya¹, Kazuyoshi Oohara¹, Takumi Ochiai¹, Yoshiho Masuda²,
Atsushi Hiraiwa¹, Michiko Kusunoki², Hiroshi Kawarada¹

¹School of Science and Engineering, Waseda University, Tokyo 169-8555, Japan

²Eco Topia Science Institute, Nagoya University, Aichi 464-8603, Japan

1. Contact resistivity of CNT

To apply carbon nanotube (CNT) to electron devices, metallic properties of CNT forest as electrode can be applicable from nano size via structure of Si-ULSI to large metal contact of SiC power device. Densely grown ($\sim 10^{12} \text{ cm}^{-2}$) CNT has been realized by remote plasma CVD (RPCVD CNT)^[1,2]. CNT synthesized with SiC surface decomposition method (CNT on SiC) exhibits the most densely packed CNT forest ($\sim 10^{13} \text{ cm}^{-2}$)^[3,4]. Comparing RPCVD CNT and CNT on SiC using conductive atomic force microscopy (c-AFM), very low contact resistivity of $\sim 5 \times 10^{-9} \Omega \text{ cm}^2$ has been exhibited. Here we report the measurement and evaluation of Au electrode deposited CNT on SiC electric properties.

2. AFM current mapping of CNT forests

CNT on SiC is synthesized on the C-face (000 $\bar{1}$) on-axis n-type 4H-SiC substrate ($\sim 10^{-2} \Omega \text{ cm}$) with SiC surface decomposition method^[3,4]. This CNT is double-wall dominant, densely aligned ($\sim 10^{13} \text{ cm}^{-2}$). Au 100 nm/ Ti 30 nm is sputtered on CNT forest as top electrode. CNT on SiC substrate is fixed using conductive paste (Ag), and current-voltage properties are observed with 2-probe method.

3. Electrical current behavior of CNT-SiC interface

CNT on SiC I-V curve shows rectification at CNT-SiC interface which stems from the Schottky barrier formation. Since SiC has low resistivity, CNT-SiC contact is expected to have a Schottky barrier thin enough to form ohmic contact by tunneling. Fig.1 shows the secondary ion mass spectroscopy (SIMS) result on SiC and CNT surface. During the SiC surface deposition in high temperature annealing, the nitrogen (donor) in SiC decomposition region is piled up and donor in bulk substrate is out diffused to SiC-CNT contact region. From the current-voltage relationship, the current value is $\sim 1 \mu\text{A}$ at 16 mV applied by c-AFM probe ($\sim \Phi 10 \text{ nm}$), while $\sim 6 \mu\text{A}$ by Au electrode deposition ($\sim \Phi 100 \mu\text{m}$). Even though the Au electrode contacting area is $\sim 10^8$ times larger than that of c-AFM, current value is only several times. Generally, lateral conductivity of CNT forest is lower than horizontal conductivity. However, the nearly ideally packed CNT causes the lateral conducting paths. In case of c-AFM (Fig.2), conducting path spreads to the comparable size of Au electrode ($\sim \Phi 100 \mu\text{m}$). Conducting paths of Au electrode deposition (Fig.3) also spreads, yet the spreading ratio is respectively small. CNT-SiC contact resistivity cannot be estimated because the conducting paths are expanded, but c-AFM probe-CNT contact resistivity can be estimated to be $\sim 5 \times 10^{-9} \Omega \text{ cm}^2$ from the size of probe contact area.

1 D.Yokoyama, H.Kawarada *et al.*, APL 47.4 (2008)

2 Y. Yamasaki, Y. Awano *et al.*, APEX 3, 055002 (2010)

3 M. Kusunoki *et al.*, APL 77, 531 (2000)

4 M. Kusunoki *et al.*, APL 87, 103105 (2005)

Corresponding author: M. Inaba

E-mail: inaba-ma@ruri.waseda.jp

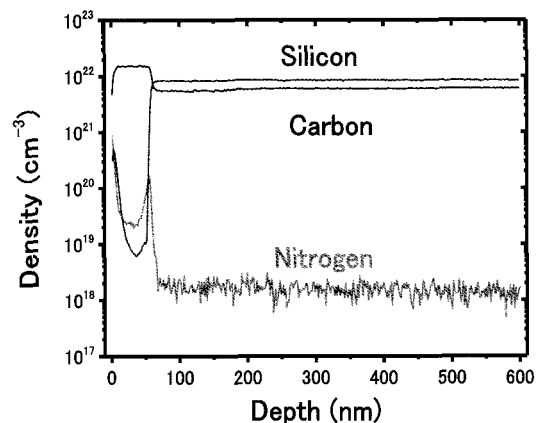


Fig.1 Nitrogen density by SIMS

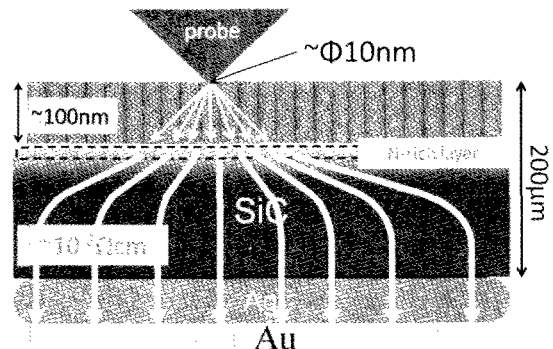


Fig.2 Current paths in case of using c-AFM ($\Phi 10 \text{ nm}$)

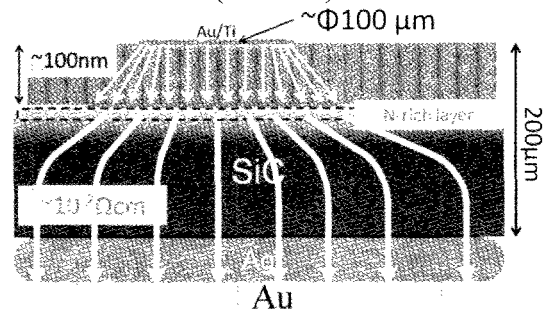


Fig.3 Current paths in case of Au electrode ($\Phi 100 \mu\text{m}$)

Raman Imaging Spectroscopy of Horizontally Aligned Single-Walled Carbon Nanotubes on Crystal Quartz

○ Saifullah Badar, Daisuke Hasegawa, Taiki Inoue, Shohei Chiashi, Shigeo Maruyama

Department of Mechanical Engineering, The University of Tokyo, Tokyo, 113-8656, Japan

Horizontally Aligned Single Walled Carbon-Nanotubes (HASWNTs) hold great promise for future field effect transistors (FET), high frequency transistors and other semiconductor electronic devices. Crystalline quartz substrates with several different surface cuts have been shown to give near perfect horizontal alignment of the nanotubes. This alignment of nanotubes on the substrate is driven by interaction between the nanotubes and quartz crystal lattice [1]. Recent Raman spectrographic studies have shown that the nanotubes grown on these substrates show clear up-shifts in the G-band of the spectra [2]. These up-shifts have been hypothesized to stem from compressive strain along the axis of the nanotubes [3].

In this study, we have used line scanning Raman spectroscopic imaging to study the G-band shifts of HASWNTs. The presence of both kinds of nanotubes, i.e. nanotubes with Raman G-band up-shifts and without up-shifts, were observed to exist simultaneously on the same substrate. Also, the G-band intensity for the unshifted nanotubes was higher than a typical nanotube with G-band up-shifts. The interaction with the substrate affects the intensity of the Raman G-band peaks.

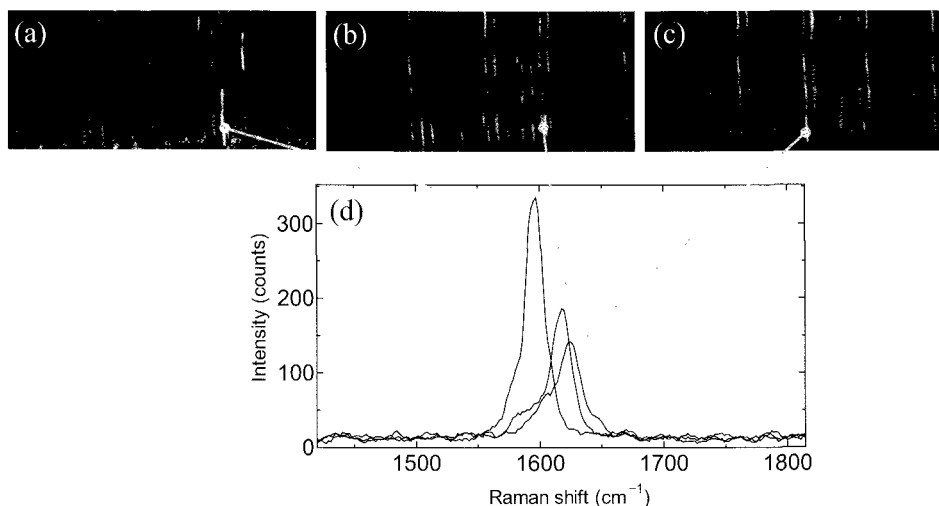


Fig 1: (a), (b) and (c) show the Raman G-band intensity image of the same area for peaks at 1591cm^{-1} , 1613cm^{-1} and 1621cm^{-1} respectively. (d) shows the G-band peak intensity and position for the brightest nanotube.

[1] Xiao J. *et al*, Nano Lett. (2009) 9, 4311.

[2] Ding L. *et al*, Nano Res (2009) 2,903.

[3] Ozel T. *et al*, ACS Nano (2009) 3, 2217.

Corresponding Author: Shigeo Maruyama

Email: maruyama@photon.t.u-tokyo.ac.jp

TEL: +81-3-5841-6421, FAX: +81-3-5800-6983

Fabrication and characterization of individually suspended DWCNTs

○Tomoya Kitagawa¹, Ryo Kitaura¹, Yuhei Miyauchi², Yasumitsu Miyata¹, Kazunari Matsuda²
and Hisanori Shinohara¹

¹*Department of Chemistry & Institute for Advanced Research, Nagoya University, Nagoya 464-8602, Japan*

²*Institute for Chemical Research, Kyoto University, Uji, Kyoto 611-0011, Japan*

The physical properties of carbon nanotubes (CNTs) strongly depend on their structure: chirality, defects and the number of walls. A free-standing individual double-wall carbon nanotube (DWCNT) is an ideal system to investigate how the number of walls, namely the layer-layer interaction, affects the properties of CNTs. In this study, we have focused on fabrication of free-standing individual DWCNTs devices and investigated the correlation between their structure and optical transitions using transmission electron microscopy (TEM) and Rayleigh scattering spectroscopy[1], respectively.

Suspended DWCNTs devices were prepared by using chemical vapor deposition. Briefly, Co and Mo bimetal catalyst nanoparticles were deposited onto pre-fabricated substrate possessing electrodes and a penetrating slit of $\sim 10 \mu\text{m} \times 1.5 \text{mm}$, which was followed by alcohol catalytic chemical vapor deposition (ACCVD) at 1173 K using ethanol as a carbon source. Figures 1 and 2 show a TEM image and corresponding electron diffraction pattern of a suspended DWCNT bridged between electrodes. The TEM image clearly shows that the suspended CNT is surely a DWCNT, which is consistent with the observed electron diffraction pattern. Based on the electron diffraction pattern, we have determined that the DWCNTs have chiral indices of (41,1)/(25,12) or (42,1)/(25,13). Figure 3 shows a Rayleigh scattering spectrum of a suspended DWCNT showing several peaks arising from optical transitions between the van-Hove singularities of each layer. In the presentation, details of the device preparation and further analyses of diffraction pattern and Rayleigh spectrum will be discussed.



Fig. 1 TEM image of a suspended DWCNT.

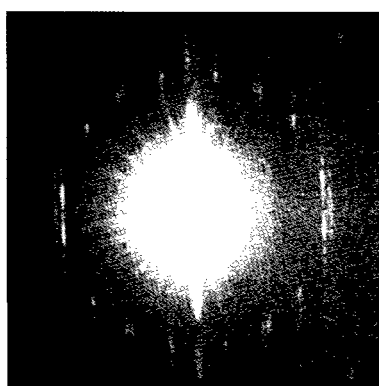


Fig. 2 Electron diffraction pattern of a suspended DWCNT.

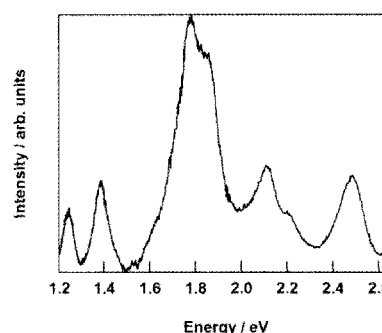


Fig. 3 Rayleigh scattering spectrum of a suspended DWCNT.

[1] M. Y. Sfeir, *et al.*, *Science* **306**, 1540 (2004).

Corresponding Author: Ryo Kitaura, Hisanori Shinohara

TEL: +81-52-789-2482, **Fax:** +81-52-747-6442, **E-mail:** r.kitaura@nagoya-u.jp, noris@nagoya-u.ac.jp

Crystal structure analysis of MWNT forests

○Hiroshi Furuta^{1,2}, Akimitsu Hatta^{1,2}

¹ *Electronic and Photonic Systems Engineering, Kochi University of Technology,*

² *Institute for Nanotechnology, Kochi University of Technology, Kochi, 782-8502, Japan*

Carbon nanotube (CNT) forests, vertically aligned high-density CNTs grown on substrates, attract researcher's attention because their excellent properties of large surface area, uniformity in length, and also the possibility in mass-scale production in widely spreading CNT application fields. It is known the unique and outstanding functional properties (physical, chemical, electrical, and optical etc.) of carbon nanotubes (CNTs) are directly derived from their unique nano-scale structures, such as (a) high-density field emission current of patterned emitter using a high-density CNT forest, (b) anisotropic electrical conductivity of horizontally placed /grown CNTs on substrates, and (c) anisotropic optical absorption for vertically aligned CNTs grown on substrates. Thus, detailed crystal structure analysis of the CNT forests is quite important and has been desired to improve the functional properties (including physical, chemical, electrical and thermal and so on) of CNT forests.

We reported a novel crystal structure analysis method [1] for the vertically aligned MWNT forests by $2\theta/\phi$ scanning cross-sectional XRD measurements, in which crystal structures (layer number, alignment factor, and d002 interlayer spacing) of the MWNT forests including their statistical composition were obtained. In the report [1], the estimated layer numbers of MWNTs in the MWNT forests were consistent with the distribution of the layer numbers observed by TEM, and the alignment factor derived from the XRD spectra showed good agreements with the cross-sectional SEM images. Analysis of the cross-sectional XRD, SEM and Raman spectroscopy of the MWNT forests of various structures, grown with various conditions, will be discussed in this presentation.

Figure 1 shows $2\theta/\phi$ XRD spectra of the thermal CVD MWNT forests grown at various temperatures. The $2\theta/\phi$ angles of the d(002) peak were reduced with decreasing the growth temperature, which means the increase of d(002) spacing of MWNTs in the forests.

We believe the cross-sectional XRD method, which reveal the statistical information of the crystal structure (layer number, alignment factor, d002 interlayer spacing) of MWNT forests, will be a powerful and convenient tool to improve the functional properties of MWNT forests for the future electrical, mechanical, chemical, optical applications.

[1] H. Furuta et al, "Crystal Structure Analysis of Multiwalled Carbon Nanotube Forests by Newly Developed Cross-Sectional XRD Measurement", *Appl. Phys. Express* 3, 105101 (2010).

Corresponding Author: H. Furuta
Tel: +81-(0)887-57-2211, Fax: +81-(0)887-57-2120,
E-mail: furuta.hiroshi@kochi-tech.ac.jp,
Web site: hiroshifuruta.wordpress.com

This work was supported by Iketani Science and Technology Foundation, Nippon Sheet Glass Foundation for Materials Science and Engineering, and JSPS KAKENHI (No. 24560050), Grant-in-Aid for Scientific Research (C).

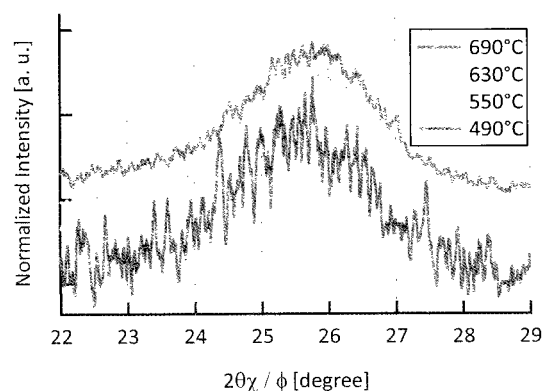


Fig.1. $2\theta/\phi$ XRD spectra of MWNT forests grown at various temperature.

Photovoltaic Properties of Single-Walled Carbon Nanotube/Silicon Heterojunction Solar Cells

○Daichi Kozawa¹, Kazushi Hiraoka², Yuhei Miyauchi^{1,3}, Shinichiro Mouri¹, and Kazunari Matsuda¹

¹*Institute of Advanced Energy, Kyoto University, Uji, Kyoto 611-0011, Japan*

²*Hitachi Zosen Corporation, 2-2-11 Funamachi, Taisho, Osaka 551-0022, Japan*

³*Japan Science and Technology Agency, PRESTO, 4-1-8 Honcho Kawaguchi, Saitama 332-0012, Japan*

Carbon nanotubes have attracted a great deal of interest for photovoltaic applications due to their excellent physical and electronic properties, including a band gap that is widely tunable by controlling the tube diameter and high carrier mobility along their one-dimensional axis [1-3]. Recently, the heterostructures of carbon nanotubes and Si have been extensively studied to realize highly efficient photovoltaic cells. However, the roles of the single-walled carbon nanotube (SWNT) network and Si layer in the photovoltaic processes are not well understood. Thus, the photovoltaic properties of SWNT/*n*-Si solar cells should be understood in detail to improve their conversion efficiency. We report the photovoltaic properties of SWNT/*n*-Si heterojunction solar cells [4].

Figure 1 shows the photovoltaic conversion efficiency η of SWNT/*n*-Si solar cells as a function of transmittance T of the SWNT network film at 550 nm wavelength. The inset shows current density–voltage (J – V) characteristics of a typical SWNT/*n*-Si cell under light illumination. The photovoltaic conversion efficiency strongly depends on the thickness of the SWNT network and shows a maximum value of 2.4% at the optimized thickness of $T \sim 60\%$. The mechanism of photovoltaic conversion based on the results from the incident photon to charge carrier efficiency spectra and detailed analysis of current–voltage curves using the equivalent circuit model will be discussed in the presentation.

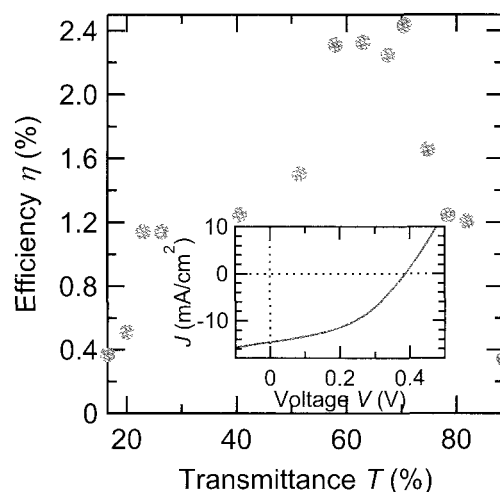


Fig.1 Photovoltaic conversion efficiency as a function of transmittance T . The inset shows current density–voltage (J – V) characteristics of a typical SWNT/*n*-Si cell under light illumination.

[1] Z. Li *et al.*, *ACS Nano* **3**, 1407 (2009).

[2] L. Pang *et al.*, *Nanotechnology* **21**, 105203 (2010).

[3] J. Yi *et al.*, *Nano Lett.*, **11**, 1901 (2011).

[4] D. Kozawa *et al.*, *Appl. Phys. Exp.* **5**, 042304 (2012).

Corresponding Author: D. Kozawa

Tel: +81-774-38-3465, Fax: +81-774-38-3467,

E-mail: d-kozawa@iae.kyoto-u.ac.jp

Micro-fabrication of stretchable and robust interconnects of conductive CNT rubbers on a stretchable substrate

○Atsuko Sekiguchi¹, Takeo Yamada^{1,2}, Kazufumi Kobashi¹, Motoo Yumura¹ and Kenji Hata^{1,3}

¹ Nanotube Research Center, National Institute of Advanced Industrial Science and Technology (AIST), Tsukuba, 305-8565, Japan

² Research Planning Office for Nanotechnology, Materials and Manufacturing National Institute of Advanced Industrial Science & Technology (AIST), Tsukuba, 305-8565, Japan

³ Japan Science and Technology Agency (JST), Kawaguchi, Japan

Stretchable and robust conductors are key and inevitable elements in the development of wearable and ambient electronics, which have many potential applications in biological devices, robotic skins, wearable displays and power-generating systems. The conductive rubber composed of single walled carbon nanotube (SWNT) and fluorinated copolymer is one of the promising materials as elastic conductor for these applications with its mechanical stretchability and robustness.

In this study we succeeded in the micro-fabrication of the conductive CNT rubber on the polydimethylsiloxane (PDMS) substrate by combining lithography technique and transfer process. This process is advantageous to implement the conductive CNT rubber interconnects into the integrated circuits containing the transistors, capacitors and/or sensors of nano-materials and organic materials.

We deposited thin and flat film of conductive CNT rubber on Si substrate with thickness of approximately 15 μm by spray coating of buckey gel. In the film, SWNT shows the configuration like trunks of a tree enabling simultaneous realization of a rubber-like mechanical properties and electrical conductivity. To achieve the surface flatness enough for conformal resist coating, the film is hot-pressed by mirror-like finishing plate. Then, micro-patterning process is carried out on the SiO_2/Si substrate to prevent the process damage to a rubber substrate. The conductive CNT rubber is patterned by reactive ion etching with oxygen plasma. Finally the patterned conductive CNT rubber is transferred to a rubber substrate, in which PDMS is spin-coated on the patterned structure followed by immersion in KOH aqueous solution to dissolve SiO_2 and Si substrate.

The fabrication process established here could be a key technology to realize the physically adaptable and durable integrated circuits with the conductive CNT rubber as interconnects.

Corresponding Author: K. Hata

Tel: +81-29-861-4654, Fax: +81-29-861-4851,

E-mail: kenji-hata@aist.go.jp

Optimizing dispersion structure of SWNT for high electrically-conductive rubber composites

○Howon Yoon¹, Motoi Yamashita¹, Seisuke Ata¹, Motoo Yumura^{1,2}, Kenji Hata^{1,2*}

¹ *Technology Research Association for Single Wall Carbon Nanotubes (TASC), Tsukuba, Ibaraki, 305-8565, Japan*

² *Nanotube Research Center, National Institute of Advanced Industrial Science and Technology (AIST), Tsukuba, Ibaraki, 305-8565, Japan*

Carbon nanotubes (CNTs) have a wide range of potential applications in many industrial areas due to their outstanding electrical and mechanical properties. Ever-increasing interest in applying CNTs in many different fields has led to continued efforts to develop dispersion technique. To employ CNTs as effective reinforcement in composites, proper dispersion has to be guaranteed. However, single-walled carbon nanotubes (SWNTs) are supplied in the form of heavily entangled bundles, resulting in inherent difficulties in dispersion.

This research investigates that the effects of various dispersion methods such as high shear flow, ultrasonication and milling, on morphology of SWNTs and their interactions in the fluid phase. Furthermore, it is demonstrated that the relation between SWNT dispersion and the electrical property of SWNT/rubber composites.

The dispersibility and bundle exfoliation of SWNTs have been quantitatively evaluated using Raman spectroscopy, laser diffraction and zeta-potential measurement. It was found that the dispersion state of SWNTs for higher electrical property of rubber composites containing 10 wt% SWNTs is dependent on decreasing the particle size of SWNTs and increasing G/D ratio and the value of zeta-potential (Fig.1). Especially, the dispersion by High-pressure jet-mill and Nanomizer shows the enhanced electrical conductivity compared to other dispersion methods. The results indicate that these two techniques are effective to minimize the shortening of SWNTs and form debundled mesh structure, leading to higher electrical conductivity.

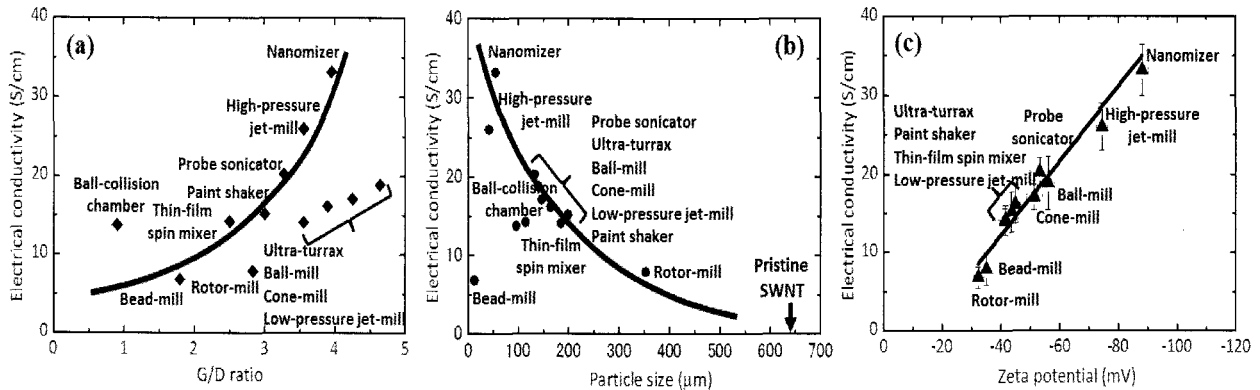


Fig.1 Characterization of SWNT dispersion structure in liquid state by (a) Raman spectroscopy, (b) Laser diffraction and (c) Zeta-potential.

Corresponding Author: K. Hata

Tel: +81-29-861-4654, Fax: +81-29-861-4851,

E-mail: kenji-hata@aist.go.jp

Super-Growth SWNT/rubber composite with extruder for commercial applications

○Seisuke Ata¹, Takaaki Mizuno¹, Howon Yoon¹, Motoo Yumura², Kenji Hata²

¹Technology Research Association for Single Wall Carbon Nanotubes (TASC), 1-1-1 Higashi, Tsukuba, Ibaraki 305-8565, Japan

²Nanotube Research Center, National Institute of Advanced Industrial Science and Technology (AIST), Japan

Electrically conductive elastomers or rubbers have a variety of applications such as electro-magnetic shielding, vacuum sealing and in flexible electronic devices. Previously, we reported high performance conductive rubber with long and high aspect ratio single wall carbon nanotubes, synthesized by water-assisted chemical vapor deposition, denoted as “supergrowth” (SG-SWNT).

In spite of several advantages of such SG-SWNT conductive rubber, its industrial mass production was an important issue to be solved. While the technological challenges for SG-SWNT mass production has been addressed through a pilot plant (production capacity of 100g/h), a similar process for SG-SWNT/rubber (resin) composites needed to be established. Here, we demonstrate such a scalable process for mass production of conductive SG-SWNT /rubber (resin) composites, with a specially designed extrusion set-up.

Matrices such as rubber and resin are kneaded with SG-SWNT, insider the extrusion set-up, followed by their molding into desired shapes. Versatility of this process allowed for forms ranging from sheets to tapes and blocks to be fabricated with the SG-SWNT/rubber (resin) composite. Further, the shape-formability is limited only by the shape of the mould. To achieve this, the rotation blades of the extruder were custom-designed to avoid scission and damage of long, high aspect ratio SG-SWNT. Further, molding conditions such as blade rotation speed (rpm), temperature and duration were optimized for each matrix (fluorinated rubber and polyurethane rubber).

The resulting SG-SWNT/rubber composites showed identical electrical conductivity and elasticity compared to its smaller counterparts made by wet, laboratory-scale processes. Thus, easy scalability is established without loss of functionality. In addition, the conductivities of SG-SWNT/fluorinated rubber are 100-times higher than similar composites made with other conductive fillers (carbon-black, multi-wall carbon nanotubes and single-wall carbon nanotubes). Thus, we are able to retain the advantage of SG-SWNTs and establish a mass production protocol for SG-SWNT rubber composites.

Corresponding Author: K. Hata

Tel: +81-22-861-4654, Fax: +81-22-861-4851,

E-mail: kenji-hata@aist.go.jp



Fig.1 SG-SWNT/fluorinated rubber sheet with extruder.(200um×60mm×12m)

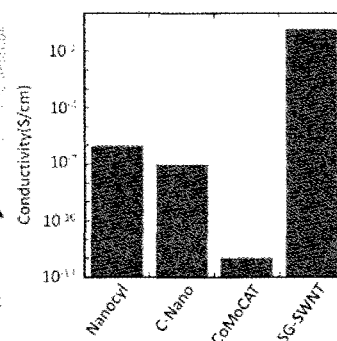


Fig. 2 Conductivity of various kinds of CNT and fluorinated rubber composites with extruder.

Ion-Gel Transistors on Thick Films in a Single Chiral State of (6,5) Single-Wall Carbon Nanotubes

○Kudo Hikaru¹, Yuki Nobusa², Hiromichi Kataura³, Taishi Takenobu², Kazuhiro Yanagi¹

Tokyo Metropolitan Univ.¹, Waseda Univ.², AIST/CREST³

Recent progress of separation techniques enables us to get metallic, semiconducting or single chiral SWCNTs [1]. Semiconducting SWCNTs have better heat durability and chemical stability than organic materials, and flexibility than inorganic materials. Therefore it is of great importance to investigate semiconducting characteristic of SWCNTs for development of a next-generation flexible electronics devices. Transistor performance of SWCNTs is significantly influenced by the morphology of the SWCNTs network. Thus, it was difficult to find out the intrinsic semiconducting property caused by the electronic structure of SWCNTs.

In recent years, however, by using ion gel as gate dielectrics, a carrier control of all the SWCNTs that served as the channel was achieved. As a result, it is known that the FET characteristic reflecting the density of states of SWCNTs tend to appear. In the previous research, the mixed chiral state of semiconducting SWCNTs was used. In this research, in order to investigate relationships between intrinsic characteristic and FET performance, we used a thick film of high purity (6,5) single chiral SWCNTs which were obtained by gel separation and density gradient ultracentrifugation.

CoMoCAT SG65 SWCNTs were used as a starting material. We separated the (6,5) chiral by combination of gel chromatography and density gradient ultracentrifugation. We formed a thick film of (6,5) SWCNTs (the thickness was approximately 600nm) as a channel. After that, an ion gel was put on it as gate dielectrics. Then we measured its FET characteristics.

Figure1 shows the transfer characteristics of the FET. The on/off current ratios were good, approximately 10^4 . The highest carrier mobility was $46 \text{ cm}^2\text{V}^{-1}\text{s}^{-1}$.

[1] H. Liu et al., *Nature Commun.* **2**, 309 (2011), M. Kawai et al., *J. Am. Chem. Soc.* **134**, 9545 (2012).

Corresponding Author: K. Yanagi
Tel: +81-42-677-2494,
Fax: +81-42-677-2483,
E-mail: yanagi-kazuhiro@tmu.ac.jp

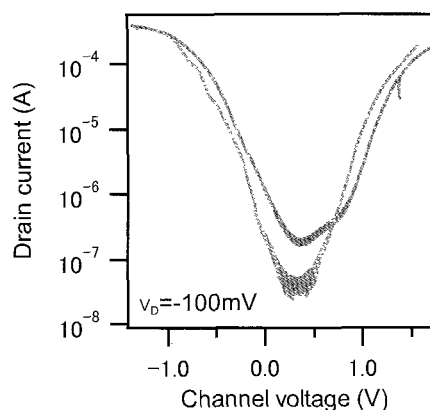


Fig1. Transfer characteristics of (6,5) SWCNT-ion gel transistor.

Synthesis and Electrical Conductivity of Polymer/CNT Composite Using the Reaction Injection Molding (RIM) Method

○Hoang The Ban, Masahiro Shigeta, Mitsugu Uejima

Technology Research Association for Single Wall Carbon Nanotubes (TASC)

Higashi 1-1-1, Tsukuba, Ibaraki, 305-8562, Japan

Polymer/CNT composite combines the advanced mechanical property of polymer and the outstanding electrical and thermal conductivities of the carbon nanotubes (CNT). The fabrication of polymer/CNT composites has been carried out via three processes, i.e., dry, wet, and *in situ* polymerization. Because of the fact that all these processes have their strong and weak points, it is necessary to develop new processes for the mass production of highly functional and low cost polymer/CNT composite materials.

We have recently reported that the electrical conductivity of the polymer/CNT composite could be remarkably improved through the enhancement of the π - π stacking interaction between CNT surfaces and the conjugated C-C double bonds located in the main chains of the cyclic olefin polymer synthesized from the *in situ* ring opening metathesis polymerization in the organic solution.¹ On the other hand, we have also found that the CNT percolation network in the polymer/CNT composite might be controlled via adjusting the size and shape of the polymer composite particles synthesized from the *in situ* emulsion polymerization in the aqueous solution.² Although the presence of solvents in the fabrication of polymer/CNT composites effectively improved the homogeneous dispersion of CNT into the polymer matrixes, it is a costly and energy consumed process. This work thus reports our recent results on the development of a very simple and efficient process for the fabrication of the polymer/CNT composite based on the reaction injection molding (RIM) method wherein the costly solvent removal process was absolutely omitted.

A typical fabrication process of the polymer/CNT composite using RIM method is shown in Fig.1. CNT used in this work is the supergrowth CNT (SGCNT), and polymer is the cyclic olefin polymer (COP). The significant difference between the RIM and the other fabricating methods is that SGCNT is directly dispersed into a highly reactive cyclic olefin monomer liquid instead of a polymer matrix. As soon as the monomer/CNT liquid and catalyst are mixed and injected into the mold cavity at elevated temperatures, a polymerization chemical reaction will occur to form a completed polymer/CNT composite product which was then directly collected from the mold without any further treatments.

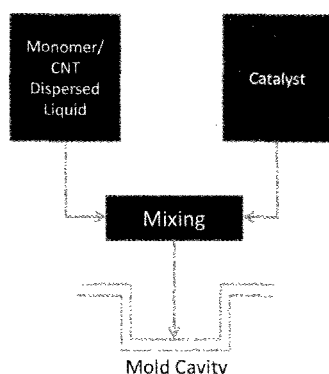


Fig.1: RIM fabrication process of polymer/CNT composite

In order to improve the homogeneous dispersion of CNT into the monomer liquid, we have developed effectively assisted dispersed agents. In fact, adding a small amount of the assisted dispersed agent into the monomer/CNT liquid dramatically increased its homogeneity. Accordingly, the electrical conductivity of the RIM-based COP/CNT composite sample was found extremely high up to $\sim 10^{-3}$ S/cm even at very low CNT contents (< 0.1 wt%).

¹H.T.Ban; T.Nagamune; M.Shigeta; M.Uejima, *Polymer Preprints*, Japan, Vol.61, No.1, 1225, 2012.

²H.T.Ban; T.Nagamune; M.Shigeta; M.Uejima, *The 42nd Fullerenes-nanotubes-Graphene General Symp.*, p.155, 2012.

Corresponding Author: Hoang The Ban

Tel: 080-2346-1028, E-mail: hoang@tasc-nt.or.jp

Fabrication of biotin-labeled double-walled carbon nanotubes for a specific biosensor

Yuka Nagaya, Akihiro Kuno, Koji Tsuchiya, and Hirofumi Yajima

Department of Applied Chemistry, Faculty of Science, Tokyo University of Science
1-3 Kagurazaka, Shinjuku-ku, Tokyo 162-8601, Japan

Double-walled carbon nanotubes (DWNTs) have attracted a great deal of attention in their specific optical properties and possible technological applications in various fields because of the possession of advantageous features of both single-walled carbon nanotubes (SWNTs) and multi-walled carbon nanotubes (MWNTs), such as electrical properties and thermal and mechanical stabilities. Recently we reported the fabrication of a novel field effect transistor (FET) type biosensor with a high sensitivity using DWNTs, the outer wall of which was modified by chemical oxidation. The FET-type biosensor using DWNT achieved the ultrasensitive detection for 250aM bovine serum albumin (BSA) solution, in spite of the unspecific substrate. In order to gain ultrasensitive biosensor for “specific” substrate, the present study aims to produce biotin-labeled DWNTs, which are allowed to specifically react with avidin.

DWNTs were oxidized by mixture of sulfuric acid and nitric acid (3:1) to create carboxyl groups on their surface. The oxidized DWNTs are then allowed to react with 5-(biotinamido)pentylamine through amine coupling using 1-ethyl-3-(3-dimethylaminopropyl) carbodiimide hydrochloride (EDC) and sulfo-NHS.

The obtained DWNTs were measured by Fourier transform infrared spectroscopy (FTIR) to structure of the DWNTs, examined the reactivity with avidin by isothermal titration calorimetry (ITC). This study suggested the possibility of producing an ultrasensitive biosensor for specific substrate using biotin-labeled DWNTs.

*Corresponding Author: Hirofumi Yajima

Tel: +81-3-3260-4272(ext.5760), Fax: +81-3-5261-4631,

E-mail: yajima@rs.kagu.tus.ac.jp

Labeling of mannose to acid-treated double-walled carbon nanotubes for a sensitive and specific biosensor

○Shuhei Takesue, Akihiro Kuno, Koji Tsuchiya, and Hirofumi Yajima*

*Department of Applied Chemistry, Faculty of Science, Tokyo University of Science
1-3 Kagurazaka, Shinjuku-ku, Tokyo 162-8601, Japan*

Double-walled carbon nanotubes (DWNTs) are expected to apply ultrasensitive biosensors based on field-effect transistors (FETs) because of their superior electrical properties. In the present study, for specific FET-type biosensors, we prepared the mannose-labeled DWNTs through an EDC/NHS amine coupling method.

The preparation process consists of the following two steps. (1) DWNTs were oxidized by mixture of sulfuric acid and nitric acid (3:1 ratio) to create carboxyl acid groups on their surfaces. (2) The modified carboxyl acid groups were activated by 1-ethyl-3-(3-dimethyl aminopropyl)-carbodiimide hydrochloride and *N*-hydroxysuccinimide (NHS) to form NHS ester, which is allowed to react with the amine group of *p*-aminophenyl mannose.

The functional groups on the DWNT surface were characterized by Fourier transform infrared absorption (FTIR) spectroscopy. Figure 1 shows the FTIR spectra of *p*-aminophenyl mannose and mannose-labeled DWNT. Fig.1 confirms that the amine group of *p*-aminophenyl mannose and the carboxyl group of DWNTs were coupled to form an amide bond. Now we are trying to detect the amount of concanavalin A specifically bonded with the mannose groups of DWNTs.

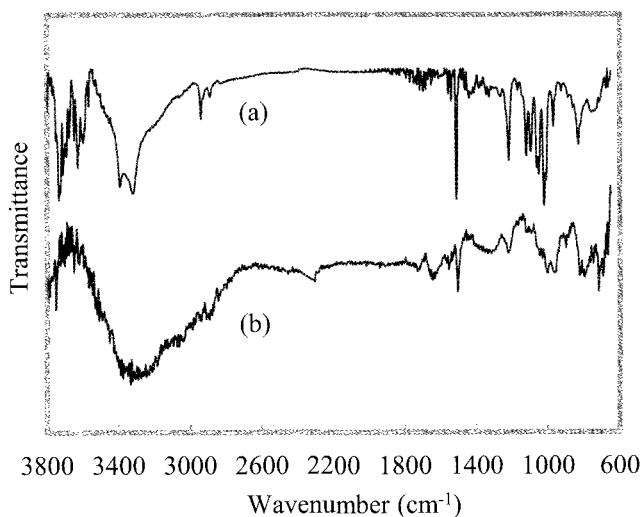


Fig.1 FTIR spectra of (a) aminophenyl mannose and (b) mannose-labeled DWNT.

*Corresponding Author: Hirofumi Yajima

Tel: +81-3-3260-4272(ext.5760), Fax: +81-3-5261-4631,

E-mail: yajima@rs.kagu.tus.ac.jp

Formation of homogeneous and high density thin-film of single-wall carbon nanotube by dip coating

○Maki Shimizu^{1,2}, Shunjiro Fujii^{1,2}, Takeshi Tanaka¹, Hiromichi Kataura^{1,2}

¹ *Nanosystem Research Institute, National Institute of Advanced Industrial Science and Technology (AIST), Tsukuba, Ibaraki 305-8562, Japan*

² *JST, CREST, Kawaguchi, Saitama, 332-0012, Japan*

Single-wall carbon nanotubes (SWCNTs) have great potential to fabricate thin and highly transparent 2D material. Especially, the semiconducting SWCNTs (s-SWCNTs) can be applied to thin film transistors (TFTs). However, their commercial use has not been realized yet because of the difficulties in controlled, reproducible assembly of SWCNT thin films. We reported the preparation of s-SWCNT thin films for TFTs by drop coating method [1]. However, it was difficult to control the concentrations of surfactant and SWCNTs because the method includes evaporation process, resulting not only poor reproducibility of SWCNT density but also high inhomogeneity due to coffee stain effect. In this study, we fabricated thin films by dip coating which does not include evaporation process. This method enabled us to control the concentration of SWCNT and surfactant. We investigated the concentration dependence to know the optimum condition to get the high density individual SWCNT network that suits for high performance TFTs.

We prepared twelve kinds of solutions comprising different combinations of the concentrations of SWCNT (0.1, 0.2, 0.4 mg/ml) and sodium deoxycholate (0.1, 0.25, 0.5, 1 wt%). The 3-aminopropyltriethoxysilane functionalized SiO₂/Si substrates were dipped in these solutions for one day. Then the substrates were immersed in water to remove the remaining surfactant.

Figure 1 shows the atomic force microscopy images of the thin films. The density of SWCNTs was greatly influenced by the concentrations of the SWCNTs and surfactant. The high density thin films were obtained when the surfactant concentration was low and the SWCNT concentration was high. When the SWCNT density was too high, however, the thick bundles were observed. In the presentation, transport properties of these thin films and variability of the devices will be discussed.

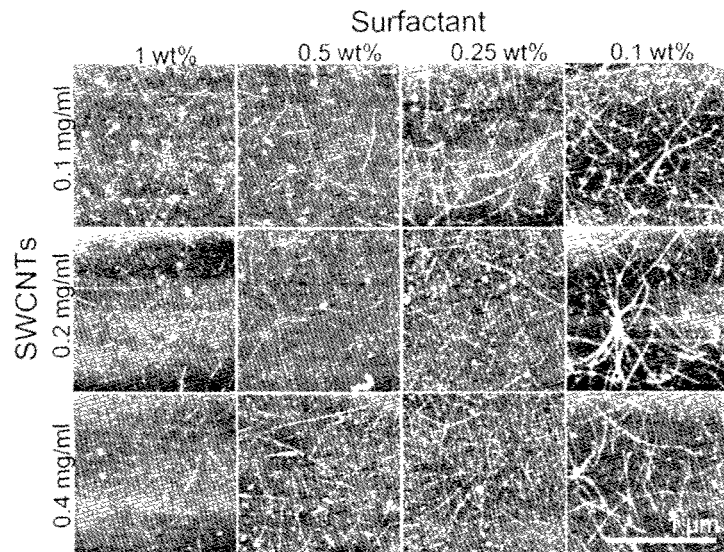


Fig.1 AFM images of the thin films formed from twelve different concentration solutions

[1] S. Fujii *et al.* Phys. Stat. Sol. B 248 (2011) 2692

Corresponding Author:

Hiromichi Kataura

Tel:+81-29-861-2551, Fax: +81-29-861-2786,

E-mail: h-kataura@aist.go.jp

Conduction-Type Control of Carbon Nanotube Field-Effect Transistors by Pd and Ti Overlayer Doping

○Satoshi Ishii^{1,2}, Masato Tamaoki¹, Shigeru Kishimoto^{1,2}, Takashi Mizutani¹

¹ Department of Quantum Engineering, Nagoya University, Nagoya, 464-8603, Japan

² Venture Business Laboratory, Nagoya University, Nagoya, 464-8603, Japan

Carbon nanotube field-effect transistors (CNTFETs) have been expected to be applied for the complementary logic circuit, and therefore both the p- and n-type CNTFETs are required. In order to implement n-channel CNTFETs, the CNTFETs with Al overlayer was reported [1]. This was explained by the doping effect of the Al overlayer. In this study, we propose the conduction-type control of the CNTFETs by charge transfer from metal overlayers with different work functions (Pd ($\phi=5.1$ eV) and Ti ($\phi=4.4$ eV)) deposited onto the side surface of the CNT channel, as shown in Fig. 1.

The graphitic carbon (G-C) contacts were used to study the doping effects (Fig. 1), since the CNTFETs with G-C contacts were confirmed to show ambipolar behaviors [2]. The conduction properties of the devices were measured in the nitrogen-gas filled glove box after baking the fabricated devices in vacuum without exposure to air.

The device without overlayer showed p-dominant ambipolar behavior (Fig. 2(a)), as reported previously [2]. On the other hand, the device with Pd overlayer showed the p-channel behavior (Fig. 2(b)). In contrast, the device with Ti overlayer showed n-channel behavior (Fig. 2(c)).

These results can be explained based on the energy-band diagrams of each device as follows. The energy band of the device without metal overlayer can be drawn as shown in the inset of Fig. 2(a), taking into account the Fermi level of the G-C contacts [2]. On the other hand, in the case of the device with Pd overlayer, the electrons are expected to transfer from the CNTs to the Pd overlayer due to the larger work function of Pd as compared to the CNT ($\phi=4.8$ eV). That is, hole doping in the CNT. This makes the barrier height for electrons higher than that for holes (inset of Fig. 2(b)). In the case of the device with Ti overlayer, the electrons are expected to transfer from the Ti overlayer to the CNTs due to the smaller work function of Ti as compared to the CNT. That is, electron doping in the CNT. This makes the barrier height for holes higher than that for electrons (inset of Fig. 2(c)).

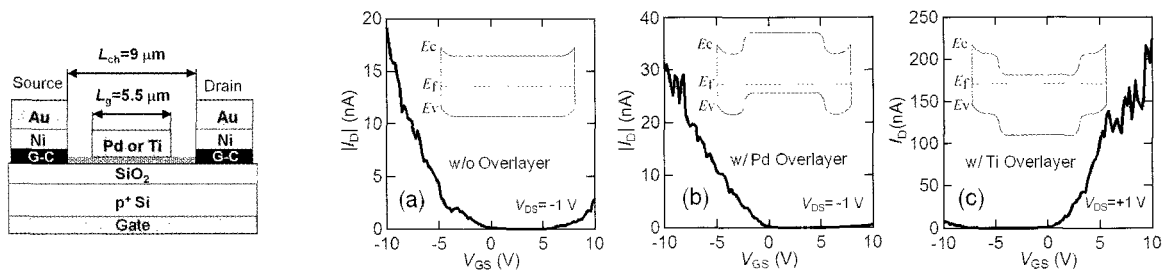


Fig. 1 Schematic of the CNTFET with metal overlayer. Fig.2 I_D - V_{GS} characteristics and schematic energy-band diagrams of the CNTFETs (a) without overlayer, (b) with Pd overlayer, and (c) Ti overlayer.

[1] H. Oh *et al.* Appl. Phys. Lett. **88**, 103503 (2006).

[2] M. Tamaoki *et al.* to be published in Appl. Phys. Lett. (2012).

Corresponding Author: T. Mizutani, E-mail: tmizu@nucc.nagoya-u.ac.jp, Tel: +81-52-789-5230

This work is partially supported by Grant-in-Aid for Young Scientists (B) and Scientific Research on Priority Areas from MEXT

Switchable thermal conductivity enhancement of phase change composites with single walled carbon nanotube inclusions

o Sivasankaran Harish¹, Kei Ishikawa¹, Taiki Inoue¹, Shohei Chiashi¹, Junichiro Shiomi¹,
Shigeo Maruyama¹

¹*Department of Mechanical Engineering, The University of Tokyo, 7-3-1 Hongo, Bunkyo-ku, Tokyo 113-8656, Japan.*

Thermal energy storage using phase change alkanes is often employed in waste heat recovery, solar energy storage etc. However, utilizing this technology for large scale applications is often hindered by the low thermal conductivity of the composite which inhibits the energy storage and release rate. Recently, Zheng et al. [1] demonstrated an efficient technique using graphite suspensions to tune the thermal and electrical conductivity using temperature regulation. In this work, we report the thermal conductivity enhancement of phase change alkanes with single walled carbon nanotube (SWNT) inclusions which has a less increase in the fluid viscosity also performs in a similar manner comparable to that of graphite suspensions. Thermal conductivity measurements in solid and liquid state were carried out using a transient hot wire technique. In the liquid state a nominal increase in thermal conductivity was observed which is in consistent with the predictions of effective medium theory. When the composite was frozen, nearly a two fold increase in thermal conductivity was observed due to the formation of aggregated networks which dramatically increases the heat transport path.

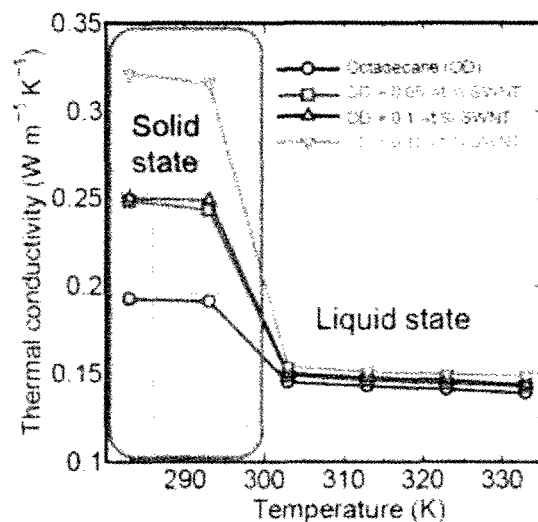
References

[1] R. Zheng et al. Nature Communications, 2, 2011.

Corresponding Author: S. Harish

Tel: +81-80-3279-1605

E-mail: harish@photon.t.u-tokyo.ac.jp



***In-situ* transmission electron microscopy study on electric properties of a junction between a gold nanoparticle and carbon nanotubes**

○Motoyuki Karita, Koji Asaka, Hitoshi Nakahara, and Yahachi Saito

Department of Quantum Engineering, Nagoya University, Furo-cho, Nagoya 464-8603

Carbon nanotubes (CNTs), which have excellent mechanical and electric properties such as high thermal conductivity and high current-carrying capacity, are promising materials as interconnect wires for microelectronic devices. To realize CNT-based devices by utilizing these superior properties, it is highly required to clarify electric properties at junctions between CNTs and metals. In this study, structural changes and electric properties of a CNT-gold nanoparticle (Au NP)-CNT junction were studied during the passage of a current by *in-situ* transmission electron microscopy (TEM).

CNTs were attached to an edge of a Au plate of 50 μm thickness by dielectrophoresis, and then Au was deposited on CNTs. A free end of an Au-deposited CNT was brought into contact with a tip of an Au-coated tungsten needle inside a TEM. By applying an electric current to the CNT, Au NPs on the CNT disappeared and the CNT was cut. An Au NP on the Au plate was picked by using the CNT1 and was attached to the tip of the CNT1 (Fig. 1). Then, the tip of the CNT2 was brought into contact with the Au NP on the CNT1 tip (Fig. 2(a)).

Figure 2 shows a time sequential series of high-resolution images of the CNT-Au NP-CNT junction. When the bias voltage was increased to 1.60 V, the current increased to 44.4 μA . At the same time, the Au NP started to shrink (Fig. 2(b)). After a further increase of current to 54.5 μA , the Au NP disappeared. When the bias voltage was increased to 2.19 V, the current increased from 65.4 μA to 113 μA and the two CNTs were reconnected (as shown by arrows in Fig. 2(c)). The total resistance of the CNT bridge decreased from 100 $\text{k}\Omega$ for the CNT-Au NP-CNT junction (Fig. 2(a)) to 39 $\text{k}\Omega$ for the reconnected CNT (Fig. 2(c)).

Corresponding Author: Motoyuki Karita
E-mail: karita@surf.nuqe.nagoya-u.ac.jp
Tel&Fax: +81-52-789-3714, +81-52-789-3703

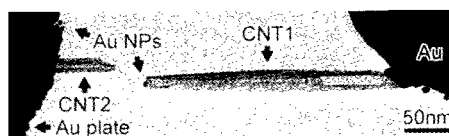


Fig. 1 A TEM image of cut CNTs. A dark spherical particle on the CNT1 is an Au NP picked out of the Au plate.

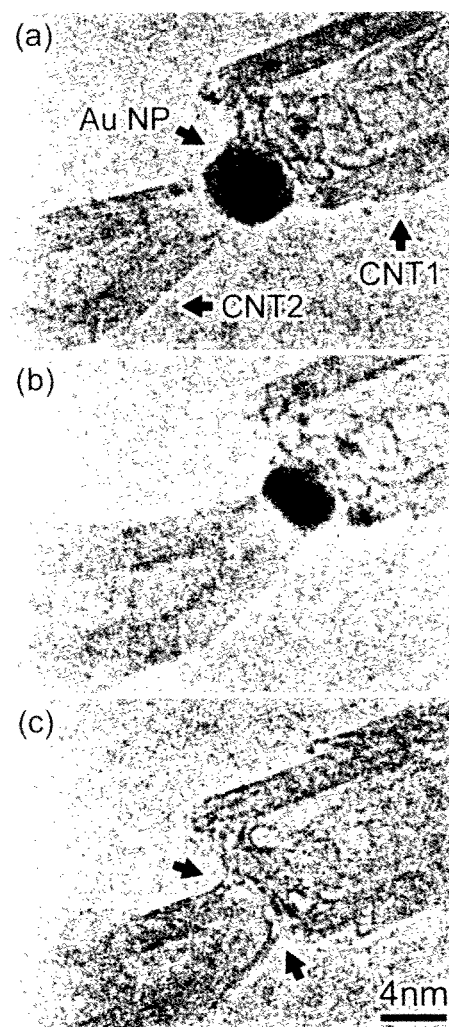


Fig. 2 A time sequential series of high resolution images of the CNT-Au NP-CNT junction.

Synthesis of carbon nanotubes conjugated with distance-controlled nanoparticles using gas-liquid interfacial plasmas

○Toshiro Kaneko, Qiang Chen, Rikizo Hatakeyama

Department of Electronic Engineering, Tohoku University, Sendai, 980-8579, Japan

Carbon nanotubes (CNTs) conjugated with nanoparticles have attracted much attention due to their high catalytic activity, unique photosensitive reactivity, and so on. To realize the highly-ordered structure of gold nanoparticles (AuNPs) on the CNTs, single-walled carbon nanotubes (SWNTs) are utilized as a template and are conjugated with the AuNPs synthesized by a gas-liquid interfacial discharge plasma (GLIDP) using ionic liquids (ILs) [1-3].

The SWNTs are dispersed in the IL (2-Hydroxyethylammonium formate) which consists of amino and carboxyl groups, and the discharge plasma is generated on the IL. In this experimental condition, the plasma ions with high energy are irradiated to the IL and can dissociate the IL into the amino and carboxyl groups, which bond to the surface of the SWNTs. When the Au chloride (HAuCl_4) is dissolved in the IL with the functionalized SWNTs (f-SWNTs), the Au chloride is reduced by the IL and the AuNPs are selectively synthesized on the functional (amino and carboxyl) groups bonding to the SWNTs. Since the density of the functional groups can be controlled by the plasma ion irradiation parameter, such as irradiation energy, time, and so on, the density of the AuNPs can also be controlled.

Figure 1 presents transmission electron microscope (TEM) images of the AuNPs synthesized on the f-SWNTs, which have been treated in the IL for plasma irradiation time (b) $t_{\text{pi}} = 1$ min and (c) $t_{\text{pi}} = 10$ min, argon gas pressure $P_{\text{gas}} = 60$ Pa, and discharge current $I_{\text{D}} = 1$ mA. Here the TEM image of the SWNTs which are not previously treated by the plasma irradiation ($t_{\text{pi}} = 0$ min) is also presented as a reference in Fig. 1(a). It is found that the mono-dispersed AuNPs are synthesized on the f-SWNTs when the SWNTs are previously treated by the plasma irradiation, while only a few AuNPs are observed on the SWNTs in the absence of the plasma irradiation. In addition, the distance between the AuNPs becomes small with an increase in the plasma irradiation time. This result means that the distance between the AuNPs can be controlled by functionalization of the SWNTs using the plasma ion irradiation in the IL.

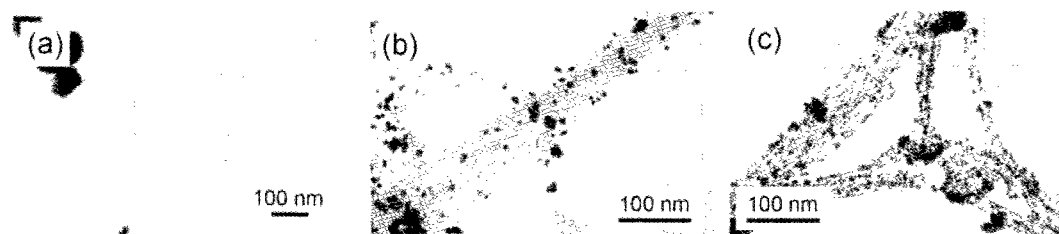


Fig.1 TEM images of the AuNPs synthesized on the f-SWNTs. (a) $t_{\text{pi}} = 0$ min, (b) $t_{\text{pi}} = 1$ min, (c) $t_{\text{pi}} = 10$ min.

[1] T. Kaneko, K. Baba, and R. Hatakeyama, *J. Appl. Phys.* **105**,103306 (2009).

[2] T. Kaneko, K. Baba, T. Harada, and R. Hatakeyama, *Plasma Proc. Polym.* **6**, 713 (2009).

[3] T. Kaneko, Q. Chen, T. Harada, and R. Hatakeyama, *Plasma Sources Sci. Technol.* **20**, 034014 (2011).

Corresponding Author: Toshiro Kaneko

Tel: +81-22-795-7116, Fax: +81-22-263-9375,

E-mail: kaneko@m.tohoku.ac.jp

Electrochemical durability of single-wall carbon nanotube electrode against anodic oxidation in water

○Shigekazu Ohmori¹ and Takeshi Saito¹

¹ Nanotube Research Center, National Institute of Advanced Industrial Science and Technology, Ibaraki, 305-8565, Japan

The electrochemical capability of single-wall carbon nanotube (SWCNT) electrodes is investigated to establish their reliability in practical applications. Direct current (DC) voltage of +10, +8, and +6 V is applied across the SWCNT anode and Pt cathode in water, and the electrochemical fracturing behavior of SWCNTs is analyzed using transmission electron microscopy and atomic force microscopy (Figure 1). A considerable number of short SWCNTs, with lengths of less than 200 nm, are observed to be electrochemically generated.

This result suggests that the anodic corrosion of SWCNTs occurs even in water, a non-electrolyte liquid (Figure 2). Raman spectroscopy and a comparison study of the anodization behavior of SWCNTs with narrow (0.9 nm) and wide (1.8 nm) diameters indicate that the durability of narrow SWCNTs is lower than that of the wide SWCNTs.

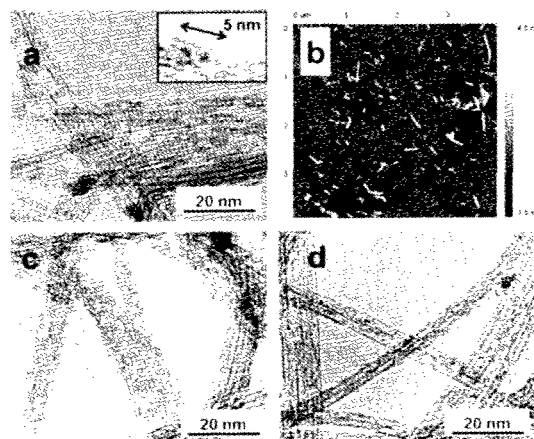
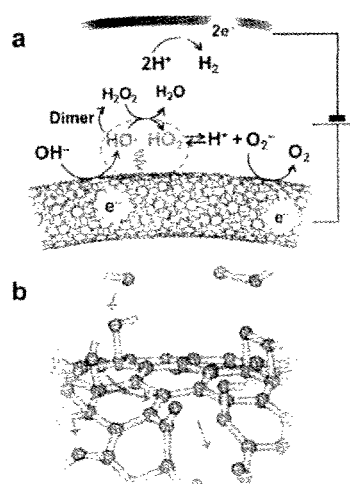


Figure 1. Typical TEM images of SWCNTs after the electrochemical reaction at anode voltages of +10 V (a), +8 V (c), and +6 V (d), and AFM image of short SWCNTs extracted from the sample subjected to +10 V bias (b) by cross-flow filtration with pore size of 200 nm [1].



→ R. Erni, *et. al.*, ref. 2.
 G.M. Psfogiannakis *et. al.*, ref. 3.
 → A. bagri *et. al.*, ref. 4.

- [1] S. Ohmori, *et. al.*, *ACS Nano*, 4(7) (2010), 3606–10.
 [2] R. Erni, *et. al.*, *Phys. Rev. B*, 82 (16) (2010), 165443 1-6
 [3] G.M. Psfogiannakis, *et. al.*, *J. Am. Chem. Soc.*, 131 (42) (2009), 15133–15135.
 [4] A. Bagri, *et. al.*, *J. Phys. Chem. C*, 114 (28) (2010), 12053–12061.
 [5] S. Ohmori, *et. al.*, *Carbon*,
<http://dx.doi.org/10.1016/j.carbon.2012.06.023>.

Corresponding Author: T. Saito
 Tel: +81-29-861-4863
 E-mail: takeshi-saito@aist.go.jp

Figure 2. Schematic representation showing the anodization mechanism, that is, the production of oxidants on the surface of the SWCNT electrode (a), and a possible reaction pathway that results in the oxidative degradation of SWCNTs (b).

Patterned Carbon Nanotubes Thin Films Fabricated by Polystyrene-Nanosphere Templating

○Yuki Kuwahara^{1,2}, Takayoshi Hirai², Takeshi Saito^{1,2}

¹ Nanotube Research Center, National Institute of Advanced Industrial Science and Technology (AIST), Tsukuba, 305-8565, Japan

² Technology Research Association for Single Wall Carbon Nanotubes (TASC), Tsukuba, 305-8562, Japan

Because of their excellent electronic property, carbon nanotubes have been studied aiming at their transparent conducting films (CNT-TCFs). In addition to the substitution of ITO, the application of CNT-TFTs a new flexible device is prospective. As for CNT-TCFs, the optimal film morphology for the high optical transparency and low electrical resistivity is one of the controversial issues.^[1] Therefore, it would be important to study the film fabrication techniques and control their morphology. Such investigation will contribute to further improvements in conductivity and transparency of CNT-TCFs.

It is well-known that the close-packed layer of ordered latex particles forms a hexagonal pattern that is frequently used as a template. In this study, we have fabricated honeycomb-shape CNT thin films by the templating method using polystyrene spheres (PSs), and investigated the relationship between the performance as CNT-TCFs and the film morphology.

CNTs were dispersed in aqueous solutions of 1 wt% sodium cholate (SC) by using a tip-type ultrasonicator. For the fabrication of the honeycomb-shape CNT thin films, we combined PS template and filtration methods. At first, the PSs latex solution was filtered through nitrocellulose membrane filter to form self-assembled close-packed layers on the membrane. Then, the CNT dispersion was poured on it and washed with ample amounts of Millipore water. After removing PSs using 1,2-dichlorobenzene, CNT films were transfer to glass substrates according to the method described by Wu *et al.*^[2] Patterned CNT films were observed by using SEM, AFM, and optical microscopy. The surface resistance and transparency of CNT films were also characterized.

Figure 1 shows the optical image of CNT film. According to the PSs packing structure, honeycomb-shape CNT thin film is formed on glass substrate. The details of the other results will be reported in this presentation.

[1] N. Wakamatsu *et al.* Adv. Funct. Mater. **19**, 311 (2009).

[2] Z. Wu *et al.*, Science **305**, 1273 (2004).

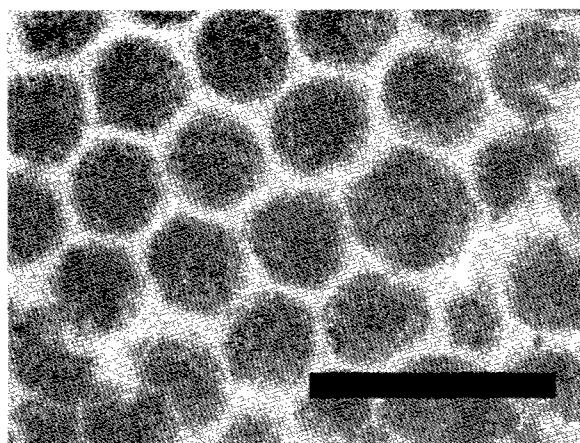


Fig.1 Optical image of the honeycomb-shape CNT thin film on a glass substrate. Scale bar is 10 μm .

Corresponding Author: T. Saito
Tel: +81-29-861-4863, Fax: +81-29-861-4413,
E-mail: takeshi-saito@aist.go.jp

Fabrication of stable p-n junction diode with Cs encapsulated single-walled carbon nanotubes

○Yoshihiro Abiko, Toshiaki Kato, Rikizo Hatakeyama, Toshiro Kaneko

Department of Electronic Engineering, Tohoku University, Sendai, 980-8579, Japan

Single-walled carbon nanotubes (SWNTs) attract a great deal of attention due to their outstanding electrical features, which can be useful to next-generation nanoelectronic devices. It is well known that a pristine SWNTs field effect transistor (FET) shows p-type semiconducting characteristics and accommodation of various dopant atoms, molecules, and compounds makes it possible to modify the intrinsic electronic properties of SWNTs. According to our previous researches for the transport property of individual SWNT, alkali-metal- and halogen-encapsulated SWNTs are found to exhibit n-type and p-type semiconducting behaviors under the FETs configuration, respectively. This indicates that alkali-metal and halogen atoms operate as an electron donor and acceptor for SWNT, respectively [1-3]. As a next step of this study, we attempted to fabricate a p-n junction diode with atom-encapsulated SWNTs thin films.

Atom encapsulation was carried out by a plasma ion irradiation method [4]. In this study, Cs was used as a dopant atom. It is found that the transport properties of Cs encapsulated SWNTs-FETs are changed from p-type to n-type semiconducting characteristics and are stable under the various environments, such as air and water conditions. The n-type characteristics are observed even after the high temperature (~350 °C) annealing. This indicates that it is possible to fabricate the stable SWNTs p-n junction diode with Cs encapsulated SWNTs thin films. In order to fabricate the p-n junction diode, position selective Cs encapsulation was carried out by covering the half of SWNTs thin film channels with a conventional photo-lithographical technique. The diode like electrical characteristics can be observed for position selectively Cs encapsulated SWNTs, which indicates that the p-n junction diode structure should be formed by our established position selective plasma irradiation method.

[1] T. Izumida *et al.* Appl. Phys. Lett. **89**, 093121 (2006).

[2] J. Shishido *et al.* Jpn. J. Appl. Phys. **47**, 2044 (2008).

[3] T. Kato *et al.* Appl. Phys. Lett. **95**, 083109 (2009).

[4] R. Hatakeyama *et al.* J. Phys. D: Appl. Phys. **44**, 174004 (2011).

Corresponding Author: Y. Abiko

Tel: +81-22-795-7046, Fax: +81-22-263-9225,

E-mail: abiko12@ecei.tohoku.ac.jp

Nanotube-Based Self-Standing Carbon Films for Supercapacitors

○Ricardo Quintero, Dong Young Kim, Kei Hasegawa, Yuki Yamada, Atsuo Yamada,
and Suguru Noda*

Department of Chemical System Engineering, The University of Tokyo, Japan

Study on the application of carbon nanotubes (CNTs) and other carbon nanostructures to supercapacitor electrodes is being conducted. Although we previously developed self-standing electrodes for high-power Li batteries from oxidized few-walled carbon nanotubes (Ox.FWCNTs) [1], other low cost all-carbon electrodes have not been extensively researched. The approach in the present work is the systematic combination of low cost capacitive materials, such as activated carbon (AC), with carbon nanotubes which provide high electrical conductivity and a structural matrix. The dispersion conditions are set to keep the length and conductivity of carbon nanotubes. Moreover, since the electrodes are self-standing, no binding materials are added. Because of this, this work aims to fabricate an array of flexible electrodes with different performances in terms of capacitance and specific power, able to be used on a case-by-case basis.

To prepare the electrodes, different amounts of single-walled CNTs (SWCNTs) (2-4 nm diameter, 500 μm length) [2] and FWCNTs (8 nm diameter, 400 μm length) [3] were mixed with Ox.FWCNTs and AC, through the ultrasonication of their aqueous (SDBS 1wt% solution) and ethanol dispersions. The electrodes were obtained by vacuum filtration over PTFE membrane filters after extensive rinse of the surfactant. Cyclic voltammetry (CV) and impedance measurements in a three-electrode cell with H_2SO_4 1M as electrolyte, were used to measure gravimetric capacitance and redox behavior, sheet resistance was determined by four point probe instrument and SEM imaging was used to analyze the electrodes structure. The results in Figure 1 show how the SWCNT electrode has higher capacitance than the FWCNT one, probably due to the larger specific surface area for the former. The combination electrode SWCNT - AC exhibits the contribution to capacitance from the particulate AC confined in the nanotube matrix. There is a decrease in capacitance with scan rate, which suggests its suitability to a specific scan rate range application. Performance of the Ox.FWCNTs electrode involves redox reactions between the surface functional groups and the electrolyte, which yield high pseudocapacitance.

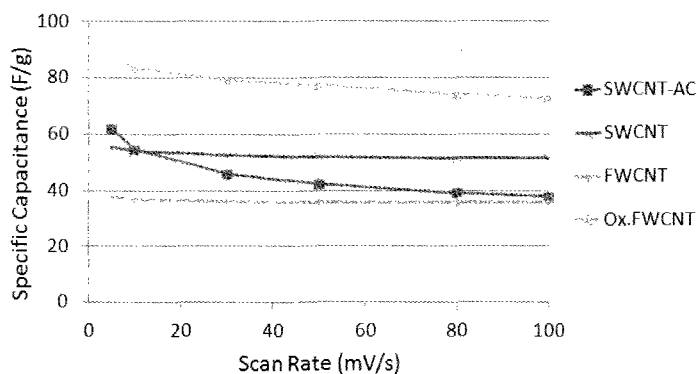


Figure 1. Galvanostatic rate capability of CNT-based selfstanding carbon nanostructures.

- [1] S.W. Lee, et al., *Energy Environ. Sci.*, 2012, **5**, 5437.
 [2] D.Y. Kim, et al., *Carbon*, 2012, **50**, 1538.
 [3] D.Y. Kim, et al., *Carbon*, 2011, **49**, 1972.

Corresponding Author: S. Noda

Tel: +81-3-5841-7330, Fax: +81-3-5841-7332, E-mail: noda@chemsys.t.u-tokyo.ac.jp

Controlled Functionalization of Carbon Nanotubes with Antibody

Yoko Iizumi¹, Toshiya Okazaki¹, Yuzuru Ikehara², Mutsuo Ogura³, Masako Yudasaka¹

¹ *Nanotube Research Center,* ² *Research Center for Medical Glycoscience*

³ *Nanotsystem Research Institute, National Institute of Advanced Industrial Science and Technology, Tsukuba, Ibaraki, Japan*

Complex formation of single-walled carbon nanotubes (CNT) with biological molecules is an important technique for medical application of CNTs. The protein attachment to CNTs enhances the CNT dispersion in aqueous solutions and increases the biocompatibility of CNT. Nucleic acids attachments would be useful for the gene therapy. The CNT's structure-selective attraction of DNA may create a new type of gene therapy technique. We have been studying the complex formation process of CNTs with antibodies, in which biological functions of antibodies is maintained.

Firstly, the antibody was attached to CNTs following the conventional method. The CNTs (CoMoCAT) were mixed with SDS, followed by vigorous sonication and centrifugation. The CNTs coated with SDS were individually dispersed in the centrifugation supernatant. The SDS attached on CNTs were replaced by phospholipid PEG (PLPEG) and PLPEG-IgG by putting SDS-CNT, PLPEG, and PLPEG-IgG in a dialysis membrane tubes and left in water for several days. Here, IgG was a mouse antibody, and it was attached to PLEG by reacting amino groups of IgG with NHS group placed at the end of PLPEG. The obtained complex was designated as IgG-CNT. The compound IgG-CNT showed the optical properties characteristic of CNTs, however, the IgG function of specific adsorption of protein G (PrG) was deactivated. The production process of IgG-CNT was variously improved; however, it was difficult to obtain IgG-CNT that maintains the IgG function. It was suspected that PLPEG conjugated with IgG improperly or IgG interacted with CNTs, resulting in the inhibition of IgG-PrG specific coupling. Since the conventional method was not necessarily adequate for the IgG-CNT preparation, several new methods have been challenged to prepare IgG-CNT, and some of which have shown better results for IgG-PrG specific coupling, which are going to be shown in the presentation.

Contact: T. Okazaki (toshi.okazaki@aist.go.jp)

M. Yudasaka (m-yudasaka@aist.go.jp)

Selective Extraction of Semiconducting Single-Walled Carbon Nanotubes by Fullerodendrons

H. Suzuki,^{1,2} T. Okazaki,^{2,1,*} Y. Iizumi,² M. Tange,² T. Wada,³ T. Tajima,³ Y. Takaguchi,³
and S. Iijima²

¹Department of Chemistry, Tsukuba University, Tsukuba 305-8577, Japan

²Nanotube Research Center, AIST, Tsukuba 305-8565, Japan,

³Graduate School of Environmental Science, Okayama University, Okayama 700-8530, Japan

Hydrogen gas has been expected as an ultimate clean energy source, which can be used in fuel cells to generate electricity. Many researchers have therefore been studied on photocatalytic hydrogen generation. For example, a photoinduced electron transfer system consisting of SWCNT and fullerodendrons (Fig. 1) can be utilized for a light harvesting antenna [1]. The electron immigration from C₆₀ moiety to methylviologen dication (MV²⁺) induces the MV⁺ radicals. In the presence of MV⁺, hydrogen gas is effectively generated from water with the assistance of colloidal PVA (polyvinylalcohol)-Pt catalyst. However, the mechanism of high efficiency of hydrogen generation is not yet clear. We here report spectroscopic characterizations of the fullerodendron-SWCNTs composite systems. Figure 2 shows the Raman spectrum of fullerodendrons extracted HiPco tubes (red line) together with the pristine HiPco nanotubes (solid line). There are two peaks at 180 cm⁻¹ and 270 cm⁻¹ that correspond to the radial breathing modes (RBM) of semiconducting and metallic SWCNTs, respectively. The RBM intensity of metallic SWCNTs extracted by fullerodendrons apparently decreases compared to the pristine HiPco tubes. The result indicates that fullerodendrons more strongly interact with semiconducting SWCNTs than the metallic counterparts, which may be one of the reasons for the efficient hydrogen generation in the fullerodendron-SWCNT system.

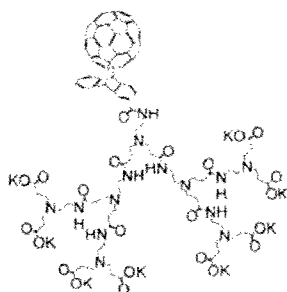


Figure 1. Molecular model of fullerodendrons.

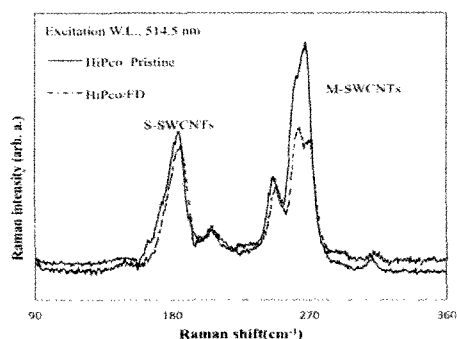


Figure 2. Raman spectrum of fullerodendron-extracted HiPco tubes (broken line), together with the reference spectrum of the pristine HiPco tubes (solid line).

[1] T. Tajima et al., *Adv. Mater.*, 23, 5750 (2012).

e-mail: toshi.okazaki@aist.go.jp

Fabrication and properties of chemically doped semiconducting single-walled carbon nanotubes/Si heterojunction diodes

○Mao Shoji^{1,3}, A.Nakano¹, Hironori Ogata^{1,2,3}

¹Graduate School of Engineering, Hosei University, Koganei, 184-8584, Japan

²Department of Chemical Science and Technology, Hosei University, Koganei, 184-8584, Japan

³Research Center for Micro-Nano Technology, Hosei University, Koganei 184-0003, Japan

Since the high carrier mobility, SWNTs are expected to the application to the various kinds of the electronic devices. Especially, semiconducting SWNTs(S-SWNTs) are direct band-gap materials and expected to be useful for photonic and optoelectronic applications¹. The S-SWNTs are reported to show unipolar p-type behavior under ambient conditions and various chemical doping have been reported to convert from p-type to n-type².

In this study, we fabricated the various types of p-n diodes based on chemically doped n-SWNTs /p-Si hetero junction and characterized their diode properties.

The SWNTs used in this study were purchased from Aldrich(CoMoCAT (0.8 ± 0.1 nm in diameter)). The SWNTs were dispersed in 1,2-dichlorobenzene at 0.5 mg/mL by ultrasonication and SWNTs thin film was fabricated on the p-type Si wafer in which layers of Cr and Au were deposited on the backside by using airbrush. Three kinds of viologen molecule(benzyl viologen(BV), ethyl viologen(EV), methyl viologen(MV)) was doped to SWNT films with various conditions. Finally, Ag was deposited at 100 nm. The schematic of SWNTs/Si device is showed in Fig. 1.The current density-voltage(J-V) curve was measured both dark and AM1.5G condition(100 mW/cm²).

Fig. 2 shows one example of the J-V characteristics of BV-doped SWNTs/p-Si device(transmittance of SWNT film at 550 nm is 45%). The rectification characteristic of the device has improved by BV doping. The detailed properties of the devices will be presented.

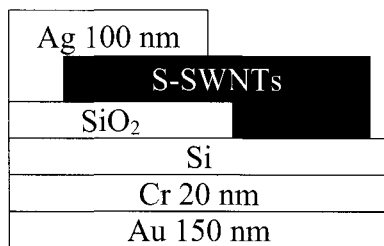


Figure 1. Structure of SWNTs/Si device

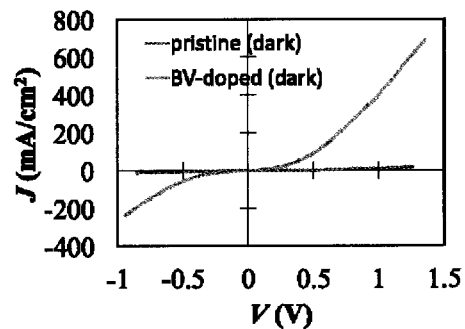


Figure 2. J-V characteristics of pristine and BV-doped SWNTs/p-Si device

Corresponding Author: Hironori Ogata,
Tel: +81-42-387-6229, Fax: +81-42-387-6229,
E-mail: hogata@hosei.ac.jp

Structural deformation of functionalized multi-walled carbon nanotubes in the macrophage of rat subcutaneous soft tissue over long time

○Yoshinori Sato¹, Atsuro Yokoyama², Eiko Nakazawa³, Minfang Zhang⁴, Masako Yudasaka⁴, Kenichi Motomiya¹, Kazuyuki Tohji¹

¹Graduate School of Environmental Studies, Tohoku University, Sendai 980-8579, Japan

²Graduate School of Dental Medicine, Hokkaido University, Sapporo 060-8586, Japan

³Advanced Microscope Systems Design, Hitachi High-Technologies Corporations, Hitachinaka 312-8504, Japan

⁴National Institute of Advanced Industrial Science and Technology, Tsukuba 305-8566, Japan

Carbon nanomaterials (CNMs) such as carbon nanotubes (CNTs) and carbon nanohorns (CNHs) have attractive in the application for drug delivery systems, biosensors, and biomaterials. Although carbon materials are believed to be unchangeable or non-biodegradable within the living body, the stability and metabolism of CNMs are of great significance for the human bodies and biogeocenosis as a fundamental knowledge. Recently, Kagan and colleagues reported on the enzymatic biodegradation of carboxylated single-walled carbon nanotubes (COOH-SWCNTs) *in vitro*, in neutrophils[1]. In contrast, to our knowledge, the chemically-modified short CNTs or CNHs was taken into not neutrophils but macrophages, *in vivo*. It is a commonplace to say that oxidative ability of macrophages to foreign body is much weaker than that of neutrophils. Are CNMs biodegraded in macrophage *in vivo*? Here, we report on the implantation of multi-walled carbon nanotubes (MWCNTs) modified with carboxyl groups, in the subcutaneous tissue of rats over 2 years and the structural deformation of these MWCNTs in phagocytes studied using high-resolution transmission electron microscopy (HRTEM) and Raman scattering spectroscopy.

[1] V. E. Kagan *et al.* Nat. Nanotech. **5**, 354 (2010).

Corresponding Author: Yoshinori Sato

Tel: +81-22-795-3215, Fax: +81-22-795-3215

E-mail: hige@ncsimd.kankyo.tohoku.ac.jp

Ultrathin aligned CNTs film by combining AC electric field with liquid flow

○Jun Matsui¹, Shigeru Kaida¹, Tokuji Miyashita¹

¹*Institute of Multidisciplinary Research for Advanced Materials, Tohoku University, Sendai, 980-8577, Japan*

Since the discovery of carbon nanotubes (CNTs), CNTs have attracted much interest in the wide area from electric devices to composites because of their remarkable electrical, optical and mechanical properties. Since CNTs exhibit most of their remarkable properties along the tube axis, it is important to prepare a well-aligned uniform CNT film by a cost-effective and facile fabrication process. In this paper, we present a simple and versatile technique, which combines AC electric field with liquid flow to prepare aligned CNT ultrathin films. The aligned film was characterized with atomic force, polarized Raman spectrum and conductivity measurement. Moreover, a liquid crystal alignment of a liquid crystal using the CNTs ultrathin film was also demonstrated.

SWCNTs that had been synthesized using HiPco method were purchased from Unidym Inc.

SWCNTs were treated with acid to be dispersed in water and the acid-treated SWCNTs were aligned by combining AC electric field with liquid flow. Figure 1 shows the set up for preparing aligned SWCNT ultrathin film. A rectangular glass vessel with two ITO electrodes were used a deposition cell. SWCNTs water dispersion was placed on the cell and a solid substrate was place between the ITO electrodes. Then AC electric field was applied between the electrodes and the substrate was withdrawn from the dispersion with a constant speed. We found that aligned SWCNT film was deposited from the edge of the substrate and with optimizing deposition condition, such as concentration of SWCNT, AC voltage, AC frequency, and withdrawal speed, an aligned SWCNTs film with nanometer thickness was prepared onto a solid substrate (Figure 2). In the presentation, we will show a liquid crystal alignment using the CNTs ultrathin film

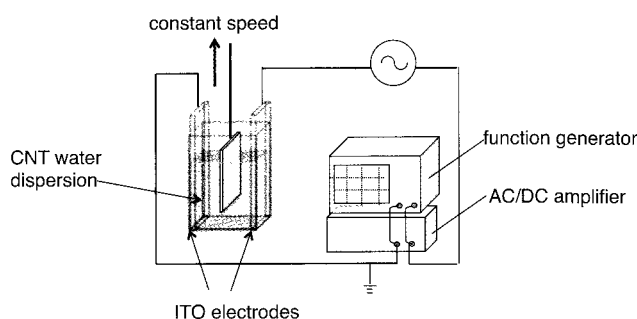


Figure 1 Schematic of the setup for fabrication of aligned SWCNTs ultrathin film by combination of AC electric field and liquid flow.

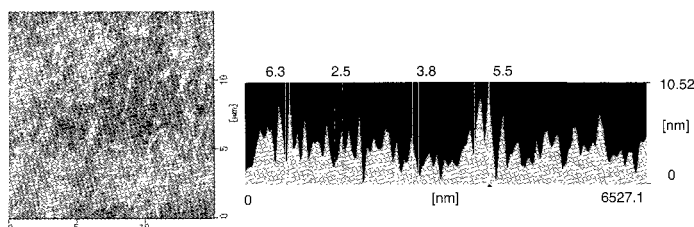


Figure 2 AFM image of acid-treated SWCNT transferred onto an APTS-treated glass substrate and height profiles across the sample surface.

Corresponding Author: J. Matsui

Tel: +81-22-217-5639, Fax: +81-22-217-5639,

E-mail: jun_m@tagen.tohoku.ac.jp

Encapsulation of C₆₀ into the Single Chirality State of (11,10) Single Wall Carbon Nanotubes

○Masatoshi Kawai¹, Toru Igarashi¹, Haruka Kyakuno¹,
Toshiya Okazaki², Yutaka Maniwa^{1,3}, Kazuhiro Yanagi¹

¹ Tokyo Metropolitan University, ² AIST, ³ JST-CREST

Single-wall carbon nanotubes (SWCNTs) encapsulating organic molecules (peapods) exhibit unique physical and chemical properties. However, a mixed electronic structure state of surrounding SWCNTs has impeded a detailed understanding of the properties of peapods. Recent advancement of purification techniques for SWCNTs enable us to obtain high-purity metallic, semiconducting, and single-chiral state of SWCNTs samples. However, most of the obtained single-chiral SWCNTs are limited with the diameter of less than 1.0 nm. The diameter is not enough inner hollow space to encapsulate organic molecules. For the purpose, we reported the successful extraction of a single-chiral state of SWCNTs with (11,10) chirality which has 1.45nm diameter, and their peapods [1]. In this study, we tried to fill C₆₀ into the (11,10) SWCNTs and investigate their Raman characteristics.

We prepared (11,10) SWCNTs for encapsulation by two steps density-gradient ultracentrifugation; metal/semiconductor sorting and cesium chloride sorting (CsCl sorting). Semiconducting SWCNTs was obtained by using iodixanol as density medium, and (11,10) single-chiral SWCNTs was achieved by the CsCl sorting [1]. Then a thick film of (11,10) SWCNTs were formed on a small glass substrate. This substrate was sintered with C₆₀ twice at 600K for 24 hours in high vacuum for encapsulation. After encapsulating, the plate was chemically washed with toluene and annealed at 500 degree in high vacuum to remove C₆₀ attaching outside of the SWCNTs.

Figure 1 shows the Raman spectrum of (11,10) peapod. The Ag(2) mode of the encapsulated C₆₀ was identified to be 1464cm⁻¹, and the presence of C₆₀ inside the samples was observed by transmission electron microscope. In addition, a shift of the radial breathing mode of (11,10) was clearly observed by encapsulation C₆₀.

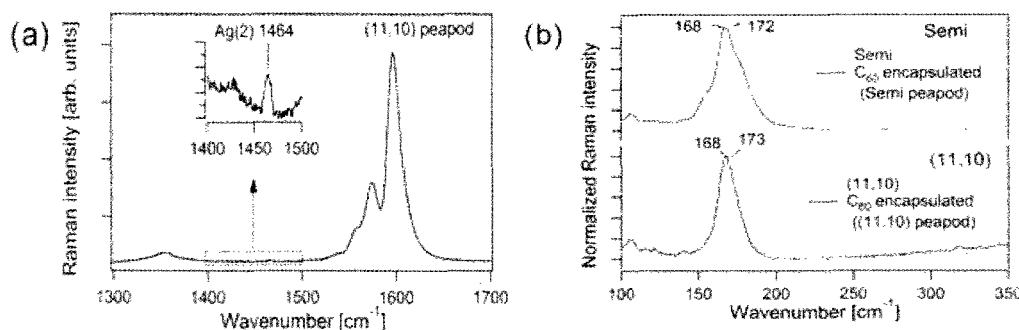


Fig1. (a) The Ag(2) peak of encapsulated C₆₀ was enlarged and is presented in the inset. (b) The changes of the Raman peaks of the radial breathing modes by encapsulation C₆₀ into Semi and (11,10), respectively.

[1] Kawai, Yanagi *et al.* J. Am. Chem Soc. 134, 9545 (2012)

Corresponding Author: K. Yanagi

Tel: +81-42-677-2494, Fax: +81-42-677-2483,

E-mail: yanagi-kazuhiro@tmu.ac.jp

Optical Properties of Perylene/Single-Walled Carbon Nanotube Composites

○Takuya Tsunekawa,¹ Takeshi Koyama,¹ Koji Asaka,² Yahachi Saito,²
Hideo Kishida,¹ and Arao Nakamura^{1,3}

¹Department of Applied Physics, Nagoya University, Chikusa, Nagoya 464-8603, Japan

²Department of Quantum Engineering, Nagoya University, Chikusa, Nagoya 464-8603, Japan

³Toyota Physical and Chemical Research Institute, Nagakute 480-1192, Japan

Single-walled carbon nanotubes (SWNTs) have enough space to encapsulate other molecules, and can be used as a one-dimensional reactor. One-dimensionally limited space inside SWNTs makes it possible to synthesize some unique oligomer and polymer molecules which cannot be synthesized in non-limited space. Graphene nanoribbons were synthesized from coronene and perylene molecules inside SWNTs [1], and recently sulfur-terminated graphene nanoribbons were synthesized from TTF molecules inserted in SWNTs [2]. In this study, we synthesized dimeric perylene molecules from perylene monomers (chemical structures of perylene monomer and dimeric perylene molecule are shown in Figure 1).

Perylene/SWNT composites were synthesized by using a vapor phase method. Two types of SWNTs were used in this study, they were produced by the high pressure carbon monoxide method (HiPCO, tube diameter ~ 1.0 nm) and the arc plasma jet method (Meijo-SO, tube diameter ~ 1.4 nm). SWNT films (thickness ~ 300 nm, diameter ~ 4 nm) were prepared by filtration after annealing at 550°C in air to open end-cap of SWNTs. The SWNT film on a glass substrate and perylene powder (1 mg) were inserted into a quartz tube and sealed in vacuum ($\sim 3 \times 10^{-5}$ Torr). The quartz tube was heated in a muffle furnace at 400°C for 20 h. The film samples taken out from the quartz tube were washed by toluene to remove residual perylene molecules attaching outside the tube walls. The obtained samples will be referred to as pery(D)@SWNT. We also prepared SWNT films as reference samples by the same process described above without perylene powder.

Figure 2 shows Raman scattering spectra of SWNT and pery(D)@SWNT film samples with the excitation wavelength of 633 nm (SWNTs used are Meijo-SO). We can observe so-called G-band (1566 and 1591 cm^{-1}) and D-band (1324 cm^{-1}) originating from SWNTs in both samples, while other several peaks are observed at 1060 , 1256 , 1287 , 1361 and 1545 cm^{-1} in pery(D)@SWNT film sample. Since these peak frequencies are in good agreement with those of the dimeric perylene molecule obtained by the first principle calculations [3], these peaks are attributed to dimeric perylene molecules. In contrast, these peaks are weak in Raman spectra excited with 488-nm light, while strong peaks assigned to perylene monomers are observed, which indicates the change of the resonance condition. Absorption spectra also support the presence of dimeric perylene molecules.

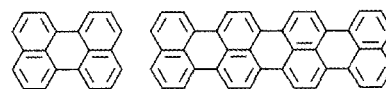


Fig. 1. Chemical structures of perylene monomer (left) and dimeric perylene molecule (right).

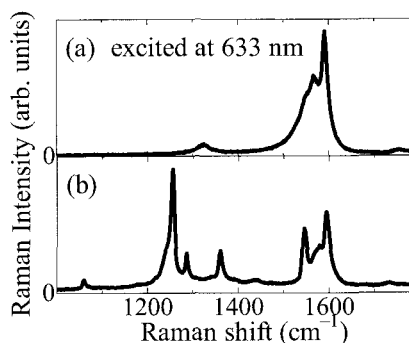


Fig. 2. Raman scattering spectra of (a) SWNT and (b) pery(D)@SWNT film samples.

[1] A. V. Talyzin *et al.*, Nano Lett. **11**, 4352 (2011).

[2] T. W. Chamberlain *et al.*, ACS Nano **6**, 3943 (2012).

[3] N. U. Zhanpeisov *et al.*, Int. J. Quantum. Chem. **105**, 368 (2005).

Corresponding Author: Takeshi Koyama

Tel: 052-789-4452, **Fax:** 052-789-5316, **E-mail:** koyama@nuap.nagoya-u.ac.jp

Difference in encapsulated AgBr lifetime between ^{12}C NTs and ^{13}C NTs under electron beam irradiation

○Keita Kobayashi¹, Takeshi Saito^{2,3}, Masaharu Kiyomiya³, Hidehiro Yasuda¹

¹ Research Center for Ultra-High Voltage Electron Microscopy, Osaka University, 7-1 Mihogaoka, Ibaraki, Osaka 567-0047, Japan

² Nanotube Research Center, National Institute of Advanced Industrial Science and Technology (AIST), Tsukuba 305-8565 Japan

³ Technology Research Association for Single Wall Carbon Nanotubes (TASC), Tsukuba 305-8562, Japan

Since inner space of a carbon nanotubes (CNTs) can store unstable nano materials stably even under harsh environmental conditions such as under UV laser light irradiation [1], CNTs have been widely utilized as a "test-tube" for investigating novel nano materials. In particular, CNTs encapsulating nano materials have been used to investigate the structural properties of novel low dimensional nano materials by transmission electron microscopy (TEM).

However, because structure of CNTs is susceptible to knock-on damage caused by incident electron beam, TEM observations of nano materials encapsulated within CNTs is difficult at a high electron dose rate. Although low-voltage TEM observation using aberration-corrected TEM has been developed as one of the solution of the problem, deployment of such an aberration-corrected TEM is not easy due to its price yet.

While, the development of nanotubes which are stable under electron beam irradiation is a possible alternative solution of the problem. According to a recent report by Meyer and co-workers, CNTs consisting of ^{13}C are expected as a probable candidate of the nanotube having stability under electron beam irradiation.

In this study, we compared lifetime of CNTs-encapsulated AgBr between CNTs with natural abundance of ^{12}C (AgBr@ ^{12}C NTs) and those enriched in ^{13}C (AgBr@ ^{13}C NTs), to investigate the isotope effect on the stability of CNTs under TEM observation condition.

Figure 1 shows the intensity ratio of the EDX spectra of Br and Ag in AgBr@ ^{12}C NTs and AgBr@ ^{13}C NTs exposed to electron beam irradiation at 120 kV as a function of electron dose. The plot of AgBr@ ^{12}C NTs clearly shows that $I_{\text{Br L}\alpha}/I_{\text{Ag L}\alpha}$ decreases with increasing electron dose. In contrast, the EDX spectra of AgBr@ ^{13}C NTs suggest that $I_{\text{Br L}\alpha}/I_{\text{Ag L}\alpha}$ is hardly decreases as the electron dose is increased; therefore AgBr is more stable within ^{13}C NTs than ^{12}C NTs. Since the cost of producing ^{13}C NTs by eDIPS method [3] is about 250,000 JPY/g [4], we believe using ^{13}C NTs as the "test tube" is a reasonable solution of the problem.

[1] K. Kobayashi *et al.* Adv. Mater. **22**, 3156 (2010). [2] J. C. Meyer *et al.* Phys. Rev. Lett. **108**, 196102 (2012). [3] T. Saito *et al.* J. Nanosci. Nanotechnol. **8**, 6153 (2008). [4] Tomoe Shokai, Private communication (2011).

Corresponding Author: K. Kobayashi

Tel: +81-6-6879-7941, Fax: +81-6-6879-7941,

E-mail: kobayashi-z@uhvem.osaka-u.ac.jp

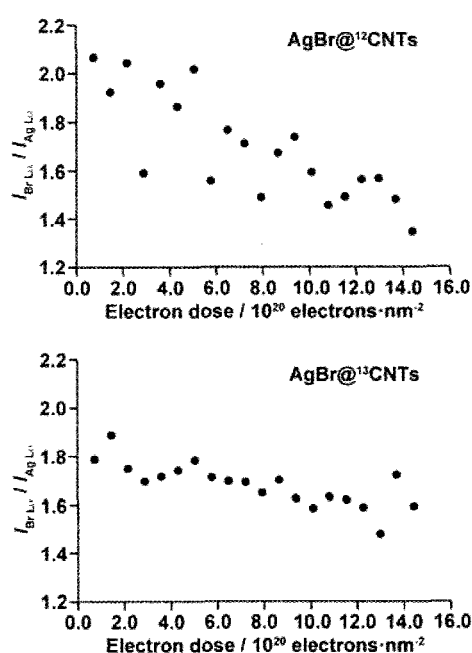


Fig. 1 The intensity ratio of the EDX spectra of Br and Ag in the AgBr@ ^{12}C NTs and AgBr@ ^{13}C NTs exposed to electron beam irradiation as a function of electron dose

Fabrication and characterization of structurally uniform conducting polymers within carbon nanotubes

○Kenshi Miyaura, Yasumitsu Miyata, Ryo Kitaura, Hisanori Shinohara

*Department of Chemistry & Institute for Advanced Research, Nagoya University,
Nagoya 464-8602, Japan*

Hybrid materials of conducting polymers and carbon nanotubes (CNTs) have attracted much attention because of their potential applications in optoelectronics such as solar cells [1]. In previous reports, however, polymers are adsorbed on the surface of nanotubes and their hybrid and electronic structure has not clarified yet. To understand their intrinsic electronic properties and inter-molecular interaction, the structural control of polymers is one of the most important challenges. To shed light on this issue, we have focused our attention to the encapsulation of polymer inside within CNTs, which offer a confined space to control polymer structure.

Here, we report the fabrication and characterization of conducting polymers inside CNTs. As a precursor molecule, sexithiophene (6T, Fig.1a) is selected because of its high filling ratio (more than 95 %) in CNTs as confirmed in our previous study [2]. After a vapor phase doing process, 6T is polymerized through thermal annealing to produce polythiophene in CNTs (PT@CNTs, Fig.1b). High-resolution TEM observations reveal that the presence of a single or double long chain inside CNTs (Fig.1c). Similar images are observed for almost all of the CNTs investigated, which indicates the formation of polythiophene from 6T. For optical characterization, the PT@CNTs are then purified by using density gradient ultracentrifugation (DGU) as shown in Fig.1d. The purified PT@CNTs clearly show a prominent absorption peak around 500 nm originating from encapsulated polymers (Fig. 1e). The presence of polymers is also confirmed by using Raman and photoluminescence spectroscopy. The present hybrids provide an ideal system for unraveling the optoelectronic properties of CNT-conducting polymer hybrids.

References

[1] D. J. Bindl *et al.* *Nano Lett.*, 11, 455 (2011) [2] K. Miyaura *et al.* The 42th FNTG General Symposium.

Corresponding Author :

Hisanori Shinohara

Tel:052-789-3660 Fax: 052-747-6442

E-mail:noris@cc.nagoya-u.ac.jp

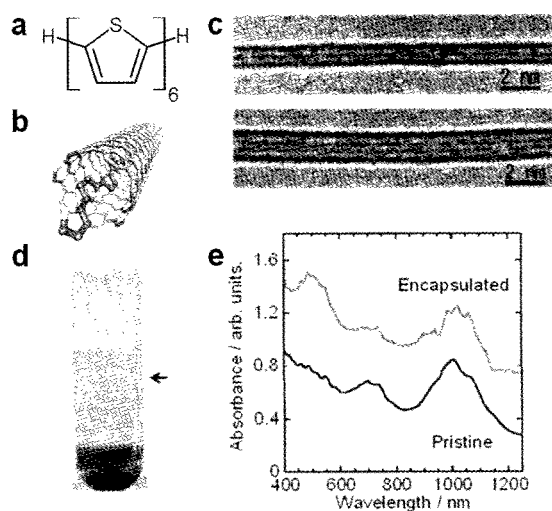


Fig.1. (a) Molecular structure of Sexithiophene. (b) Schematic illustration of PT@CNT. (c) HRTEM images of single and double chains of polythiophene in CNTs. (d) photograph of a centrifugal tube after DGU. (e) Optical absorption spectra of pristine and PT@CNT samples. The PT@CNT sample is collected from the layer indicated by an arrow in panel d.

Amphoteric Carrier Doping to Semiconducting Single-Wall Carbon Nanotubes by TTF and F₄TCNQ Encapsulation

○Yasuhiro Ito^{1,2}, Shunjiro Fujii^{1,2}, Maki Shimizu^{1,2}, Takeshi Tanaka¹, Hiromichi Kataura^{1,2}

¹ Nanosystem Research Institute, National Institute of Advanced Industrial Science and Technology (AIST), Tsukuba, Ibaraki, 305-8562, Japan

² Japan Science and Technology Agency, CREST, Kawaguchi, Saitama, 330-0012, Japan

Semiconducting single-wall carbon nanotubes (s-SWCNTs) have been demonstrated as great potential materials for flexible and transparent thin-film transistor (TFT) applications. For further applications such as the building blocks of CMOS type logic circuits, n- and p-type s-SWCNTs are highly desired. Encapsulation of electron or hole donating molecules inside s-SWCNTs (so-called peapods) is one of the best ways to control the carrier of s-SWCNTs. For encapsulating molecules, tetrathiafulvalene (TTF) and 2,3,5,6-tetrafluoro-7,7,8,8-tetracyano-quinodimethane (F₄TCNQ) are good candidates as n-type and p-type dopants, respectively. In this work, we prepared TTF and F₄TCNQ peapods using high purity s-SWCNTs and fabricated TFTs. Optical properties of these peapods and transfer characteristics of TFTs were measured.

High purity s-SWCNTs were separated from APJ SWCNT (Meijo Nanocarbon) using gel column chromatography. TTF and F₄TCNQ peapods were prepared by a sublimation method. Thin films on SiO₂/Si substrates were fabricated by drop coating method [1]. Then Pd/Au electrodes were deposited by vacuum evaporation as a source and a drain. Figure 1 shows the transfer characteristics of back-gated TFTs measured under vacuum. It is clearly seen that electron on-current for TTF@s-SWCNT-TFT is larger than that for s-SWCNT-TFT. On the other hand, electron on-current of F₄TCNQ@s-SWCNT-TFT is very low, meaning almost pure p-type behavior. These results show that electron and hole carrier densities can be controlled by molecular encapsulation. This is the first evidence that both n- and p-type TFTs can be fabricated using molecular encapsulated s-SWCNTs.

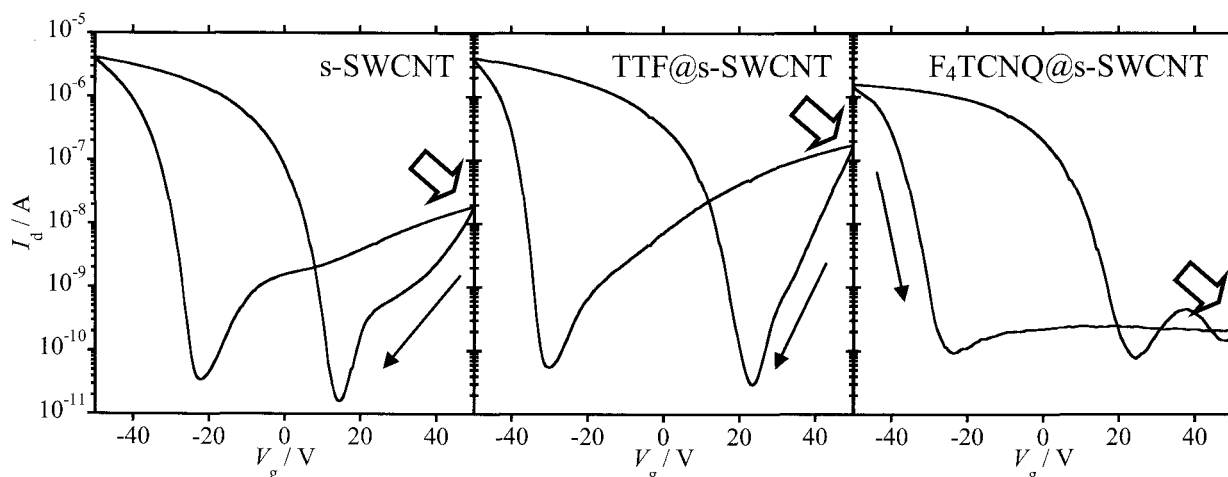


Fig. 1 Transfer characteristics of the s-SWCNT- and peapod-TFTs under vacuum (8.6×10^{-6} Torr). The channel length and width are 100 and 200 μm , respectively. The drain-source voltage is -1 V.

[1] S. Fujii *et al.*, *Phys. Stat. Sol. B* **248**, 2692 (2011).

Corresponding Author: Hiromichi Kataura

E-mail: h-kataura@aist.go.jp **Tel:** +81-29-861-2551, **Fax:** +81-29-861-2786

Microwave-assisted exfoliation of graphite in organic solvents without using strong oxidants

○Haruya Okimoto, Ryota Tada, Masahito Sano

¹ Department of Polymer Science and Engineering, Yamagata University, Yonezawa, 992-8510, Japan

Recently, a great interest in graphene electronics has aroused in flexible/printable electronic devices. Several wet processes for synthesis of graphene were reported. Among various strategies pursued, reduction of graphene oxide (GO) is one of the most widely used methods. However, this method involves reactions with strong oxidants such as KMnO_4 and requires strong reducing agents like hydrazine. In practical applications, however, a method without strong chemicals is desirable. For this purpose, microwave-assisted reaction is a very promising method because it is known that microwave irradiation can shorten the reaction time and achieve high-yields. In fact, rapid heating by microwave has been used in oxidizing graphite for graphene synthesis [1]. Here, we report microwave-assisted synthesis of exfoliated graphene in organic solvents without strong oxidants.

Expanded graphite powder is added to several kinds of organic solvents in a test tube. Each mixture is mixed and placed in a microwave reactor. It is subjected to 15 min of 200 watt microwave irradiation. The mixture was centrifuged at 8000 rpm for 20 minutes to remove unreacted graphite powder.

In the case of N, N-dimethylformamide (DMF) and acetone as a solvent, graphite was not exfoliated. When chloroform or dichloromethane was used, graphite was exfoliated and the supernatant attained a brown color. The dispersion was stable for months without significant precipitation.

Chemical functionalities of the exfoliated sheets were studied using XPS. C_{1s} shows a main peak of oxygen-free sp^2 carbon. Any oxides peaks were significantly smaller than those of graphene oxide made by Hummers method. In addition, Cl_{2p} peak was observed in the exfoliated graphene. This means that a part of the graphene is functionalized by chlorine. The thickness was measured to be 2-5 nm.

Presently, the mechanism of exfoliation is not clear. DMF, which can disperse graphene relatively well, do not produce graphene by microwave irradiation. It should be noted that only chlorinated organic solvents were able to exfoliate graphite. It suggests that active species produced as a result of decomposition of chlorinated solvents by microwave irradiation have caused exfoliation as well as dispersion of graphene.

[1] P.L. Chiu et al., *J. Am. Chem. Soc.*, **134**, 5850(2012).

Corresponding Author: H. Okimoto Tel: +81-238-26-3074, Fax: +81-238-26-3074,

E-mail: haruya@yz.yamagata-u.ac.jp

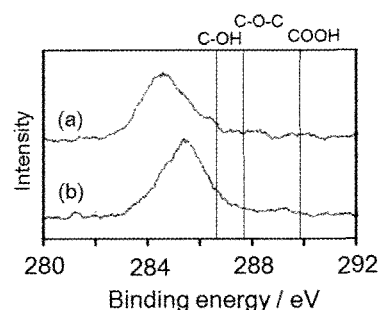


Fig1 XPS spectra of graphene oxide using (a) chloroform and (b) dichloromethane

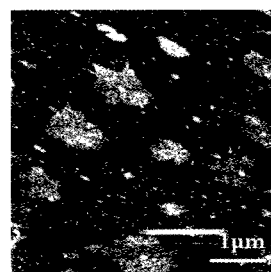


Fig 2 AFM image of graphene oxide using chloroform

Raman characterization of patterned graphene directly synthesized by alcohol chemical vapor deposition

○Yusuke Kito, Hiroya Yamauchi, Tomoya Kamizyukoku, Manabu Suzuki,
Takahiro Maruyama and Shigeya Naritsuka
*Department of Materials Science and Engineering, Meijo University,
1-501 Shiogamaguchi, Tempaku, Nagoya 468-8502, Japan*

Graphene has been attracting much attention from its superior characteristics [1]. For the sake of application, patterning of graphene is another important issue. We focus on a special technique, where the patterned catalyst is used to shape the graphene. To optimize conditions, both temperature and growth time are varied and the quality of the grown layers is characterized by Raman spectroscopy.

300nm-thick Ni catalyst deposited on a sapphire was patterned into small pieces with $20 \times 400 \mu\text{m}^2$ area using photolithography. After annealing the catalyst, graphene was grown with supplying ethanol vapor into H_2 ambient. Growth temperature and time were changed between 750 and 850 °C, and between 5 and 15 min, respectively.

Raman spectra in Fig.1 show not only D, G peaks but also G' peak, which indicates patterned graphene was successfully grown under these conditions. As shown in Fig.2, G'/G peak ratio decreased with time in the samples grown at 850°C. On the contrary, it stayed constant when the layer was grown at 750°C. In other words, the thickness of the graphene increased with time at 850°C but it stayed constant at 750°C. It is possibly explained by the penetration-impediment mechanism of carbon atoms through the graphene. The D/G peak ratio in Fig.3 suggests the improvement of the crystal quality during growth. The defect related peaks were recovered faster at higher temperature of 850°C.

[1] K.S.Novoselov et al., Science 306 (2994) 025102.

Corresponding author: Shigeya Naritsuka

Phone: +81-52-838-2386, Fax: +81-52-832-1172

E-mail: narit@meijo-u.ac.jp

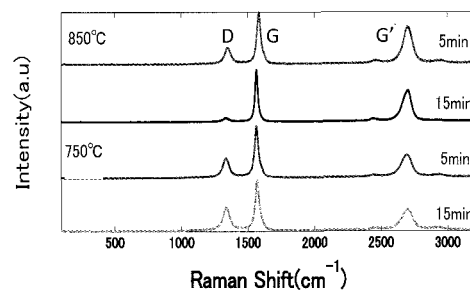


Fig.1 Raman spectra

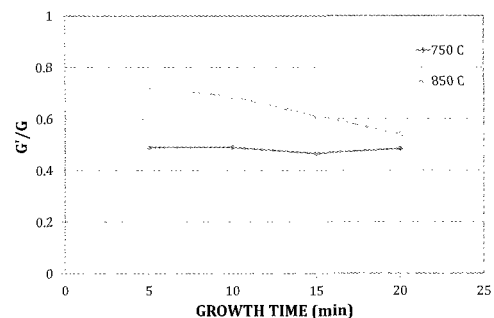


Fig.2 Raman G'/G peak ratio dependence on growth time.

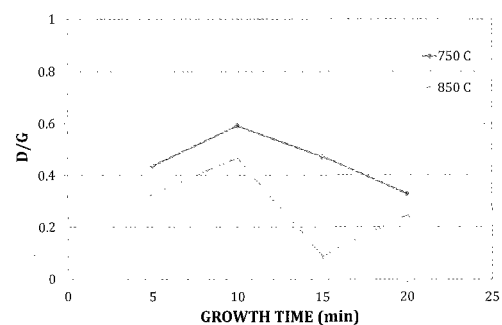


Fig.3 Raman D/G peak ratio dependence on growth time.

Characterization of interface between hexagonal graphene domains grown on hetero-epitaxial Cu films

○Yui Ogawa¹, Kenji Kawahara², Masahiro Miyashita¹, Masaharu Tsuji^{1,2}, Hiroki Ago^{1,2,*}

¹ Graduate School of Engineering Sciences, Kyushu University, Fukuoka, 816-8580, Japan

² Institute for Materials Chemistry and Engineering, Kyushu University, Fukuoka, 816-8580, Japan

CVD growth of graphene on Cu foil has been widely studied, because it enables large-scale single-layer growth with low cost. However, the CVD graphene grown on Cu foil is polycrystalline and has many domain boundaries due to the formation of a number of graphene nuclei with different orientations [1]. Since the domain boundaries limit the physical properties, it is very important to investigate the domain structure of CVD graphene [2,3]. We previously demonstrated the orientation-controlled growth of graphene by employing hetero-epitaxial Co and Cu films [4-6], but it is still unclear how the developing graphene domains merge together to form a uniform graphene film. Here, we report the detailed characterization of the interface of adjacent graphene domains (Figure 1).

Large hexagonal-shaped graphene domains were grown by ambient-pressure CVD with CH₄ on the hetero-epitaxial Cu(100) film and characterized by optical microscope, SEM, AFM, and Raman mapping measurements. The graphene domain shows two main relative orientations, 0° and 30°. Only when the orientation of neighboring domains is identical (0°, in the right merged domains of Figure 1), we observed defect and wrinkle-free interface. However, in some cases, a clear boundary was observed even for the 0° case, as was usually observed for the 30°-rotated domains. These results suggest that unifying orientation of graphene domains is a possible approach for the seamless atomic connection. We will also discuss the effect of domain boundary on carrier mobility. Our work is expected to offer a new approach for the synthesis of a single-crystalline graphene free from domain boundaries.

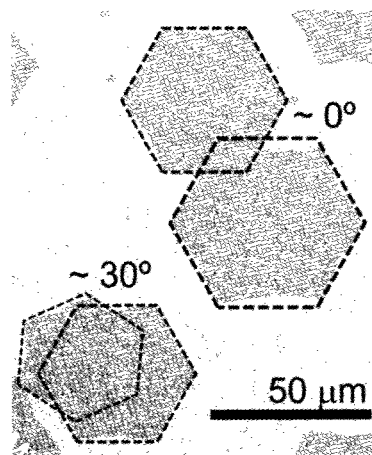


Figure 1 SEM image of two merged graphene domains. Angles between two domains are 0° (right) and 30° (left).

Reference;

[1] P. Y. Huang *et al.*, *Nature* **469**, 389 (2011). [2] Q. Yu *et al.*, *Nat. Mater.* **10**, 443 (2011). [3] C. M. Orofeo *et al.*, *Carbon* **50**, 2189 (2012). [4] H. Ago *et al.*, *ACS Nano* **4**, 1414 (2010). [5] B. Hu *et al.*, *Carbon* **50**, 57 (2012). [6] Y. Ogawa *et al.*, *J. Phys. Chem. Lett.* **3**, 219 (2012).

Corresponding Author: Hiroki Ago (Tel&Fax: +81-92-583-7817, E-mail: ago@cm.kyushu-u.ac.jp)

CVD Growth of Mono- and Bi-Layer Graphene from Ethanol

○Xiao Chen, Pei Zhao, Bo Hou, Shohei Chiashi and Shigeo Maruyama

Department of Mechanical Engineering, The University of Tokyo, Tokyo 113-8656, Japan

Graphene, a monolayer of sp^2 -bonded carbon atoms with a honeycomb structure, has triggered numerous fundamental studies due to its unique properties such as superb mechanical strength and quantum transport. Due to the fact that mechanically-exfoliated graphene [1] cannot fulfill the practical requirement of electronic applications, the development of large-scale, high-quality graphene production methods have been motivated. Among these methods, chemical vapor deposition (CVD) on polycrystalline metal substrates has attracted most attention recently, because of its low cost and operation simplicity. Many kinds of carbon precursors have been employed to synthesize graphene, such as methane [2], ethane [3] and ethanol [4]. Here we report a systematic study on CVD growth of graphene on Cu and Ni substrates from ethanol. Ethanol has proven effective in the synthesis of high-purity single-walled carbon nanotubes [5], and it is expected that these advantages would also apply in the synthesis of graphene.

Results show that compared with widely-used methane, ethanol is also capable of synthesizing high-quality, large-scale graphene. Figure 1 shows the scanning electron microscope (SEM) images of graphene on metal substrates. We investigated the growth parameters for Cu substrate, to show that precise

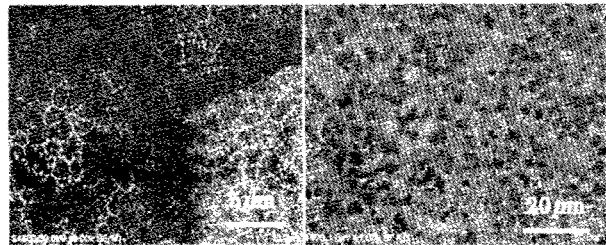


Fig.1 SEM image of graphene on Cu (left) and Ni (right).

layer control (mono- or bi-layer) can be achieved. To explain these results, we conducted carbon isotope CVD experiments, using $^{12}C_2H_5OH$, $^{13}C_2H_5OH$, and $^{13}CH_3^{12}CH_2OH$ precursors and Raman spectroscopy to track carbon atoms. Based on these experiments, we propose the growth mechanism models of graphene growth on both Cu and Ni substrates.

[1] K. S. Novoselov, A. K. Geim, *et al.*, *Science* **306**, 666 (2004).

[2] A. Reina, *et al.*, *Nano Lett.* **9**, 30 (2008).

[3] J. Coraux, *et al.*, *Nano Lett.* **8**, 565 (2008).

[4] Y. Miyata, *et al.*, *Appl. Phys. Lett.* **96**, 263105 (2010).

[5] S. Maruyama, *et al.*, *Chem. Phys. Lett.* **360**, 229 (2002).

Corresponding Author: S. Maruyama

Tel: +81-3-5841-6421, Fax: +81-3-5841-6408,

E-mail: maruyama@photon.t.u-tokyo.ac.jp

Direct growth of hexagonal domain graphene on SiO₂ substrate

○Toshiaki Kato, Rikizo Hatakeyama, Toshiro Kaneko

Department of Electronic Engineering, Tohoku University, Sendai 980-8579, Japan

Graphene is a monolayer carbon sheet including high carrier mobility, flexibility, and high optical transmittance [1]. These properties are advantageous if graphene is to be used as a component in electrical devices such as field effect transistors, solar cells, and various gas and chemical sensors. Chemical vapor deposition (CVD) is one of the most promising methods of growing graphene, which can produce large, relatively high-quality graphene sheets. However, the graphene growth by CVD is limited only to the metal catalyst surfaces such as Ni, Cu, or Co, which is one of the most serious problems for the practical application of graphene as electrical devices. Thus, the development of the method for the direct growth of graphene on the insulating substrate, especially on a SiO₂ substrate, is highly required.

Recently, we have established a novel, simple, and scalable method for the direct growth of graphene on the insulating substrate by plasma CVD [2]. It is revealed that by adjusting the growth parameters using plasma CVD, the graphene layer can be grown along the interface of the Ni layer and the SiO₂ substrate instead of on top of the Ni layer. After removing the top Ni layer, high-quality single- or few-layer graphene sheets are found to be directly grown on the entire substrate area in large scale (10 × 10 mm). Interestingly, at the initial growth stage, the hexagonal domain structure of graphene can be observed in our method. Since the hexagonal domain graphene structure should appear only when graphene has a single domain structure, it can be possible to realize a direct growth of single domain large scale graphene on a SiO₂ substrate with our established novel approach.

- [1] Toshiaki Kato, Liying Jiao, Xinran Wang, Hailiang Wang, Xiaolin Li, Li Zhang, Rikizo Hatakeyama, and Hongjie Dai, *Small* 7, 574 (2011).
- [2] Toshiaki Kato and Rikizo Hatakeyama, Abstracts of the 42nd Fullerenes-Nanotubes-Graphene General Symposium, p 37 (2012).

Corresponding Author T. Kato

E-mail: kato12@ecei.tohoku.ac.jp

Tel&Fax: +81-22-795-7046 / +81-22-263-9225

First-Principles Study of Carbon-Impurity States in Hexagonal Boron-Nitride Monolayer

○Yoshitaka Fujimoto, Takashi Koretsune, and Susumu Saito

Department of Physics, Tokyo Institute of Technology, Tokyo 152-8551, Japan

Two-dimensional hexagonal boron-nitride (h-BN) monolayer is a fascinating material from the viewpoint of basic nanophysics and potential applications in nanoelectronics because of having large band gap. The substitutional doping with impurities often offers the new route to tune the electronic properties such as modulation of band gap and enhancement of electrical conductivity. The carbon doping into h-BN monolayer has been implemented using electron beam irradiation [1], and it was found that the electronic properties of h-BN monolayer are changed from insulating to metallic [2]. It was also found that boron atoms in h-BN monolayer sheet are usually replaced by carbon atoms under substitutional-doping processes. Therefore, the electronic structure of the C-doped h-BN sheet, where a boron atom is substituted with a carbon atom, should generate donor states below the conduction-band minimum.

In this work, we study the electronic structures of carbon-donor-states of h-BN monolayer sheet using first-principles density-functional calculations (Fig. 1). In the presentation, we show the relationship between strain effects and donor states of C-doped h-BN monolayer. It is found that the impurity states become relatively shallow states when biaxial strains are applied. Especially, the compressive strains cause donor states to move considerably toward the conduction-band minimum. We also discuss how the relationship between the donor states and the conduction-band minimum is determined.

This work was partly supported by grants-in-aid from MEXT Japan through Global Center of Excellence Program of Nanoscience and Quantum Physics of Tokyo Institute of Technology.

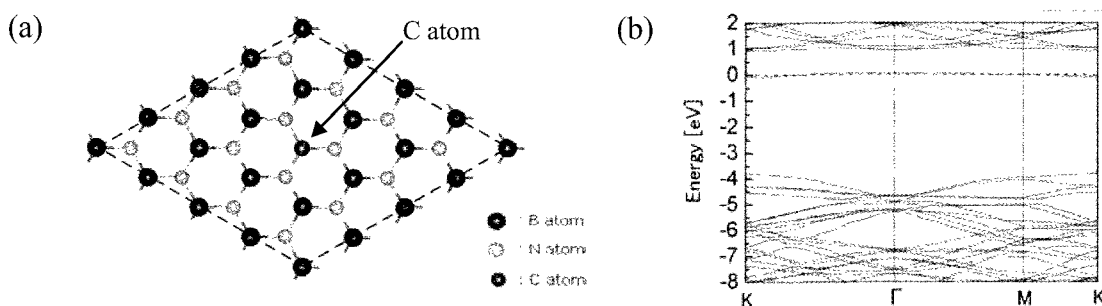


Figure 1 (a) Atomic geometry and (b) energy band of carbon impurity in hexagonal boron-nitride monolayer.

[1] O. L. Krivnek, M. F. Chisholm, V. Nicolosi, T. J. Penycook *et al.*, *Nature* **464**, 571 (2010).

[2] X. Wei, M. S. Wang, Y. Bando, and D. Golberg, *ACS Nano* **5**, 2916 (2011).

Corresponding Author: Yoshitaka Fujimoto

TEL: +81-3-5734-2368, FAX: +81-3-5734-2368, E-mail: fujimoto@stat.phys.titech.ac.jp

Electronic Structures of Bilayer Graphene under Electric Field

Satoru Konabe and Susumu Okada

Graduate School of Pure and Applied Sciences, University of Tsukuba, 1-1-1 Tennodai, Tsukuba, Ibaraki 305-8571, Japan

Graphene and graphite thin films are now considered to be key materials for electronic devices in the next generation due to their perfectly planner atomic network structure and a remarkable high carrier mobility. Graphene is a metal with a vanishing density of states at the Fermi energy due to the emergence of two linear dispersion curves at the Fermi level. These linear dispersion bands lead to massless electrons near the Fermi energy, which makes for a rich variety of interesting physics in these systems. On the other hand, it is urging us to realize graphene-based structures with finite fundamental gap for its semiconductor device usage. Indeed, It has been demonstrated that the electronic structure of graphene is tunable by forming the bilayer structures. For instance, bilayer graphene is a metal, a semimetal, and a semiconductor depending on the mutual stacking arrangements[1]. Furthermore, the external electric field can tune the electronic structure of bilayer graphene with Bernal (AB) stacking arrangement [2]. Therefore, the bilayer graphene with AB stacking is now considered to be the possible candidates for a constituent of semiconductor electronic devices. In this paper, based on the density functional theory with the effective screening medium method, we theoretically study the electronic structure of bilayer graphene under an electric field with various stacking arrangements, since both the electric field and the mutual stacking arrangement are essential and important for designing the device properties of bilayer-graphene.

We found that the bilayer graphene with AB stacking arrangement under an electric field is a semiconductor with small direct energy gap around the K point. The calculated gap energy strongly depends on the field strength: The gap monotonically increase with increase of the electric field and then saturate 0.25 eV at about 0.5 V/Å. In sharp contrast, electronic structure of bilayer graphene with the other stacking arrangements, i.e. AA, bridge, hollow, and rotation (Fig. 1), does not depend on the external electric field. Bilayer graphene with AA, bridge, hollow, and rotation stacking arrangements are a metal, a semiconductor, a semimetal, and a metal, respectively [1]. By applying the electric field, these bilayer graphene almost keep their electronic structure without external field.

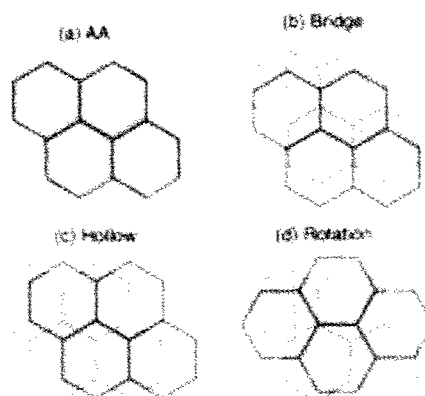


Fig. 1, Geometric structures of bilayer graphene. Black and gray lines denote the graphene network for upper and lower layers, respectively.

References

- [1] S. Okada and T. Kobayashi, *pJn. J. Appl. Phys.* **48** (2009) 050207.
 [2] M. Otani and S. Okada, *J. Phys. Soc. Jpn.* **79** (2010) 073701.

Satoru Konabe

Phone: +81-29-853-5600(ext.8233), E-mail: konabe@comas.frsc.tsukuba.ac.jp

Raman scattering study on the X-ray irradiation effect of graphene

○Toshiya Murakami¹, Kazuki Yamazaki¹, Susumu Kamoi², Noriyuki Hasuike²,
Hiroshi Harima², Kenji Kisoda³, Chihiro Itoh¹

¹Department of Material Science, Wakayama University, Wakayama, 640-8510, Japan

²Department of Electronics, Kyoto Institute of Technology, Kyoto 606-8585, Japan

³Department of Physics, Wakayama University, Wakayama, 640-8510, Japan

Graphene is one of the promising materials for future-nano-electronic devices due to its unusual electronic property. Because of strong interplay between structure and electronic states in graphene, structural modification changes its electronic properties.[1] To realize graphene-based devices, the defect formation in sp^2 carbon network is an important technique to modify the local structure of graphene. Although defects on graphene induced by electron beam irradiation has been studied,[2] the primary process and dynamics are not fully understood. In contrast, because the excitation process of X-ray is dominated by inner-core excitation, it is easy to control the defect in graphene.

Here, we report the results of Raman scattering study on X-ray irradiation effect of graphene. Graphene samples grown by CVD method on the Cu/MgO(100) substrates were irradiated by soft X-ray (277 eV). Figure 1 shows Raman spectra of the as-grown and the X-ray irradiated graphene. The X-ray irradiation enhanced D bands. The enhancement demonstrates that X-ray irradiation generates defects in graphene. Furthermore, we found X-ray irradiation led to low frequency-shift of 2D band. Because of the strong correlation between the excitation process of 2D band and the electronic structure of graphene, this frequency-shift suggests the X-ray irradiation modifies the electronic structure of graphene.

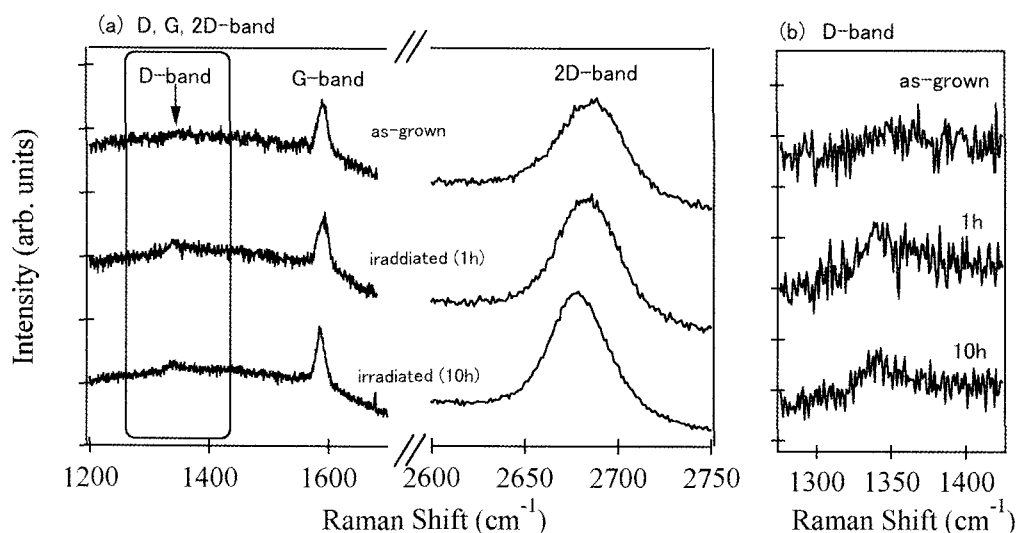


Figure 1 Raman spectra of the as grown and the X-ray irradiated graphene.

[1] Y. W. Son, et. al., Phys. Rev. Lett. **97** (2006) 216803

[2] D. Teweldebrhan, et. al., Appl. Phys. Lett. **94** (2009) 013101

Corresponding Author: T. Murakami

Tel: +81-73-457-8532

E-mail: murakami@sys.wakayama-u.ac.jp

Edge Effects on Thermoelectric Power of Graphene Nanoribbons: First-Principles Simulation

○Teppei Kato¹, Shinji Usui², Takahiro Yamamoto^{1,3}

¹*Dept. of Electrical Engineering, Tokyo Univ. of Science, Chiyoda-ku, Tokyo 102-0073, Japan*

²*QuantumWise Japan KK, Shinjuku-ku, Tokyo 160-0023, Japan*

³*Dept. of Liberal Arts, Tokyo Univ. of Science, Chiyoda-ku, Tokyo 102-0073, Japan*

Graphene nanoribbons (GNRs) are expected to be potential candidates for new functional materials because of their novel physical properties originating from edge structures of GNRs. In this work, we systematically investigated the thermoelectric power of GNRs with zigzag-type edges (ZGNRs) using Atomistix ToolKit 12.2.0 [1,2] combined with Esfarjani's method [3]. The definition of ZGNR structure is shown in Fig.1(a).

Figure 1(b) displays the calculated thermoelectric powers $S(E)$ of ZGNRs with various widths as a function of electron energy E . In the regimes of $|E| > 1\text{eV}$, sharp peaks appear at the energy corresponding to lowest energy sub-band edge. In addition, the sign of these peaks is positive for $E > 1\text{eV}$, whereas negative for $E < 1\text{eV}$. In other words, the carrier is electron for $E > 1\text{eV}$, whereas hole for $E < 1\text{eV}$.

These results are similar to our previous results for GNR with armchair-type edges (AGNRs) [4]. The inset of Fig. 1(b) shows $S(E)$ of ZGNTs near the Fermi energy. The sign of $S(E)$ is negative in the $E > 0$ regime and is positive in the $E < 0$ regime. This is opposite to the higher energy regime of $|E| > 1\text{eV}$. Moreover, we found that the low-energy $S(E)$ is remarkably varied for $n=3$ to 6, while is not for $n \geq 7$. These results can be understood from the energy-band structures of the edge states.

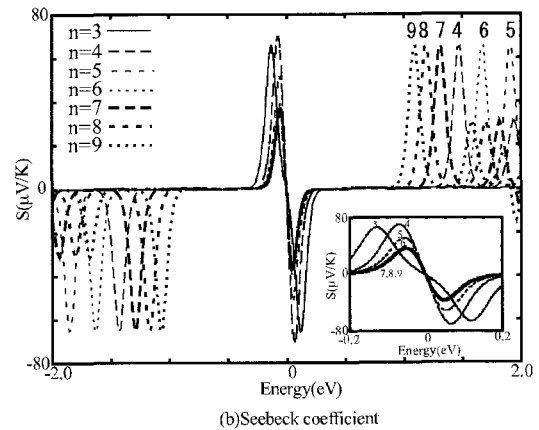
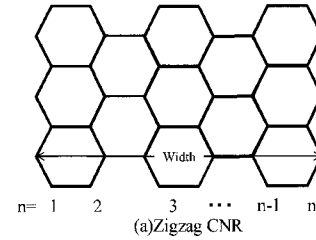


Fig.1 (a) Definition of the width of ZGNRs (b) Thermoelectric powers of ZGNR with various widths.

[1] <http://www.quantumwise.co.jp>

[2] M. Brandbyge, et al., *PRB* **65**, 165401 (2002)

[3] K.Esfarjani, M. Zebarjadi, and Y. Kawazoe, *PRB* **73**, 085406 (2006)

[4] 26pPSB-60, The 67th annual JPS meeting

Corresponding Author: Takahiro Yamamoto

Tel&FAX: +81-3-5213-0990,

E-mail: takahiro@rs.tus.ac.jp

Wave Packet Dynamics Simulations on Electrical Conduction in Graphene Nanoribbons

Yukihiro Takada¹, ○Kengo Takashima², Takahiro Yamamoto¹

¹ *Department of Liberal Arts, Tokyo University of Science, Tokyo, 102-0073, Japan*

² *Department of Electrical Engineering, Tokyo University of Science, Tokyo, 102-0073, Japan*

Nanocarbon materials consisting of hexagonal network of carbon atoms, such as carbon nanotubes (CNTs) and graphene, have been widely intrigued by their fascinating electronic properties. The electronic transport in such hexagonal network systems displays unusual features in apparent conflict with the common view that low-dimensional systems are generally subject to Anderson's localization. For example, both metallic CNTs and graphene nanoribbons (GNRs) are demonstrated the presence of perfectly conducting channel even in the presence of impurities, when the impurity potential range is much longer than the C-C bond length [1-3]. On the other hand, they show Anderson's localization in the presence of short-ranged impurities that cause scattering between K and K' points. Although the underlying physics of impurity scattering effects have been discussed in detail thus far [1-3], the impurity-concentration dependence of the mean free path and localization length of CNTs and GNRs with short-ranged impurities, which are important for materials design, has not been clarified yet.

In this study, we systematically investigate the electronic transport properties of GNRs using the wave-packet dynamics method, focusing particularly on the impurity concentration and ribbon width dependence [4, 5]. We describe Hamiltonian of GNRs by the nearest-neighbor π -orbital tight-binding model. In wave-packet dynamics simulations for quantum transport calculation, we numerically solve the time-dependent Schrödinger equations under several initial conditions and obtain the time-developed wave functions at each time step. The wave-packet dynamics simulation enables us to treat long GNRs with micrometer length, which are comparable to realistic GNR lengths. Details of our simulation results will be discussed in the presentation.

[1] T. Ando, and H. Suzuura, *J. Phys. Soc. Jpn.* **71**, 2753 (2002).

[2] K. Wakabayashi, Y. Takane, and M. Sigrist, *Phys. Rev. Lett.* **99**, 036601 (2007).

[3] M. Yamamoto, Y. Takane, and K. Wakabayashi, *Phys. Rev. B* **79**, 125421 (2009).

[4] Y. Takada *et al.*, *Jpn. J. Appl. Phys.* **51**, 02BJ01 (2012).

[5] H. Ishii, N. Kobayashi, and K. Hirose, *Appl. Phys. Lett.* **1**, 123002 (2008).

Corresponding Author: Y. Takada

Tel & FAX: +81-3-5123-0990,

E-mail: ytakada@rs.tus.ac.jp

Multiple Dirac points of graphene on a quasiperiodic superlattice

○Masayuki Tashima¹ and Naomichi Hatano²

¹ *Department of Physics, The University of Tokyo, Komaba, Meguro, Tokyo 153-8505, Japan*

² *Institute of Industrial Science, The University of Tokyo, Komaba, Meguro, Tokyo 153-8505, Japan*

We report the appearance of new Dirac cones in the energy spectrum of graphene superlattice under an external quasiperiodic potential. Park *et al.* reported that new Dirac cones appear around the original Dirac point in the energy spectrum of graphene under a periodic potential [1]. The positions of the new cones were given by the period of the potential. We have discovered much more Dirac cones for graphene under a *quasiperiodic* potential.

The new Dirac cones are of strong interest for fundamental study as well as for application of assembling nano structure of graphene. However, calculation of the energy spectrum of graphene under a complicated potential is necessary for further development. For this purpose we develop a new method of solving the eigenvalue problem of the first-order differential Hamiltonian and apply the method to the study of the energy spectrum of graphene under a quasiperiodic potential.

Suppose that the potential consists of two terms.

$$H = H_0 + V_1 + V_2 \quad (1)$$

We first solve the eigenvalue problem of a separated Hamiltonian with each potential term.

$$H_1 = H_0 + V_1 \quad , \quad H_1 \psi_1 = E_1 \psi_1 \quad (2.a)$$

$$H_2 = H_0 + V_2 \quad , \quad H_2 \psi_2 = E_2 \psi_2 \quad (2.b)$$

The eigenvalue of the original Hamiltonian is given by the summation of the eigenvalues of the separated Hamiltonians and its eigenstate is given by the multiplication of the eigenstates of the separated Hamiltonian.

$$H\psi = E\psi \quad (3.a)$$

$$\psi = \psi_1 \psi_2 \quad , \quad E = E_1 + E_2 \quad (3.b)$$

If the Hamiltonian has a quasiperiodic potential, which can be written as the summation of periodic potentials whose periodicities are mutually irrational, we first solve the eigenvalue problems of the Hamiltonians with each periodic potential to obtain the final answer. We note that this method is only applicable to the first-order differential Hamiltonian. It is a generalization of a calculation for the Floquet operator [2].

We apply the above method to the study of a graphene under an external quasiperiodic superlattice potential. We especially focus on the effect of quasiperiodicity to the energy spectrum. We predict that many new Dirac cones appear in the energy spectrum and their positions reflect the quasiperiodicity of the external potential.

[1] C. -H. Park *et al.* Phys. Rev. Lett. **101**, 126804 (2008).

[2] A.G. Fainshtein *et al.* Phys. Rep. **210**, 111-221 (1992).

Corresponding Author: M. Tashima

Tel: +03-5452-6154, Fax: +03-5452-6155,

E-mail: tashima@iis.u-tokyo.ac.jp

Sheet resistivity for nitrogen doped graphene film grown on Cu foil by sonication mist CVD

○Takahiro Mizuno, Morio Takizawa[†], Shunji Bandow

*Department of Materials Science and Engineering, Meijo University,
1-501 Shiogamaguchi, Tenpaku, Nagoya 468-8502, Japan*

[†]*Sekisui NanoCoat Technology, 36 Hama-machi, Gamagohri 443-8623, Japan*

In many electronic devices, transparent conductive films are used as touch panel for signal input and solar cell for light transmission, so on. Nowadays, most of the transparent conductive films are made of ITO, and hence serious problem occurs on stable supply of rare indium metal. In order to settle out this problem, graphene is attracted as an exchangeable material to make transparent conductive films. For the use of transparent conductive film, low sheet resistivity as low as a few hundreds Ω/sq with visual light transmittance better than 80 % are required. Although there are several papers reporting the attainment of these hurdle values [1,2], it still remains reproducibility problem.

One effective way to decrease sheet resistivity of graphene is to dope hetero atoms to the carbon network. Nitrogen doping is a candidate and there are several papers reporting the evidence of nitrogen doping [3,4]. However, systematic study on the sheet resistivity against the doping rates of nitrogen has not been achieved so far. In the present study, we introduce a newly developed method of sonication driven mist CVD method for preparing nitrogen doped graphene on Cu foil. Preparation details will be explained in the poster. Essence of this technique is to use methanol (MeOH) solution including nitrogen source. Here we used methylated melamine resin (Sanwa Chemicals, MW-30) as a nitrogen source and its concentration in MeOH is widely varied between 0.001 and 2 %. Growth of nitrogen doped graphene is conducted at 925 °C with mist inlet rate of 0.4 mL/min under 3% H₂/Ar flow of 1.3 L/min for 2 min. Sheet resistivity was measured by 4-terminal method by using chemically peeled film on quartz plate and the transmittance was measured in the UV visible region. From the magnitude of transmittance at 550 nm, we evaluated the number of layers. Figure 1 represents normalized sheet resistivity (sheet resistivity per one graphene sheet) with respect to melamine concentration in MeOH as a mist source liquid. Interestingly, one can find that the magnitude of sheet resistivity drops around 0.01 % melamine region, suggesting that effective nitrogen doping for reducing the sheet resistivity can be realized only in narrow window region.

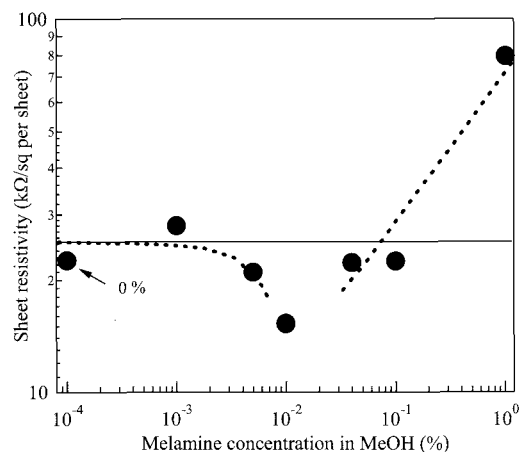


Fig.1. Change of normalized sheet resistivity against melamine concentration in MeOH liquid for mist generation.

[1] X. Li *et al.*, *Nano Lett.* **9**, 4359 (2009).

[2] S. Bae *et al.*, *Nature Nanotech.* **5**, 574 (2010).

[3] Y. Wang *et al.*, *ACS Nano* **4**, 1790 (2010).

[4] H. Wang *et al.*, *ACS Catal.* **2**, 781 (2012).

Corresponding Author: Shunji Bandow, **E-mail:** bandow@meijo-u.ac.jp, **Tel&Fax:** +81-52-834-4001

Simulated Image of Suspended Graphene by Helium Ion Microscope

○Yoshiyuki Miyamoto

Nanosystem Research Institute, AIST, Central 2, 1-1-1 Umezono, Tsukuba, 305-8568, Japan

Non-destructive measurement is demanded for analyzing nano-scaled structure. Recent advent of helium ion microscope (HIM) [1] open a new way for material characterization without sample preparation before the measurement. Intensity of secondary emitted electrons is monitored as a function of impact point of the scanned He^+ ion beam. With the narrowest beam size 0.25 nm[1], one can expect to take lattice image of graphene whose hexagonal pattern has diameter of 0.28 nm.

In this presentation, the intensity of secondary emitted electron depending on the impact point of the He^+ ion on a suspended graphene sheet was estimated by means of the first-principles molecular dynamics (MD) based on the time-dependent density functional theory (TDDFT) by using a code *FPSEID*[2].

Fig.1 (a) shows several impact point of the He^+ ion with incident kinetic energy of 30 KeV as same as experimental condition[1]. A significant difference in intensities of secondary emitted electrons depending on the impact point was obtained by TDDFT-MD simulation which suggests a possibility of taking an image of hexagonal pattern of the graphene as a schematic of Fig. 1 (b).

Details of computational conditions and mechanisms of electron emission upon He^+ collision will be discussed.

All calculations were done by using the Earth Simulator. This work was performed under collaboration with Prof. H. Zhang and Prof. A. Rubio. The author is supported by Research Organization of Information Science and Technology at Tokyo Office.

[1] B. M. Ward *et al.* *J. Vac. Sci. Tech.* **B24**, 2871 (2006).

[2] O. Sugino and Y. Miyamoto, *Phys. Rev.* **B59**, 2579 (1999); **B66**, 089901(E) (2002).

Corresponding Author: Y. Miyamoto

Tel: +81-29-849-1498, Fax: +81-29-861-3171,

E-mail: yoshi-miyamoto@aist.go.jp

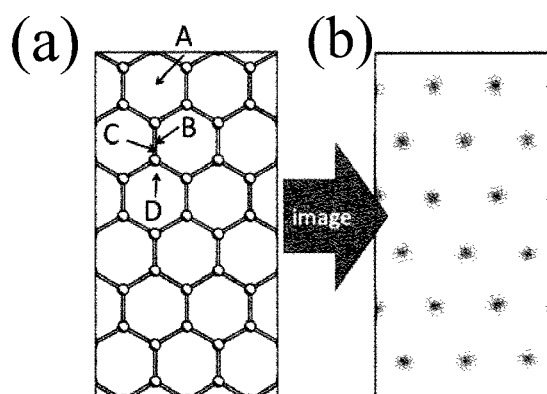


Fig.1 (a) Impact points A-D tested by current simulation. (b) Schematic of the image obtained by intensity profile of secondary emitted electron as a function of the impact points.

Lattice matching and band gap opening in graphene and h-BN stacked thin films

○Yuki Sakai and Susumu Saito

*Department of Physics, Tokyo Institute of Technology
2-12-1 Oh-okayama, Meguro-ku, Tokyo 152-8551, Japan*

Graphene and hexagonal boron nitride (h-BN) based heterostructures have been intensively studied both experimentally and theoretically in recent years. For instance, tunnel currents between two graphene monolayers through h-BN layers have been studied [1]. It has been also demonstrated that new Dirac points appear in graphene on h-BN substrate due to the periodic potential of h-BN [2]. In parallel with these experimental studies, we have investigated geometries and electronic properties of three-dimensional graphene/h-BN superlattices within the framework of the density functional theory [3-5]. Stable stacking sequences of the superlattices have been identified. In addition, interesting electronic properties of these superlattices have been revealed. On the other hand, thin films composed of finite layers of graphene and h-BN layers should be also important systems. Theoretically, it has been suggested that a graphene/h-BN stacked finite layer system could have a finite band gap due to broken symmetry in graphene layers [6, 7]. Although there is an intrinsic difference in in-plane lattice constants of graphene and h-BN, lattice matching between graphene and h-BN layers is assumed in these works. The lattice matching should be an important issue to be addressed since whether the lattice matching could occur or not is non-trivial. In this work, we address this important issue within the framework of the density functional theory. To the best of our knowledge, relative stabilities of commensurate phases with lattice matching and incommensurate phases without lattice matching of graphene/h-BN thin films are not fully understood except for bilayer systems composed of graphene and h-BN monolayer [8]. We thus study relative stabilities of commensurate and incommensurate phases of thin film systems. It is found that interlayer binding energy values of commensurate and incommensurate phases increase as the number of layers increases. The energy difference between the two phases is also found to exhibit a similar dependence on the layer number. We also report electronic properties of these thin film systems. Some commensurate phases are found to possess finite band gaps whereas an induced band gap should be almost canceled out in incommensurate phases.

- [1] L. Britnell, *et al.* Nano Lett. **12**, 1707 (2012)
- [2] M. Yankowitz, *et al.* Nature Phys. **8** 382 (2012)
- [3] Y. Sakai, T. Koretsune, and S. Saito, Phys. Rev. B **83**, 205434 (2011)
- [4] M. Sakurai, Y. Sakai, and S. Saito, J. Phys. Conf. Ser. **302**, 012001 (2011)
- [5] Y. Sakai and S. Saito, Mater. Res. Soc. Symp. Proc. **1407**, 1407-AA08-03 (2012)
- [6] G. Giovannetti *et al.* Phys. Rev. B **76**, 073103 (2007)
- [7] R. Quhe *et al.* NPG Asia Mater., **4**, e6 (2012)
- [8] B. Sachs *et al.* Phys. Rev. B **84**, 195414 (2011)

Corresponding Author: Y. Sakai

E-mail: y-sakai@stat.phys.titech.ac.jp

Synthesis and Optical Properties of Graphene Quantum Dots

oNaoto Fuyuno¹, Daichi Kozawa¹, Yuhei Miyauchi^{1,2}, Shinichiro Mouri¹, and Kazunari Matsuda¹

¹*Institute of Advanced Energy, Kyoto University, Uji, Kyoto 611-0011, Japan*

²*Japan Science and Technology Agency, PRESTO, 4-1-8 Honcho Kawaguchi, Saitama 332-0012, Japan*

Graphene quantum dots (GQDs), which are edge-bound nanometer-size graphene pieces, have attracted a great deal of interest from the viewpoints of fundamental physics and optical device application. The optical properties of GQDs have not been well understood because the synthesis of GQDs was difficult. Recently, however, Peng *et al.* reported a simple method to synthesize GQDs by means of acid treatment of pitch-based carbon fibers [1]. For further investigation of optical properties of GQDs, it is important to control the size, because the optical properties are expected to strongly depend on the size due to the quantum confinement effect.

In the present study, we synthesized the GQDs by the acid treatment of carbon fibers with changing the reaction time and temperature to control the size of the GQDs and investigated how the size affects the optical properties. Figure 1 shows photoluminescence (PL) and absorption spectra of the GQDs treated in an acid for 16 (GQDs-16h) and 48 hours (GQDs-48h) at 80 °C. The broad absorption peaks of the GQDs are observed. The PL peaks are observed around 2.2 eV at the excitation energy of 3.54 eV. The energy positions slightly shift from 2.19 eV for GQDs-16h to 2.32 eV for GQDs-48h. The energy peak shift is attributed to the different size of GQDs because the confinement energy could be larger for small GQDs, and the longer reaction time makes the size of the GQDs smaller due to deeper etching by an acid. These results indicate that the PL emission energy can be controlled through the size change of the GQDs by the reaction time.

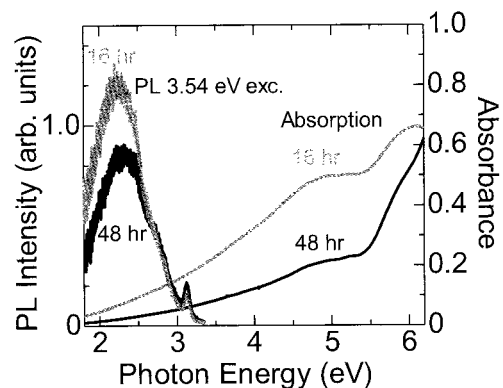


Fig. 1 PL and absorption spectra of GQDs synthesized at 80 °C with different reaction times. The PL spectra were measured separately in the high (> 2.48 eV) and low energy range.

[1] J. Peng *et al.*, *Nano letters* **12**, 844 (2012).
Corresponding Author: N. Fuyuno
Tel: +81-774-38-3465, Fax: +81-774-38-3467,
E-mail: fuyuno.naoto.67n@st.kyoto-u.ac.jp

First-principles study on geometries and electronic structures of halogen-terminated armchair graphene nanoribbons

○Hideyuki Jippo and Mari Ohfuchi

Fujitsu Laboratories Ltd., 10-1 Morinosato-wakamiya, Atsugi, Kanagawa 243-0197, Japan

Graphene nanoribbons (GNRs) have attracted attention as promising nanostructures for electronic applications of graphene. Although graphene itself is a semimetal, GNRs can open up a finite band gap as a function of the ribbon width. Recently the bottom-up approach to atomically precise fabrication of armchair GNRs (AGNRs) has been reported [1]. This approach also enables us to produce AGNRs with intended edge termination. In theoretical point of view, hydroxyl group (OH)-terminated AGNRs have been studied with first-principles methods [2]. In this article, we investigate AGNRs terminated by halogen atoms such as fluorine (F) and chlorine (Cl) using density functional theory, because they are likely to be realized by the bottom-up approach.

We examine H-, F- and Cl-terminated AGNRs (H-AGNRs, F-AGNRs and Cl-AGNRs) with widths $N = 7$ and 19. We have found the most stable geometries of H-AGNRs have a planar configuration, but those of F- and Cl-AGNRs have rippled edges, where the pairs of halogen atoms are displaced up and down alternately, as shown in Fig. 1. The ripples are strongly localized to the edges and almost the same between the ribbons for $N = 7$ and 19. The difference in the height of the halogen atoms is 1.84 Å for F-AGNRs and 2.96 Å for Cl-AGNRs. This rippled structure has been already found for hydroxyl group-terminated AGNRs [2]. We next evaluate the termination energy per termination atom E_T . We have found that the most stable termination is brought about by F atoms ($E_T(\text{F}) - E_T(\text{H}) = -1.7$ eV; $E_T(\text{Cl}) - E_T(\text{H}) = 0.1$ eV). We also investigate their energy band structures. The energy band gaps of H-, F- and Cl-AGNRs are 1.56, 1.10 and 1.16 eV for $N = 7$ (see Fig. 2) and 0.59, 0.44 and 0.51 eV for $N = 19$. The energy band gaps of F- and Cl-AGNRs are narrower than those of H-AGNRs, but wider than those of OH-AGNRs (0.8 eV for $N = 7$ and 0.3 eV for $N = 19$ [2]).

In summary, halogen-terminated AGNRs ($N = 7$ and 19) have edge ripples and their energy band gaps are narrower than those of H-terminated AGNRs.

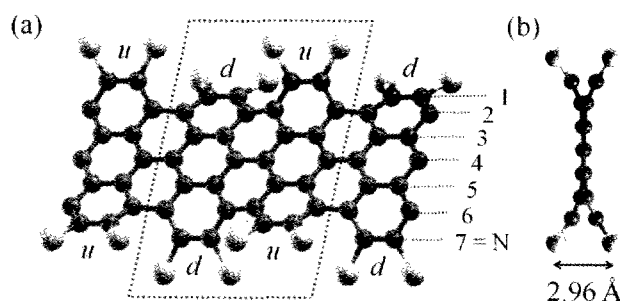


Fig.1. (a) Perspective and (b) side views of the most stable geometry for Cl-terminated armchair graphene nanoribbon with a width $N = 7$. The dark and light gray spheres represent C and Cl atoms, respectively. The symbols of u and d stand for “up” and “down” for the rippled edge, respectively. The unit cell is indicated by the dotted lines.

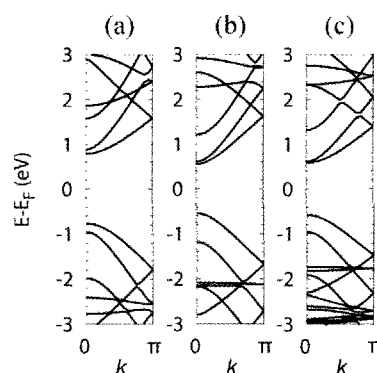


Fig.2. Energy band structures of (a) H-, (b) F- and (c) Cl-terminated armchair graphene nanoribbons with a width $N = 7$.

[1] J. Cai *et al.*, Nature **466**, 470 (2010). [2] P. Wagner, *et al.*, Phys. Rev. B **84**, 134110 (2011).

Corresponding Author: H. Jippo

Tel: +81-46-250-8843, Fax: +81-46-250-8274, E-mail: jippo.hideyuki@jp.fujitsu.com

Novel spintronic phenomena arising from pore-edge polarized spins of ferromagnetic graphene nanomeshes

○N. Kosugi, Y. Hashimoto, K. Sakuramoto, K. Takeuchi, S. Kamikawa, Y. Yagi, J. Haruyama, G. Hashimoto¹, K. Fujita¹, Y. Kato¹, S. Katsumoto¹, Y. Iye¹, P. Zhao², S. Maruyama², A. Rao³,
Faculty of Science and Engineering, Aoyama Gakuin University, 5-10-1 Fuchinobe,
Sagamihara, Kanagawa 252-5258, JAPAN

¹Institute for Solid State Physics, Tokyo University, 5-1-5 Kashiwanoha, Chiba
277-8581, JAPAN

²Tokyo University, 7-3-1 Hongo, Bunkyo-ku, Tokyo 113-8656 Japan

³Clemson University, Dept. Chemistry, Clemson, SC 29634, USA

Abstract: A variety of exciting phenomena has been experimentally reported in graphenes, while mostly none has experimentally reported on edge-related issues. There are two kinds of atomic structures in graphene edges; arm chair [1] and zigzag edges. Theoretically, zigzag edge yields a flat energy band, which makes electrons localize around the edge. The localized electrons are spontaneously spin-polarized due to strong electron interaction arising from extremely high electron density of states (edge states). It realizes research of spin-based phenomena and those applications to novel spintronic devices, interestingly in spite of a material consisting of only carbon atoms with sp^2 orbitals. However, it is difficult to experimentally observe edge-spin-related phenomena, because lithographic fabrication of graphene edges easily introduces disorder, defects, and damages.

In contrast, we have, for the first time, found a large-amplitude ferromagnetism [2] and related spin-phenomena (anomalous magnetoresistance(MR) oscillations) [3] arising from hydrogen-terminated zigzag-pore edges of 1~5-layer graphene nanomeshes with honeycomb like arrays of low-defect hexagonal nanopores, which were fabricated by non-lithographic method using nano-porous alumina template as an etching mask. Here, in the poster, we will present novel spin-based phenomena observed in the above-mentioned ferromagnetic graphene nanomeshes with different structures. Increasing the inter-pore spacing (e.g., from 20nm to 30 nm and 40 nm) allows emission of polarized spins localizing at the pore edges to bulk regions. In the samples, we observe ferromagnetic-like hysteresis loops and spin pumping effect (saw-tooth like MR oscillations) for magnetic fields applied perpendicular to the graphene plane and parallel with the plane, respectively. The correlation with edge polarized spins is discussed.

It is highly expected that in the present graphene nanomeshes, modulating a flat band and introducing polarized spins from pore edges to bulk graphene regions must open a door to novel all-carbon spintronic devices with strong spin coherence (e.g., all-carbon spin FETs, spin pumping devices, spin filtering devices).

References:

- [1] T. Shimizu, J. Haruyama et al., *Nature Nanotech.* **6**, 45 (2011)
- [2] K. Tada, J. Haruyama et al., *Phys.Rev.Lett.* **107**, 217203 (2011.11- 2012.3)
- [3] T. Shimizu, J. Haruyama et al., *Appl.Phys.Lett.* **100**, 023104 (2012)

Corresponding Author Junji Haruyama

E-mail J-haru@ee.aoyama.ac.jp

Tel&Fax 042-759-6256 & 6524

Magnetic behaviors sensitive to foreign-atom termination of pore-edge in graphene nanomeshes

○K. Takeuchi, K. Sakuramoto, N. Kosugi, Y. Hashimoto, Y. Yagi, J. Haruyama P. Zhao¹,
S.Maruyama¹, A. Rao²,

*Faculty of Science and Engineering, Aoyama Gakuin University, 5-10-1 Fuchinobe,
Sagamihara, Kanagawa 252-5258, JAPAN*

¹*Tokyo University, 7-3-1 Hongo, Bunkyo-ku, Tokyo 113-8656 Japan*

²*Clemson University, Dept. Chemistry, Clemson, SC 29634, USA*

Abstract: Although a variety of exciting phenomena has been experimentally reported in graphenes, mostly none has experimentally reported on edge-related phenomena. Basically, there are two kinds of atomic structures in graphene edges; the so-called arm chair [1] and zigzag edges. Zigzag edge theoretically produces a flat energy band and, thus, electrons localize around the edge. The localized electrons are spontaneously spin-polarized due to strong electron interaction originated from extremely high electron density of states (i.e., edge states), resulting in appearance of (anti)ferromagnetism. Moreover, the phenomena are highly sensitive to edge termination of foreign atoms (e.g., hydrogen, oxygen, nitride, boron). It is attractive and extremely useful that a material consisting of only carbon atoms with sp^2 orbitals allows them. Mostly none has, however, reported on experimental observation of edge-derived spin phenomena, because lithographic fabrication of graphene edges easily introduces disorder.

In contrast, we have reported on a large-amplitude ferromagnetism at room temperature [2] arising from hydrogen(H)-terminated zigzag-pore edges of graphene nanomeshes (GNMs) with honeycomb like arrays of low-defect hexagonal nanopores, which were fabricated by non-lithographic method using nano-porous alumina template as an etching mask. Here, in the poster, we will present correlation of magnetism with termination of the pore edges by foreign atoms. In oxygen (O)-terminated GNMs, the ferromagnetism observed in the H-terminated GNMs changes to weak diamagnetism due to formation of C=O bonds and consequent appearance of spin paring at pore edges. In contrast, we find that boron (B)-terminated GNMs exhibit ferromagnetism like the case of the H-terminated GNMs. This can be interpreted by association with breaking the symmetry of spin-up and spin-down physical properties of the inter-pore regions, which correspond to nanoribbons, with the B-doped nano-pore edges [3]. The case of nitrogen termination will be also presented.

It is highly expected that termination of pore edges by foreign atoms can control magnetism and realize high-efficiency controllable graphene magnets, which are ultra-light (wearable), flexible, invisible, and rare-element free.

References:

[1] T.Shimizu, J.Haruyama et al., *Nature Nanotech.* **6**, 45 (2011)

[2] K. Tada, J. Haruyama et al., *Phys.Rev.Lett.* **107**, 217203 (2011.11- 2012.3)

[3] T. B. Martins et al., *Phys.Rev.Lett.* **98**, 196803 (2007)

Corresponding Author Junji Haruyama

E-mail J-haru@ee.aoyama.ac.jp

Tel&Fax 042-759-6256 & 6524

Electronic structures of hexagonal boron nitride with topological line defects

○Yoko Tomita^{1,2}, Susumu Okada^{1,2}

¹ Graduate School of Pure and Applied Sciences, University of Tsukuba,
1-1-1 Tennoudai, Tsukuba, Ibaraki 305-8571, Japan

² CREST, Japan Science and Technology Agency, 7 Gobancho, Chiyoda-ku
Tokyo 102-0076, Japan

Imperfection, such as vacancies, edges, and topological defects, in materials with translational symmetry usually leads to peculiar electron states around them. Indeed, topological line defects in graphene and carbon nanotubes modulate their metallic electronic properties and induce peculiar localized states around the defects [1,2]. Hexagonal boron nitride (h-BN) possesses a planar honeycomb lattice but is made of cation and anion atoms, so that h-BN is an insulator with a large band gap around 5eV. By analogy with graphene with imperfection, h-BN with topological line defects also possesses unusual electron states around the imperfection. However, theoretical works on electronic structures of topological line defects in h-BN are still limited [3]. In this work, we consider the formation of asymmetric line defects and study their electronic structures by the first-principles calculation.

We first prepare $(6\sqrt{3}\times 2)$ rectangle repeated unit cell of h-BN and produce an asymmetric line defect along the zigzag direction by implanting dimer atoms, $XX=BN$, BB , or NN , which induces fused pentagonal and octagonal rings. Optimized atomic positions and electronic structures are calculated by the ab-initio pseudopotential method.

All topological line defects induce deep impurity-like bands within the fundamental gap of bulk h-BN. Since they have large dispersion along the defect line, they will capture electrons or holes supplied in h-BN and show the one-dimensional-like carrier conduction along the defect line.

Though all impurity-band states are localized around the defect line, they have different characters depending on the kinds of implanted atoms.

Calculated formation energies of BN , BB , and NN line defects are 4.76, 4.36, and 9.36eV, respectively. Thus, the BN line defect is difficult to appear in h-BN under a usual crystal-growth condition. Perhaps, the BB line defect appears in the case of B-rich growth condition.

References

- [1] S. Okada, T. Kawai, K. Nakada, J. Phys. Soc. Jpn, **80** (2011) 013709.
- [2] S. Okada, K. Nakada, K. Kuwabara, K. Daigoku, T. Kawai, Phys. Rev. B **74** (2006) 121412(R).
- [3] X. Li, X. Wu, X. C. Zeng, J. Yang, ACS Nano **6** (2012) 4104.

Corresponding Author: Y.Tomita

Tel: +81-29-853-5600, Fax: +81-29-853-5924,

E-mail: cosmiceye@comas.frsc.tsukuba.ac.jp

Hole-doping to CVD graphene induced by electron beam resist

○Yui Ogawa¹, Masaharu Tsuji^{1,2}, Hiroki Ago^{1,2,*}

¹ Graduate School of Engineering Sciences, Kyushu University, Fukuoka, 816-8580, Japan

² Institute for Materials Chemistry and Engineering, Kyushu University, Fukuoka, 816-8580, Japan

Graphene is an attractive two-dimensional material for electronics applications due to its extraordinarily high carrier mobility [1,2]. The growth of graphene on metal catalysts, such as Ni and Cu, using chemical vapor deposition (CVD) is a promising approach for the production of large-area graphene for the device applications [3,4]. Generally, a large graphene film is transferred onto an insulating substrate and patterned by lithography in order to fabricate the devices [5]. Thus, understanding the effects of chemicals in the lithographic processes is important to develop the performance of graphene device. In this study, we present unexpected hole-doping induced by the electron beam (EB) resist, ZEP520A (ZEON corporation), on the graphene field-effect transistor (g-FET).

Large-area and uniform single-layer graphene was grown by CVD with CH₄ and H₂ gases on a hetero-epitaxial Cu film [6]. Then the graphene film was transferred onto SiO₂ (300 nm)/Si substrate using PMMA and etching solution. ZEP 520 A (inset of Figure 1) was used as the EB resist to make graphene patterns as well as to design the electrode patterns. After each lithography process, the resist was lifted-off and graphene was cleaned by vacuum annealing at 200 °C. FET measurements were carried out under vacuum condition ($\sim 1.7 \times 10^{-4}$ Pa). We changed the total coating time of the EB resist on graphene and found that the longer coating time results in a shift of the Dirac point by ca. +20 V, as shown in Figure 1. This indicates hole-doping to graphene by the EB resist. We consider that Cl atoms in the EB resist act as electron acceptor. On the other hand, the carrier mobility of graphene did not change significantly even after the contact with the EB resist; 2840.7 and 3150.4 m²/Vs for 2 days and 6 days contact, respectively. These results can be useful to realize high performance g-FET.

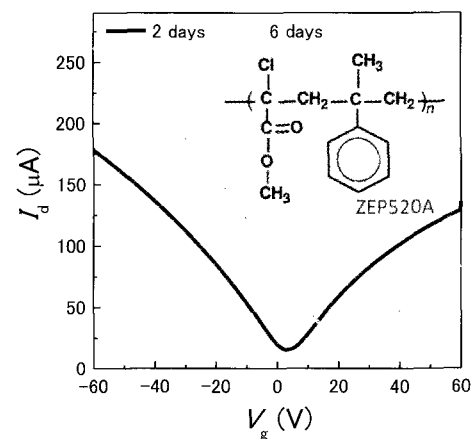


Figure 1 Transfer curve of back-gated g-FET. The dark and light lines show the contact with EB resist for 2 and 6 days, respectively. The inset shows chemical structure of ZEP 520A.

Reference;

- [1] K. S. Novoselov *et al.*, *Nature* **438**, 197 (2005). [2] K. I. Bolotin *et al.*, *Solid State Phys.* **146**, 351 (2008). [3] A. Reina *et al.*, *Nano Lett.* **9**, 30 (2009). [4] X. Li *et al.*, *Science* **324**, 1312 (2009). [5] J. W. Suk *et al.*, *ACS Nano* **5**, 6916 (2011). [6] Y. Ogawa *et al.*, *J. Phys. Chem. Lett.* **3**, 219 (2012).

Corresponding Author: Hiroki Ago (Tel&Fax: +81-92-583-7817, E-mail: ago@cm.kyushu-u.ac.jp)

Fabrication of freestanding graphene nanoribbons devices for in-situ TEM characterization

○Shoji Suzuki, Ryo Kitaura*, Yuki Sasaki, Keiichi Kamon, Yasumitsu Miyata and Hisanori Shinohara*

Department of Chemistry and Institute for Advanced Research, Nagoya University, Nagoya, 464-8602, Japan

Edge structure, defects and width of graphene nanoribbons (GNRs) significantly affect their physical properties; for example, spin polarized edge states appear when the edge of GNR is zigzag[1]. Therefore, to fully understand the intrinsic properties of GNRs, the combination of TEM-based structural characterization and the physical property measurements is essential. For this purpose, we have focused on fabrication of TEM sample holder compatible with electronic properties measurements and the TEM-compatible device where GNRs are suspended between two electrodes for electronic properties measurement. Figure 1 shows schematic representation of the TEM-compatible device. In this presentation, we report a preparation of TEM-compatible GNRs device and newly developed TEM holder for in-situ characterization of GNRs.

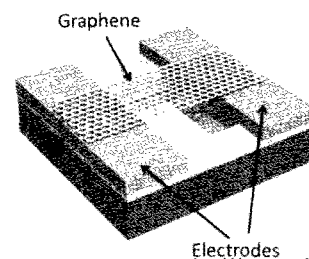


Fig. 1 A schematic illustration of the graphene device

To prepare high quality pure graphene is crucial to fabricate freestanding GNR device. To obtain high quality graphene, we have performed chemical vapor deposition (CVD) at 1323 K using methane as a carbon source and copper as a substrate. After the CVD growth, copper substrate was etched off, and graphene was directly transferred onto the pre-fabricated substrate possessing electrodes and the penetrating hole. After the preparation of the suspended graphene, H₂ plasma etching was performed to clean the surface of the suspended graphene. We have investigated several conditions of plasma treatment to obtain impurity-free suspended graphene. The freestanding clean graphene was patterned using electron beam lithography to obtain freestanding GNRs device.



Fig. 2 A photograph of the developed TEM sample holder.

Figure 2 shows the developed TEM sample holder having 4 electrode pads to make electric contact between the pads and electrodes on the TEM-compatible devices. Using this holder, we can perform TEM observation and electronic properties measurements simultaneously. In the presentation, details of the device preparation and characterization of GNRs devices using the TEM sample holder will be presented.

[1] M. Fujita, et. al., *J. Phys. Soc. Jap.*, 65, 1920, (1996)

Corresponding Author: Ryo Kitaura and Hisanori Shinohara

Tel & Fax: 052-789-2482 & 052-747-6442, E-mail : r.kitaura@nagoya-u.jp and noris@nagoya-u.jp

The effects of graphene-layer thickness on I - V characteristics of CNT-FETs with graphene contacts

○Masato Tamaoki¹, Shigeru Kishimoto^{1,2}, and Takashi Mizutani¹

¹Department of Quantum Engineering, Nagoya University, Nagoya 464-8603, Japan

²Venture Business Laboratory, Nagoya University, Nagoya 464-8603, Japan

Recently, CNT-FETs with graphene contacts have been fabricated and shown to have small contact resistance [1][2]. It is important to fully understand the electrical property of the graphene contacts for improving the device performance. In this study, we have studied the effects of graphene layer thickness on CNT-FET I - V characteristics.

Fabricated CNT-FETs with graphene contacts is shown Figure 1. Amorphous carbon (a-C)/Ni/Au tri-layer structure was formed at the source and drain electrode regions, which was followed by graphitization annealing at 800°C for 15 min in a vacuum. Two types of devices were fabricated with different a-C/Ni thicknesses keeping the thickness ratio between a-C and Ni constant. Control devices with Au contacts were also fabricated as references. The formation of graphene layer was confirmed by Raman spectroscopy as shown Figure 2. In the case of thick a-C/Ni layers, the thickness of graphene layers was thick (judged from the width of 2D peak) and the G/D ratio was large, suggesting that the quality of the graphene layers with thick a-C was better than that of the thin a-C. Both types of CNT-FETs have shown p-type conduction in air. Figure 3 shows the maximum transconductance ($g_{m,max}$) for three types of CNT-FETs. In the case of thin graphene layers, $g_{m,max}$ is larger than the device with Au contacts. In the case of the device with thick graphene layers with better quality however, it was smallest among the three-types of the devices. This means that the contact resistance in the CNT-FETs with graphene contacts is small for the devices with thin graphene layers and large for the devices with thick graphene layers. This suggests that the contact resistance in the present CNT-FETs with graphene contacts is dominated by the inter-graphene resistance.

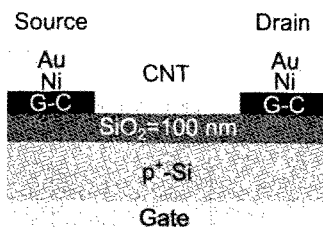


Fig.1 Schematic cross section of a CNT-FET with graphene contacts.

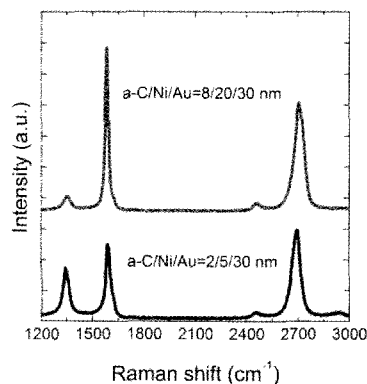


Fig.2. Raman scattering spectra of graphitic carbon layers..

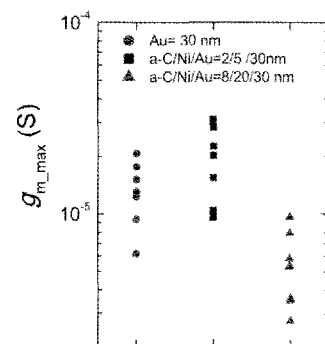


Fig.3. Measured maximum transconductance of the CNT-FETs with graphene contacts and Au

[1] Y. Chai *et al.* IEEE Trans. ED. **59**, no. 1, pp. 12-19, (2012).

[2] M.Tamaoki *et al.* to be published in Appl. Phys. Lett. (2012)

Corresponding Author: T. Mizutani Tel: +81-52-789-5230, E-mail: tmizu@nuee.nagoya-u.ac.jp

Synthesis of Nanocarbon Composites Based on Reduced Graphene Oxides

○Elly Indahyanti, Hiroyuki Yokoi, Kazuto Hatakeyama, Yasumichi Matsumoto

*Graduate School of Science and Technology, Kumamoto University,
Kumamoto, 860-8555, Japan*

Composites of carbon nanotubes (CNTs) and reduced graphene oxide (rGO) have promising applications as organic field-effect transistors (FETs), electrode materials for electrochemical supercapacitors and sensor for environment contamination due to their excellent electrical, thermal, and mechanical properties [1-3]. However, information about combination of rGO and nanocarbon is limited. The aim of this study was to synthesize composites of CNTs and rGO by chemical vapor deposition (CVD) process. GO nanosheets were produced following the Hummers' method [4] and deposited on the silicon oxide substrate. The GO nanosheets were reduced by photoreaction process to obtain rGO nanosheets [5]. Thus, CNTs were grown on top of the rGO by CVD process with catalysts Co and Fe. The product was analyzed with Field Emission Scanning Electron Microscopy (FE-SEM) and Raman Spectroscopy. The SEM images and Raman spectras show that the combination of CNTs as nanocarbon materials and rGO has occurred. CNTs with open ends are also characterized on the substrate.

[1] Bing Li *et al. Adv. Mater.* **22**, 3058-3061, 2010.

[2] Ting Lu *et al. Journal of Electroanalytical Chemistry* **661**, 270-273, 2011.

[3] Fangxin Hu *et al. Analytica Chimica Acta*, **724**, 40-46, 2012.

[4] Hummers W.S. and Offeman R.E., *J. Am. Chem. Soc.* **80**, 1339, 1958.

[5] Matsumoto Y. *et al. J. Phys. Chem.* **115**, 19280-19286, C2011.

Corresponding Author: Hiroyuki Yokoi

Tel: +81-96-342-3727,

E-mail: yokoihr@kumamoto-u.ac.jp

First-principles simulations of graphene dual-double gate transistors: implementation of gate electric field

○Mari Ohfuchi

Fujitsu Laboratories Ltd., 10-1 Morinosato-wakamiya, Atsugi, Kanagawa 243-0197, Japan

Graphene has shown great promise for use in future nanoelectronics. At the nanoscale, it is important to fully understand the intrinsic transport properties under gate electric fields. In this study, we develop a method to introduce the effect of multiple gates into first-principles electronic transport calculations. We also report the simulations of a graphene Dual-Double (DD) gate transistor having four gates in all as the first case.

All calculations are performed using density functional theory (DFT) code [1]. We adopt the nonequilibrium Green's function (NEGF) method. The gates are modeled as surface charge. The electrostatic potential is analytically calculated from the surface charge and added as external potential while the nonequilibrium electronic structure is self-consistently determined under the source-drain bias voltages V_{SD} . The source-drain current I_{SD} is evaluated by integrating the transmission based on the electronic structure according to the Landauer formula. Model of the graphene DD gate transistor and I_{SD} - V_{SD} curves obtained for four cases (DD gate (nn), DD gate (pn), double gate, and w/o gate) are shown in Fig. When we put surface charge of 10^{13} cm^{-2} to all the gates (DD gate (nn)), the current is almost the same as that for single double gate (double gate). When we set the surface charge to the opposite sign for the left and right gates (DD gate (pn)), we have found that the current becomes even smaller than that without gates (w/o gate). This might correspond to the large resistance in ballistic pnp junctions [2], which will be examined using this method in the future.

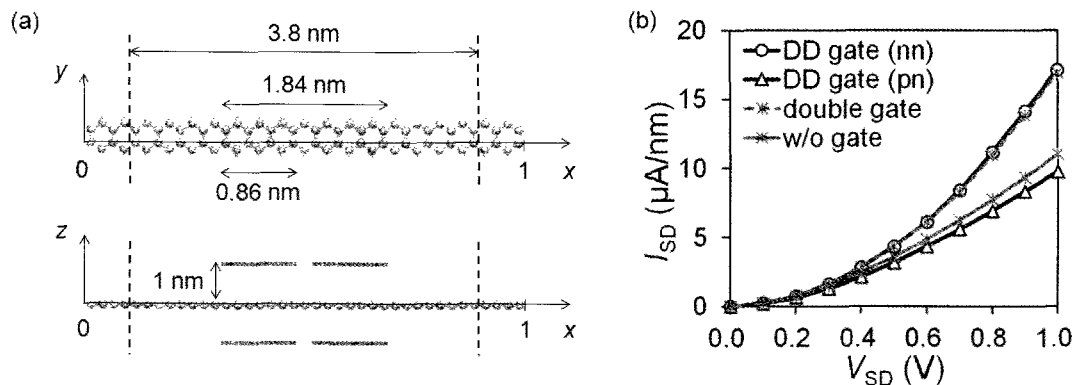


Fig. (a) Schematic diagram of a graphene dual-double (DD) gate transistor. The gray spheres represent carbon atoms. Both sides in the transport direction (x) (source and drain) are semi-infinite graphene leads. The broken lines indicate the boundary between the center region and the leads. In the y and z directions, only atoms of the unit cell are shown. The gray rectangles and lines denote the positions of the gates. The left and right ones of DD gates are 0.12 nm away from each other. The connected one of the left and right gates into a length of 1.84 nm is called single double gate. (b) The source-drain currents I_{SD} as a function of the source-drain bias voltage V_{SD} .

[1] T. Ozaki, Phys. Rev. B 67, 155108 (2003); <http://www.openmx-square.org/>.

[2] R. Gorbacev *et al.*, Nano Lett. 8, 1995 (2008).

Corresponding Author: Mari Ohfuchi

Tel: +81-46-250-8194, Fax: +81-46-250-8274, E-mail: mari.ohfuchi@jp.fujitsu.com

Apoptotic Mechanism of RAW264.7 Induced by Carbon Nanohorns

Mei Yang¹, Minfang Zhang¹, Yoshio Tahara¹, Sumio Iijima^{1,2}, Masako Yudasaka^{1*}

¹ *Nanotube Research Center, National Institute of Advanced Industrial Science and
technology 5-2, Tsukuba, Japan*

² *Department of Material Science and Engineering, Meijo University, Nagoya, Japan*

Single-walled carbon nanohorns (CNHs), which are prepared by the CO₂ laser ablation of graphite without metal catalysts, have high potential for applications to drug delivery, diagnostic imaging, and photo-hyperthermia therapy. Same as the other nanocarbons, CNHs are easily captured by macrophages [1]. Although *in vitro* and *in vivo* studies showed that CNHs have low acute toxicity, this undesired accumulation in macrophages can potentially lead to long-term toxicity and strongly limits the bio-application of CNHs. Recently, it has been shown that CNHs is cytotoxic when a large amount of CNHs were internalized in murine macrophage RAW 264.7. The cell death was necrotic/apoptotic, which is discussed on the basis of lysosomal membrane destabilization and the generated ROS [2]. We discussed the details of apoptosis mechanism caused by CNHs in RAW264.7 in this presentation.

We used the CNHs treated by light-assisted oxidation with hydrogen peroxide. They were dispersed in cell medium without using any dispersants, and the cell medium dispersion of CNHs was used for the cell experiments. The CNH concentration in the cell culture medium was 1-100 µg/ml. After 48 h incubation, RAW 264.7 cells took up 1- 140 pg/cell of CNHs. The cytotoxicity became apparent after the 48 h incubation, when the cell proliferation inhibition and cell death increased with the CNH concentration. At the same time, Caspase 3 was activated, suggesting that the apoptotic cell death proceeded. Mitochondrial membrane potential was examined by using JC-1 probe, which tended to decrease by the CNHs. ROS generation was enhanced by CNH, which was appreciably suppressed by deactivation of mitochondrial electron transport chain complexes I and III. These results suggest that the CNHs accumulated in the lysosomes could cause the apoptosis via disturbing the mitochondrial activity.

[1] J. Miyawaki, et al. *ACS Nano*, 3, 1399-1406, 2009.

[2] Y Tahara, et al. *Biomaterials*, 33, 2762-2769, 2012.

Synthesis of carbon nanohorns dispersed with metallic nanoparticles by gas-injected arc-in-water method

○Noriaki Sano¹, Tatporn Suntornlohanakul^{1,2,3}, Chantamanee Poonjarernsilp^{1,4}, Daisuke Hirama¹, Kosuke Taniguchi¹, Tatsuhiko Norimoto¹, Taiga Ishii¹, Hajime Tamon¹, Tawatchai Charinpanitkul²

¹ Department of Chemical Engineering, Kyoto University, Kyoto, 615-8510, Japan

² Center of Excellence in Particle Technology, Department of Chemical Engineering, Faculty of Engineering, Chulalongkorn University, Patumwan, Bangkok 10330, Thailand

³ International School of Engineering, Faculty of Engineering, Chulalongkorn University, Patumwan, Bangkok 10330, Thailand

⁴ Department of Chemical Engineering, Faculty of Engineering, Rajamangala University of Technology Krungthep, 2 Nanlinchee Rd., Tungmahamek, Sathon, Bangkok 10120, Thailand

It can be expected that carbon nanohorns (CNHs) [1] are useful for many applications for their unique structural characteristics, for example catalyst support, electrode materials, drug delivery, etc. Dispersing metallic nanoparticles in CNHs should enhance the ability of the CNHs for some applications because nanoparticles of specific nanoparticles can give catalytic or magnetic properties to CNHs. The present study tried to elucidate the influence of the metallic components on the product structures of metal-dispersed CNHs in the synthesis process by gas-injected arc-in-water (GI-AIW) method using metal-carbon composite electrode [2].

The set-up of the GI-AIW method is explained in a literature [2]. A hollow graphite cathode was submerged in water and narrow graphite rod anode was inserted in the hole of the cathode to generate arc discharge. N₂ was supplied to the cathode hole during the arc discharge. To produce the CNHs dispersed with metallic nanoparticles, the anode rod was drilled axially, and powers or wires of specific metallic components are stored therein. In this study, we stored Pd together with Ni in the anode hole to produce Pd-Ni alloy nanoparticles. An example TEM image of CNHs dispersed with Pd-Ni alloy particles is shown in Fig. 1. As shown in Fig. 2, it was revealed that the component ratio (Ni/Pd ratio) in alloy-dispersed CNHs significantly decrease with the initial Ni/Pd ratio stored in anode. This result suggested that the thermal properties such as boiling point would be important criteria to estimate the component ratio in metallic nanoparticles dispersed in the CNHs produced by this way. To observe the influence of this aspect, a variety of metallic components (W, Nb, Fe, Ni, Au, Mo, Cu, etc.) were stored with Pd in the anode when CNHs were synthesized. In these experiments, some clear trends which determined the metallic components in the products were found. The knowledge obtained here will be fundamentally useful to synthesize CHNs dispersed with metallic nanoparticles having specific components to maximize their performance in any application.

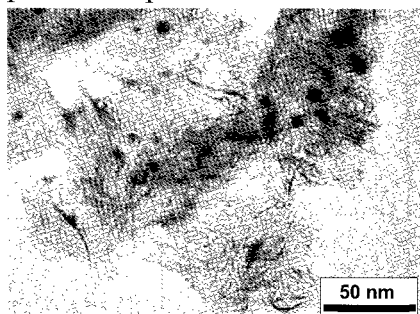


Fig. 1 TEM image of CNHs dispersed with Pd-Ni alloy nanoparticles

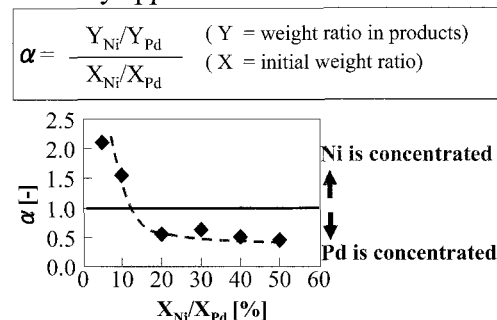


Fig. 2 Concentration factor of Ni in Pd-Ni alloy dispersed in CNHs vs. initial Ni/Pd ratio

[1] S. Iijima, M. Yudasaka, *et al.* Chem. Phys. Lett. **309**, 165 (1999).

[2] C. Poonjarernsilp, N. Sano, *et al.* Carbon, **49**, 4920 (2011).

Corresponding Author: N. Sano Tel: +81-75-383-2684, Fax: +81-75-383-2654, E-mail: sano@cheme.kyoto-u.ac.jp

Vibronic interaction in the forbidden electronic transition of polyynes and cyanopolyynes

○Tomonari Wakabayashi, Yoriko Wada, Makiko Tomioka

Department of Chemistry, Kinki University, Higashi-Osaka, 577-8502, Japan

The linear chain carbon molecules of hydrogen-end-capped polyynes and cyanopolyynes, are intriguing as possible precursors for infinitely long, one-dimensional atomic chains of carbon, namely carbyne. The electronic structure of these molecules is also an important subject upon making conducting materials. Optical spectroscopy is one of the promising tools for investigating the electronic structure of these molecules. However, some low-lying excited states of polyynes are not accessible directly by a simple electric-dipole transition. The electronic transition can be *forbidden* by symmetry. Even under the case for the symmetry-forbidden transition, the electronic transition becomes allowed by incorporating activation or deactivation of a specific mode of molecular vibration. Here, we examined symmetry rules for the vibronic transitions for polyynes and cyanopolyynes, observable in the near UV regions. These transitions are usually orders of magnitude weaker than those for the fully allowed transition appearing in the UV.

First, we observed near UV emission bands of hydrogen-end-capped polyyne molecules in hexane by resonant excitation with UV-laser photons tuned to the allowed transition in the UV [1]. The forbidden transition is activated along with the excitation of a trans-bending π_g mode of vibration. Second, we observed intensification of the vibronic bands in the near UV by absorption spectroscopy for polyyne-iodine molecular complexes [2]. The symmetry for the complex is substantially deviated from the cylindrical symmetry. Also, electronic transition of the polymeric iodine unit can promote the transition of polyyne molecules. The effect of formation of the complex is detectable by infrared absorption spectroscopy [3]. Major IR absorption lines for hydrogen-end-capped polyyne molecules are red-shifted and some new lines are intensified. Skeletal deformation of the polyynic carbon chain becomes easier for the polyyne-iodine complex relatively to the intact polyyne molecules. Finally, we observed absorption bands in the UV for cyanopolyynes [4]. According to the loss of inversion symmetry, the molecules show absorption features of substantial intensity on the low-energy side of the fully allowed transition in the UV. When cyanopolyynes are embedded in a crystalline form of a molecular complex with α -cyclodextrin, the near UV transitions are intensified again, indicating the modification of the vibronic interaction within the cyanopolyyne molecule.

[1] T. Wakabayashi *et al.* Chem. Phys. Lett. **446**, 65 (2007).

[2] Y. Wada *et al.* J. Phys. Chem. B **115**, 8439 (2011).

[3] Y. Wada *et al.* Chem. Phys. Lett. **541**, 54 (2012).

[4] T. Wakabayashi *et al.* Carbon **50**, 47 (2012).

Corresponding Author: T. Wakabayashi

Tel: +81-6-6721-2332, Fax: +81-6-6723-2721,

E-mail: wakaba@chem.kindai.ac.jp

Methanol oxidation reaction characteristics of carbon nanomaterials with PtRu-support

○Masahiro Ozaki¹, Yoshiyuki Suda¹, Hirofumi Takikawa¹, Hideto Tanoue¹,
Hitoshi Ue², Kazuki Shimizu³

¹ Toyohashi University of Technology, ²Tokai Carbon Co., Ltd.,

³Shonan Plastic Mfg. Co., Ltd.

Direct methanol type fuel cell (DMFC) has been attracting attention as a power source for mobile devices. Increase of power generation efficiency and power output is required for commercialization. We have developed carbon electrodes for DMFC using different carbon nanomaterials on which a metal catalyst is supported. In this study, we discussed the effect of methanol oxidation reaction characteristics on the property of carbon nanomaterials.

We used three carbon nanomaterials, Vulcan XC-72 (Vulcan), arc black (AcB) ⁽¹⁾, and carbon nanocoil (CNC). Table 1 shows the characterization of carbon nanomaterials.

Table 1. Characterization of carbon nanomaterials.

	Specific surface (m ² /g)	Volume resistivity (Ω · cm)	Shape
Vulcan	237	0.43	Clusters of 30 nm particles
AcB	153	7.4	Clusters of 50 nm particles
CNC	115	1.9	Helical fiber

We supported metal catalysts, Pt and Ru by the reduction method using sodium borohydride. The loading amount was determined by thermal gravimetric analysis (TGA) and the amounts of Pt and Ru were set to be 20 and 10 wt. %, respectively.

The methanol oxidation reaction was analyzed by a three-electrode cell; PtRu catalyst, saturated KCl/Ag/AgCl electrode, and Pt sheet electrode were respectively used as working, reference and counter electrodes. 1M H₂SO₄ + 1M CH₃OH was used as an electrolytic solution. The voltage scan range and rate were 0 - 1.5 V and 20 mV/s, respectively.

Figure 1 shows the measurement results. The current around 0.8 V which indicates the methanol oxidation reaction, was higher in the order of Vulcan, CNC, and AcB.

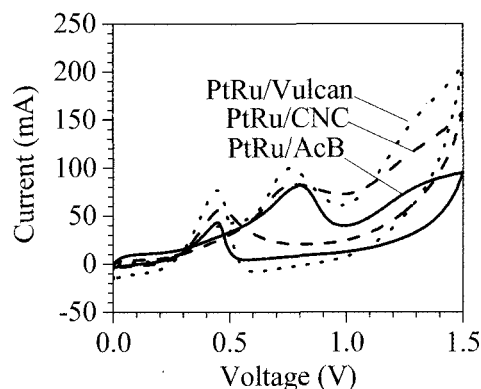


Fig.1 Catalytic actives for methanol oxidation reaction in 1M H₂SO₄ + 1M CH₃OH at room temperature.

This work has been partly supported by the Research Project of the Venture Business Laboratory from Toyohashi University of Technology (TUT); the Core University Programs (JSPS-CAS program in the field of "Plasma and Nuclear Fusion") from the Japan Society for the Promotion of Science (JSPS); and a Grant-in-Aid for Scientific Research from JSPS.

References

[1] S. Oke, et al.: Chem. Eng. J., 143, 225-229 (2008).

Corresponding Author: Yoshiyuki Suda

Tel: +81(0)532 44 6726, Fax: +81(0)532 44 6757, E-mail: suda@ee.tut.ac.jp

IR spectra of polyynes-iodine complexes in nonpolar solvents

○Yoriko Wada¹, Yusuke Morisawa², Tomonari Wakabayashi^{1,2}

¹Department of Chemistry, Interdisciplinary Graduate School of Science and Engineering,
Kinki University, Higashi-Osaka 577-8502, Japan

²Department of Chemistry, School of Science and Engineering, Kinki University,
Higashi-Osaka 577-8502, Japan

Polyynes, $H(C\equiv C)_nH$ ($n \geq 2$), are sp-hybridized linear carbon chain molecules with two hydrogen atoms at both ends. We have reported that a molecular complex is formed from polyynes and iodine molecules by photoinduced reaction. The composition of the polyynes-iodine complex was determined to be 1:3 for polyynes: I_2 ratio from the concentration-dependence experiment. The 1H - and ^{13}C -NMR spectra showed that the polyynes-iodine complex has C_2 symmetry [1].

Very recently, we measured IR spectra of polyynes-iodine complexes, $C_{2n}H_2I_6$ ($n=5-7$), for structural characterization of these complexes [2]. Figure 1 shows IR spectra of $C_{10}H_2$ (upper panel) and $C_{10}H_2I_6$ (lower panel). We detected CH-bending π_u mode and CH-stretching σ_u mode of $C_{10}H_2$ at 625 cm^{-1} and 3306 cm^{-1} , respectively. A signal at 1236 cm^{-1} and a weak signal at 2191 cm^{-1} were assigned to a combination of CH-bending $\pi_g + \pi_u$ mode and CC-stretching σ_u mode of $C_{10}H_2$, respectively. In the spectrum for $C_{10}H_2I_6$, signals were red shifted from 625 cm^{-1} to 610 cm^{-1} for CH-bending π_u mode and from 3306 cm^{-1} to 3085 cm^{-1} for CH-stretching σ_u mode by formation of complex. As for the CC-stretching σ_u mode of $C_{10}H_2I_6$ at 2182 cm^{-1} , signal was intensified by formation of complex. There are two noticeable signals at 866 and 1345 cm^{-1} in the spectrum of $C_{10}H_2I_6$ which have appeared by formation of complex. According to molecular orbital calculations for $C_{10}H_2$, there are fundamental transitions for CC-stretching σ_u modes in this region. Therefore, we consider that these new signals at 866 and 1345 cm^{-1} in $C_{10}H_2I_6$ are intensified CC-stretching σ_u modes by formation of the complex. We can consider that the six iodine atoms are surrounding the polyynic carbon chain, because CH-bending and CH-stretching modes show red shift and CC-stretching modes are intensified by formation of complex. The results of IR and NMR spectra suggest that an iodine unit, I_6 , in $C_{10}H_2I_6$ lies at equator of $C_{10}H_2$.

[1] Y. Wada et al. *J. Phys. Chem. B* **115**, 8439 (2011).

[2] Y. Wada et al. *Chem. Phys. Lett.* **541**, 54 (2012).

Corresponding Author: T. Wakabayashi

Tel: +81-6-6730-5880 (ex. 4101), Fax: +81-6-6723-2721, E-mail: wakaba@chem.kindai.ac.jp

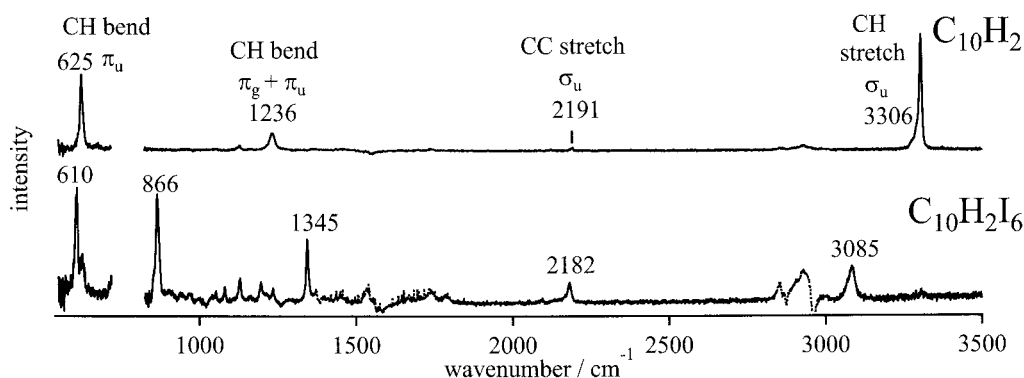


Fig. 1. IR spectra of $C_{10}H_2$ (upper panel) and $C_{10}H_2I_6$ (lower panel).

Formation of carbon nanocapsules from silicon nanoparticles deposited on a carbon nanotube heater

○Tomohiro Terada, Koji Asaka, Hitoshi Nakahara, and Yahachi Saito

Department of Quantum Engineering, Nagoya University, Furo-cho, Nagoya 464-8603

The formation of carbon nanocapsules from silicon (Si) nanoparticles deposited on a carbon nanotube (CNT) by Joule heating was studied by *in situ* transmission electron microscopy (TEM).

CNTs were attached to an edge of a gold (Au) plate by dielectrophoresis, and Si was deposited on the surface of the CNTs at 773 K by electron beam evaporation. A free end of a Si-deposited CNT was brought into contact with a tip of an Au-coated tungsten needle inside a transmission electron microscope. The formation of carbon nanocapsules on the surface of Si nanoparticles by Joule heating of the CNT was observed by *in situ* TEM, and the current and bias voltage applied to the CNT were simultaneously measured.

Figure 1(a) shows a TEM image of a Si-deposited CNT bridging between Au electrodes. When the bias voltage was increased to 1.46 V, a current of 43.4 μA suddenly passed through the CNT. At the same time, some Si nanoparticles lying on the CNT disappeared (Fig. 1(b)). At a bias voltage of 1.60 V, the current increased to 49.3 μA and a carbon nanocapsule encapsulating Si nanoparticle was formed, as indicated by an arrow in Fig. 1(c). An application of the bias voltage up to 2.04 V led to the rise in current to 90.7 μA , and Si nanoparticles were completely disappeared and only carbon nanocapsules were left on the surface of the CNT, as indicated by arrows in Fig. 1(d). Figure 2 shows a high-resolution TEM image of carbon nanocapsules observed after the disappearance of Si nanoparticles. They have a multilayered structure, and the interlayer spacing is about 0.35 nm, corresponding to that of (002) planes of graphite.

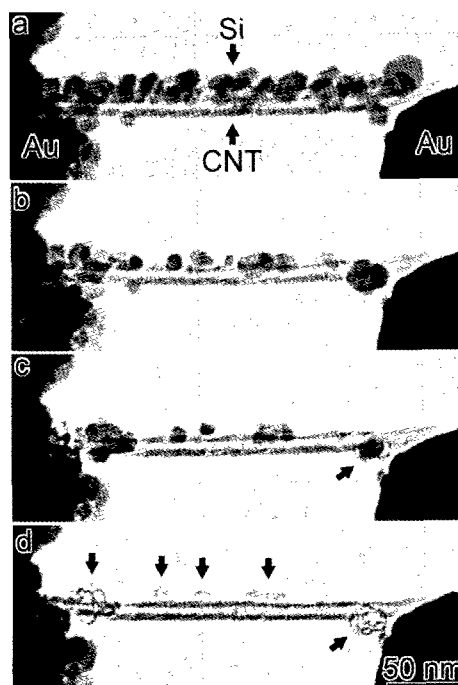


Fig. 1. A time sequential series of TEM images of the formation of carbon nanocapsules from Si nanoparticles deposited on a CNT.

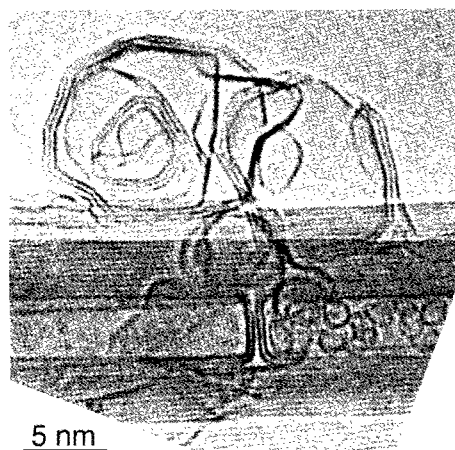


Fig. 2. A high-resolution TEM image of carbon nanocapsules lying on the surface of the CNT.

Corresponding Author: Tomohiro Terada
 Tel: +81-52-789-3714, Fax: +81-52-789-3703,
 E-mail: terada@surf.nuqe.nagoya-u.ac.jp

Distribution of Lanthanum containing carbon nanocapsules in the DC arc cathode deposit

○Kazunori Yamamoto¹, Shin-ichi Shamoto¹, Takeshi Akasaka²

¹Quantum Beam Materials Synthesis Research Group, Quantum Beam Science Directorate,
Japan Atomic Energy Agency, Tokai-mura, Naka-gun, Ibaraki 319-1195, Japan

²Life Science Center of Tsukuba Advanced Research Alliance, University of Tsukuba, Ibaraki
305-8577, Japan

The discovery of endohedral fullerenes [1,2] has triggered a new exciting field of research, where a variety of new endohedral carbon nanostructures, such as nanocapsules [3,4] and nanotubes [5] have been produced. Several materials such as pure metals, alloys, and carbides have been nanoencapsulated in carbon. Although these “carbon nanoencapsulates” are very important compounds due to their potential application for the disposal of radioactive waste metals, such as rare earth and actinide [6], they are still laboratory materials, and their very low conversion efficiency from starting metal/carbon mixtures to the carbon nanoencapsulates, resulting from the present synthetic technology, is certainly one of the main explanations of present status. Nearly 20 years after their discovery, therefore, no real large-scale industrial application of carbon nanoencapsulates has yet started.

Historically, the conventional DC arc discharge experiments provided carbon nanocapsules containing nanocrystals of LaC_2 in carbonaceous deposit on cathode [3,4]. Figure 1 shows one of typical powder X-ray diffraction profiles of the cathode deposit. Although LaC_2 is very reactive with H_2O and easily converts to $\text{La}(\text{OH})_3$ in humid air, diffraction peaks of LaC_2 crystals were observed in Figure 1, which means the LaC_2 crystals are in carbon nanocapsules and are protected from water molecules. Recently we have found that no nanoencapsulates were observed in the center of the cathode deposit, and that the nanoencapsulates were concentrated under outer-shell of the cathode deposit. Distribution of the nanoencapsulates and the formation process in the cathode deposit will be discussed.

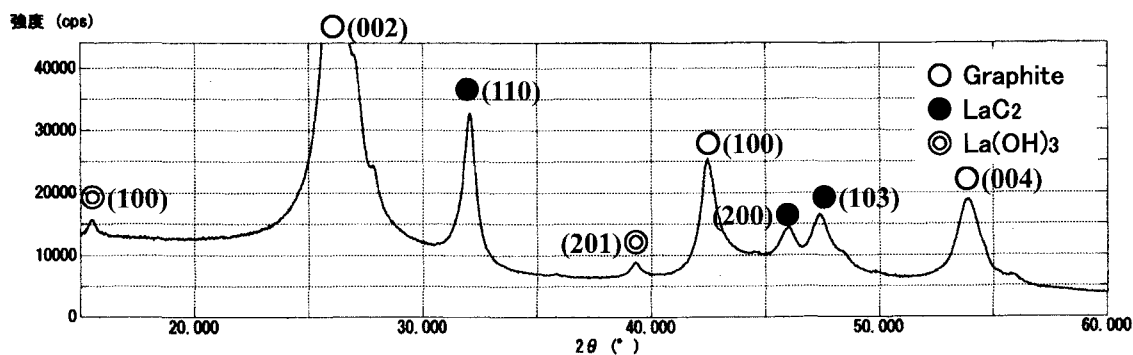


Fig. 1 Typical powder X-ray diffraction profile of the cathode deposit.

- [1] J.R. Heath *et al.*, *J. Am. Chem. Soc.*, **107**, 7779 (1985). [2] Y. Chai *et al.*, *J. Phys. Chem.*, **95**, 7561(1991).
[3] R.S. Ruoff *et al.*, *Science*, **259**, 336(1993). [4] M. Tomita *et al.*, *Jpn. J. Appl. Phys.*, **32**, L280(1993).
[5] S. Seraphin *et al.*, *Appl. Phys. Lett.*, **63**, 2073(1993). [6] K Yamamoto *et al.*, *Prog. Nucl. Energy*, **47**, 616(2005).

Corresponding Author: K. Yamamoto, Tel: +81-29-282-6474,

E-mail: yamamoto.kazunori@jaea.go.jp

Dependence of carbon nanocoil length on sonication time

○Koji Maruyama¹, Yoshiyuki Suda¹, Hideto Tanoue¹, Hirofumi Takikawa¹,
Hitoshi Ue², Kazuki Shimizu³, Yoshito Umeda⁴

¹ *Department of Electrical and Electronic Information Engineering,
Toyohashi University of Technology, Toyohashi, 441-8580, Japan*

² *Fuji Research Laboratory, Tokai Carbon Co., Ltd.*

³ *Shonan Plastic Mfg. Co., Ltd.*

⁴ *Fundamental Research Department, Toho Gas Co., Ltd.*

Carbon nanocoil (CNC) is expected to be applied to nanodevice because of its unique form and high conductive property. We conducted isolated dispersion of CNC into water. CNC was synthesized by using the chemical vapor deposition (CVD) and was used as the starting material as shown in Fig. 1(a). CNC length before dispersing was about from 20 to 30 μm . CNC (10 mg) was dispersed for 5 to 120 min in 100 ml deionized water and 1g (1wt %) sodium dodecyl sulfate by homogenization using a homogenizer (Nihonseiki, US-600T). The dispersed solution was kept below 20 degrees during dispersion. A drop of 40 μl of suspension was dropped onto carbon-coated TEM grids and observed by a scanning electron microscopy as shown in Fig. 1(b). It was found that CNCs were cut after dispersion. Fig. 2 shows a correlation between sonication time and CNC length. As the increase of sonication time, a number of long CNCs of over 10 μm decreased and a number of short CNCs of under 6 μm increased. At 90 and 120 min of dispersion times, there were few long CNCs and many short CNCs in the dispersed solution.

This work has been partly supported by the Research Project of the Venture Business Laboratory from Toyohashi University of Technology (TUT); the Core University Programs (JSPS-CAS program in the field of "Plasma and Nuclear Fusion") from the Japan Society for the Promotion of Science (JSPS); and a Grant-in-Aid for Scientific Research from JSPS.

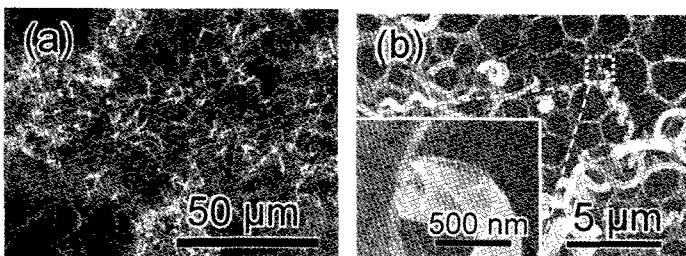


Fig. 1 SEM micrographs of (a) as-grown CNCs and (b) dispersed CNCs on TEM grid.

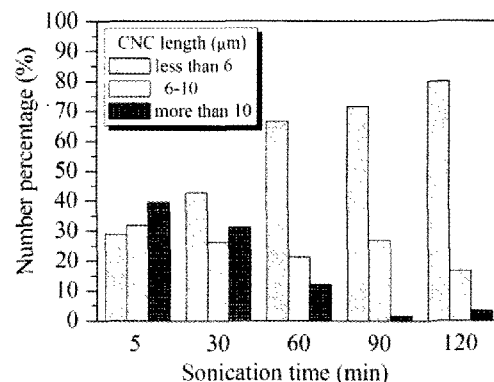


Fig. 2 Relationship between sonication time and CNC length.

Corresponding Author: Yoshiyuki Suda

Tel: +81-532-44-6726, Fax: +81-532-44-6757, E-mail: suda@ee.tut.ac.jp

Doping of Fullerene to Iron Oxide Nanotubes

○Yuki Shiraki, Yuki Mishina, Shunji Bandow

*Department of Materials Science and Engineering, Meijo University,
1-501 Shiogamaguchi, Tenpaku, Nagoya 468-8502, Japan*

Characteristic of nanotube structure is simply described by large surface area, which stems from usable inner surface surrounding a molecular sized space spread inside the tube. Recently, many tubule structured nanomaterials are reported such as vanadium oxide, TiO₂, ZrO₂, Al₂O₃ and Fe₂O₃, so on [1-5] after finding of carbon nanotubes [6]. Fullerene filling in the carbon nanotube is widely studied with a viewpoint whether or not the encapsulated fullerenes modify the nanotube electronic structure [7]. In addition, co-deposited film of MoO₃ and C₆₀ has a potential ability as an organic solar cell due to effective charge transfer from C₆₀ to MoO₃ [8]. Such charge transfer would modify the band scheme and lowers optical absorption energy to visible light region from UV. Since the band gaps of most metal oxides are in UV region, it is necessary to find effective charge transfer materials in order to realize some photo-activities triggered by visible light irradiation.

Generally, the interaction will occur in the contact region, hence the nanotube structure is one of ideal structure for the doping of guest molecules. In the present study, we prepared iron oxide nanotubes by the sol-gel method previously reported [9] and examined the fullerene doping.

Fullerene dopings were carried out by the liquid phase method using C₆₀ and C₆₀(OH)_n. For C₆₀ doping, iron oxide nanotubes were dispersed in toluene solution of C₆₀ and sonicated for 1 hour. Then the sample was observed by TEM. Fullerene hydroxide was prepared by the patent method [10] and checked by thermogravimetry. C₆₀(OH)_n thus obtained was dissolved in ethanol and iron oxide nanotubes were dispersed in this solution. After making such colloidal dispersion, we sonicated the solution for 1 hour and observed by TEM. Figure 1 indicates summary of TEM observations. Figures 1a, b and c are, respectively, pristine iron oxide nanotube, iron oxide nanotube after C₆₀ doping and those after C₆₀(OH)_n. From these figures, one can easily find that some circular contrasts associated with C₆₀(OH)_n are seen only in Fig. 1c, which suggests that the hydrophilic nature is needed to interact with iron oxide nanotubes.

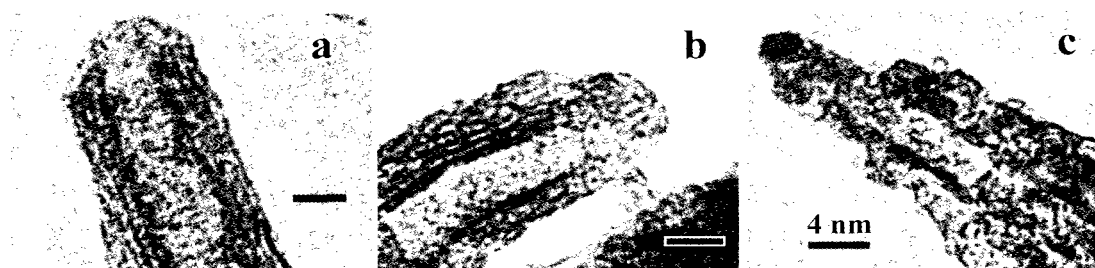


Fig. 1. TEM images of (a) pristine, (b) after C₆₀ doping and (c) after C₆₀(OH)_n doping iron oxide nanotubes. Bar in each panel represents 4 nm.

[1] M.E. Spahr *et al.*, *Angew. Chem.* **37**, 1263 (1998). [2] G. Armstrong *et al.*, *Chem. Commun.* 2454 (2005). [3] G. Shen *et al.*, *J. Nanotechnol.* **4**, 730 (2007). [4] S. Kobayashi *et al.*, *J. Am. Chem. Soc.* **124**, 6550 (2002). [5] S. Kobayashi *et al.*, *Chem. Mater.* **12**, 1523 (2000). [6] S. Iijima, *Nature* **354**, 56 (1991). [7] C.H.L. Quay *et al.*, *Phys. Rev. B* **76**, 073404 (2007). [8] N. Ishiyama *et al.*, *Appl. Phys. Lett.* **99**, 133301 (2011). [9] Y. Shiraki *et al.*, 42nd FNTG, **3P-49**. [10] P2007-031090.

Corresponding Author: Shunji Bandow, **E-mail:** bandow@meijo-u.ac.jp, **Tel&Fax:** +81-52-834-4001

Supercooled and Glassy Water Confined in Zeolite Templated Carbon

○Haruka KYAKUNO¹, Kazuyuki MATSUDA², Yusuke NAKAI¹, Tomoko FUKUOKA¹,
Yutaka MANIWA^{1,3}, Hiroto NISHIHARA⁴, and Takashi KYOTANI⁴

¹ *Department of Physics, Faculty of Science, Tokyo Metropolitan University, Hachioji,
192-0397, Japan*

² *Institute of Physics, Faculty of Engineering, Kanagawa University, Yokohama, 221-8686,
Japan*

³ *JST, CREST, Kawaguchi 332-0012, Japan*

⁴ *Institute of Multidisciplinary Research for Advanced Materials, Tohoku University, Sendai,
980-8577, Japan*

Zeolite Templated Carbon (ZTC) is a new porous carbon synthesized using the nanochannels of zeolite Y. (Fig.1) The novel characteristics of ZTC are its uniform nanopores with a diameter of ~ 1.2 nm, a long range periodicity derived from the parent zeolite Y, and high specific surface area of up to 4000 m²/g. A proposed model for ZTC is buckybowllike nanographenes assembled into a three-dimensionally regular network^[1].

In the previous work, we carried out NMR measurements, x-ray diffraction (XRD) experiments, and classical molecular dynamics (MD) calculations to clarify the structure and phase behavior of water confined in nanopores of ZTC. It was indicated that the confined water can be supercooled below 200 K, and at the lower temperatures is not crystalline ice but a kind of an amorphous solid, which can be characterized by distorted hydrogen bond networks with very few dangling-bonds.

In this work, we investigated isobaric specific heat capacity C_p of the confined water by means of differential scanning calorimetry (DSC) and gained more insight for its supercooled states. As shown in Fig.2, we successfully determined the C_p , and its temperature dependence shows similar characteristics to that of structural changes analyzed by XRD experiments and MD calculations. Also the glass transition temperature T_g was possibly estimated to be ~ 150 K, consistent with that proposed by NMR measurements.

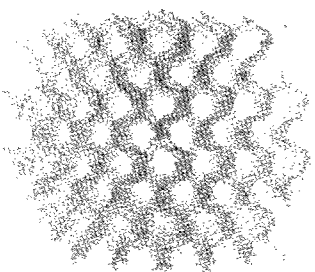


Fig.1 Possible structural model proposed for ZTC solid.

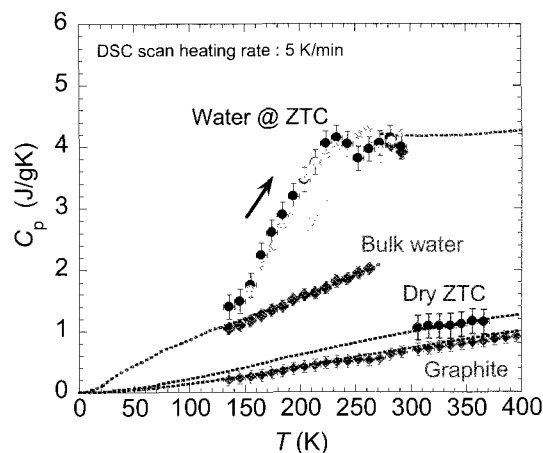


Fig.2 Temperature dependence of specific heat capacity C_p obtained by DSC measurements. As for the data of the confined water, contribution from ZTC framework was eliminated.

Reference: [1] H. Nishihara *et al.* Carbon **47**, 1220 (2009).

Corresponding Authors: Yutaka MANIWA TEL: +81-42-677-2490, E-mail: maniwa@phys.se.tmu.ac.jp

Haruka KYAKUNO TEL: +81-42-677-2498, E-mail: h-kyakuno@phys.se.tmu.ac.jp

Microscopic study of Zeolite Templated Carbon (ZTC) by using ^{13}C NMR spectroscopy

○Kensuke Yamada¹, Yusuke Nakai¹, Kazuyuki Matsuda², Yutaka Maniwa^{1,3},
Hiroto Nishihara⁴, and Takashi Kyotani⁴

¹ *Department of Physics, Graduated School of Science and Engineering,
Tokyo Metropolitan University, Tokyo 192-0397, Japan*

² *Institute of Physics, Faculty of Engineering, Kanagawa University, Yokohama, 221-8686,
Japan*

³ *JST, CREST, Kawaguchi 332-0012, Japan*

⁴ *Institute of Multidisciplinary Research for Advanced Materials, Tohoku University, Sendai,
980-8577, Japan*

Zeolite Templated Carbon (ZTC) is a new allotrope of carbon synthesized using zeolite Y as a template. The novel characteristics of ZTC are the highest surface area of carbon materials (4000 m²/g), three-dimensional structure composed of buckybowls (Fig. 1), and uniform nanopores with a diameter about 1.2 nm. [1] Except these findings of its structure, most of physical properties have not been clarified. In this work, we carried out ^{13}C NMR measurements as a microscopic probe to reveal the electronic properties of ZTC.

^{13}C NMR spectrum at 4.2 K is shown in Fig. 2. The asymmetric spectrum indicates a typical anisotropic powder pattern. We also measured the nuclear spin-lattice relaxation time T_1 with a saturation recovery method. From this measurement, we found the temperature dependence of T_1 obeys a characteristic behavior in metals, the Korringa law ($1/T_1 \propto T$).

Details of our experiments including comparison with other allotropes of carbon (graphite, fullerene, and carbon nanotube) will be reported.

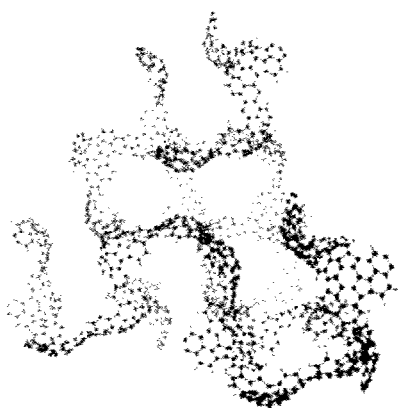


Fig.1 Structural model of ZTC. [1]

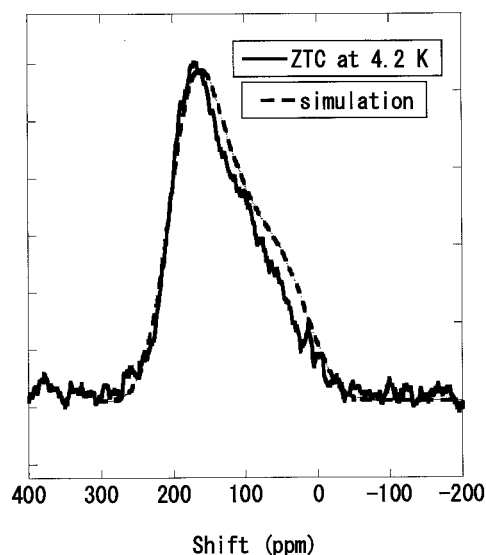


Fig.2 ^{13}C NMR spectrum of ZTC at 4.2 K and simulated powder pattern spectrum.

[1] H. Nishihara *et al.*, Carbon **47** 1220 (2009).

Corresponding Author: Yutaka Maniwa

Tel: +81-42-677-2490, E-mail: maniwa@phys.se.tmu.ac.jp

Measurement of electric property of carbon nanocoil in scanning electron microscope

○Ryuji Kunimoto¹, Taiichiro Yonemura¹, Yoshiyuki Suda¹, Hideto Tanoue¹, Hirofumi Takikawa¹, Hitoshi Ue², Kazuki Shimizu³, Yoshito Umeda⁴

¹ Department of Electrical and Electronic Information Engineering, Toyohashi University of Technology, Toyohashi 441-8580, Japan

² Fuji Research Laboratory, Tokai Carbon, Co., Ltd., Oyama 410-1431, Japan

³ Development Department, Shonan Plastic Mfg. Co., Ltd., Hiratsuka 254-0807, Japan

⁴ Technical Research Institute, Toho Gas Co., Ltd., Tokai 476-8501, Japan

Carbon nanocoil (CNC) is predicted to have a high mechanical strength^[1], and we focus on the elongation of CNC. The purpose of this study is to measure the electrical resistance of CNC when it is elongated under the tensile load. CNC was synthesized in our laboratory by chemical vapor deposition^[2]. Making electrical contact with the both ends of CNC enables us to measure the CNC electrical property. Fig. 1 shows a schematic of the experimental setup.

A manipulator with a tungsten probe tip (W-tip) is mounted in a scanning electron microscope (SEM) and connected to the stage through a multimeter. An oxide film is formed on an Si substrate. Al film is partially deposited on the SiO₂/Si substrate and connected to the stage using a silver paste. CNC installation on the Al-coated SiO₂/Si substrate was performed by a focused ion beam (FIB). The procedure is the following. First, we picked up one CNC from as-grown CNCs on substrate using a tungsten probe equipped in FIB and fixed CNC with the probe by irradiating Pt ion beam. Lower part of the picked-up CNC was cut by Si ion beam and the upper part of several μm length remained. Then the CNC was transferred to the Al-coated SiO₂/Si substrate and we attached one end of the CNC to the end of Al film by irradiating Pt ion beam.

This work has been partly supported by the Research Project of the Venture Business Laboratory from Toyohashi University of Technology (TUT); the Core University Programs (JSPS-CAS program in the field of "Plasma and Nuclear Fusion") from the Japan Society for the Promotion of Science (JSPS); JSPS KAKENHI Grant Number 24360108; and MEXT KAKENHI Grant Number 24110708.

[1] L. Ci, *et al.*: *Mater. Lett.*, **43**, 291 (2000)

[2] M. Yokota, *et al.*: *Journal of Nanosci. Nanotechnol.*, Vol.10, pp.3910–3914 (2010)

Corresponding Author: Yoshiyuki Suda

Tel: +81-532-44-6726, Fax: +81-532-44-6757, E-mail: suda@ee.tut.ac.jp

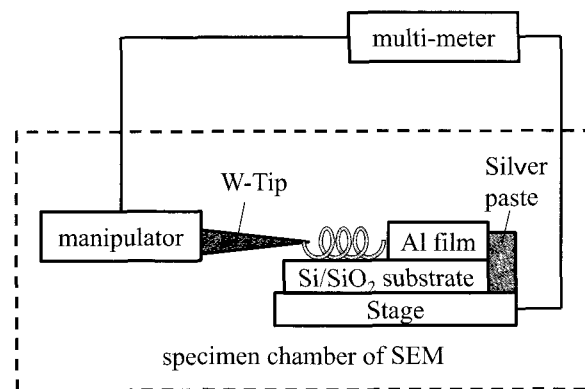


Fig. 1 A schematic of the experimental setup for the measurement of the electrical resistance of CNC

Development of CNT-based Polymer Electrolyte Fuel Cell Electrocatalyst

○Tsuyohiko Fujigaya^{1,2}, Mohamed Reda Berber¹ and Naotoshi Nakashima^{1,2,3}

1 Department of Applied Chemistry, Graduate School of Engineering.

Kyushu University, 744, Motoooka Nishi-ku Fukuoka, 819-0395, Japan

2 WPI I²CNER, Kyushu University, 744 Motoooka, Nishi-ku, Fukuoka, 819-0395, Japan

3 JST-CREST, 5 Sanbancho, Chiyoda-ku, Tokyo 102-0075, Japan

Fuel cell is key technology to convert hydrogen energy into electric power quite efficiently. Especially, polymer electrolyte fuel cell (PEFC) is promising candidate for the energy source of car, portable electronic device, and house. Carbon nanotube (CNTs) have been emerged as a better conductive supporting material for catalyst nanoparticle than conventional material such as carbon black due to their excellent electron conductivity, better electrochemical durability and fibrous structure. The key issue to utilize the CNTs as a supporting materials is to develop a proper method to immobilize the metal nanoparticle onto CNT surface. We have reported **PBI** adsorbed onto the surface of CNTs and acts as the good dispersant of CNTs [1]. By taking the advantage of uniform wrapping of **PBI** on CNTs surface, we utilized this composite (CNT/**PBI**) as a novel carbon supporting materials for the loading of platinum (Pt) nanoparticles to fabricate a electrocatalyst for PEFC. As the result, the CNTs/**PBI** show better efficiency of Pt loading than that of pristine CNTs due to the coordination between Pt ion and **PBI** (Fig. 2), where CNT, PBI and Pt as a electron path, proton path and reaction site, respectively. The obtained electrocatalyst (CNT/**PBI**/Pt) shows excellent Pt utilization efficiency mainly due to the formation of ideal interfacial structure around Pt [2,3].

We fabricated the PEFC membrane electrode assembly (MEA) using acid-doped **PBI** and acid-doped CNT/**PBI**/Pt as a electrolyte membrane and electrocatalyst, respectively, and measured the fuel cell performance using hydrogen and air as fuels [4]. Interestingly, PEFC showed higher power density than the control MEA using carbon black (CB) in place of CNTs (Fig. 2). We assumed the the ideal nano- and micro-structure provided by the CNT/**PBI**/Pt in the electrocatalyst layer lead the better performance [5]. In addition, the durability of CNT-based PEFC was evaluated.

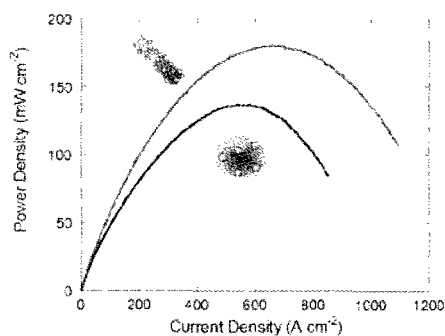


Fig. 2 Power density curves of CNT-based MEA (left) and CB-based MEA (right).

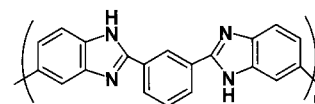


Fig. 1 Chemical structure of PBI.

- [1] *Adv. Funct. Mater.* **18**, 1776-1782 (2008). [2] *Small* **5**, 735-740 (2009). [3] *Carbon* **47**, 3227-3232 (2009). [4] *J. Mater. Chem.* **21**, 1187-1190 (2011). [5] *Unpublished data*

発表索引
Author Index

Author Index

～ A ～

Abe, Shigeaki	1P-50
Abe, T.	1-15
Abiko, Yoshihiro	2P-35
Achiba, Yohji	1-1, 1P-15, 1P-33
Ago, Hiroki	3S-6, 2-6, 3-13, 3P-8, 3P-25
Akasaka, Takeshi	1-4, 2-3, 1P-19, 1P-21, 3P-36
Akasaka, Tsukasa	1P-50
Akiyama, Kazuhiko	1-9, 1P-16, 1P-18
Akiyama, Wataru	1P-26
Akizuki, Naoto	2P-1, 2P-11
Akutsu, Makoto	1-5
Alzubaidi, Ayar	1-3
Amagai, Yuri	1-4
Amemiya, Kenta	1P-34
Ando, Tsuneya	2P-13
Aoki, N.	1-15
Aoki, Nobuyuki	1P-26, 2P-10
Aonuma, Shinji	1P-40
Aonuma, Shuji	1-14
Aoyagi, Shinobu	1P-5
Arai, Shigeo	3-5
Asaka, Koji	2P-31, 3P-2, 3P-35
Ata, Seisuke	2P-22, 2P-23

～ B ～

Baba, Keisuke	1P-24
Badar, Saifullah	1P-45, 2P-17
Balch, Alan L.	1P-19
Bandow, Shunji	3P-17, 3P-38
Berber, Mohamed Reda	3P-42
Bird, Jonathan	1-15, 1P-26, 2P-10
Bissett, Mark	2-6

～ C ～

Cannon, James	2P-15
Charinpanitkul, Tawatchai	3P-31
Chen, Qiang	2P-32
Chen, Xiao	3P-9
Chiashi, Shohei	1P-29, 1P-43, 1P-45, 2P-3, 2P-15, 2P-17, 2P-30, 3-9, 3P-9
Chiba, Kazuki	1-9
Cho, Soon Cheon	1P-20
Cong, Chunxiao	3-11

～ D ～

Dang, Jing-Shuang	1-7, 1P-7
Doi, Tatsuya	1P-26
Doi, Yuta	1P-9
Dresselhaus, Mildred S.	3-11
Duclaux, Laurent	1P-40

～ E ～

Einarsson, Erik	3-9
Eitoku, Takeshi	2P-2
Endo, Tomoaki	1P-23

～ F ～

Ferry, P. K.	1-15
Fujigaya, Tsuyohiko	3P-42
Fujii, Shunjiro	1P-47, 2P-28, 3-4, 3P-5
Fujimoto, Yoshitaka	3P-11
Fujita, Kazuhiro	3P-22
Fukuda, H.	1-15
Fukuoka, Naoya	1P-36
Fukuoka, Tomoko	3P-39
Fukuzumi, Shunichi	1-8
Furuta, Hiroshi	2P-19
Futaba, Don	1P-30, 2-5
Fuyuno, Naoto	3P-20

～ G ～

Gezuhara, Kengo	3-12
Gorgoll, Ricardo Mizoguchi	1P-25
Guldi, Dirk M.	2-3, 1P-13

～ H ～

Harano, Koji	1P-11, 1P-25, 1P-27
Harigaya, Kikuo	3-10
Harima, Hiroshi	3P-13
Harish, Sivasankaran	2P-30
Haruta, Naoki	1-6
Haruyama, Junji	3P-22, 3P-23
Hasdeo, Eddwi	2P-6
Hasegawa, Daisuke	1P-45, 2P-17
Hasegawa, Kai	1P-32, 3-1
Hasegawa, Kei	2P-36
Hasegawa, Tadashi	1-4
Hashida, Toshiyuki	3-3
Hashiguchi, Masahiko	1P-8

Hashimoto, Kenro	1-1, 1P-15	Imahori, Hiroshi	1-13
Hashimoto, Yasuki	3P-22, 3P-23	Inaba, Masafumi	2P-16
Hashimoto, Yoshiaki	3P-22	Inaguma, Masayasu	1P-30
Hasuike, Noriyuki	3P-13	Indahyanti, Ellya	3P-28
Hata, Kenji	1P-30, 2-5, 2P-21, 2P-22, 2P-23	Inoue, Daisuke	1P-42
Hatakeyama, Kazuto	3-12, 3P-28	Inoue, Taiki	1P-43, 1P-45, 2P-17, 2P-30
Hatakeyama, Rikizo	1-5, 1P-20, 1P-46, 2P-32, 2P-35, 3P-10	Inukai, Eri	2P-14
Hatano, Naomichi	3P-16	Irie, Stephan	1P-10
Hatta, Akimitsu	2P-19	Ishibashi, K.	1-15
Hayakawa, Ryoma	2-4	Ishibashi, Koji	2P-10
Hayashi, Daisuke	1P-50	Ishiguro, Yuki	1P-34
Hayashi, Terutake	1-12	Ishii, Satoshi	2P-29
Herranz, M. Angels	2-3	Ishii, Taiga	3P-31
Higo, Junki	1-4	Ishii, Yosuke	1-3
Hirai, Daisuke	2P-12	Ishikawa, Kei	2P-30
Hirai, Takayoshi	1P-44, 2P-34	Iso, Y.	1-15
Hiraiwa, Atsushi	2P-16	Isobe, Hiroyuki	1P-31
Hirama, Daisuke	3P-31	Ito, Toshiyuki	1-16, 1P-24
Hiramatsu, Norihiro	1P-43	Ito, Yasuhiro	3P-5
Hirano, Atsushi	1P-38	Ito, Yoshito	3-13
Hiraoka, Kazushi	2P-20	Ito, Yosuke	1P-33
Hirata, Chika	1P-1	Itoh, Chihiro	1-2, 3P-13
Hisama, Kaoru	1P-29	Itoh, Sachiko	1P-50
Hitosugi, Shunpei	1P-31	Iwamura, Munechiyo	3-7, 2P-1, 2P-11
Hoang, The Ban	2P-25	Iye, Yasuhiro	3P-22
Homma, Naoki	2P-3	Izumi, Yudai	3-9
Homma, Yoshikazu	1P-43, 2P-3	Izumida, Wataru	2-6, 2P-5
Honda, Kazuya	2P-8	~ J ~	
Hongyou, Ken-ichi	2P-4	Jang, Jin	1-11
Horikoshi, Yoshiji	1-10	Jeyadevan, Balachandran	1P-48
Hoshi, Kazuaki	1P-44	Jippo, Hideyuki	3P-21
Hou, Bo	3P-9	~ K ~	
Huziwarra, Masazumi	1P-32	Kaida, Shigeru	2P-41
~ I ~		Kamei, Yuki	3-12
Igarashi, Toru	3P-1	Kamikawa, Shota	3P-22
Ihara, Kazuki	1P-39	Kamizyukoku, Tomoya	3P-7
Iijima, Sumio	1P-36, 1P-49, 3-16, 3-17, 2P-38, 3P-30	Kamoi, Susumu	3P-13
Iizuka, Tadashi	1P-49	Kamon, Keiichi	3P-26
Iizumi, Yoko	2P-37, 2P-38	Kaneko, Tomoaki	3-10
Ikeda, Akinobu	1P-10	Kaneko, Toshiro	1-5, 1P-20, 1P-46, 2P-32, 2P-35, 3P-10
Ikehara, Yuzuru	2P-37	Kanno, Manabu	1P-2, 1P-3, 1P-10
Ikuma, Naohiko	1P-9, 1P-12, 1P-17	Kano, Kazumasa	1-12

Karita, Motoyuki	2P-31	Kondo, Hiroki	1P-36
Kasama, Yasuhiko	1P-22, 1P-23, 2-2	Kono, Hirohiko	1P-2, 1P-3, 1P-10
Kataura, Hiromichi	1P-32, 1P-38, 1P-41, 1P-47, 2P-14, 2P-24, 2P-28, 3-1 3-4, 3P-5	Koretsune, Takashi	3-6, 3P-11
Kato, Haruhisa	2P-2	Kosugi, Naoki	3P-22, 3P-23
Kato, Teppei	3P-14	Koyama, Takeshi	3-13, 3P-2
Kato, Toshiaki	1-5, 1P-46, 2P-35, 3P-10	Kozawa, Daichi	2P-20, 3P-20
Kato, Yuto	3P-22	Kramberger, Christian	3-9
Katsumoto, Shingo	3P-22	Kudo, Hikaru	2P-24, 3-1
Kawabata, Youhei	1P-16	Kunimoto, Ryuji	3P-41
Kawachi, Kazuhiko	1P-22, 1P-23	Kuno, Akihiro	2P-26, 2P-27
Kawahara, Kenji	3P-8	Kurabuchi, Yuta	1P-40
Kawai, Hideki	1P-32, 3-1	Kurotobi, Kei	2-1
Kawai, Masatoshi	3P-1	Kusunoki, Michiko	2P-16
Kawai, Takeshi	1P-35	Kuwahara, Yuki	1P-44, 2P-34
Kawarada, Hiroshi	2P-16	Kwon, Eunsang	1P-23
Kawasaki, Shinji	1-3	Kyakuno, Haruka	3P-1, 3P-39
Kawashima, Yuki	1-8	Kyotani, Takashi	3P-39, 3P-40
Kawasuzuki, Tomoya	1P-29	~ L ~	
Kawazoe, Tadashi	3-7	Lee, Haeseong	1-11
Kiba, Takayuki	1P-50	Levêque, Jean-Marc	1P-40
Kim, Dong Young	2P-36	Liu, Gang	1-14, 1P-28, 1P-40
Kimura, Takahide	1-14, 1P-28, 1P-40	Liu, Huaping	1P-41
Kinoshita, Toyohiko	3-9	Lu, Jing	1-4
Kishida, Hideo	3-13, 3P-2	Lu, Xing	1P-19
Kishida, Hirotaka	1-12	~ M ~	
Kishimoto, Shigeru	2P-29, 3P-27	Maeda, Kenji	2P-10
Kisoda, Kenji	1-2, 3P-13	Maeda, Yasushi	1P-42
Kitagawa, Tomoya	2P-18	Maeda, Yutaka	1-4, 1P-21
Kitaura, Ryo	1P-5, 2P-14, 2P-18, 3-5, 3P-4, 3P-26	Mahjoub, Akram	1-15
Kito, Yusuke	3P-7	Manako, Takashi	3-16
Kiyomiya, Masaharu	1P-44, 3P-3	Maniwa, Yutaka	2P-8, 3P-1, 3P-39, 3P-40
Kobayashi, Kazufumi	2P-21	Martin, Nozario	2-3
Kobayashi, Keita	3P-3	Maruyama, Koji	3P-37
Kobayashi, Nagao	1P-21	Maruyama, Masashi	1P-13, 2-2
Kobayashi, Toshihisa	1P-50	Maruyama, Mina	1P-4
Kodama, Takeshi	1-1, 1P-15	Maruyama, Shigeo	1P-29, 1P-43, 1P-45, 2P-15, 2P-17, 2P-30, 3-9, 3P-9, 3P-22, 3P-23
Koh, Heeyuen	2P-15, 3-9	Maruyama, Takahiro	1P-34, 1P-35, 1P-36, 1P-37, 3P-7
Koinuma, Michio	3-12	Masuda, Yoshiho	2P-16
Kokubo, Ken	1-12, 1P-9, 1P-12, 1P-17	Matsuda, Kazunari	2P-1, 2P-11, 2P-18, 2P-20, 3-7, 3P-20, 3P-39, 3P-40
Komatsu, Ken-ichirou	1P-23	Matsui, Jun	1-4, 2P-41
Komatsu, Naoki	1-14, 1P-28, 1P-40	Matsumoto, Yasumichi	3-12, 3P-28
Komuro, Takashi	2-2		
Konabe, Satoru	3-8, 3P-12		

Matsumura, Sachiko	1P-49	Nakahara, Hitoshi	2P-31, 3P-35
Matsunaga, Masahiro	2P-10	Nakai, Yusuke	2P-8, 3P-39, 3P-40
Matsuo, Yutaka	1P-8, 1P-13, 2-2	Nakamura, Arao	3-13, 3P-2
Meikle, Grace	1P-45	Nakamura, Eiichi	1P-11, 1P-13, 1P-25, 1P-27
Michihata, Masaki	1-12	Nakamura, Kenta	1P-43
Mihara, Junya	1-13	Nakamura, Maki	3-17
Mikie, Tsubasa	1P-9	Nakamura, Takashi	1P-2, 1P-3
Minami, Kosuke	1P-27	Nakamura, Toshiya	2P-14
Mishina, Yuki	3P-38	Nakamura, Yuji	1P-12, 1P-17
Mitoma, Nobuhiko	3-15	Nakanishi, Ryo	3-5
Miura, Shogo	1-11	Nakanishi, Takeshi	2P-13
Miyamoto, K.	1-15	Nakanishi, Waka	1P-31
Miyamoto, Katsuhiko	1P-26	Nakanishi, Yusuke	1-9, 1P-18
Miyamoto, Yoshiyuki	3P-18	Nakano, Atsushi	2P-39
Miyashita, Masahiro	3P-8	Nakano, Kaichiro	3-16
Miyashita, Tokuji	2P-41	Nakano, Shun	1P-44
Miyata, Yasumitsu	2P-14, 2P-18, 3-5, 3P-4, 3P-26	Nakashima, Naotoshi	3P-42
Miyauchi, Yuhei	2P-1, 2P-11, 2P-18, 2P-20, 3-7, 3P-20	Nakatsu, Ryo	1P-32, 3-1
Miyaura, Kenshi	3P-4	Nakazawa, Eiko	2P-40
Miyazawa, Kunichi	1P-1	Narituka, Shigeya	1P-34, 1P-35, 1P-36, 1P-37, 3P-7
Mizorogi, Naomi	1P-19, 1P-21, 2-3	Nguyen, Thanh Cuong	3-14
Mizuno, Takaaki	2P-23	Nihey, Fumiyuki	1P-39
Mizuno, Takahiro	3P-17	Nii, Hiroyuki	2P-4
Mizutani, Takashi	2S-4, 2P-29, 3P-27	Niitsu, Naoyuki	1P-2, 1P-3, 1P-10
Momiyama, Daiki	1P-26	Nishida, Tomoko	1P-5
Morisawa, Yusuke	3P-34	Nishihara, Hirotomo	3P-39, 3P-40
Moriyama, Hiroshi	1-11, 1P-14	Nishinaga, Jiro	1-10
Motomiya, Kenichi	2P-40	Nishiyama, Satoko	3-4
Mouri, Shinichiro	2P-1, 2P-11, 2P-20, 3-7, 3P-20	Nitta, Hirohisa	1P-11
Murai, Ryota	1-12	Nobusa, Yuki	2P-24
Murakami, Tatsuya	3-17	Noda, Shoko	1-9, 1P-18
Murakami, Toshiya	1-2, 3P-13	Noda, Suguru	2P-36
Murakoshi, Koshi	1-5, 1P-46	Noguchi, Syunsuke	2P-4
Muranaka, Atsuya	1P-21	Noguchi, Takuya	1P-29
Murata, Yasujiro	1P-5, 2-1	Noiri, Eisei	1P-27
Muro, Takayuki	3-9	Norimoto, Tatsuhiko	3P-31
~ N ~		Nouchi, Ryo	3-15
Nagaoka, Tomoya	3-2	Nugraha, Ahmad Ridwan Tresna	2P-6, 2P-7
Nagasawa, Hiroshi	1P-33	~ O ~	
Nagase, Shigeru	1-4, 1P-19, 1P-21, 2-3	Ochiai, Takumi	2P-16
Nagaya, Yuka	2P-26	Ochiai, Yuichi	1-15, 1P-26, 2P-10
Nakagawa, Hamazo	2P-4	Ogata, Chikako	3-12
Nakagawa, Koji	1P-9	Ogata, Hironori	1-16, 1P-24, 2P-39

Ogawa, Yui	3P-8, 3P-25	~ S ~	
Ogura, Mutsuo	2P-37	Sado, Yuki	1P-5
Oh, Jaebuem	1-11	Saito, Riichiro	2-6, 2P-5, 2P-6, 2P-7, 3-11
Ohfuchi, Mari	3P-21, 3P-29	Saito, Susumu	1P-6, 3-6, 3P-11, 3P-19
Ohkubo, Kei	1-8	Saito, Takeshi	1P-39, 1P-44, 2P-33, 2P-34, 3P-3
Ohmori, Shigekazu	2P-33	Saito, Yahachi	2P-31, 3P-2, 3P-35
Ohtsu, Motoichi	3-7	Sakai, Seiji	1P-22
Okabe, Yuta	3-18	Sakai, Takenobu	1-3
Okada, Hiroshi	2-2	Sakai, Yuki	3P-19
Okada, Susumu	1P-4, 2P-9, 3-8, 3-14, 3P-12, 3P-24	Sakurai, Shunsuke	1P-30
Okamoto, Koji	1P-27	Sakakibara, Satoshi	1P-34, 1P-37
Okazaki, Toshiya	1S-1, 1-1, 2P-2, 2P-37, 2P-38, 3P-1	Sakuramoto, Kenshi	3P-22, 3P-23
Okimoto, Haruya	3P-6	Sanders, Gary	2P-7
Okuda, Shin-ichi	1P-23	Sankaran, R. Mohan	3S-5
Olmstead, Marilyn M.	1P-19	Sano, Masahito	3P-6
Omatsu, T.	1-15	Sano, Noriaki	3P-31
Omatsu, Takashige	1P-26	Sasaki, Fusako	1P-39
Omori, Mamoru	3-3	Sasaki, Masahiro	1P-22
Ono, Akira	1P-33	Sasaki, Yuki	3P-26
Ono, Shin	1P-42	Sato, Kentaro	2P-6, 3-11
Oohara, Kazuyoshi	2P-16	Sato, Shin-Ichiro	1P-50
Osada, Yukihiko	1P-48	Sato, Shintaro	2P-3
Oshima, Takumi	1-12, 1P-9, 1P-12, 1P-17	Sato, Tohru	1-6
Otani, Minoru	3-14	Sato, Yoshinori	1P-48, 2P-40
Otsuji, Taiichi	1S-3	Satou, Akira	1S-3
Ouchi, T.	1-15	Sekiguchi, Atsuko	2P-21
Ozaki, Masahiro	3P-33	Shamoto, Shin-ichi	3P-36
		Shiba, Kiyotaka	1P-49
		Shibata, Rena	1P-44
		Shibuya, Megumi	2P-16
~ P ~		Shigeta, Masahiro	2P-25
Pac, Chyongjin	1-11	Shimizu, Kazuki	3-18, 3P-33, 3P-37, 3P-41
Poonjarernsilp, Chantamane	3P-31	Shimizu, Maki	2P-28, 3P-5
Prassides, Kosmas	1S-2	Shimomura, Shuichi	1P-1
		Shinohara, Hisanori	1-9, 1P-5, 1P-18, 2P-14, 2P-18, 3-5, 3P-4, 3P-26
~ Q ~		Shiomi, Junichiro	1P-29, 2P-15, 2P-30
Quintero, Ricardo	2P-36	Shiraki, Yuki	3P-38
		Shirasu, Keiichi	3-3
~ R ~		Shiromaru, Haruo	1-1, 1P-15
Ranjit, Ghosh	1P-36	Shoji, Mao	1-16, 2P-39
Rao, Apparao	3P-22, 3P-23	Slanina, Zdenek	1P-19, 1P-21
Ryu, Misun	1-11	Song, Ha Yong	1-3
Ryzhii, Victor	1S-3	Stanton, Christopher	2P-7

Subramaniam, Chandramouli	2-5	Tashima, Masayuki	3P-16
Suda, Yoshiyuki	3-18, 3P-33, 3P-37, 3P-41	Tateishi, Hikaru	3-12
Sunayama, Yuuki	1P-48	Tatsumi, Yuki	2P-5
Suntornlohanakul, Tatporn	3P-31	Tatsuki, Yasumitsu	1P-40
Suzuki, Hironori	2P-38	Terada, Tomohiro	3P-35
Suzuki, Manabu	3P-7	Thanh, Cuong Nguyen	3-14
Suzuki, Mitsuaki	1P-19	Thurakitseree, Theerapol	3-9
Suzuki, S.	1-15	Tobita, Hiromi	2-2
Suzuki, Shoji	3P-26	Tohji, Kazuyuki	2P-40
Suzuki, Shinzo	1P-33	Tomioka, Makiko	3P-32
		Tomita, Yoko	3P-24
~ T ~		Toriumi, Naoto	1P-26
Tachika, Hideyuki	1-12	Toyama, Kiyohiko	3-16
Tada, Ryota	3P-6	Toyohiro, Chikyow	2-4
Tahara, Yoshio	3-17, 3P-30	Tsuchiya, Koji	3-2, 2P-26, 2P-27
Tajima, Tomoyuki	2P-38	Tsuji, Masaharu	3P-8, 3P-25
Takada, Tomoya	1P-50	Tsunekawa, Takuya	3P-2
Takada, Yukihiro	3P-15	Tsuzuki, Mayumi	1P-47
Takaguchi, Yutaka	2P-38		
Takahashi, Yoshiyuki	3-2	~ U ~	
Takaki, Yuki	1P-29	Uchiyama, Kouya	1P-14
Takano, Yuta	2-3	Ue, Hitoshi	3-18, 3P-33, 3P-37, 3P-41
Takashima, Kengo	3P-15	Ueda, Kiyoshi	1P-3
Takashima, Tadashi	1P-42	Uejima, Mitsugu	2P-25
Takaya, Yasuhiro	1-12	Ueno, Hiroshi	1P-12, 1P-17
Takenobu, Taishi	2P-24	Ueno, Takao	1P-8
Takesue, Shuhei	2P-27	Umeda, Yoshito	3P-37, 3P-41
Takeuchi, Erina	1-9, 1P-16	Umeyama, Tomokazu	1-13
Takeuchi, Keigo	3P-22, 3P-23	Umino, Takanori	1P-43
Takeuchi, Shigeki	1P-32	Uo, Motohito	1P-50
Takikawa, Hirofumi	3-18, 3P-33, 3P-37, 3P-41	Urabe, Yasuko	1P-41
Takizawa, Morio	3P-17	Usui, Shinji	3P-14
Tamaoki, Masato	2P-29, 3P-27		
Tamon, Hajime	3P-31	~ W ~	
Tanada, Hiroki	1-12	Wada, Takaaki	2P-38
Tanaka, Kazuaki	2P-10	Wada, Yoriko	3P-32, 3P-34
Tanaka, Kazuyoshi	1-6	Wakabayashi, Tomonari	3P-32, 3P-34
Tanaka, ken	1P-22	Wakahara, Takatsugu	1P-1
Tanaka, Takeshi	1P-38, 1P-41, 1P-47, 2P-28, 3-4, 3P-5	Wakayama, Yutaka	2-4
Tange, Masayoshi	2P-2, 2P-38	Wang, Wei-Wei	1-7, 1P-7
Tanigaki, Katsumi	3-15	Wang, Zhipeng	1-16
Taniguchi, Kosuke	3P-31	Wang, Zhiyong	1-9, 1P-18
Taniguchi, Takaaki	3-12	Warner, Jamie H.	3-5
Tanoue, Hideto	3-18, 3P-33, 3P-37, 3P-41	Watanabe, Satoshi	2P-12
		Watanabe, Takahito	2-2

Watari, Fumio	1P-50	~ Z ~	
Wei, Xiaojun	2P-10	Zhang, Minfang	2P-40, 3P-30
		Zhao, Li	1-14
~ Y ~		Zhao, Pei	3P-9, 3P-22, 3P-23
Yagi, Yuko	3P-22, 3P-23	Zhao, Xiang	1-7, 1P-7
Yahagi, Tatsuou	2P-10		
Yajima, Hirofumi	2P-26, 2P-27, 3-2		
Yajima, Takatoshi	1P-37		
Yamada, Atsuo	2P-36		
Yamada, Kensuke	3P-40		
Yamada, Michio	1-4, 1P-21		
Yamada, Takao	2P-21		
Yamada, Takeo	2-5		
Yamada, Yoichi	1P-22		
Yamada, Yuki	2P-36		
Yamaguchi, Hiroya	3P-7		
Yamaguchi, Takashi	3-16		
Yamamoto, Go	3-3		
Yamamoto, Kazunori	3P-36		
Yamamoto, Takahiro	2P-3, 2P-12, 3P-14, 3P-15		
Yamamoto, Yuki	1-2		
Yamamoto, Yuta	3-5		
Yamanaka, Ayaka	2P-9		
Yamasaki, Takashi	1P-31		
Yamashita, Motoi	2P-22		
Yamauchi, Akiko	1P-49		
Yamazaki, Kaoru	1P-2		
Yamazaki, Kazuki	3P-13		
Yanagi, Kazuhiro	1P-32, 2P-8, 2P-24, 3-1, 3P-1		
Yang, Mei	3P-30		
Yasuda, Hidehiro	3P-3		
Yasuda, Toku	1-14		
Yawaka, Yasutaka	1P-50		
Yokoi, Hiroyuki	3P-28		
Yokoyama, Atsuro	1P-49, 2P-40		
Yonemura, Taiichiro	3P-41		
Yoon, Howon	2P-22, 2P-23		
Yoshida, Kazuma	3-13		
Yoza, Kenji	1P-14		
Yu, Ting	3-11		
Yudasaka, Masako	1P-49, 2P-37, 2P-40, 3-16, 3-17, 3P-30		
Yuge, Ryota	3-16		
Yumura, Motoo	1P-30, 2-5, 2P-21, 2P-22, 2P-23		

複写をご希望の方へ

フラーレン・ナノチューブ・グラフェン学会は、本誌掲載著作物の複写に関する権利を一般社団法人学術著作権協会に委託しております。

本誌に掲載された著作物の複写をご希望の方は、(社)学術著作権協会より許諾を受けて下さい。但し、企業等法人による社内利用目的の複写については、当該企業等法人が社団法人日本複写権センター((社)学術著作権協会が社内利用目的の複写に関する権利を再委託している団体)と包括複写許諾契約を締結している場合にあつては、その必要はございません(社外頒布目的の複写については、許諾が必要です)。

権利委託先：一般社団法人学術著作権協会

〒107-0052 東京都港区赤坂 9-6-41 乃木坂ビル 3階

電話：03-3475-5618 FAX：03-3475-5619 E-Mail：info@jaacc.jp

注意：複写以外の許諾(著作物の引用、転載・翻訳等)に関しては、(社)学術著作権協会に委託致しておりません。直接、フラーレン・ナノチューブ・グラフェン学会へお問い合わせください。

Reprographic Reproduction outside Japan

- ・ Making a copy of this publication

Please obtain permission from the following Reproduction Rights Organizations (RROs) to which the copyright holder has consigned the management of the copyright regarding reprographic reproduction.

- ・ Obtaining permission to quote, reproduce; translate, etc.

Please contact the copyright holder directly.

Users in countries and regions where there is a local RRO under bilateral contract with Japan Academic Association for Copyright Clearance(JAACC) are requested to contact the respective PROs directly to obtain permission.

Users in countries or regions in which JAACC has no bilateral agreement are requested to apply for the license to JAACC.

Japan Academic Association for Copyright Clearance (JAACC)

Address : 9-6-41 Akasaka, Minato-ku, Tokyo 107-0052 Japan

Website : <http://www.jaacc.jp/>

E-mail : info@jaacc.jp

TEL : 81-3-3475-5618 FAX : 81-3-3475-5619

2012年9月5日発行

第43回フラーレン・ナノチューブ・グラフェン総合シンポジウム 講演要旨集

<フラーレン・ナノチューブ・グラフェン学会>

〒113-8656 東京都文京区本郷 7-3-1

東京大学大学院工学系研究科 機械工学専攻
丸山研究室内

Tel : 03-3830-4848

Fax : 03-3830-4848

E-mail : fntg@photon.t.u-tokyo.ac.jp

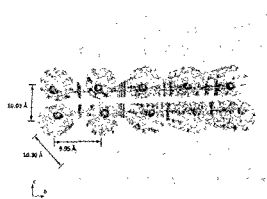
URL : <http://fullerene-jp.org>

印刷 / 製本 (株) 仙台共同印刷

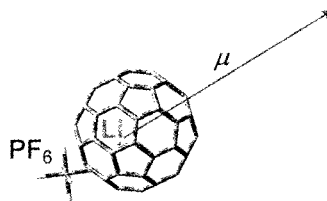


リチウム内包フラーレンは $\text{Li}^+@C_{60}$

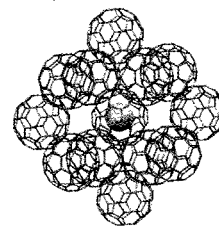
(株) アイデアスター、東北大学、名古屋大学、理化学研究所の共同研究によって、その存在が克明に示されました。(published online: 20 June 2010/DOI:10.1038/NCHEM.698)



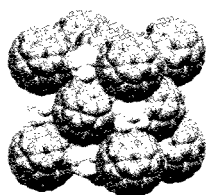
初めてリチウムイオンの内包化を証明した $[\text{Li}@\text{C}_{60}](\text{SbCl}_6)$ 単結晶
—名古屋大学青柳忍先生他—



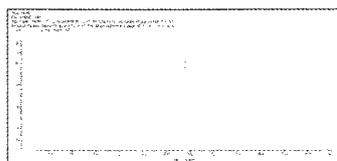
巨大な電気双極子モーメントを持つ $\text{Li}^+@C_{60} \cdot \text{PF}_6^-$ イオン対
—東北大学権根相先生—



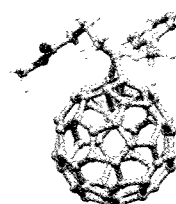
$\text{Li}^+@C_{60} \cdot nC_{60}$ クラスタ
—東北大学権根相先生—



岩塩型構造をとる $[\text{Li}@\text{C}_{60}](\text{PF}_6)$ 単結晶
—名古屋市立大学青柳忍先生他—



陰イオンモードでも $\text{Li}@\text{C}_{60}$ のピークしか観測されない $[\text{Li}@\text{C}_{60}](\text{PF}_6)$ 塩の TOF・MS スペクトル
—アイデア・インターナショナル(株)—



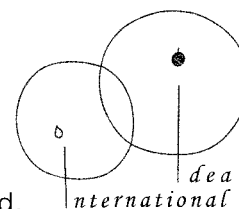
リチウムイオン内包 PCBM に成功
—東京大学松尾豊先生他—

001B01 リチウム内包フラーレンクラスター		
Li ⁺ @C ₆₀ を中心に据えてその周囲を十数個のC ₆₀ が取り囲むように凝集した粉末	1,000 mg	500,000 円
	500 mg	250,000 円
001D04 リチウム内包フラーレン PF ₆		
化学式 : $[\text{Li}@\text{C}_{60}](\text{PF}_6)$ Li ⁺ @C ₆₀ とPF ₆ ⁻ が1:1で対を成す微結晶の粉末	10 mg	210,000 円
	20 mg	390,000 円
	30 mg	570,000 円
	40 mg	747,000 円
	50 mg	930,000 円
	50mg以上のmg当たりの単価	18,600 円
TS001 リチウム内包フラーレンクラスター特別試作品		
Li ⁺ @C ₆₀ , Li, C ₆₀ の混成体粉末をAr雰囲気中で梱包したもの	1,000 mg	400,000 円
	500 mg	200,000 円

Li@C₆₀ の製造・販売

アイデア・インターナショナル株式会社

<http://www.lic60.jp>



Idea International Co., Ltd.

仙台支店・仙台開発センター
〒981-0922 宮城県仙台市青葉区鶯ヶ森1-15-35
Tel:022-342-8410

共同研究室
〒980-8579 宮城県仙台市青葉区荒巻字青葉6-6-04
東北大学未来科学技術共同研究センターハッチェリースクエア高橋研究室
Tel:022-795-3164

本社
〒802-0005 福岡県北九州市小倉北区堺町2-1-1 ライズ小倉ビル3F
Tel : 093-383-6577 Fax : 093-383-6271

Sendai Office and R&D center
1-15-35 Sagigamori, Aobaku, Sendai, Miyagi, 981-0922 Japan
+81-22-342-8410

Joint Research Center
Takahashi-Lab. Hatchery Square, Tohoku-University, 6-6-04
Aramaki Aza Aoba, Aoba-ku, Sendai, Miyagi 980-8579 Japan
+81-22-795-3164

Head Office
3F Rise Kokura Bldg. 2-1-1 Sakai-cho, Kokurakita-ku, Kitakyushu,
Fukuoka, 802-0005 Japan
+81-93-383-6577 Fax: +81-93-383-6271

溶液中の粒子のナノレベル微細化・分散に

BRANSON 超音波ホモジナイザー

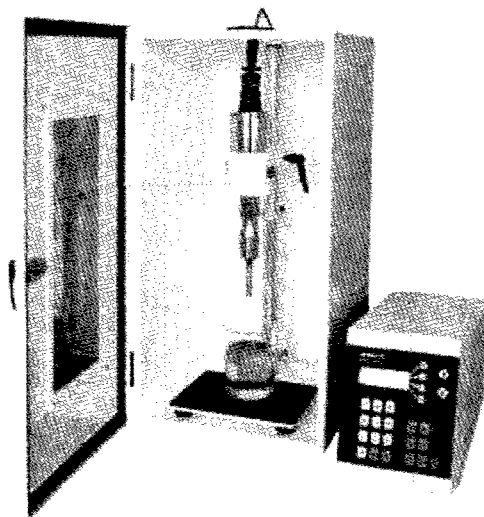
ホーン先端部の振幅の安定性を、より高めた Advance タイプ になりました。

近年のナノテクノロジーの発展及び粉体関連技術の向上により、より微細な粒子に対する乳化分散処理の要望が増えてまいりました。

超音波ホモジナイザーを使用し、均質な乳化分散処理を行い、安定させることにより製品の機能は向上します。

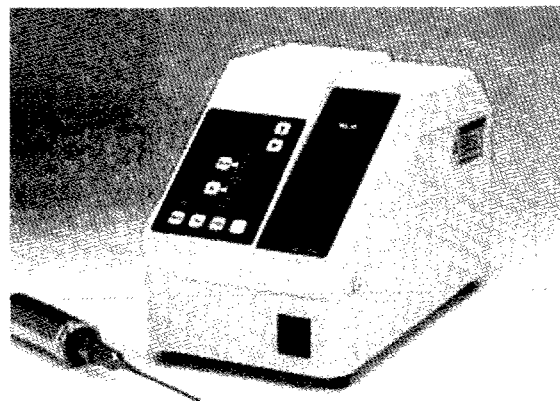
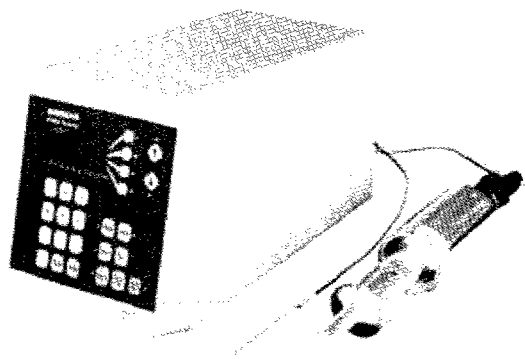
ブランソン社では 20kHz 機と、40kHz 機の 2 タイプを用意しております。

1 次粒子の凝集力にも拠りますが、20kHz 機では 100nm 程度までの分散力があります。40kHz 機は、さらに細かいレベルで分散ができる可能性があります。



20KHz 超音波ホモジナイザー
BRANSON SONIFIER シリーズ

高周波 40KHz 超音波ホモジナイザー
BRANSON SLPe シリーズ



ブランソン社の製品は、ホーン先端部の振幅の安定性が高く、強力なキャビテーションが得られ、効率良く、再現性の高い分散処理が行えます。

主なアプリケーション

分散

カーボンナノチューブ 有機顔料 無機顔料 セラミック セメント 感光体 記録材料
磁性粉 粉末冶金 酸化鉄 金属酸化物 シリカ アルミナ カーボンブラック
ポリマー ラテックス 製紙 ファンデーション

研磨剤 電池 フィラー 光触媒 触媒 ワクチン 体外診断薬 歯磨き粉 シャンプー
半導体 電子基盤 液晶 貴金属 金属 宝石 タイヤ 発酵菌類 その他

乳化

エマルジョン製剤 農薬 トナー ラテックス 界面活性剤 クリーム 乳液 クリーム 等

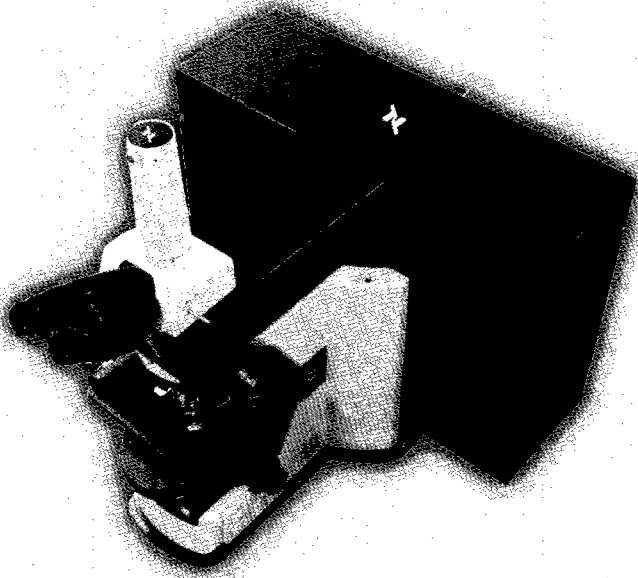
株式会社 **セントラル** 科学貿易

本社：111-0052 東京都台東区柳橋 1-8-1
Tel 03-5820-1500 Fax 03-5820-1515
URL <http://www.cscjp.co.jp/>

大阪支店：Tel 06-6325-3171 Fax 06-6325-5180
福岡営業所：Tel 092-482-4000 Fax 092-482-3797
札幌出張所：Tel 011-764-3611 Fax 011-764-3612

高速・高分解能レーザーラマン顕微鏡

RAMAN-11



グラフェンの分布を5分でイメージング

最高のイメージング性能

独自のコンフォーカル光学系採用により、理論限界に迫る空間分解能 350nm を実現。強度分布の均一なライン照明（特許取得済み）が試料上の 400 点でラマン散乱を同時に励起するため、超高速イメージングが可能です。

超高精度ピークシフト測定

焦点距離 500mm の分光器を搭載し、高波数分解能と光学系の明るさを高いレベルで両立しました。高分解能グレーティングと組み合わせることで、 0.1cm^{-1} を超える精度でピークシフトを検出。応力測定に力を発揮します。

オートメーションを追求

最大で 4 波長のレーザーを搭載でき、ソフトウェアからワンクリックで切り替えて使用できます。わざわざしい光学調整は一切不要です。グレーティングの切り替えやレーザー強度の調整などもすべてワンクリックです。



熱酸化したシリコン基板に分布するグラフェン薄膜のラマンイメージ。炭素 1 原子のシートである単層グラフェンと、二層、三層、四層の多層グラフェンが、それぞれどのように分布しているかを、わずか数分の測定時間と 350nm という高い空間分解能でイメージングしています。

※このサンプルは物質・材料研究機構の津谷大樹様よりご提供頂きました。

■RAMAN-11 標準仕様表

レーザー	532nm / 785nm / その他（電動切換）
イメージング方式	ライン照明 + ビーム走査、ほか各種モード
分光器	焦点距離 500mm 回折格子 3 枚（電動切換）
検出器	電子冷却 CCD 1,340×400 画素
光学顕微鏡	正立型 / 倒立型
空間分解能 (x / y / z)	350nm / 500nm / 1000nm (@532nm)
分光分解能 (FWHM)	1.6cm^{-1} （ピーク位置決め精度は 0.1cm^{-1} ）
ラマンシフト検出範囲	$80\text{cm}^{-1} \sim 5000\text{cm}^{-1}$

製造元

ナノフォトン株式会社

www.nanophoton.jp

販売代理店

アルバック販売株式会社

www.ulvac-es.co.jp

本社：TEL 03-5218-6011

大阪支店：TEL 06-6397-2281

名古屋支店：TEL 0564-65-2251

松本支店：TEL 0263-51-0888

仙台営業所：TEL 022-348-1315

茨城営業所：TEL 029-823-2651

姫路営業所：TEL 0791-62-3951

三重営業所：TEL 059-356-8025

北陸営業所：TEL 076-276-7901

福岡営業所：TEL 092-483-1451

熊本営業所：TEL 0968-38-1115

分析機器のエキスパートグループをめざして



株式会社 東北サイエンス

高度な技術で
安心を提供します

〒980-0811 仙台市青葉区一番町 1-17-24
TEL 022-267-6050 FAX 022-267-6343
<http://www.tohoku-science.co.jp>

Nano & Bio

— フロンティア出版のナノテクノロジー・ナノマテリアルシリーズ —

有機・無機・金属ナノチューブ

— 非カーボンナノチューブ系の最新技術と応用展開 —

編集：清水敏美(産業技術総合研究所)
木島 剛(宮崎大学)
■体裁/B5判・330頁 ■価格/57,750円(税込)

ナノ材料のリスク評価と安全性対策

— 生体・環境への影響,安全性対策・国内外動向 —

監修：豆理文夫(北海道大学)
■体裁/B5判・317頁 ■価格/57,750円(税込)

ナノ空間材料の創製と応用

編集：有賀克彦(物質・材料研究機構)
■体裁/B5判・314頁 ■価格/57,750円(税込)

自己組織化ナノマテリアル

— フロントランナー85人が語るナノテクノロジーの新潮流 —

企画：理化学研究所 フロンティア研究システム
時空間機能材料研究グループ
監修：国武豊喜(北九州市立大学/理化学研究所)
編集幹事：下村政嗣(北海道大学/理化学研究所)
山口智彦(産業技術総合研究所)
■体裁/B5判・392頁 ■価格/57,750円(税込)

グラフェンの最先端技術と拡がる応用

— グラフェンの材料科学,成長・合成技術,各種デバイス応用 —

監修：尾辻泰一(東北大学)
■体裁/B5判・242頁 ■価格/57,750円(税込)

レアメタル・希少金属リサイクル技術の最先端

— ナノ有機・メタラジーが広げるリサイクル技術 —

監修：原田幸明(物質・材料研究機構)
■体裁/B5判・313頁 ■価格/57,750円(税込)

ナノインプリントの最新技術と装置・材料・応用

— ナノインプリント技術の最先端と拡がる用途 —

編集：平井義彦(大阪府立大学)
■体裁/B5判・330頁 ■価格/57,750円(税込)

ナノオプティクス・ナノフォトニクスのすべて

— ナノ光技術の基礎から実用まで —

監修：河田 聡(大阪大学/理化学研究所)
編集：梅田倫弘(東京農工大学)
川田善正(静岡大学)
羽根一博(東北大学)
■体裁/B5判・352頁 ■価格/57,750円(税込)



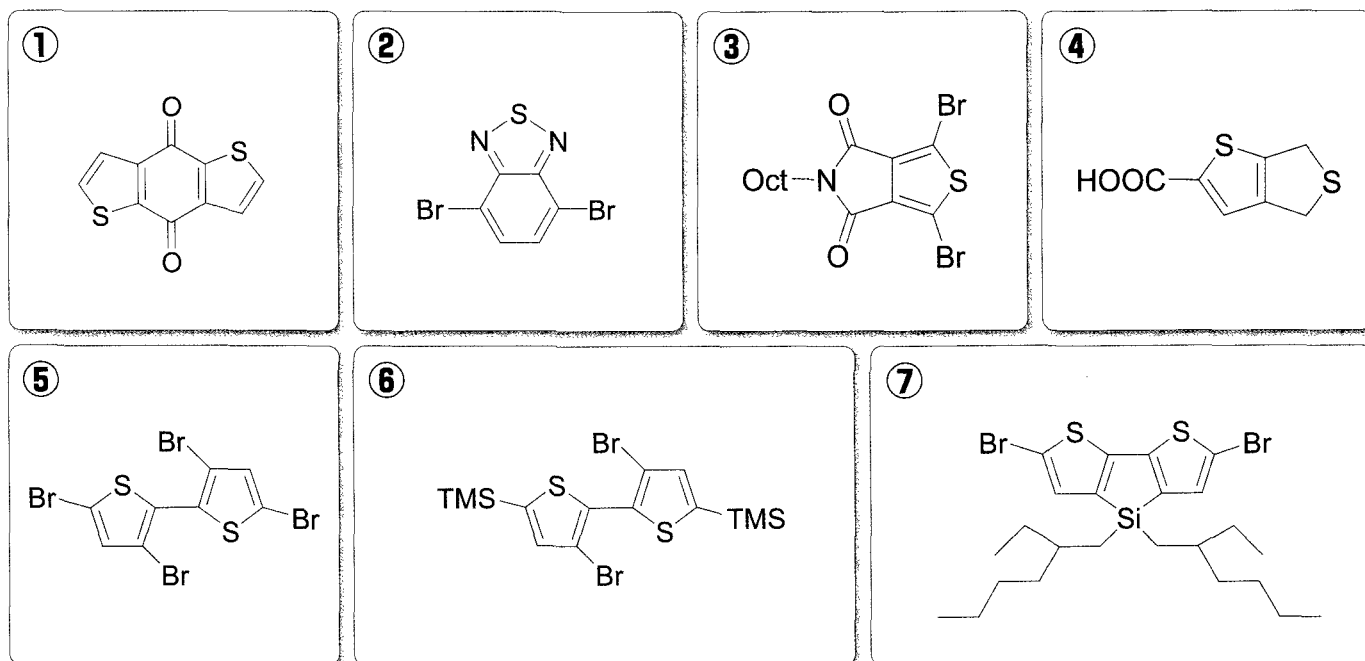
フロンティア出版

〒110-0012 東京都台東区竜泉1-21-18 TEL:03-6802-1640 FAX:03-6802-1641 E-mail:info@frontier-books.com

<http://www.frontier-books.com>

有機薄膜太陽電池材料合成用 ビルディングブロック

次世代の太陽電池として期待される有機薄膜太陽電池の研究用試薬です。
誘導化に利用しやすいよう様々なタイプの間体をラインアップしました。
材料合成にご利用下さい。



番号	コードNo.	品名	規格	容量
①	025-17321	Benzo[1,2- <i>b</i> :4,5- <i>b'</i>]dithiophene-4,8-dione	有機合成用	1g
	021-17323			5g
②	045-31961	4,7-Dibromo-2,1,3-benzothiadiazole	有機合成用	1g
	041-31963			5g
	043-31962			25g
③	042-31971	1,3-Dibromo-5-octyl-4 <i>H</i> -thieno[3,4- <i>c</i>]pyrrole-4,6(5 <i>H</i>)-dione	有機合成用	1g
	048-31973			5g
④	049-31981	4,6-Dihydrothieno[3,4- <i>b</i>]thiophene-2-carboxylic Acid	有機合成用	1g
	045-31983			5g
NEW ⑤	208-18851	3,3',5,5'-Tetrabromo-2,2'-bithiophene	有機合成用	1g
	204-18853			5g
	206-18852			25g
NEW ⑥	040-32131	3,3'-Dibromo-5,5'-bis(trimethylsilyl)-2,2'-bithiophene	有機合成用	1g
	046-32133			5g
NEW ⑦	047-32141	2,6-Dibromo-4,4'-bis(2-ethylhexyl)-4 <i>H</i> -silolo[3,2- <i>b</i> :4,5- <i>b'</i>]dithiophene	有機合成用	1g

和光純薬工業株式会社

本社：〒540-8605 大阪市中央区道修町三丁目1番2号
 東京支店：〒103-0023 東京都中央区日本橋本町四丁目5番13号
 営業所：北海道・東北・筑波・東海・中国・九州

問い合わせ先

フリーダイヤル：0120-052-099 フリーファックス：0120-052-806

URL：<http://www.wako-chem.co.jp>

E-mail：labchem-tec@wako-chem.co.jp

Hitachi Koki 日立小形超遠心機/高速冷却遠心機シリーズ

世界トップクラスの高性能、床置き・卓上、日立なら選べます!

小形超遠心機

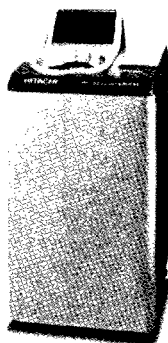
エコでスリムな床置きタイプ

himac CS-FNX Series

世界最高速150,000rpm* (CS150FNX)
世界最大遠心加速度1,050,000×g* (CS150FNX)
クラス最静音45dB(A)*
省スペース床置きタイプの小形超遠心機は日立だけ!

特長

- 世界標準の安全規格CEマーキング適合製品
- サンプルのバランスは目分量でOK!
- ロータは全て載せるだけ! (ロータクイックセッティング方式)
- エコ対応省エネモデル



仕様

形名	CS150FNX	CS120FNX	CS100FNX
最高回転速度 (rpm)	150,000	120,000	100,000
最大遠心加速度 (xg)	1,050,000	771,000	571,000
サイズ (W×D×H mm)	440×520×910		
質量 (kg)	105		
標準価格 (税別)	¥5,500,000	¥4,900,000	¥4,300,000

卓上超遠心機

コンパクトなボディに世界トップクラスの性能

himac CS150NX

世界最高速150,000rpm*
世界最大遠心加速度1,050,000×g*
世界最小コンパクトサイズ*
クラス最静音45dB(A)*

特長

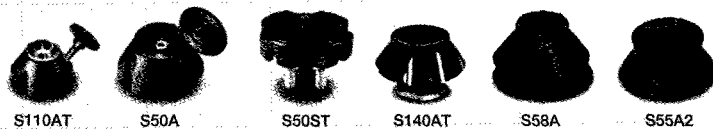
- 短い真空待ち時間
- サンプルのバランスは目分量でOK!
- ロータは全て載せるだけ!



仕様

形名	CS150NX
最高回転速度 (rpm)	150,000
最大遠心加速度 (xg)	1,050,000
サイズ (W×D×H mm)	590×582×408
質量 (kg)	97
標準価格 (税別)	¥6,000,000

*(2012年3月現在当社調べによる)



ロータ仕様

形名	S110AT	S50A	S50ST
最高回転速度 (rpm)	110,000	50,000	50,000
容量 (ml) × 本数 (本)	5.0×8	30.0×6	7.0×4
標準価格 (税別)	¥1,100,000	¥950,000	¥1,500,000
形名	S140AT	S58A	S55A2
最高回転速度 (rpm)	140,000	58,000	55,000
容量 (ml) × 本数 (本)	2.0×10	13.5×8	1.5×12
標準価格 (税別)	¥1,290,000	¥1,000,000	¥750,000

高速冷却遠心機

CR-GⅢシリーズよりもコンパクトなボディにパワフルな性能
使いやすくてスタイリッシュ

himac CR22N

最高回転速度22,000rpm

特長

- クラス最大処理容量*6L
(新ロータR9A2:クラス初*の1.5Lボトル×4本)
- クラス初*の高解像度カラー液晶タッチパネル
- 家庭の冷蔵庫やエアコンで一般的で、きめ細やかな温度制御が可能なインバータ冷凍機をクラス初*搭載。
安定した温度制御とともに省エネ効果も発揮します。
- CEマーキング適合の安全性**



仕様

形名	CR22N	CR21GⅢ	CR20GⅢ
最高回転速度 (rpm)	22,000	21,000	20,000
最大遠心加速度 (xg)	55,200	50,300	48,000
サイズ (W×D×H mm)	700×810×915		
最大処理容量	1.5L×4本	750×810×1,144 1.0L×4本	
画面表示	高解像度カラー液晶		
操作部	液晶タッチパネル		
冷凍機	全密閉型インバータロータリー (冷媒: R410A)		
質量 (kg)	290	300	
標準価格 (税別)	¥2,500,000	¥2,300,000	¥1,800,000

環境にやさしく、使いやすいスタンダード

himac CR21GⅢ

最高回転速度21,000rpm

himac CR20GⅢ

最高回転速度20,000rpm

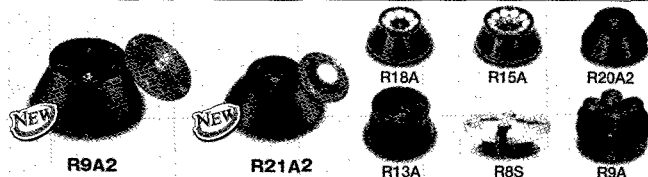
特長

- CEマーキング適合の安全性**
(床面へのアンカーボルト固定不要)
- インバランスを正確にキャッチ
- ロータは全て載せるだけ。
- ロータ自動判別機能 (特許)



*(2012年4月現在当社調べによる高速冷却遠心機比)

**CEマーキング適合外となるロータ (旧型ロータ含む) があります。詳細はお問い合わせください。



ロータ仕様

形名	R9A2	R21A2	R18A	R15A
最高回転速度 (rpm)	8,500	21,000	18,000	15,000
容量 (ml) × 本数 (本)	1,500×4	30×6	50×8	15/50×10
標準価格 (税別)	¥2,200,000	¥350,000	¥450,000	¥550,000
形名	R20A2	R13A	R8S	R9A
最高回転速度 (rpm)	20,000	13,000	8,000	9,000
容量 (ml) × 本数 (本)	50×8	250×6	50×4	1,000×4
標準価格 (税別)	¥350,000	¥770,000	¥800,000	¥1,200,000

注意: R9A2ロータはCR22N専用です。CR21GⅢやCR20GⅢでは使用できません。

【製造・販売・保守】

日立工機株式会社

URL <http://www.hitachi-koki.co.jp/himac/>

・東日本地区

東京都港区港南二丁目15番1号 品川インターシティA棟21階 TEL.03-5783-0614

・西日本地区

兵庫県西宮市津門大筒町10-20 TEL.0798-23-4125

●この広告に掲載した製品は、改善のため外観または仕様の一部を変更することがあります。 ●印刷の都合上、実際の色と異なる場合があります。 ●標準価格は仕様や構成により異なります。 ●全て税別価格となります。 ●安全のために使用環境、使用条件、据付条件が制限される場合があります。



COSMOSIL

誘導体化フラーレン用HPLCカラム

COSMOSIL[®] Buckyprep-D

- 誘導体化フラーレン用HPLCカラムを新発売
- トルエン移動相中で誘導体化フラーレンが分離可能

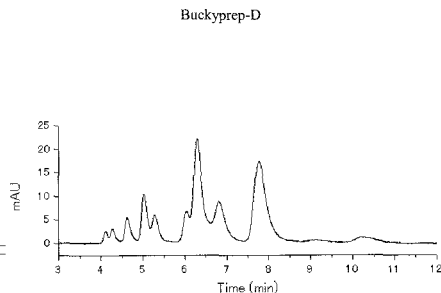
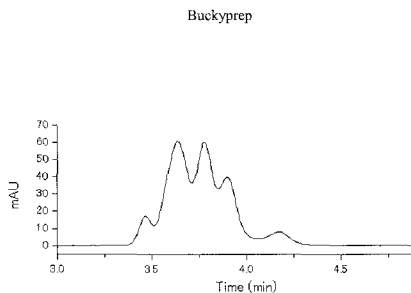
■C60インデン付加体の分析例

C60インデンは誘導体化フラーレンの一種であり、有機薄膜太陽電池のn型半導体材料として注目されている化合物です。コスモシル Buckyprep-Dを用いることにより高い分離性能が得られます。

COSMOSIL Application Data

Column: Buckyprep
 Column size: 4.6mm I.D.-250mm
 Mobile phase: Toluene
 Flow rate: 1.0 ml/min
 Temperature: 30°C
 Detection: UV 325nm

Sample: C₆₀[Indene]₂ (1.0mg/ml)
 Inj. Vol.: 1.0µl



Data courtesy of Yusuke Tajima, Dr. Sci. Organic Optoelectronics Laboratory, RIKEN (Institute of Physics and Chemistry)

NACALAI TESQUE, INC

■Buckyprepシリーズの用途

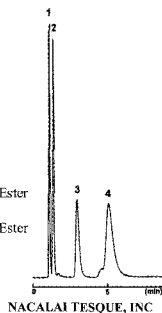
- フラーレン分離のスタンダードカラム → COSMOSIL Buckyprep
- 誘導体化フラーレンの分離 → COSMOSIL Buckyprep-D
- 金属内包フラーレンの分離 → COSMOSIL Buckyprep-M

・誘導体化フラーレン (Buckyprep-D)

COSMOSIL Application Data

Column: Buckyprep-D
 Column size: 4.6mm I.D.-50mm
 Mobile phase: Toluene
 Flow rate: 1.0 ml/min
 Temperature: 30°C
 Detection: UV325nm

Sample: 1; C₆₀ (0.125mg/ml)
 2; C₇₀ (0.250mg/ml)
 3; [6,6]-Phenyl-C₆₁ Butyric Acid Methyl Ester [PCBM] (0.125mg/ml)
 4; [6,6]-Phenyl-C₇₁ Butyric Acid Methyl Ester [[70]PCBM] (0.375mg/ml)
 Inj. Vol. 1.0µl



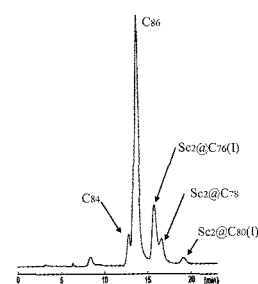
NACALAI TESQUE, INC

・金属内包フラーレン (Buckyprep-M)

COSMOSIL Application Data

Column: Buckyprep-M
 Column size: 4.6mm I.D.-250mm
 Mobile phase: Toluene
 Flow rate: 1.0 ml/min
 Temperature: 30°C
 Detection: UV312nm

Sample: Sc₂@C₇₀(I)
 Sc₂@C₇₀
 Sc₂@C₈₀(I)
 C₈₆



NACALAI TESQUE, INC

Sample courtesy of Prof. H. Shinohara, Department of chemistry, Nagoya University

詳しい情報はWeb siteをご覧ください。

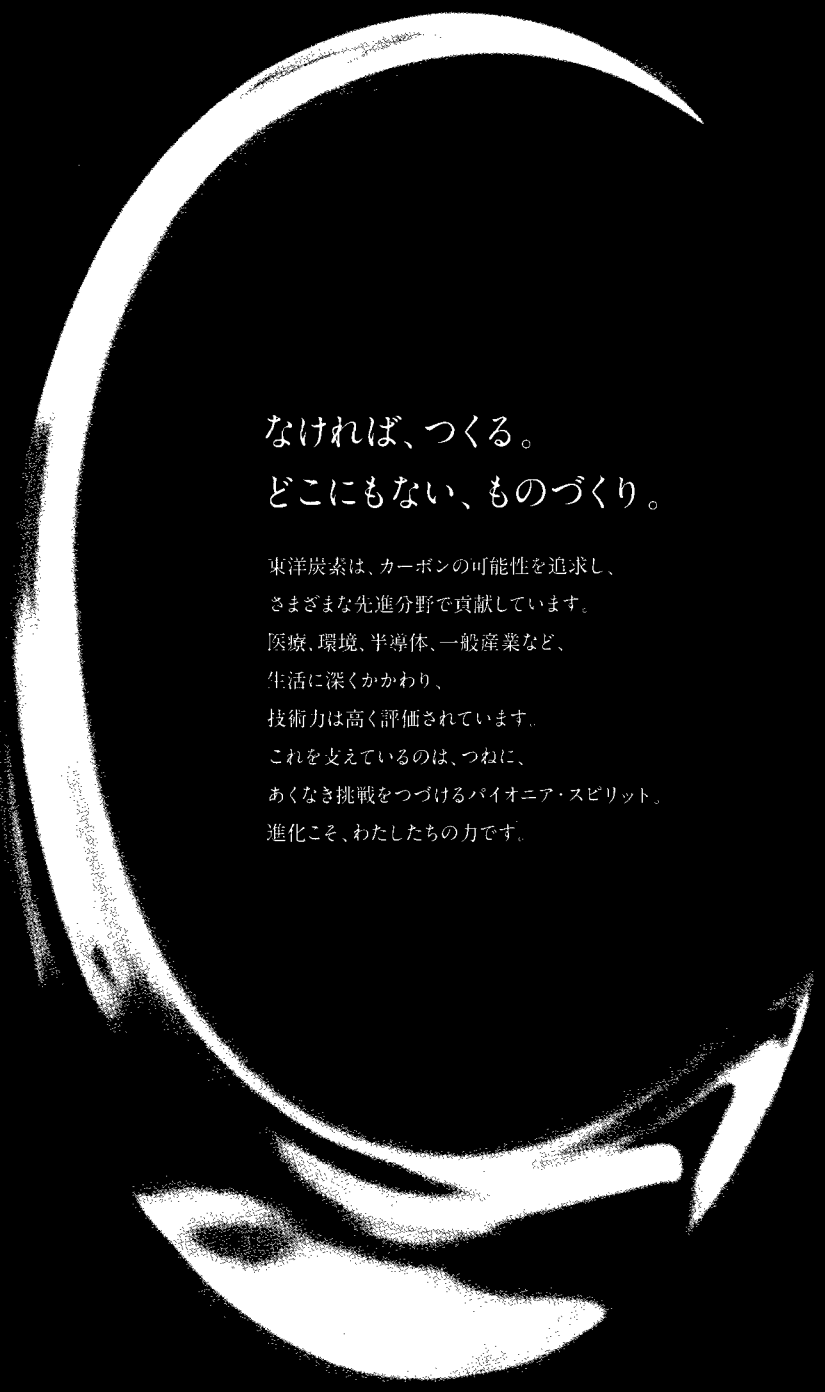
ナカライテスク株式会社

〒604-0855 京都市中京区二条通烏丸西入東玉屋町498

価格・納期のご照会 フリーダイヤル 0120-489-552

製品に関するご照会 TEL:075-211-2746 FAX:075-211-2710

Web site: <http://www.nacalai.co.jp>



なければ、つくる。
どこにもない、ものづくり。

東洋炭素は、カーボンの可能性を追求し、
さまざまな先進分野で貢献しています。
医療、環境、半導体、一般産業など、
生活に深くかかわり、
技術力は高く評価されています。
これを支えているのは、つねに、
あくなき挑戦をつづけるバイオニア・スピリット。
進化こそ、わたしたちの力です。


TOYO TANSO
Inspiration for Innovation

東洋炭素株式会社

本社 〒530-0001 大阪市北区梅田3-3-10 梅田ダイビル10F Tel 06-6451-2114 Fax 06-6451-2186 www.toyotanso.co.jp

ナノラプター NANORUPTOR[®] サンプル密閉式超音波分散装置

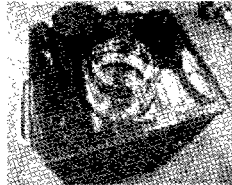
バイオの技術をナノテクへ

本装置はカーボンナノチューブ・グラフェンや燃料電池用触媒を始めとする
各種ナノ粒子を分散させる事を目的に開発いたしました。

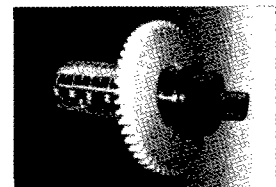
実施例：カーボンナノチューブ・グラフェンの分散、燃料電池触媒評価
納入実績：各大学、自動車メーカー、光学機器メーカー、電子部品メーカー



デモ機をご用意
しております。
どうぞお気軽に
お問い合わせ
ください。



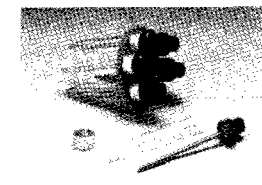
回転機構付破碎槽



標準50mlチューブ



高効率新型破碎槽



15mlチューブ



1チューブ収束装置付破碎槽



1.5mlチューブ

対象試料 / 特長

- カーボンナノチューブ、フラーレン、グラフェン等ナノ粒子
- 密閉処理（ナノリスク低減）：溶媒の蒸発・揮散やコンタミがありません。
- 多検体同時処理（100μl～20ml）：試料チューブの選択により、複数試料を同時に処理できます。
- 再現性良好：回転機構の採用により均一な超音波照射が可能です。
- 低騒音：高性能防音箱の採用により、超音波特有の騒音を防止。
- 温度制御が容易：バスタブ式なので低温から40℃まで任意に設定可能（オプション）。

NR-350仕様（予告無く変更する場合があります）

品番	NR-350
品名	密閉式超音波分散装置 Nanoruptor
超音波周波数	20 kHz
超音波出力	380,300,250,130 W (切替式)
電源	100 V、50/60 Hz、5.5 A
最低設置スペース概寸	400 (W) × 350 (D) × 680 (H) mm
発振ユニット概寸	400 (W) × 280 (D) × 160 (H) mm
処理ユニット概寸	250 (W) × 200 (D) × 300 (H) mm
消音箱概寸	400 (W) × 350 (D) × 520 (H) mm
NR-350 全体重量	36 Kg
ランタイム	599 サイクル
インターバルタイマー (ON)	0～59 秒、デジタル
インターバルタイマー (OFF)	0～59 秒、デジタル
処理本数	1本 (50 mL チューブ)～各種
付属品	高性能消音箱、電源ケーブル、 接続ケーブル、排水ポンプ、 取り扱い説明書、ユーザー登録カード
備考	NR-350は機器のみです。別途処理量に 応じたアクセサリ（ギヤ・板+チップ） をお買い求め下さい。

品名	品番	包装	希望販売価格
超音波密閉式分散装置	NR-350	1 UNIT	¥1,950,000-
50 mL チューブ用チップ	MM-50WS	1 SET	¥54,000-
使用可能チューブ：マルエム社製 50 mL ねじ口試験管			
ギヤ板	NG350-50	1 PC	¥9,000-
冷水循環器	CP80-R	1 UNIT	¥264,000-
冷水循環器接続ケーブル	TU-100	1 PC	¥15,000

販売

人と科学のステキな未来へ

コスモ・バイオ株式会社

〒135-0016 東京都江東区東陽2-2-20 東陽駅前ビル
URL: <http://www.cosmobio.co.jp>
TEL (03) 5632-9610 FAX (03) 5632-9619
販売支援部 栗原 mkurihar@cosmobio.co.jp
開発部 笹原 ksasahar@cosmobio.co.jp

製造

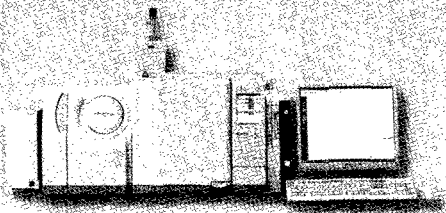
東湘電機株式会社

〒232-0027 神奈川県横浜市南区新川町5-29-2 新井ビル2F
TEL (045) 261-8388 FAX (045) 252-8935
技術部長 伊藤
e-mail: k-ito@bioruptor.jp

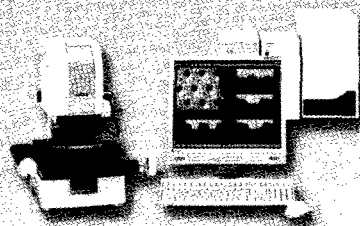
Best for Our Customers

～すべてはお客様のために～ を合言葉にナノテク新材料における最高のソリューションを提供します。

熱分解生成物・
発生ガスの分析
ガスクロマトグラフ質量分析計
GCMS-QP2010 Ultra



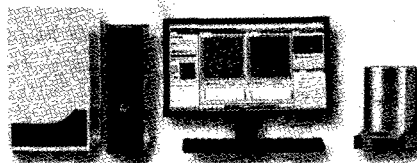
あらゆるナノテク材料を
観察・測定
ナノサーチ顕微鏡
SFT-3500



微量CNTの純度・熱特性評価
CNTの結晶性と耐熱性の評価
マイクロ熱重量測定装置
TGA-50



直径測定
精製前後の観察
CNTとポリマーコンポジット
試料の観察
走査型プローブ顕微鏡
SPM-9700

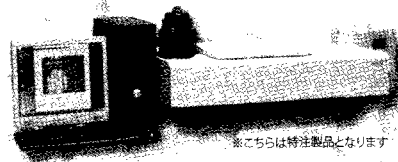


TG/DTA同時測定装置
DTG-60/60H

CNTの紫外可視近赤外
吸収スペクトル測定
紫外可視近赤外分光光度計
SolidSpec-3700



SWNTの近赤外PL
3次元分布測定
近赤外フォトルミネッセンス測定システム
NIR-PL System



紫外可視近赤外分光光度計
UV-3600



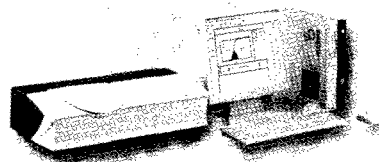
分散・凝集過程評価
高感度ナノ粒子径分布測定装置
SALD-7100H



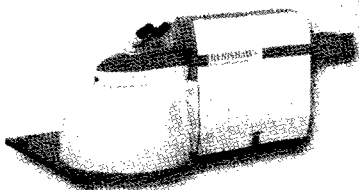
触媒元素の測定
ツインシーケンシャル形ICP発光分析装置
ICPS-8100



独自のIG法による
シングルナノ領域の粒子径評価
シングルナノ粒子径測定装置
IG-1000



直径測定
結晶性と耐熱性の評価
ラマン分光光度計
inVia シリーズ (レニショー社製)



比表面積と吸着特性
マイクロメリティクス
自動比表面積/細孔分布測定装置
トライスターII 3020シリーズ



nanotech
SHIMADZU

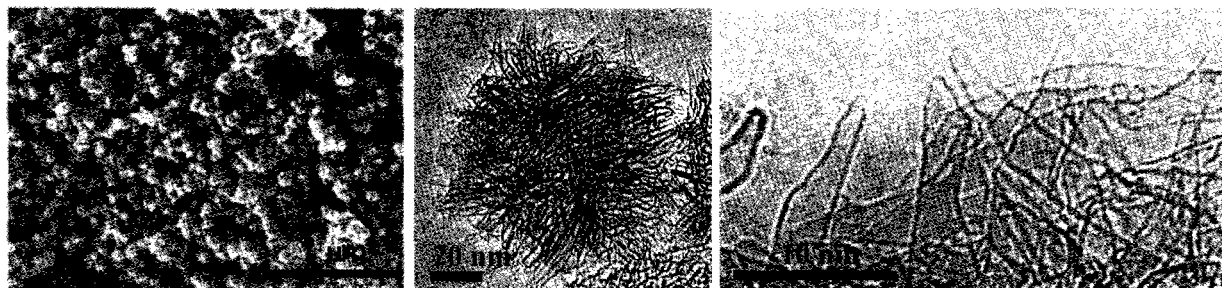
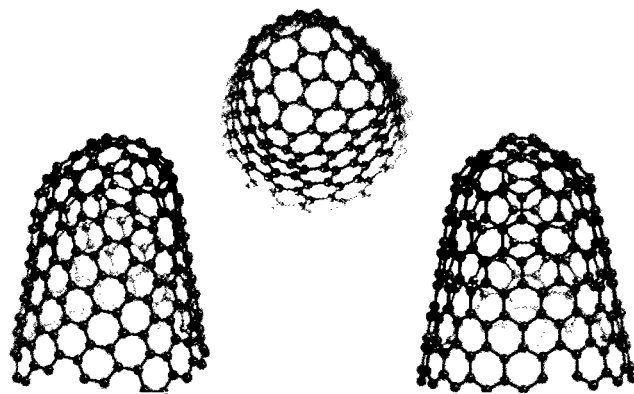
Total solutions for the future of nanotechnology

株式会社 島津製作所

分析計測事業部 グローバルマーケティング部
〒604-8511 京都市中京区西ノ京桑原町1
TEL075-823-1468 FAX075-841-9325 <http://www.an.shimadzu.co.jp>

グリーンイノベーションに貢献する革新的で実用向きの材料

カーボンナノホーン



日本電気株式会社
共通ソリューション開発本部

〒108-8423 東京都港区芝五丁目21-6(芝ダイビル)
TEL : 03-3798-6402
E-Mail : info@embedded.jp.nec.co

サンプル販売中！

1グラムからサンプルをご用意しています。
詳しくは、ホームページを御覧ください。

カーボンナノホーン サンプル販売ホームページ

<http://www.nec.co.jp/embedded/products/cnh/>



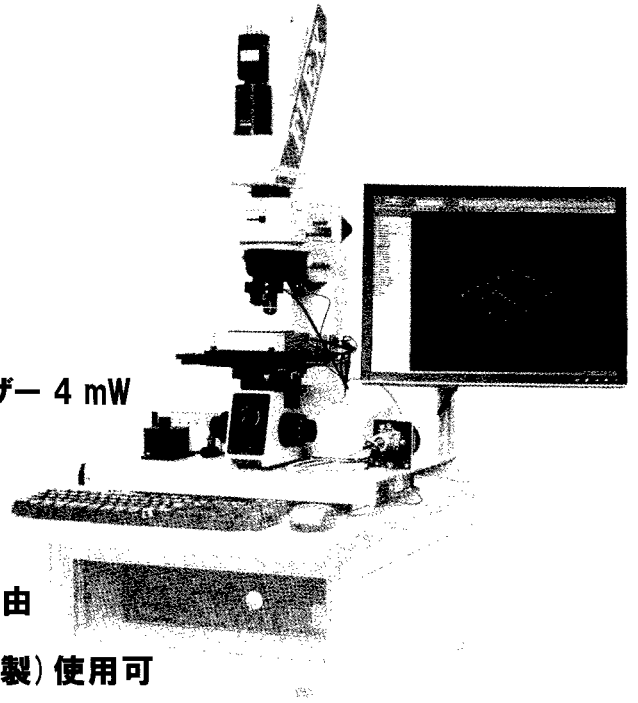
モジュラータイプの3D顕微ラマン

Nanofinder® FLEX

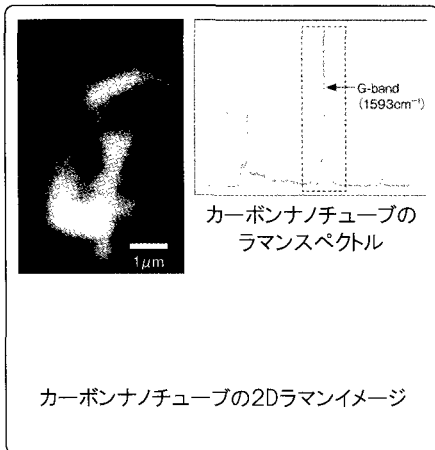
小型・低価格の3Dラマンイメージング装置

特長

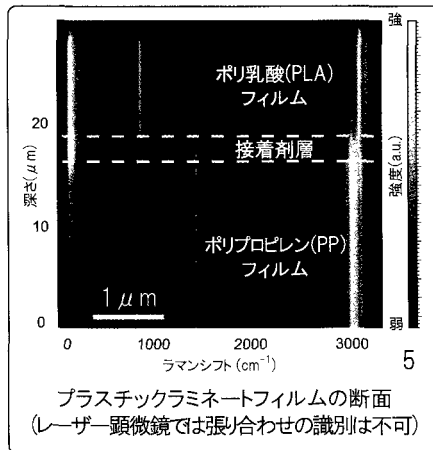
- 空間分解能 350 nm以下
- ピエゾステージ (X-Y-Z) 採用で送り精度 nm
- 高感度 (Siの4次光を1分以内に検出) 低照射レーザー 4 mW
- EMCCD検出器を搭載可能
- ラマン光学ユニットはA4サイズに凝縮
- 光ファイバーの採用でレーザー、分光器の設置場所は自由
- お手持ちのレーザー、分光器、冷却CCD (ANDOR社製) 使用可
- 定評ある Nanofinder® シリーズのソフトウェアを使用



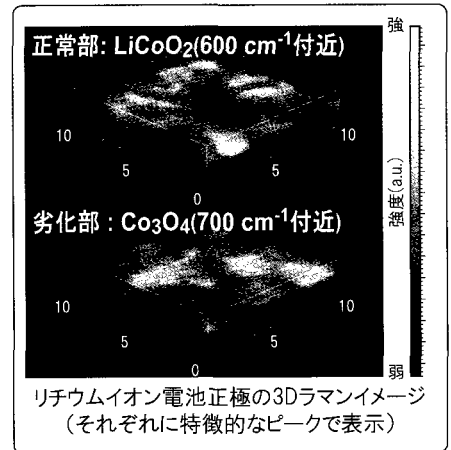
カーボンナノチューブ



ラミネートフィルム



リチウムイオン電池正極



株式会社 東京インスツルメンツ

E-Mail: sales@tokyoinst.co.jp

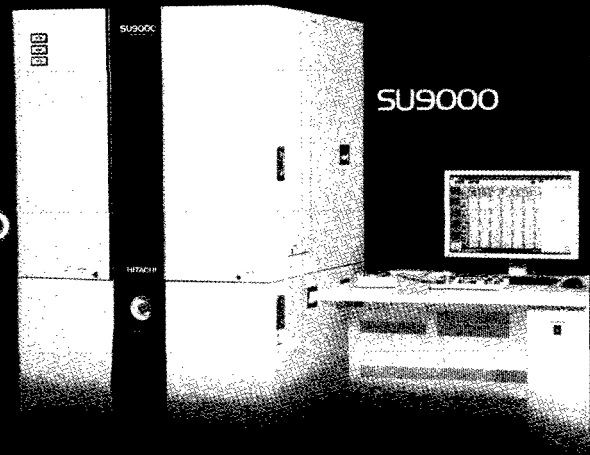
Web site: <http://www.tokyoinst.co.jp/>

本社 〒134-0088 東京都江戸川区西葛西6-18-14 Tビル TEL 03(3686)4711 FAX 03(3686)0831
大阪営業所 〒532-0003 大阪市淀川区宮原4-1-46 新大阪北ビル TEL 06(6393)7411 FAX 06(6393)7055

日立ハイテク
HITACHI



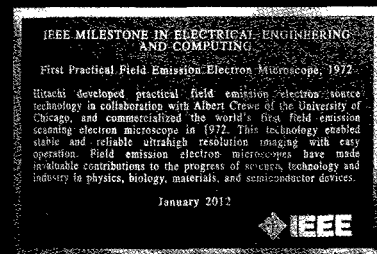
世界を変えたFE技術。 半世紀に渡る 深化の最先端へ。



「電界放出形電子顕微鏡の実用化」が
IEEEマイルストーンに認定されました。

1969年、日立はFE電子源の技術開発に着手。それからわずか3年でFE技術を実用化して、FE-SEM*1の開発に成功。以来、40年以上にわたり日立のFE技術は、高分解能なSEMやTEM*2に採用され、生物、材料、半導体などの幅広い分野で世界の科学や医学、産業の発展に大きく貢献してきたのです。

*1 電界放出形走査電子顕微鏡 *2 透過電子顕微鏡



最先端を、最前線へ。

 株式会社日立ハイテクノロジーズ

本社 〒105-8717 東京都港区西新橋一丁目24番14号 電話 ダイヤルイン (03) 3504-6111
インターネットでも製品紹介しております。以下のURLへアクセスしてください。

 <http://www.hitachi-hitec.com/science/>

北海道(札幌) (011) 707-3200

東北(仙台) (022) 264-2211

中部(名古屋) (052) 219-1670

関西(大阪) (06) 4807-2552

四国(高松) (087) 814-9911

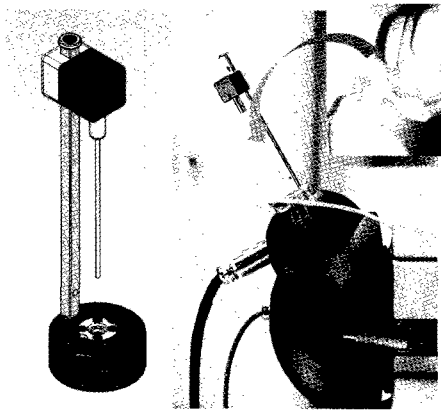
九州(福岡) (092) 778-3015

沖縄 (098) 863-8925

合成確認のためのMS

固体・粉体・液体サンプルからダイレクトに精密MS分析

ダイレクトプローブ (DIP) を取り付けけたDIPイオン源



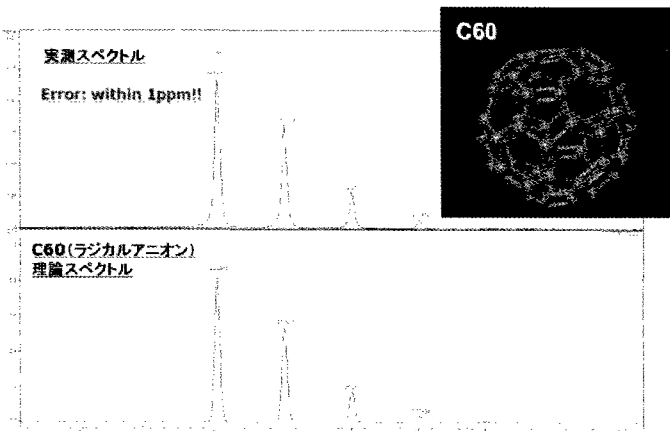
ダイレクトプローブ (左) はブルカー社イオンソースに取り付け可能です。試料調整は簡単で、ディスクのガラス管 (緑色) を粉体、または、液体のサンプルに浸し、イオン源にガラス管を差し込むだけです。



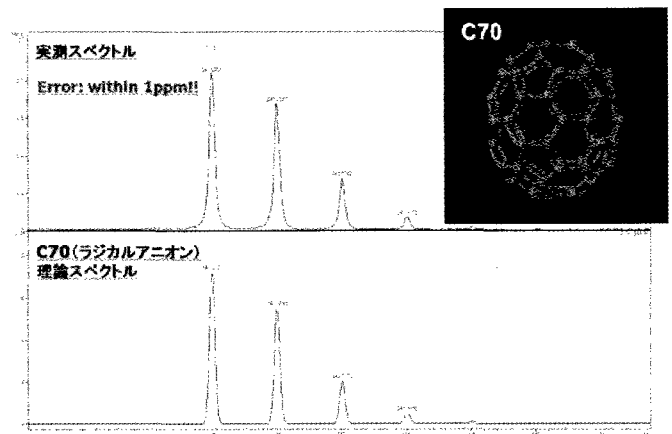
飛行時間型質量分析装置
microTOF II システム

microTOF IIIにDirectProbeを組み合わせて、フラーレンなどの粉体試料を直接測定することができます。

DirectProbe 測定スペクトル(例)



DirectProbe 測定スペクトル(例)



Bruker DaltonicsのDirectProbeはガラスキャピラリーで粉体や原液を捕捉し、そのままmicroTOF IIIに導入して測定することができます。例えばTLC(薄層クロマトグラフィー)で分離後に表層から掻き取った試料をのせて導入する、あるいは合成した試料をそのまま打ってみる、といったようにとてもスピーディーです。

Innovation with Integrity

LC/GC-TOF MS

詳しくは、www.bruker.jpをご訪問ください。

ブルカー・ダルトニクス株式会社

●営業本部・テクニカルサポートセンター
〒221-0022横浜市神奈川区守屋町3-9
TEL: 045-440-0471 FAX: 045-453-1827

●大阪営業所
〒532-0004 大阪市淀川区西宮原1-8-29 テラサキ第2ビル2F
TEL: 06-6396-8211 FAX: 06-6396-1118



微小物分析用顕微レーザーラマン

DXR Raman Microscope

微小物をかんたん確実に分析、新しい顕微ラマンシステム

- 前処理不要、1 μ mの微小物を分析
- 特許の自動光軸調整、微小物の確実な分析
- 内包物の非破壊分析、深さ方向分析
- 分析に最適な条件を、全て自動で設定
- 豊富なライブラリによるラマンスペクトル検索



サーモフィッシャーサイエンティフィック株式会社

〒221-0022 神奈川県横浜市神奈川区守屋町3-9 C棟2F ☎ 0120-753-670

E-mail: info-jp@thermofisher.com www.thermoscientific.jp

Part of Thermo Fisher Scientific

Thermo
SCIENTIFIC

非接触・非破壊による高度な薄膜解析装置 分光エリプソメーター

分光エリプソメーターは偏光解析法により、試料の膜厚および光学定数の波長分散を求める装置です。高度な測定解析が可能です。(異方性物質解析・偏光解消・ミューラー行列)

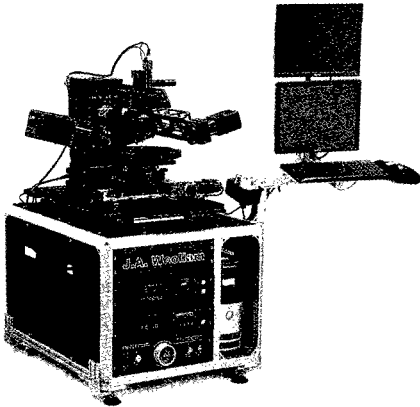
<測定解析項目>

- ・光学定数(屈折率:n, 消衰係数:k)
- ・表面層、界面層
- ・薄膜の膜厚
- ・結晶度
- ・分子種などの化学結合情報
- ・異方性
- ・膜構成物質の混合比

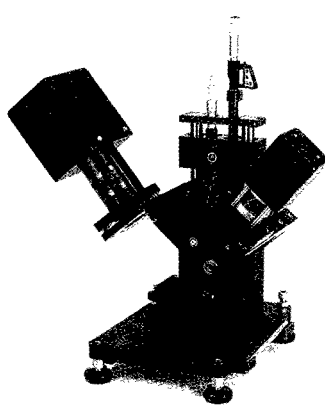
次世代のエリプソメーター 高速Ex-Situ, In-Situ測定 高速分光エリプソメーター M-2000®シリーズ

数百の波長を同時に、しかもエリプソメトリーパラメータ(Ψ ・ Δ)のフルレンジを測定します。分光データをリアルタイムで解析し、膜情報を成膜装置へフィードバックできます。

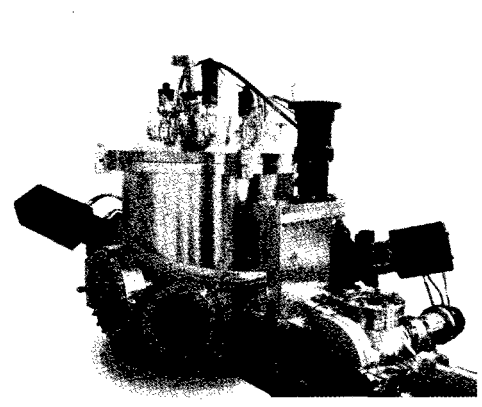
自動多入射角装置



手動多入射角装置



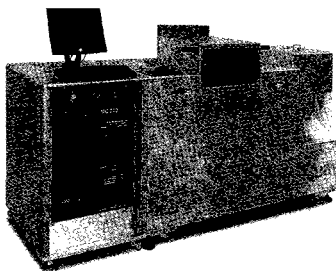
成膜装置取付 in-situ測定



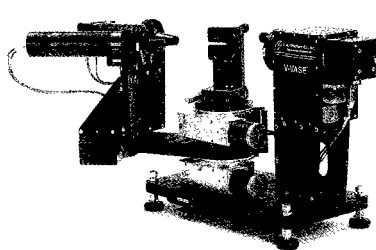
VUV真空紫外(145nm)からIR赤外域(33 μ m)まで測定可能な装置 自動多入射角分光エリプソメーター VASE®シリーズ

複数入射角で広範な波長域の分光データを同時に解析することで、薄膜の様々な情報を得ることができます。

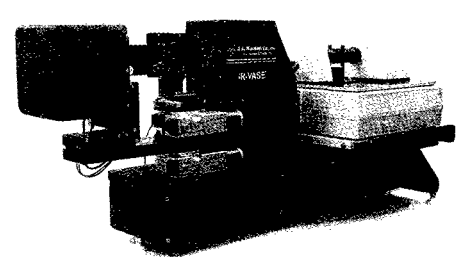
VUV-VASE (真空紫外-近赤外域測定)



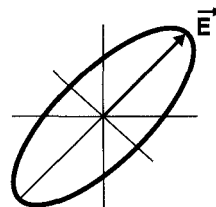
標準VASE (紫外-近赤外域測定)



IR-VASE (赤外域測定)



* サンプル測定(デモ測定または有償測定)は随時行っております。お問合せください。



ジェー・エー・ウーラム・ジャパン株式会社

〒167-0051 東京都杉並区荻窪 5-22-9 藤ビル2F

TEL. 03-3220-5871 FAX. 03-3220-5876

E-mail info@jawjapan.com

http://www.jawjapan.com

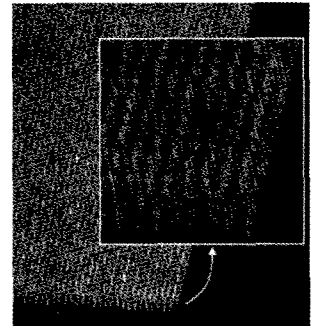
AIXTRON

アイクストロン社の

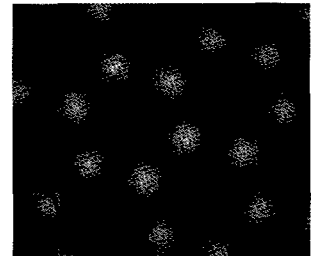
カーボンナノチューブ&グラフェン成長用CVD装置 **Black Magic**



Dense CNT



Horizontal SWCNT



Graphene

- 装置導入後、すぐに希望のCNTやグラフェンを成長可能
- オリジナルのレシピ付き「Thermal CVDとPlasma CVDの2モードに対応」
(シングルCNT用、ダブルCNT用、マルチCNT用、グラフェン用、横方向CNT用、低圧カブプロセス用、高速成長CNT用など)
- あらゆる基板サイズに対応 (研究用2"、4"、6"モデルから量産用最大300mmモデルまで)
- プラズマによる簡単クリーニングと高メンテナンス性
- 世界中の大学・研究所・企業に納入済み

アイクストロン株式会社

<http://www.aixtron.com>

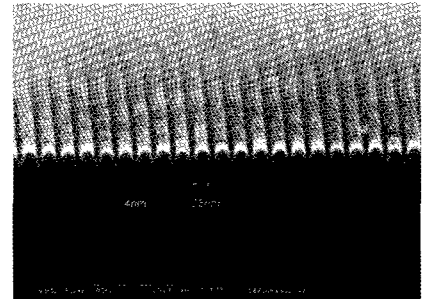
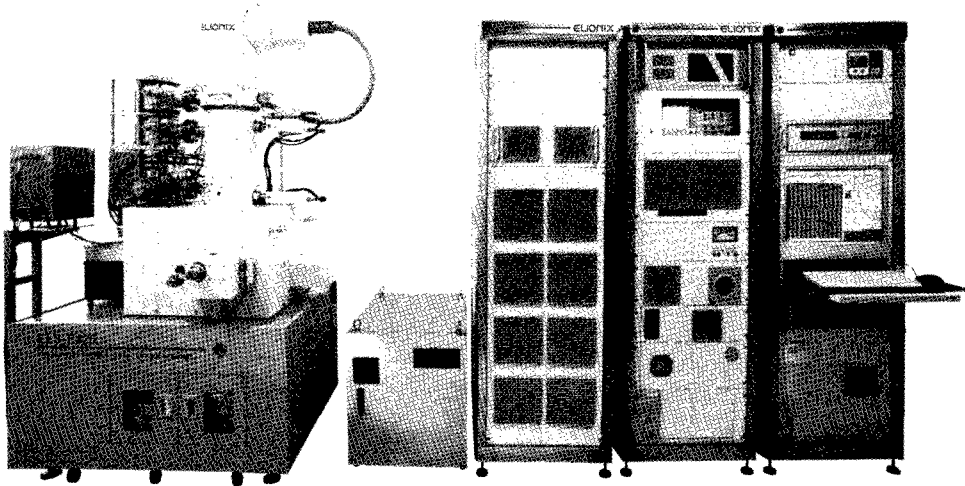
E-mail: JAPANINFO@aixtron.com

〒140-0001 東京都品川区北品川 1-8-11 Daiwa 品川 North ビル 9F TEL: 03-5781-0931 FAX: 03-5781-0940

加速電圧125kVによる高領域、低歪、高精度精細描画を実現

ELS-F125

超高精細高精度電子ビーム描画装置



最高加速電圧 125kV の照射系を採用により最小径φ1.7nm のビームが長時間安定して得られます。市販レジストにおいて 5nm 以下の細線パターンを描画可能。高領域、低歪の描画フィールドにより、均一かつ高精度な描画に成功しました。

ECR プラズマ方式によりナノインプリントモールド作成

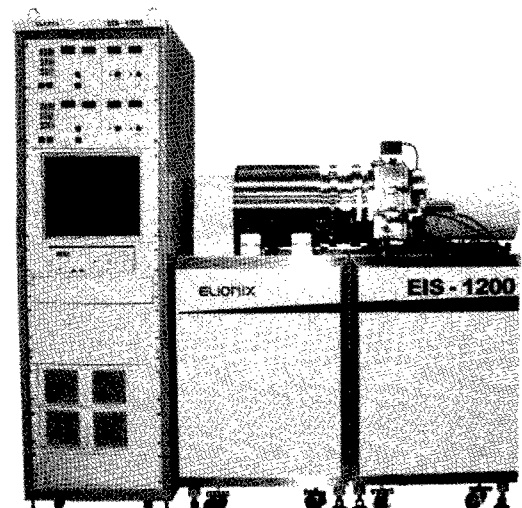
EIS-1200

ECRイオンシャワー装置

ナノインプリント用モールド作成などのナノテク分野の研究・加工で必要となる基板や、シリコン、磁性膜などのエッチングを可能です。プラズマ生成室とエッチング室が分離しているため、エッチングパラメーターとしてのビーム条件などを独立に扱えます。

操作部、表示系を全て PC 上で処理できるようにし、ユーザーフレンドリーな装置です。レシピ記憶機能、自動スケジュール機能により、様々な材料のエッチングに対応します。

ステージ温度、ビーム分布のモニター機能や、各種のプラズマ条件、ビーム加速条件の設定とスケジュール機能を用いることでレジストの熱ダメージを抑えながらプロセス設計を行うことができます。



株式会社 エリオニクス

本社・ショールーム 〒192-0063 東京都八王子市元横山町3-7-6

西日本営業所 〒563-0025 大阪府池田市城南1-9-22 (グリーンプラザ2F)

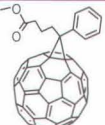
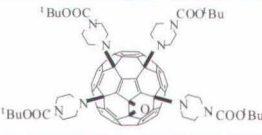
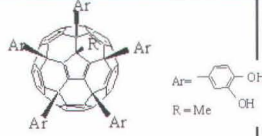
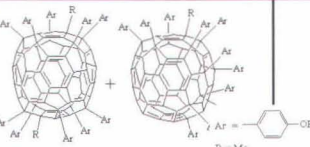
<http://www.elionix.co.jp/>

TEL 042-626-0611

TEL 072-754-6999

フラーレン販促キャンペーン実施中!

- ・フロンティアカーボン(株)では7月~9月末まで販促キャンペーン実施中です!
- ・高価格帯の高純度品、誘導体中心に**通常価格の20%割引!**
- ・対象銘柄は以下。詳細は下記代理店までお問い合わせください!

銘柄		分子構造	純度(HPLC面積%、代表値)	最低数量(g)
<u>nanom purple</u> フラーレンC60	SU		99.5/昇華精製品	2
	SUH		99.9/昇華精製品	1
	SC		99.9/昇華精製/単結晶品	1
<u>nanom orange</u> フラーレンC70	ST		97	1
	SU		98/昇華精製品	0.5
<u>nanom spectra</u> [60]PCBM <small>(phenyl C61-butrylic acid methyl ester)</small>	E100		99	1
	E100H		99.5	1
	E102		99.9	0.5
<u>nanom spectra E400</u> bis[60]PCBM <small>(bis-phenyl C61-butrylic acid methyl ester)</small>			98/異性体トータル	1
<u>nanom spectra</u> [70]PCBM <small>(phenyl C71-butrylic acid methyl ester)</small>	E110	 主成分	99/異性体トータル	0.5
	E112		99.5/異性体トータル	0.5
<u>nanom spectra Q100</u> [60]インデン付加体			99	0.5
<u>nanom spectra Q400</u> [60]インデン2付加体			99/異性体トータル	1
<u>nanom spectra J204</u> [60,70]アミノ付加体			nanom mixベースのアミノ付加体混合物	1
<u>nanom spectra H200</u> [60]5重付加体			99	1
<u>nanom spectra M100</u> [60]10重付加体			99/異性体トータル	1

【お問い合わせ先】

2012/6

- ・関東化学株式会社 試薬事業本部
〒103-0022 東京都中央区日本橋室町2-2-1 TEL:03-6214-1090 FAX:03-3241-1047
<http://www.kanto.co.jp> E-mail:reag-info@gms.kanto.co.jp
- ・第一実業株式会社 新事業推進室【担当: 鎰広(カギヒロ)】 E-mail:masaru.kagihiro@djk.co.jp
〒102-0084 東京都千代田区二番町11-19 TEL:03-5214-8579 FAX:03-5214-8503

<本資料に関するお問い合わせ先>
フロンティアカーボン株式会社 営業販売センター【担当: 梶原】
TEL:093-643-4400 FAX:093-643-4401 <http://www.f-carbon.com>
※弊社へのお問い合わせはHPよりお願いいたします。